Self-assembly and host-guest studies of heteronuclear coordination complexes

Alexander James Metherell

A thesis submitted to The University of Sheffield in partial fulfilment of the requirements for the Degree of Doctor of Philosophy

November 2014

Department of Chemistry, University of Sheffield, Sheffield S3 7HF, UK.

Author's Declaration

Except where specific references have been made to other sources, the work within this thesis is the orginal work of the author. It has not been submitted, in whole or in part, for any other degree.

Alexander James Metherell

September 2014

Abstract

This thesis is primarily concerned with the synthesis and characterisation of heterometallic polynuclear coordination structures, but also contains host-guest studies of mononuclear complexes.

Chapter One consists of an introduction to self-assembly and supramolecular chemistry. Recent examples of coordination cages are given along with previous work from the Ward group. An introduction to recent efforts in the field of heterometallic supramolecular chemistry is also given.

Chapter Two describes the use of a series of mononuclear Ru(II) complexes to act as models for the vertices of coordination cages. A simple and general synthetic procedure is described which will allow access to a wide range of substituted analogues of $[Ru(L^{H})_3]^{2+}$ as their pure *fac* and *mer* isomers. It has been shown that the *fac*-$[RuL_3]^{2+}$ complexes bind to isoquinoline N-oxide more strongly than the *mer* isomer, but much less strongly than the complete cage complex due to the presence of competing anions, which are excluded from the cage cavity.

Chapter Three describes the formation of a series of heteronuclear coordination cages from inert and labile subcomponents. The synthesis of a range of mononuclear $[RuL_2]^{2+}$ and $[RuL_3]^{2+}$ complexes as either a mixture of *mer* and *fac* isomers or pure fac is discussed, followed by the self-assembly of two heterometallic cubes $[Ru_4Cd_4(L^{1,5\text{-nap}})_{12}]^{16+}$ and $[Ru_4Co_4(L^{m\text{-Ph}})_{12}]^{16+}$, a $[Ru_4Cd_{12}(L^{p\text{-Ph}})_{12}(L^{1,4\text{-nap}})_{12}]^{32+}$ cage, the adamantoid cage $[\{Ru(L^{p\text{-Ph}})_3\}_4Ag_6]^{14+}$, and the trinuclear $[\{Ru(L^{o\text{-Ph}})_2\}_2Ag]^{5+}$.

Chapter Four describes the syntheses and characterisation of a family of asymmetric ligands based upon pyrazolyl-pyridine and catecholamide binding moeties connected by aromatic spacers. The synthesis and structural determination of a tetrameric hetero-octanuclear cyclic helicate $[Ti_4Zn_4(L^{1,3})_8(\mu\text{–}OMe)_8]$ with the ligand $H_2L^{1,3}$ is described.

Chapter Five describes the efforts towards functionalising the exterior of M_8L_{12} cages. The synthesis of the aniline functionalised ligand L^{an} is discussed, which self-assembles with Co(II) to form a $[Co_8(L^{an})_{12}]^{16+}$ cube. Functionalising the ligand with ferrocene to form L^{Fc} results in the self-assembly process with Co(II) now forming a $[Co_6(L^{Fc})_9]^{12+}$ structure.

Acknowledgements

First and foremost I would like to thank Professor Michael Ward for allowing me to work within his research group. His guidance and enthusiasm throughout my time in the group have been important to me, as well as his patience and understanding when things haven't gone to plan. Thanks Mike.

I would like to thank Dr Andy Stephenson for his diligent and tireless work helping me solve my crystal structures when I joined the group, and also his leadership and many assists he provided me on the pitch for CPFC (the Plate was for you). Dr Dan Sykes was an inspirational role model to all during his time in the group, and his 'doom and gloom' attitude helped me see the lighter side of things.

Thank you to all the other past Ward group members (Ben, Slugger, Ian, Martina, Shida and Adel) and the current bunch (Will, Ash, AJ, Liz, Jerry, Chris, Atanu, Suad and Beth) for all the useful advice and great lab (and pub) company over the years. A special mention is due for Will who has been of invaluable help with NMR and various bits of software. The Brammer group have also been a great bunch of guys to share the office, lab and pub with, so thanks to Lee (especially for the last minute viva!), Jop, Jamie, Tom, Elliot, Craig, Inigo, Rebecca and Ramida.

The technicians in the department have been of great help over the course of my PhD, particularly Harry Adams for a lot of help with X-ray crystallography; Simon and Sharon from mass spec; Jenny and Mel from elemental, and; Sue, Peter, Brian and Dr Andrea Hounslow for NMR assistance.

I would also like to thank my friends inside and outside the department for being there for the good and bad times throughout my PhD. Thanks for coming up to stay in Sheffield so much Dan, Craig, Rob, James and Liz! I also had a great time with the guys and girls of CPFC (Ed 4 golden boots).

Finally, I would like to thank my family, particularly Mum, Dad and Victoria for their support throughout my PhD, including but not limited to financial assistance, chauffeuring and cooking. Thank you Vicki for being so understanding during my final year (and furnishing the flat).

Table of Contents

List of Publications

1. A. J. Metherell and M. D. Ward, *A tetrameric hetero-octanuclear cyclic helicate formed from a bridging ligand with two inequivalent binding sites*. *RSC Advances*, 2013, **3**, 14281–14285.
2. A. J. Metherell, W. Cullen, A. Stephenson, C. A. Hunter and M. D. Ward, *Fac and mer isomers of Ru(II) tris(pyrazolylpyridine) complexes as models for the vertices of coordination cages: structural characterisation and hydrogen-bonding characteristics*. *Dalton Trans.*, 2014, **43**, 71. ('Hot Article', featured on front cover).
3. A. J. Metherell and M. D. Ward, *Stepwise synthesis of a Ru_4Cd_4 coordination cage using inert and labile subcomponents: introduction of redox activity at specific sites*. *Chem. Commun.*, 2014, **50**, 6330.
4. A. J. Metherell and M. D. Ward, *Stepwise assembly of an adamantoid Ru_4Ag_6 cage by control of metal coordination geometry at specific sites*. *Chem. Commun.*, 2014, **50**, 10979.

Abbreviations

M	Metal
L	Ligand
fac	Facial
mer	Meridional
stat	Statistical
NMR	Nuclear Magnetic Resonance
δ	Chemical shift
ppm	Parts per million
J	Coupling constant
Hz	Hertz
s	Singlet
d	Doublet
t	Triplet
m	Multiplet
ArH	Aromatic proton
ESMS	Electrospray Mass Spectrometry
ES	Electrospray
m/z	Mass to charge ratio
EA	Elemental Analysis
2θ	Angles of the diffractometer
Å	Angstrom
a, b, c	Unit cell dimensions
α, β, γ	Unit cell angles
V	Unit cell volume
Z	Formula units per unit cell
μ	Linear absorption correction
F_o, F_c	Observed and calculated structure factors
R_1, wR_2	R-indices (based on F and F_2 respectively)

CFSE	Crystal field stabilisation energy
HSAB	Hard-soft acid-base
AIBN	Azobisisobutyronitrile
Boc	tert-Butyloxycarbonyl
CBr_4	Carbon tetrabromide
CCl_4	Carbon tetrachloride
$(CD_3)_2CO$	Deuterated acetone
$(CD_3)_2SO$	Deuterated dimethylsulphoxide
CD_3CN	Deuterated acetonitrile
CD_3NO_2	Deuterated nitromethane
$CDCl_3$	Deuterated chloroform
D_2O	Deuterium oxide
DCM	Dichloromethane
DMF	Dimethylformamide
DMSO	Dimethylsulphoxide
Et_3N	Triethylamine
EtOAc	Ethyl Acetate
H_2bpp	2,6-bis(pyrazol-3-yl)pyridine
Me	Methyl
MeCN	Acetonitrile
$MeNO_2$	Nitromethane
MeOD	Deuterated methanol
MeOH	Methanol
$MgSO_4$	Magnesium sulphate
NBS	N-Bromosuccinimide
PPh_3	Triphenylphosphine
PyPz	Pyrazolyl-pyridine
THF	Tetrahydrofuran

1. Introduction

1.1 Self-assembly

Every chemist will be familiar with and have a good understanding of molecular, or covalent, synthesis. By reacting molecules with certain functionalities, a product can be rationally predicted based on centuries of accumulated chemical knowledge. Recently, a field concerning non-covalent chemistry has come to prominence. This field is known as supramolecular chemistry, or 'chemistry beyond the molecule'.[1] Whereas in molecular chemistry components are held together by covalent bonds, so-called supermolecules are held together reversibly by weak intermolecular forces.[2] The reversible formation of a supermolecule from its constituent parts under appropriate conditions is known as self-assembly. Intermolecular forces that are used in self-assembly include electrostatic interactions, hydrogen bonding,[3] π–π stacking interactions,[4] dispersion forces and hydrophobic effects.[5,6] The coordination between metals and ligands can also be included in the discussion of self-assembly when the interaction is labile.

There are several classes of self-assembly, including strict self-assembly which occurs completely reversibly under thermodynamic control, so that the supramolecular product represents a thermodynamic minimum.[6] There is also irreversible self-assembly which occurs under kinetic control, where any 'mistakes' result in the irretrievable loss of product; this type of self-assembly is of little interest in supramolecular chemistry.

1.2 Self-assembly in nature

Self-assembly is ubiquitous in nature, and as with many facets of chemistry nature is the master of its art. A well-studied example of this is the self-assembly of tobacco mosaic virus (TMV).[7] Consisting of an RNA strand and 2130 protein subunits, this simple virus spontaneously self-assembles from its constituent parts under physiological conditions (see Figure 1.2.1.). The assembly/ disassembly is dependent on the conditions and contains no covalent steps, and is termed 'strict self-assembly'.[8] The reversible nature of strict self-assembly leads to the formation of the thermodynamic product, as many kinetic products (i.e. combinations) may be tried by the system before the product lowest in energy is found.

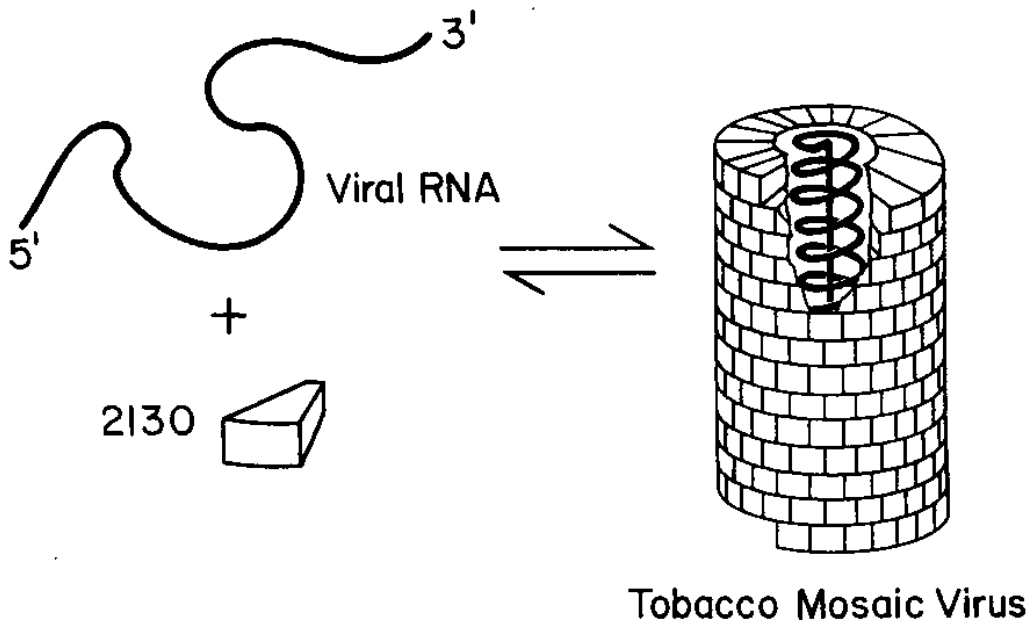

Figure 1.2.1 Self-assembly of the tobacco mosaic virus. Reproduced from Ref. 8. Copyright 1991 CNRS-Gauthier-Villars.

Nature also utilises covalent chemistry to lock a supermolecule in its self-assembled conformation. This is known as self-assembly with a covalent step, or 'self-assembly with post-modification'.[8] An example of this is the self-assembly of insulin.[9] Before the active hormone can be synthesised, the much larger polypeptide preproinsulin must first fold (i.e. self-assemble) into its native form. Disulfide bridges can then be formed between the A and B chains at the appropriate positions (the covalent step) before

proteolytic excision of the peptide to give insulin (see Figure 1.2.2). Attempts to synthesise insulin from the denatured and reduced chains A and B generally give poor yields, indicating that the initial self-assembly step is crucial in the synthesis of insulin.[5]

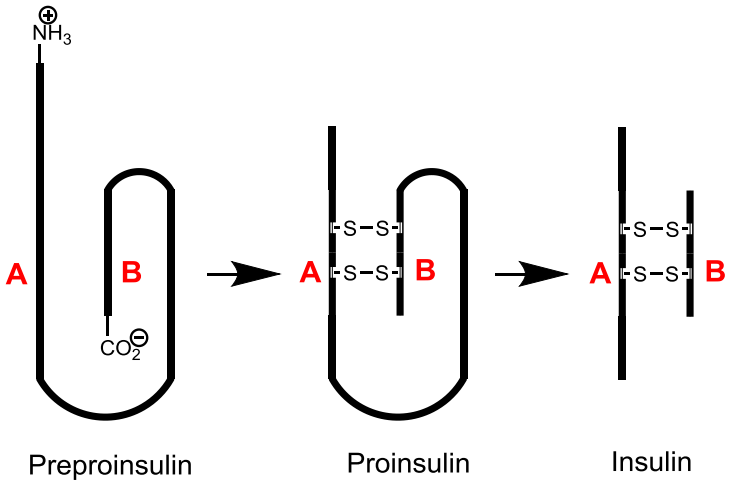

Figure 1.2.2 Self-assembly with a covalent step of preproinsulin to form insulin.[9]

Other examples of self-assembly of nature include the formation of the DNA double helix (which themselves can self-assemble into triangular motifs when crystallized),[10] and the disassembly and reassembly of ribonuclease, which spontaneously folds into its native conformation under certain conditions.[8]

1.3 Self-assembly in inorganic synthesis

1.3.1 The emergence of supramolecular chemistry

As with many areas of science, supramolecular chemistry was born in serendipitous circumstances. Pedersen's macrocyclic ethers, formed due to an impurity in his reaction mixture (see Figure 1.3.1),[11] were the first neutral molecules found that were able to bind alkali metal ions in their central cavity. This is significant for two reasons; i) the metal ion acts as a template for the large macrocycle to form around, preorganising the ligand and lowering the entropic cost of reaction; ii) alkali metal salts are rendered soluble in organic solvents such as benzene, leaving the partner anion relatively unsolvated, and hence greatly increasing the nucleophilicity of it,[5] thereby demonstrating a practical use for the host-guest chemistry which the crown ether and related ligands display.

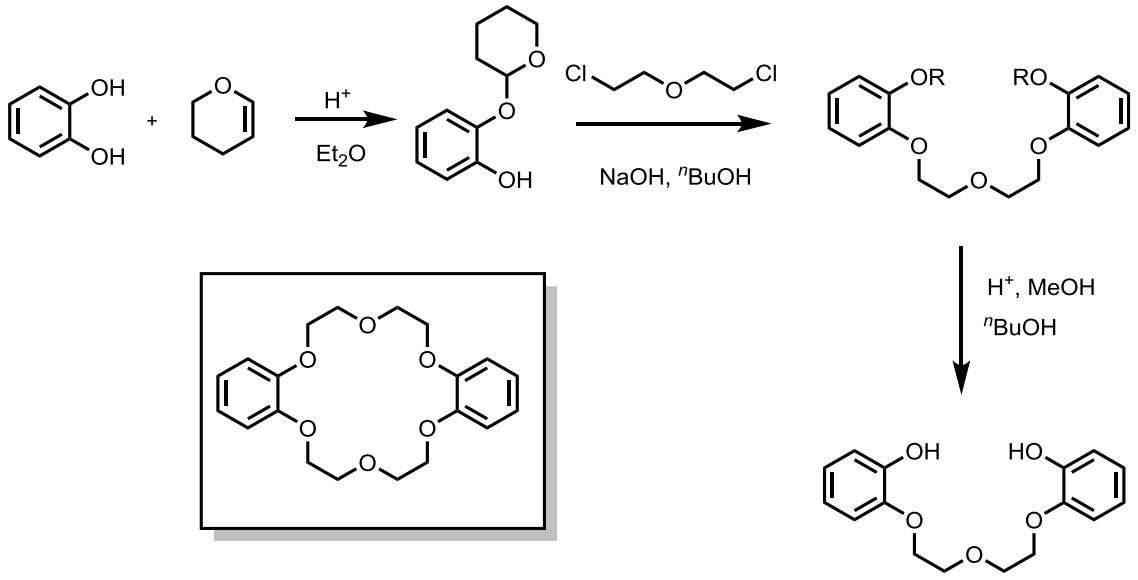

Figure 1.3.1 Intended synthesis of Pedersen's ligand, and the resulting crown ether shown in the bottom left.[11]

Since Pedersen's discovery in 1960, the field of supramolecular chemistry has moved from strength to strength, with systems of ever increasing complexity being developed. Examples include Sauvage's knots and interlinked rings[12], Whitesides' rosettes[13] and Stoddart's catenanes.[14] Jean-Marie Lehn, who was awarded the Nobel Prize for Chemistry along with Pedersen and Donald J. Cram in 1987, is pre-eminent in this field, and his initial studies included complexes of cryptands (macrobicyclic ligands).[15]

This early work focussed on the recognition of spherical metal cation guests. His work later developed into designing more complicated hosts for complex guests such as adenosine triphosphate.[1]

In the late 80s and 90s Lehn was concerned with the self-assembly of helicates and grids, moving from molecular recognition towards self-organisation.[16] By combining strands of different oligobipyridine ligands with 4-coordinate Cu(I) and 6-coordinate Ni(II), double and triple helicates can be selectively formed (see Figure 1.3.2), a phenomenon that Lehn refers to as 'programming' the system.[17]

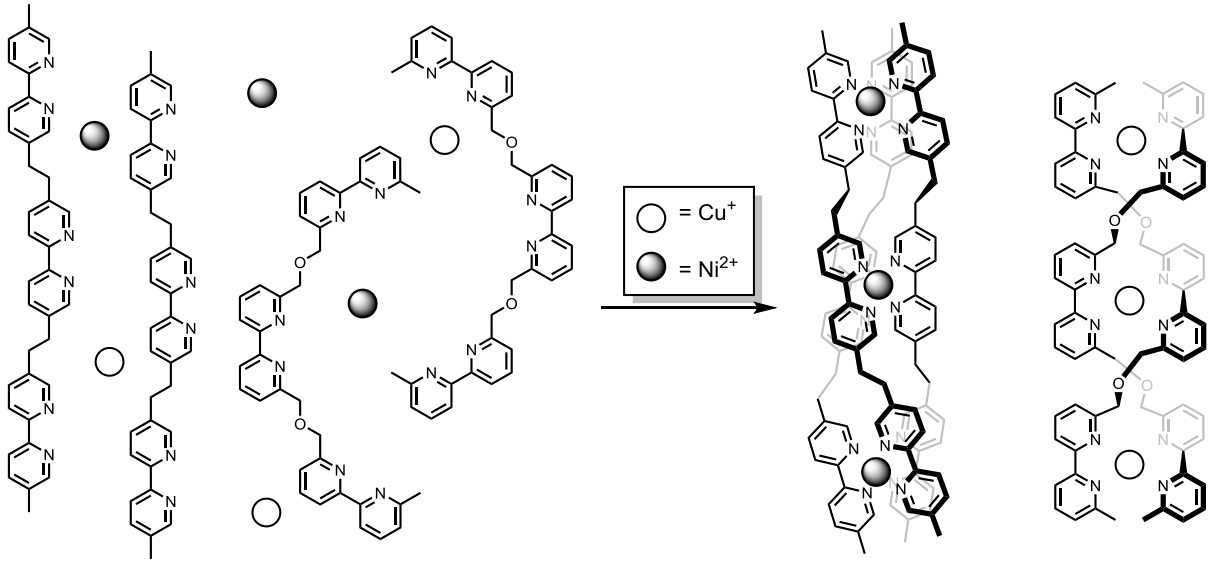

Fig 1.3.2 Self-recognition in the assembly of a double helicate and a triple helicate from a mixture of two different ligands and two different types of metal ions.[16]

As supramolecular chemistry has developed, the 'rules' governing self-assembly have become more fully understood through studying systems of low complexity such as this, enabling the designed synthesis of higher order structures.[18] Würthner describes these rules as 'molecular codes' which are used in the process of 'molecular programming'.[19]

1.3.2 From helicates to two-dimensional supramolecular structures

From these relatively simple helicates, a logical progression in the application of 'molecular programming' would be to study the assembly of two-dimensional supramolecular structures. These include squares, grids and racks, and many other structures based on simple polygons. Stang and co-workers have utilized basic coordination chemistry to form highly symmetrical pre-designed shapes from a mixture of rigid linking units.[20] This work started with 2D polygons such as simple molecular squares, but later moved on to 3D structures based on the Platonic and Archimedean solids (see Figure 1.3.3).[21] This work shows how a mixture of different units can lead to the formation of discrete supramolecular assemblies in which the shape is predetermined by the size and angle of the donor and metal acceptors.

Fujita and co-workers were one of the first to create a molecular square.[22] Using a *cis*-protected square planar metal such as palladium(II) or platinum(II) with an inert bidentate ligand such as ethylenediamine (en) as a 90^{o} corner, and reacting with a linear bridging ligand such as 4,4'-bipyridine, a near perfect square is formed (see Figure 1.3.4). When the pyridine rings are separated by a phenylene spacer, the longer bridging ligand results in the square existing in equilibrium with molecular triangles.[23] Fujita extrapolated this idea and created hexagons, linked rings and eventually 3D coordination cages.[24]

Both of the above examples employ the pre-design of a two-dimensional product by the use of particular 'molecular codes';[19] in this case, the fixed coordination geometry of both the ligands and the metal ions. It is the particular choice of a protected convergent metal and a divergent ligand that leads to the formation of the desired polygons, rather than a coordination polymer (see Figure 1.3.5).[6] Discrete supramolecular structures are formed from complementary convergent/divergent pairs, whereas a polymer would form from a divergent pair.

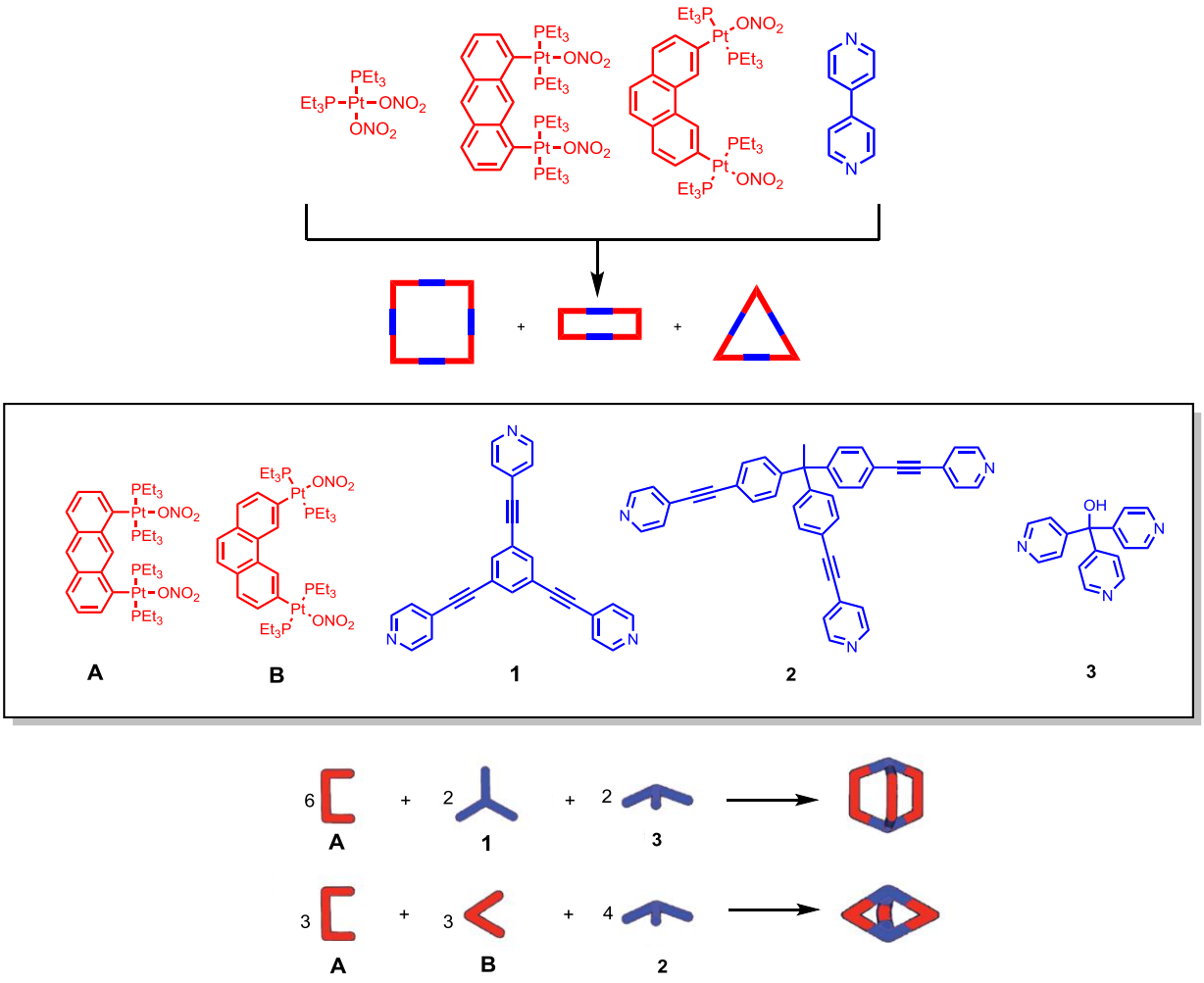

Figure 1.3.3 Representative example of Stang's work, including 2D polygons (top) and 3D polyhedra (bottom).[21]

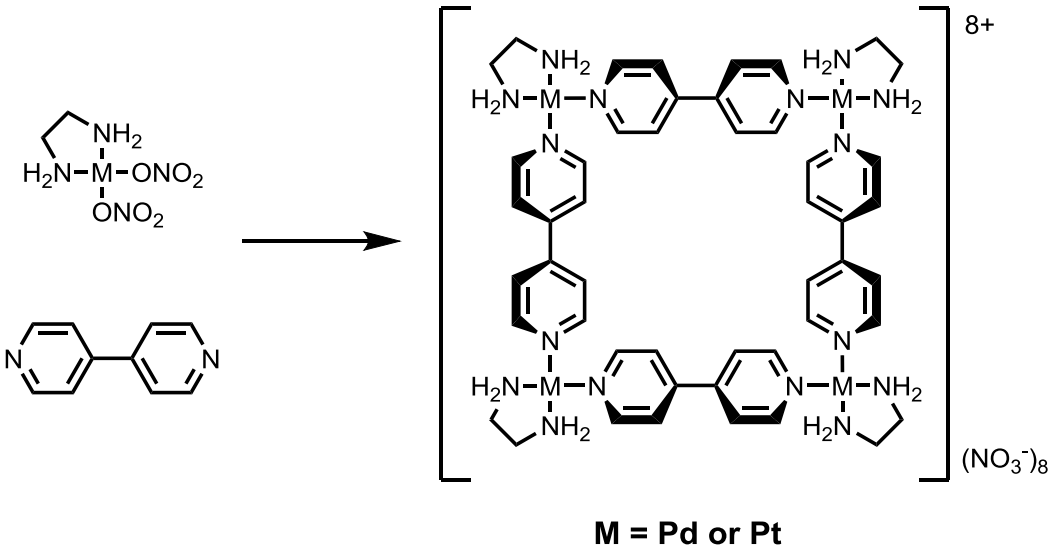

Figure 1.3.4 Fujita's molecular square.[24]

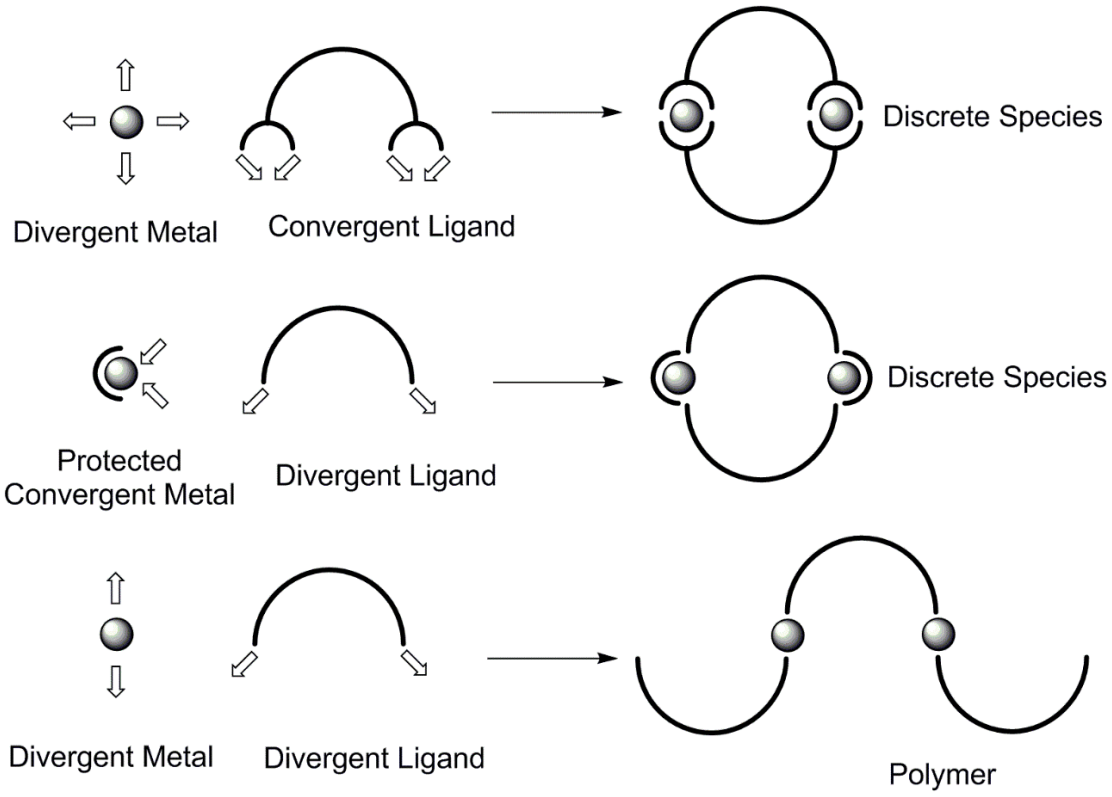

Figure 1.3.5 Design of discrete structures by choice of binding site.[6]

1.3.3 Three-dimensional coordination cages

The report of Saalfrank's adamantanoidal cage in 1988 is thought to be one of the first 3D coordination cage structures, in which a tetrahedral array of magnesium (II) ions are linked by bridging bis-enolate ligands.[25] Saalfrank expanded this idea by using transition metal dications (see Figure 1.3.6),[26] and also by extending the ligand with phenylene spacers.[27]

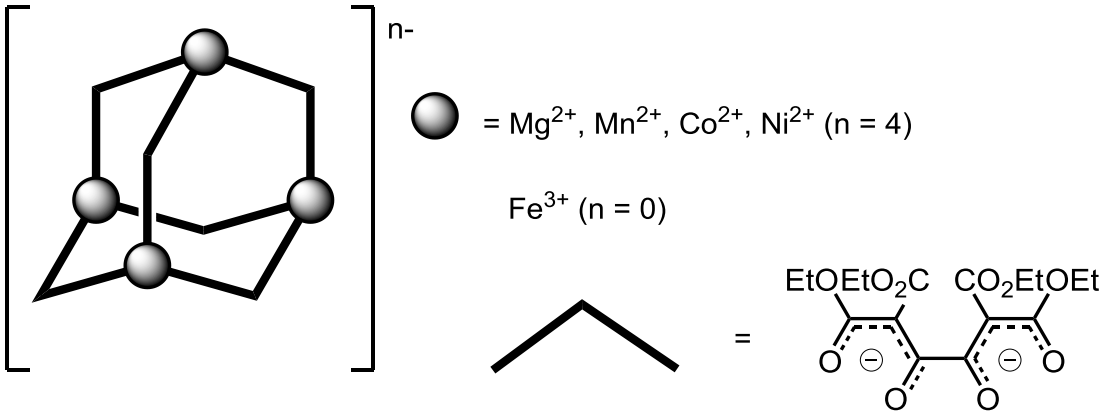

Figure 1.3.6 Saalfrank's M_4L_6 'adamantanoid' cage.[24]

In 1995, Fujita and co-workers extended their earlier work on the molecular square by synthesising a nanosized 3D cage (**1**), capable of encapsulating four adamantyl carboxylate ions within its cavity.[28] By reacting the *cis*-protected metal with a trigonal tridentate ligand, a 3D octahedral coordination cage can be formed quantitatively.[24] Fujita has since shown that this coordination cage exhibits a range of interesting properties, including host guest chemistry[29] and the use as a catalyst,[30] leading to these interesting macromolecules being called 'molecular flasks'.[31] This behaviour is driven by the hydrophobic effect, owing to the hydrophobic interior of the cage; hence in aqueous solvents, hydrophobic guests will diffuse into the central cavity of the cage in order to maximise the favourable interactions that water will have itself. This has facilitated some otherwise stubborn reactions, such as the Diels-Alder reaction of naphthalene (see Figure 1.3.7).[30] In addition to the hydrophobic effect, a significant decrease in the entropic cost of reaction results from the preorganization of reactants inside the cage.

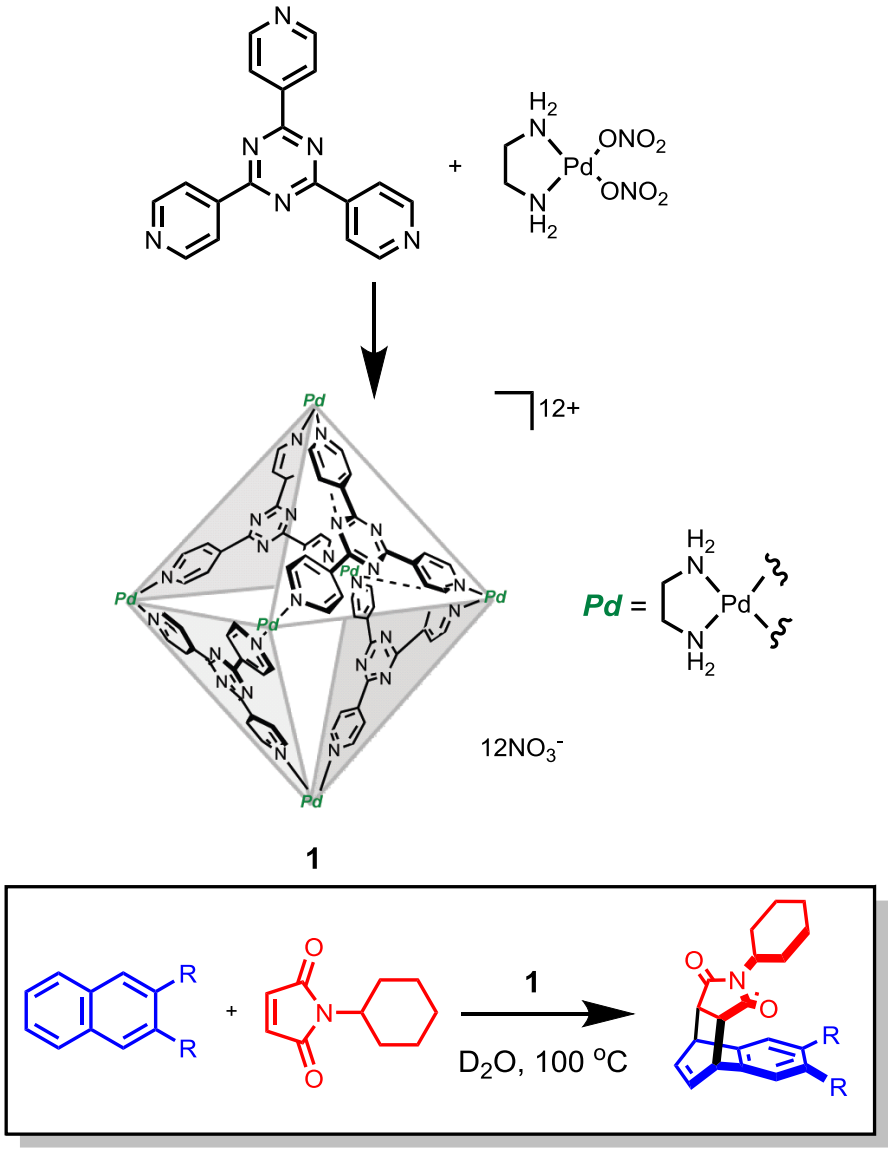

Figure 1.3.7 Top: Assembly of the M_6L_4 octahedron (**1**). Bottom: Naphthalene Diels-Alder reaction in the self-assembled molecular flask. Adapted with permission from Ref. 30. Copyright 2010 American Chemical Society.

Fujita's method for synthesising his octahedral capsule utilises what Stang describes as the 'molecular panelling' approach, in which the octahedron is prepared by bringing together eight triangular panels.[32] By modifying the position of the coordinating nitrogen atoms on the triangular ligand, and thus the connectivity of the panels, Fujita was able to form a hexahedron capsule, a square-pyramidal cone and a closed-tetrahedron.[33] His most recent work shows the formation of a staggering $M_{24}L_{48}$ series of cages, although this used a different approach and ligand family to that above.[34] These cages can be functionalised on the exterior or interior surface *via* ligand modification, drastically altering the host-

guest chemistry of the cages.[35-37] For example, with 24 inwardly directed sugar groups, precisely monodisperse silica nanoparticles can be formed within the cage cavity.

The molecular panelling approach is one method used for designing coordination cages. Another method used is the 'symmetry interaction' approach.[32] This involves using multibranched chelating ligands with rigid backbones and fixed geometries, along with labile transition metal ions or main group metals. Raymond and co-workers have defined the requisites of this design principle, principally the 'coordinate vector' and the 'chelate plane'.[38] The vector that represents the interaction between a ligand and metal is the coordinate vector (see Figure 3.3.3). When using chelating ligands, the plane orthogonal to the major symmetry axis of a metal complex is the chelate plane, in which all of the coordinate vectors of the chelating ligands lie. Any symmetric coordination complex cluster can be described in terms of the relationships between these chelate planes.

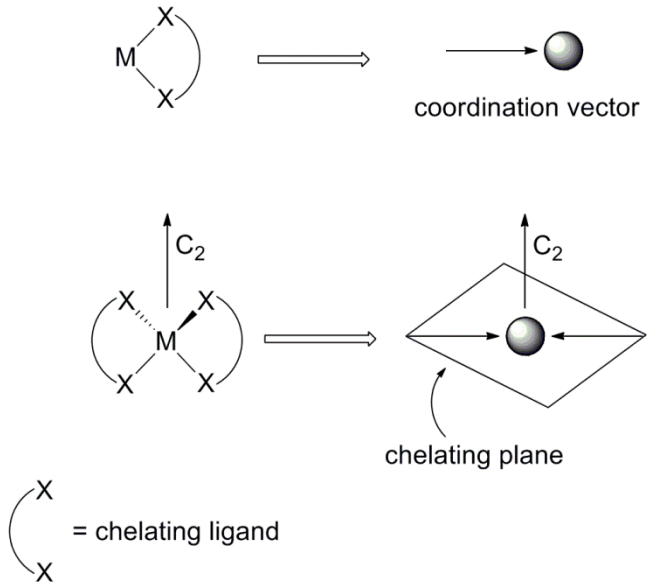

Figure 1.3.8 Raymond's definitions for coordination vectors and chelating planes.[32]

The M_2L_3 triple helicate formed in 1996 was one of the first examples from the Raymond group of a structure formed by this design approach, consisting of two gallium(III) centres linked by three rigid biscatecholamide ligands (see Figure 1.3.9).[39] Later in the same year, Raymonds first M_4L_6 cage was reported.[40] The bis-bidentate bridging ligand incorporates two hydroxamate units separated by a

phenylene spacer; the method of creating ligands with chelating binding sites separated by a rigid aromatic spacer is one that is used regularly in coordination cage chemistry.[41-44]

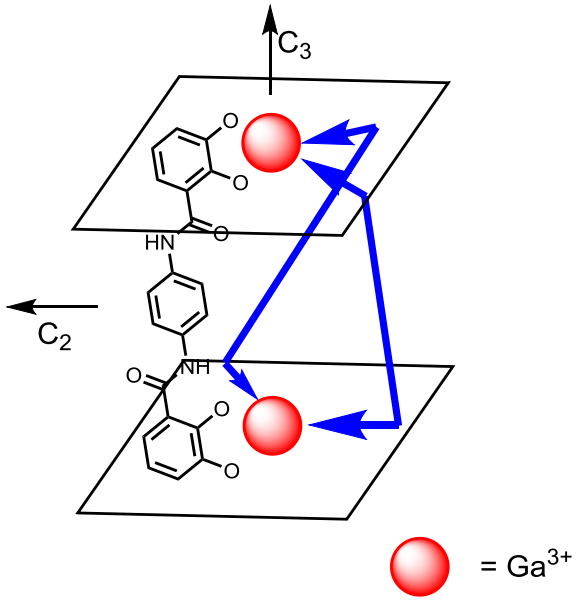

Figure 1.3.9 Raymond's D_3-symmetrical triple helicate.[32]

By changing the aromatic linker from a phenyl ring to a naphthyl unit in his biscatecholamide ligand, Raymond was able to create a M_4L_6 cage that has since proved to have many remarkable properties (see Figure 1.3.10).[45-52] The self-assembled anionic $[Ga_4L_6]^{12-}$ cage (**2**) is able to stabilize reactive intermediates such as tropylium, cationic phosphine-acetone adducts, and iminium ions due to its hydrophobic interior, as well as augmenting the performance of encapsulated catalaysts through cavity effects.[31,53] A recent example shows that the catalytic activity of Me_3PAuBr was increased 8-fold by encapsulation, and up to 67 catalytic turnovers by Me_3PAu^+ encapsulated in **2** were observed.[52]

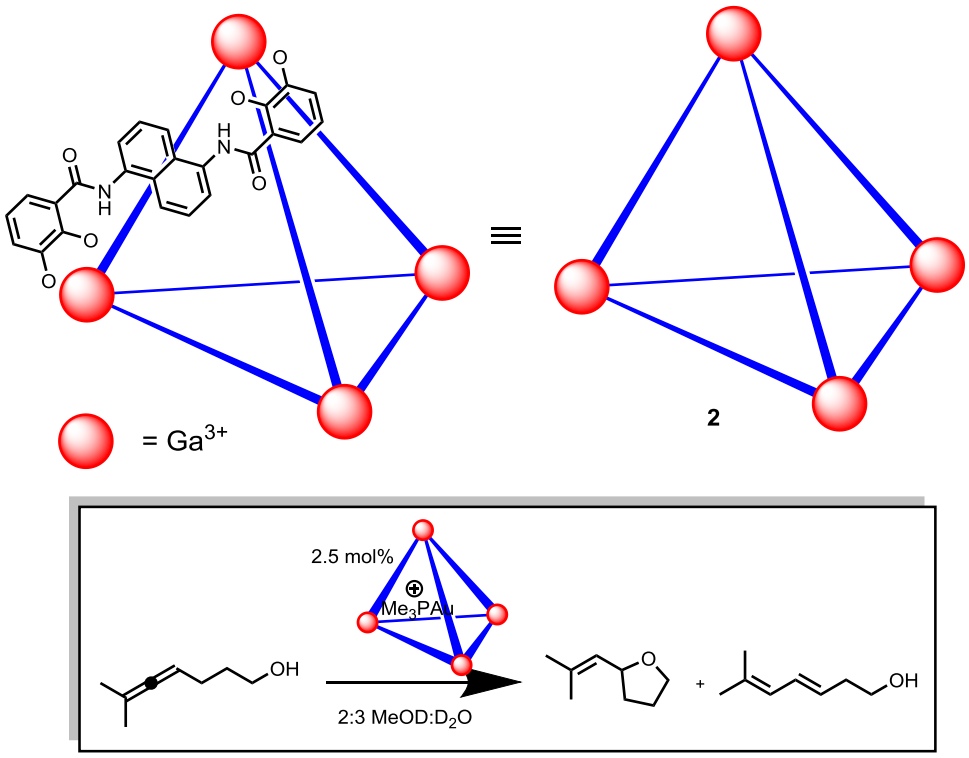

Figure 1.3.10 Raymond's $[Ga_4L_6]^{12-}$ cage (**2**), and the hydroalkoxylation reaction catalyzed by $Me_3PAu^+ \subset$**2**.[52]

The panelling approach and directional bonding approach discussed above are two methods used to construct coordination cages. Another method is 'sub-component self-assembly', an approach which Nitschke and co-workers have recently used to great effect.[54-63] Nitschke defines subcomponent self-assembly as "the construction of complex architectures from simple building blocks *via* formation of covalent bonds around metal templates".[62] This method utilises the thermodynamic template effect, in which a metal selectively binds to ligand fragments that it has a strong affinity for, and thus shifting the 'dynamic combinatorial library' to a particular product.[6]

Nitschke's most famous example of this is his anionic Fe_4L_6 tetrahedral cage (**3**).[60] In the presence of iron(II) and base, 4,4'-diaminobiphenyl-2,2'-disulfonic acid and 2-formylpyridine subcomponents condense to form the water soluble cage (see Figure 1.3.11). This cage has shown some beautiful host-guest chemistry; it is able to air-stabilize the pyrophoric P_4 molecule in aqueous solution, which can then be safely oxidized to phosphoric acid by addition of a competing guest such as benzene (see Figure 1.3.11).[59] The iron(II) cage self assembles in water, and the hydrophobic P_4 is drawn into its central

cavity due to the hydrophobic effect. The cage is also able to encapsulate SF_6, a potent greenhouse gas, and release it again under defined conditions.[56]

Nitschke has also designed a cubic cage with porphyrin-based ligands occupying the six faces of the cube, and iron(II) occupying the eight vertices.[64] This cage is able to encapsulate large aromatic guests such as buckminsterfullerene. Most recently, Nitschke has reported a Cu_8L_4 tube that is able to selectively bind and release gold guests,[65] a fluorophore incorporating M_4L_6 cage that allows nanomolar guest sensing and white-light emission,[66] and the formation of five discrete multinuclear metal-organic assemblies from one ligand.[67]

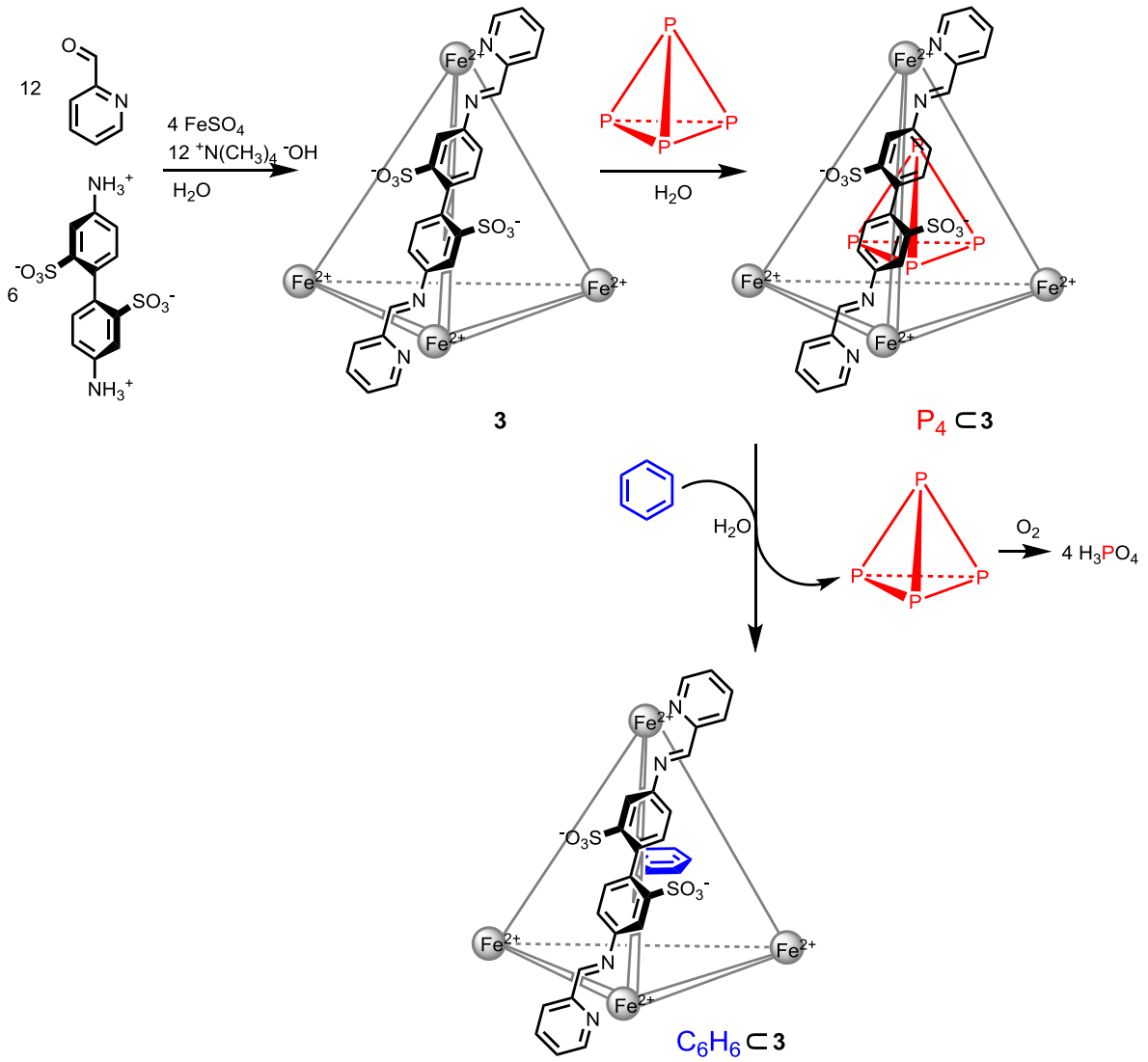

Figure 1.3.11 Subcomponent self-assembly of tetrahedral cage **3** and subsequent incorporation of P_4 followed by its controlled release by substitution with benzene.[59]

1.3.4 Functional coordination cages

Coordination cages give a great test-bed for the understanding of supramolecular theory; by designing cages methodically, the 'rules' we know concerning self-assembly become ever clearer, and new rules may be learnt. The work of Fujita, Raymond and Nitschke discussed above are great examples of this. The corollary of this is that functional structures may be formed as a result, thus propagating further research in the field so that more applications of the host-guest chemistry become discovered.[68] Their use as 'molecular flasks', so termed by Fujita,[69] is a well-known functionality of coordination cages.[31] Fujita's M_6L_4 octahedron has been shown to facilitate a number of reactions and trap reactive intermediates, as described above.[31] The catalytic activity of Raymond's M_4L_6 tetrahedron and molecular trapping abilities of Nitschke's M_4L_6 tetrahedron have also been described.[49,53]

Kobayashi and Yamanaka have shown that a capsule complex formed from the self-assembly of two cavitand and cis-protected platinum(II) units encapsulates guests that are of an appropriate molecular size to fit the cavity.[70] This builds on the earlier work of Rebek, who identified capsules that formed from a variety of hydrogen-bonding dimers.[71]

Custelcean and co-workers have used computer-aided design to form a molecular cage that is tailor-made for a specific guest.[72-74] Combination of a urea-functionalised ligand with an appropriate transition metal dication resulted in the formation of a tetrahedral cage with 12 endohedral urea protons, providing an ideal binding environment for tetrahedral oxoanions such as sulphate (see Figure 1.3.12).

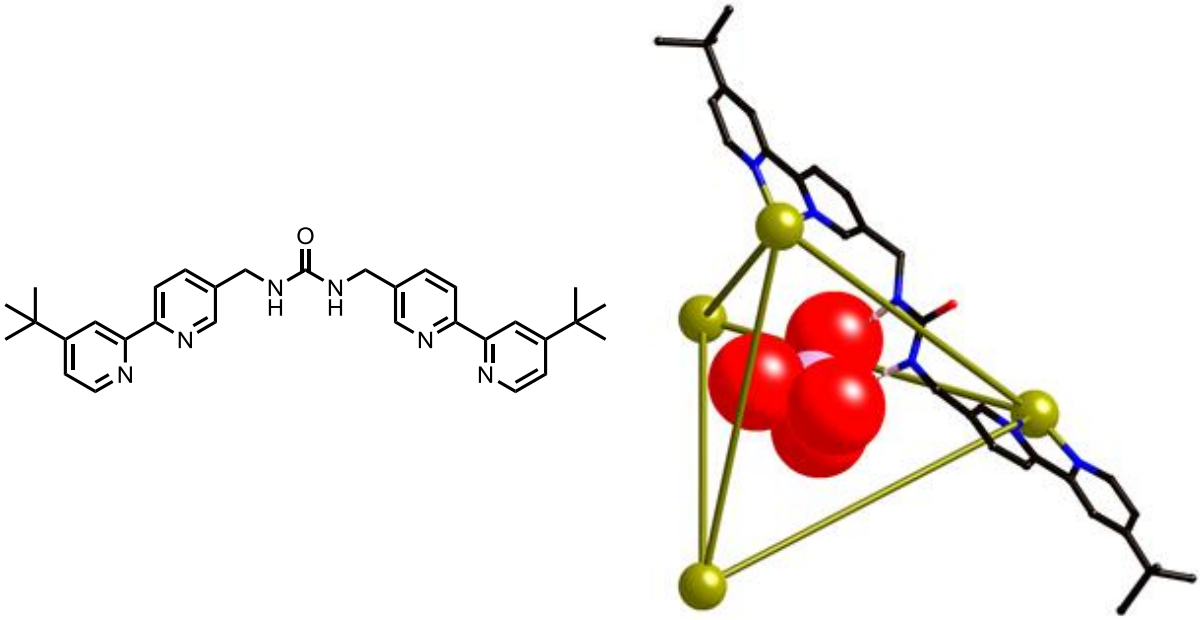

Figure 1.3.12 Left: The urea-functionalised ligand. Right: Custelcean's M_4L_6 cage with an ecapsulated SO_4^{2-} anion, emphasising the hydrogen-bonding interactions between the host and guest.

Meehan and Lindoy have used a quaterpyridine ligand previously synthesised by Lehn[75] to form a cage with iron(II) ions, and they have shown that the cage selectively binds PF_6^- over BF_4^-.[76] The same cage selectively extracts a $[Fe^{III}Cl_4]^-$ anion from a mix of Fe(II) and Fe(III) chloro species (see Figure 1.3.13).[77] The $[Fe^{III}Cl_4]^-$ anion is thought to be perfectly complementary for the cage cavity, in terms of shape, size and symmetry. This is a rare example of a supramolecular mixed-valent Fe(II)/Fe(III) inclusion assembly, and it is also believed to be the first reported example of such inclusion of a tetrahalometallate anion in a small supramolecular cage. The same authors have also reported the assembly of an expanded tetrahedral cage encapsulates four tetrahydrofuran molecules, furthering the possibilities for interesting host-guest chemistry within the cage interiors.[78]

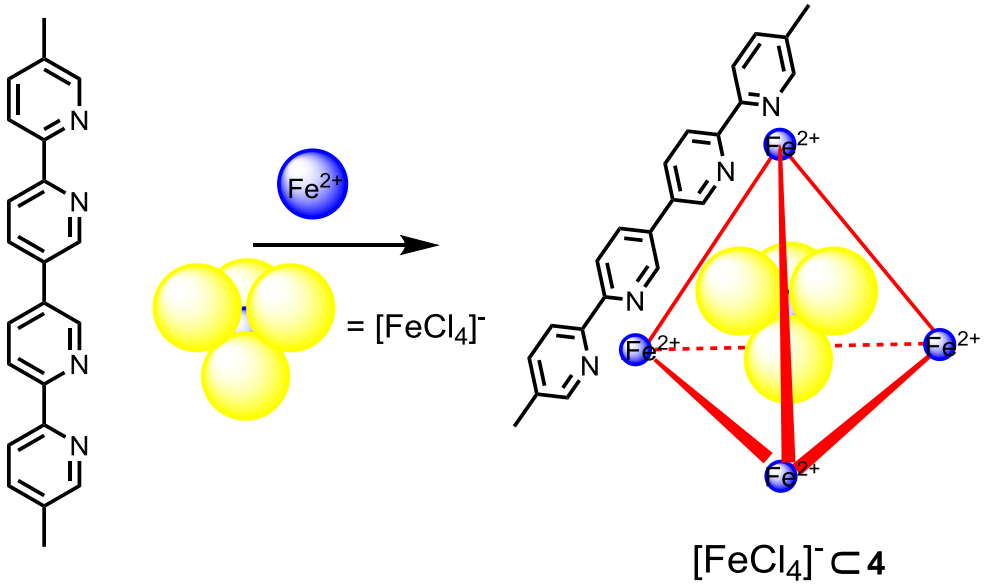

Figure 1.3.13 Schematic representation of the assembly of the tetrahedral $[Fe_4L_6]^{8+}$ host (**4**) incorporating a guest $[Fe^{III}Cl_4]^-$ anion.[77]

Therrien and co-workers have synthesised arene drug boxes; ruthenium(II) metalloprisms that bind platinum(II) or palladium(II) bis(acetylacetonate) cations within the cage cavity (see Figure 1.3.14).[79] This 'complex within a complex' approach greatly increases the cytotoxicity of the trapped complexes. This is a result of the hydrophobicity of the $[M(acac)_2]$ complexes; their insolubility in water drives them into the cage cavity. Once the box has reached the target cell, the hexaruthenium cage may open and the $[M(acac)_2]$ complex is released to the biological target. Therrien's group have also synthesised ruthenium(II) cubes that bind to duplex and human telomeric quadruplex, leading to the possibility of using octacationic arene ruthenium metalla-boxes as quadruplex DNA stabilisers.[80]

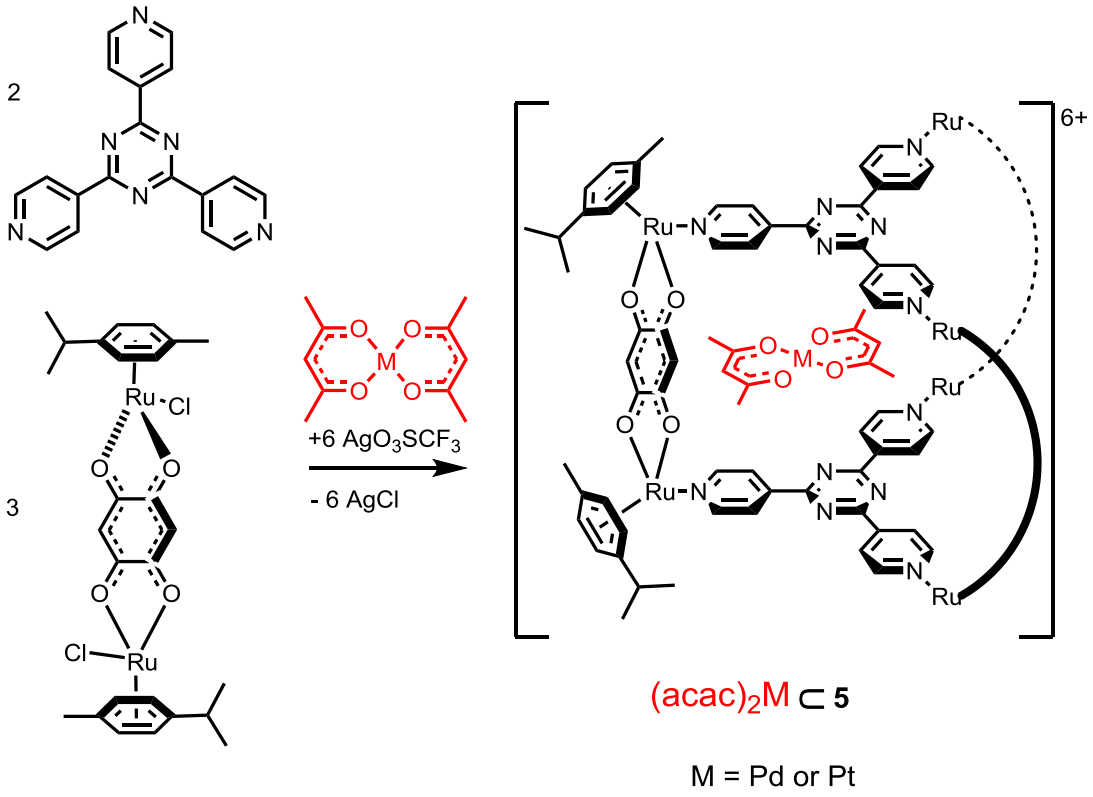

Figure 1.3.14 Therrien's self-assembled arene drug box (**5**) and its encapsulation of a [M(acac)$_2$] guest.[79]

1.4 Coordination cages in the Ward group

Ward and co-workers have been studying coordination cages for the last two decades since their initial discoveries in 1995.[42] An interest in polydentate ligands led to the study of the hexadentate ligand $[Tp^{Py}]^-$ (see Figure 1.4.1a), a member of the 'scorpionate' family of ligands, so named due to their nature of binding to metals.[81] One might expect a six-coordinate metal ion to sit in the cavity and occupy a trigonal prismatic binding geometry with the hexadentate ligand, and this is indeed the case with cobalt(II), resulting in the mononuclear complex $[Co(Tp^{Py})]^+$ (see figure 1.4.1b).[82] However, when the same ligand is reacted with Mn(II) or Zn(II), a tetrahedral cage complex of the type $[M_4(Tp^{Py})_4]^{4+}$ is formed (see Figure 1.4.1c), with each ligand chelating to three metal ions and capping a triangular face of the tetrahedron (see Figure 1.4.1d). This tetrahedral cage arises due to the greater requirement for Mn(II) and Zn(II) to adopt an octahedral coordination environment in comparison to Co(II). The rigid ligand is unable to distort to provide this environment without considerable strain, and hence the tetranuclear structure is adopted, which does allow all M(II) ions to be octahedral.

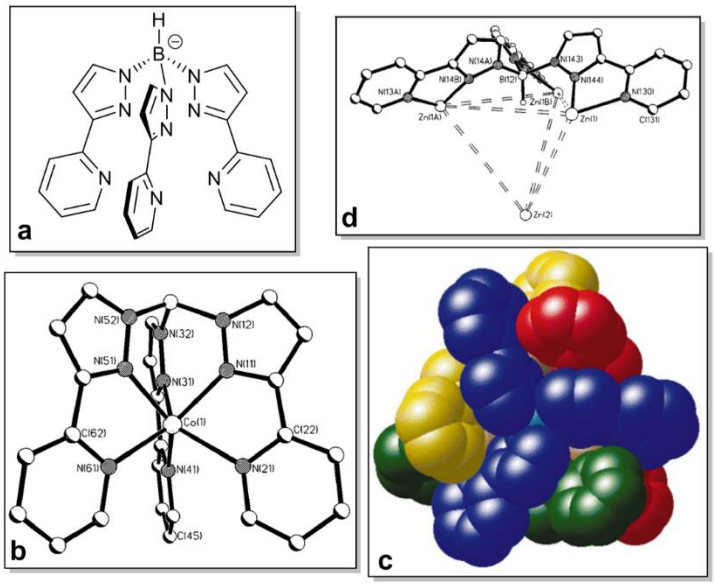

Figure 1.4.1 Anti-clockwise from top left: (a) The hexadentate ligand $[Tp^{Py}]^-$; (b) The mononuclear complex $[Co(Tp^{Py})]^+$; (c) space-filling view of the tetrahedral complex $[Zn_4(Tp^{Py})_4]^{4+}$, and; (d) $[Zn_4(Tp^{Py})_4]^{4+}$ emphasizing the face-capping nature of the ligand. Reproduced from Ref. 82 with permission from The Royal Society of Chemistry.

These results led to further studies into the nature of ligands containing bidentate pyrazolyl-pyridine units. A class of ligands combining two pyrazolyl-pyridine units separated by a rigid aromatic spacer and linked by flexible methylene hinges was born. These ligands are easily synthesised, simply requiring reaction of 3-(2-pyridyl)pyrazole under basic conditions with a (readily available) bis(bromomethyl)aromatic compound.

The first ligand of this type that was synthesised was $L^{o\text{-}Ph}$ (see Figure 1.4.2, left), which contains an ortho-phenylene spacer.[83] Reaction of this ligand with four-coordinate Cu(I) gave the double helical $[Cu_2(L^{o\text{-}Ph})_2]^{2+}$, and with Ni(II) the dinuclear $[Ni_2(L^{o\text{-}Ph})_3]^{4+}$ was formed,[84] in which one ligand acts as a bridging bidentate linkage between the two metal ions, and the other two as tetradentate-chelates, fulfilling the valence requirement of each metal. This ratio of 2M : 3L is required in all complexes of bis-bidentate ligands and six-coordinate metal ions in order for coordinative saturation of all components, an important concept in supramolecular chemistry.[6]

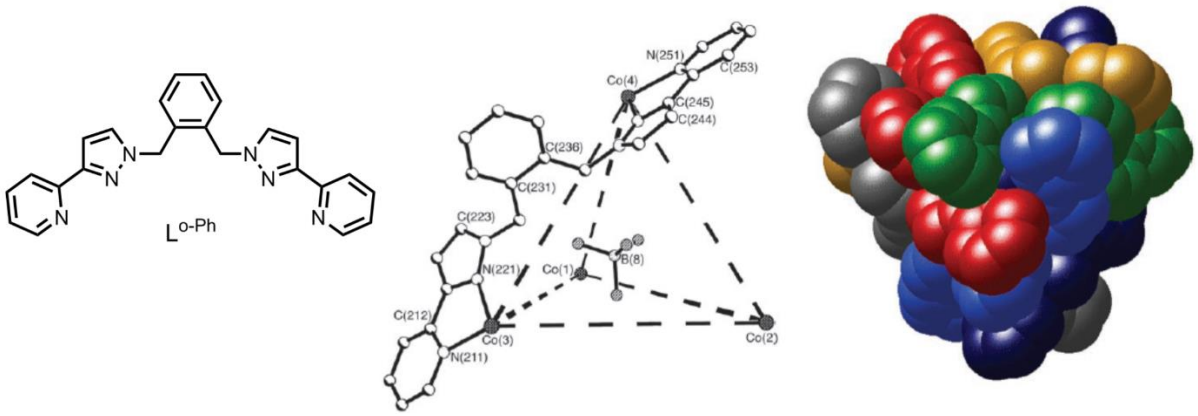

Figure 1.4.2 The bis-bidentate ligand $L^{o\text{-}Ph}$ (left), the tetranuclear cage complex $[Co_4(L^{o\text{-}Ph})_6](BF_4)_8$ showing only the internal anion (centre) and a space-filling model (right) illustrating the extensive π-stacking of the ligands. Reproduced from Ref. 82 with permission from The Royal Society of Chemistry.

Neither of the above results were particularly surprising. However, on reaction of the ligand with $Co(BF_4)_2$, a more remarkable tetrahedral coordination cage $[Co_4(L^{o\text{-}Ph})_6](BF_4)_8$ was formed (see Figure 1.4.2, centre and right). This fulfils the 2M : 3L ratio, with each ligand spanning an edge of the tetrahedron and the metal ions occupying the vertices with a *fac* tris-chelate geometry. Crystallographic studies showed that an anion was perfectly encapsulated within the cavity, interacting with the cage *via*

hydrogen bonding with the methylene CH_2 protons.[86] Reaction in the absence of a suitably fitting anion resulted in no cage formation, indicating that the central anion acts as a template for the cage to form around.[86] Another noteworthy point about the structure of the cage is that there is extensive π-stacking between different ligands. These factors all help in the formation and stabilisation of a structure of such complexity from such simple components. It is thought that the smaller ionic radius of Ni(II) in comparison to Co(II) would result in an unfavourable compression of the tetrahedral cage, thus the simple dinuclear M_2L_3 complex forms preferentially.[86]

Following this result, cages that were analogous in structure to the $[Co_4(L^{o\text{-}Ph})_6]^{8+}$ tetrahedron were synthesised with the ligands $L^{2,3\ nap}$ and $L^{3,3\ Bi}$ (see Figure 1.4.3).[85,87] The cages of $L^{2,3\ nap}$ are isostructural with those of $L^{o\text{-}Ph}$;[85] however the larger biphenyl spacer group in $L^{3,3\ Bi}$ results in an expanded tetrahedral cage in which the central anion is no longer completely encapsulated, and in which one metal has *fac* geometry and the other three have *mer* geometry. Larger anions such as hexafluorophosphate can be incorporated within the cage, and as the anions are no longer an ideal size match for the cavity, no templating effect is observed.[86] Recent work has shown that the $M_4(L^{3,3\ Bi})_6$ cages display remarkable kinetic inertness due to their mechanically entangled nature: scrambling of metal cations between the sites of pure Co_4 and Cd_4 cages to give a statistical mixture of Co_4, Co_3Cd, Co_2Cd_2, $CoCd_3$ and Cd_4 cages takes months in solution at room temperature.[88]

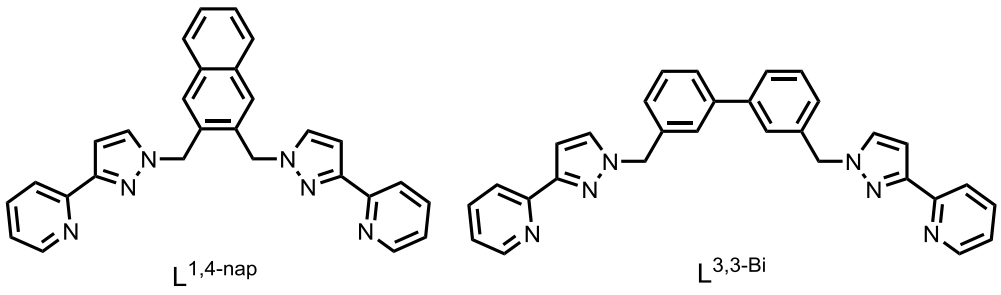

Figure 1.4.3 Ligands related to $L^{o\text{-}Ph}$ that resulted in tetrahedral cage structures.

The M_4L_6 tetrahedron is the simplest member of the 2M : 3L class of coordination cages. By varying the nature of the bis-bidentate ligands, a series of more complicated cages has been discovered. The ligand $L^{m\text{-}Ph}$ forms an open book $[M_6L_9]^{12+}$ and slanted molecular cube $[M_8L_{12}]^{16+}$ in solution with Co(II)

or Zn(II) salts (see Figure 1.4.4),[89] with both structures stabilised by extensive π-stacking of different ligands.[90]

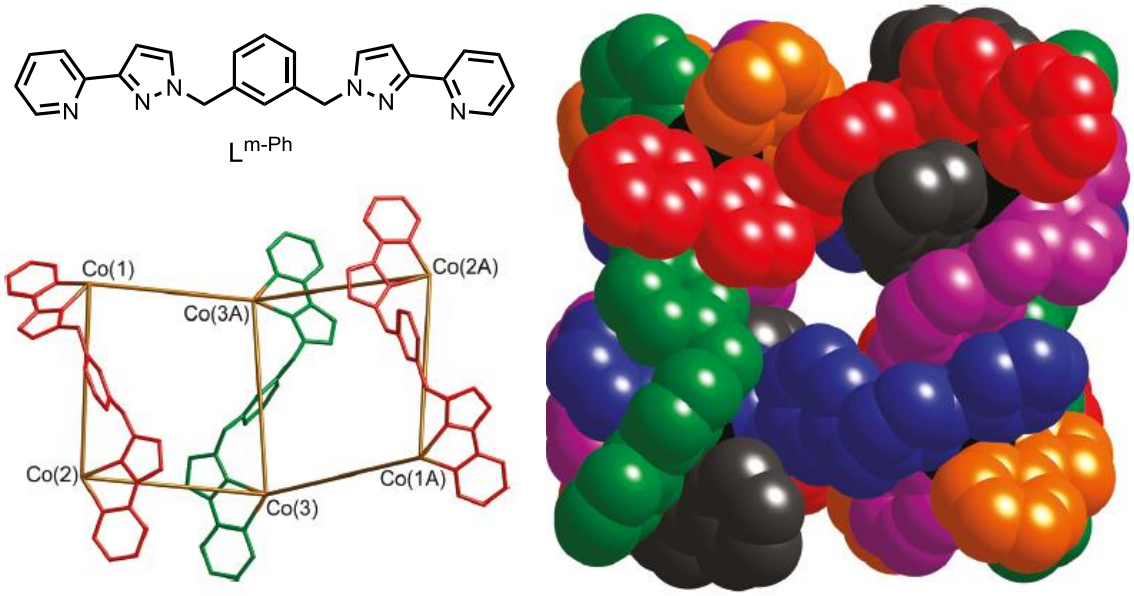

Figure 1.4.4 Clockwise from top left: The bis-bidentate ligand $L^{m\text{-}Ph}$ (top left), a space-filling view of the octanuclear cubic cage cation of $[Co_8(L^{m\text{-}Ph})_{12}](BF_4)_{16}$ (right) and the hexanuclear open book cation of $[Co_6(L^{m\text{-}Ph})_9][ClO_4]_{12}$ (bottom left) with three of the bridging ligands shown. Adapted with permission from Ref. 90. Copyright 2009 American Chemical Society.

The ligands $L^{1,5\text{-}nap}$ and $L^{9,10\text{-}anth}$ also form complex cubes, with Cu^{2+} or Zn^{2+} and Ni^{2+} or Co^{2+} respectively.[91] These cages demonstrate the importance of aromatic π-stacking in stabilizing the cage structures. In the space filling view of $[Co_8(L^{1,5\text{-}nap})_{12}](BF_4)_{16}$, the sandwiching of electron-rich naphthyl groups between electron-poor pyridyl-pyrazole units can clearly be seen (see Figure 1.4.5). These interactions help to maintain the integrity of the cage in solution, as has been observed by electrospray mass spectrometry (ESMS) and ^1H NMR studies.

Recent studies into the $[Co_8(L^{1,5\text{-}nap})_{12}]^{16+}$ cage have shown that there is selective binding within the cage interior for coumarin-type guests, located at the *fac* positions in the opposite corners of the cube.[92-94] Two components are involved in the guest binding; a polar component (the electrostatic hydrogen-bonding interactions between the coumarin carbonyl oxygen and the acidic methylene protons around

the vicinity of the cobalt(II) atom) and a non-polar component (the aromatic π-stacking between coumarin and the cage ligands).

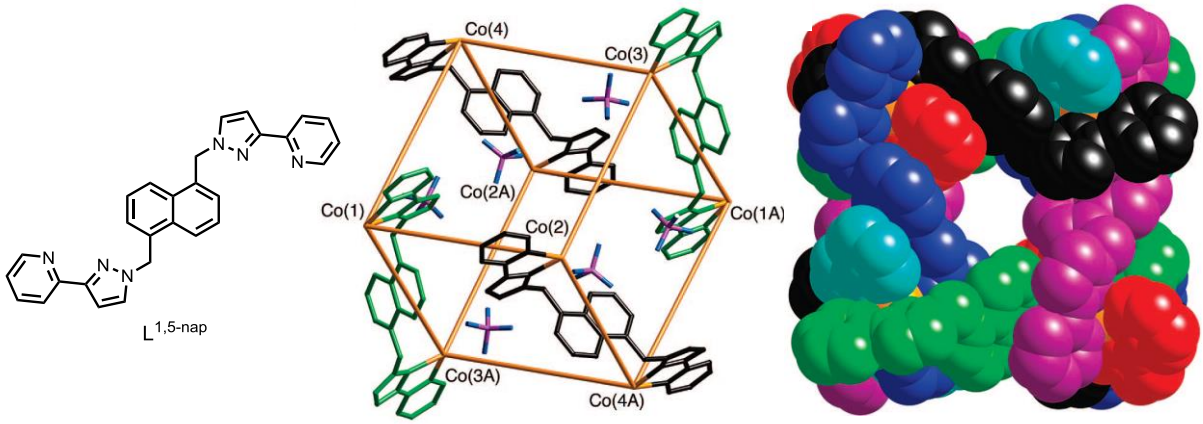

Figure 1.4.5 The bis-bidentate ligand $L^{1,5\ nap}$ (left), the octanuclear cubic cage $[Co_8(L^{1,5\text{-}nap})_{12}](BF_4)_{16}$ (centre) showing only four ligands and six anions, and a space filling view of the complete cubic cage cation. Adapted with permission from Ref. 91. Copyright 2010 American Chemical Society.

Comparison to the crystal structures of the cages formed with $L^{9,10\text{-}anth}$ show that although the cages are of the type $[M_8L_{12}]^{16+}$, they are far from isostructural with the cages of $L^{1,5\text{-}nap}$ (see Figure 1.4.6).[91] Apart from the obviously large central cavity, the other notable point about the cage is that there is no π-stacking between the anthryl groups and any other aromatic groups within the cage. Consequently, the intact cage is not detected in solution by either ^{1}H NMR or ESMS studies, and is only formed in the solid state.[91]

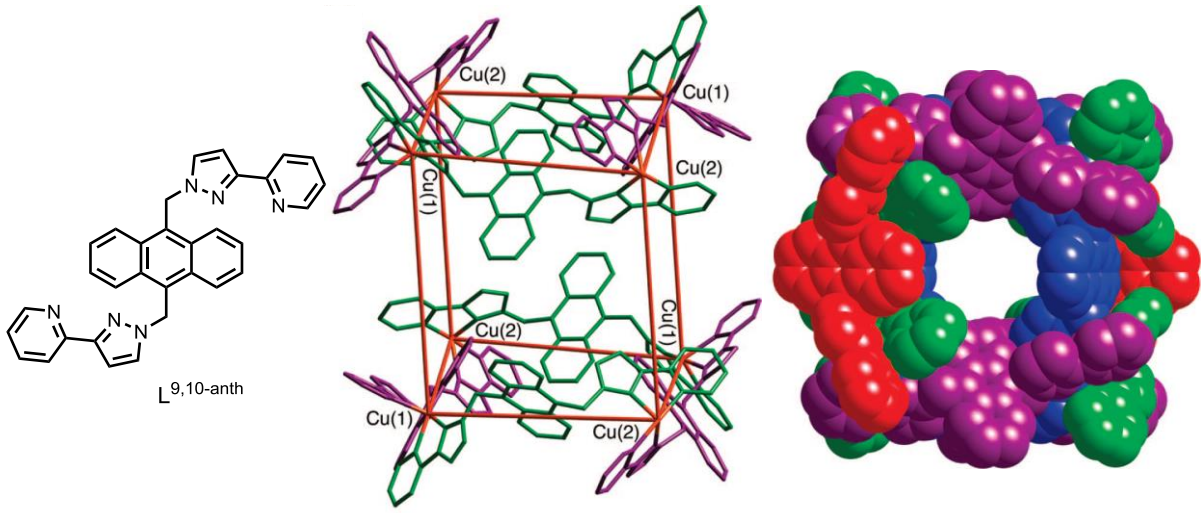

Figure 1.4.6 The bis-bidentate ligand $L^{9,10\text{-anth}}$ (left), the octanuclear cubic cage $[Cu_8(L^{9,10\text{-anth}})_{12}](BF_4)_{16}$ (centre) omitting the four vertical "pillar" ligands for clarity, and a space filling view of the complete cubic cage cation. Adapted with permission from Ref. 91. Copyright 2010 American Chemical Society.

Cages of higher nuclearity still can be formed with the ligand $L^{1,8\text{-nap}}$ (see Figure 1.4.7). With a range of M(II) ions, a truncated tetrahedral array of metal ions and ligands is formed with the general formula $[M_{12}L_{18}]^{24+}$.[95] A truncated tetrahedron is a tetrahedron that has had its vertices sliced off, generating four new triangular faces; the original four faces become hexagonal.[42] Once again, this structure follows the basic ratio of 2M : 3L as is required for bis-bidentate ligands and octahedral metal ions, and π-stacking of alternating electron-rich/ poor regions of ligands contributes to the stability of the structure in the solid state and in solution. This stacking of the ligands in the assembled cage results in a red-shift in the luminescence of the naphthalene unit (compared to the free ligand), due to a low-energy naphthyl → pyridyl-pyrazole charge-transfer band.[96] Interestingly for a closed structure, all metals have *mer* tris-chelate geometry.

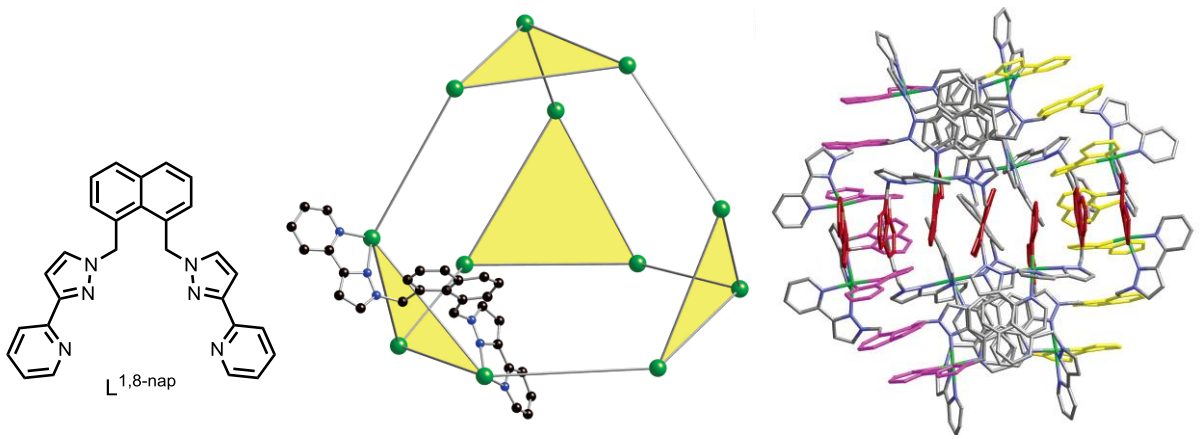

Figure 1.4.7 The bis-bidentate ligand $L^{1,8\text{-nap}}$ (left), the truncated tetrahedral cage $[Cu_{12}(L^{1,8\text{-nap}})_{18}](ClO_4)_{24}$ (centre) showing only one bridging ligand and a complete view of the complete cage cation (right) with three π-stacks highlighted in red, yellow and purple. Adapted with permission from Ref. 95. Copyright 2006 American Chemical Society.

Recent work has been conducted using the ligand $L^{p\text{-Ph}}$, and using different M(II) ions can result in the formation of three different coordination cage structures.[97,98] Reaction of $L^{p\text{-Ph}}$ with Ni(II) results in the formation of a molecular cube $[Ni_8L_{12}](BF_4)_{12}(SiF_6)_2$, whereas reaction with Cu(II) results in the formation of an unusual trigonal prism $[Cu_6L_9](BF_4)_{12}$ (see Figure 1.4.8). However, reaction with Zn(II) or Cd(II) result in the largest homoleptic cage yet seen in this series, a tetra-capped truncated tetrahedron $[M_{16}L_{24}]^{32+}$. ESMS studies have shown that this cage interconverts with the hexanuclear trigonal prism cage in solution, but it is thought that the hexadecanuclear cage is the kinetic product of crystallization and thus only crystals of this product were afforded.[98]

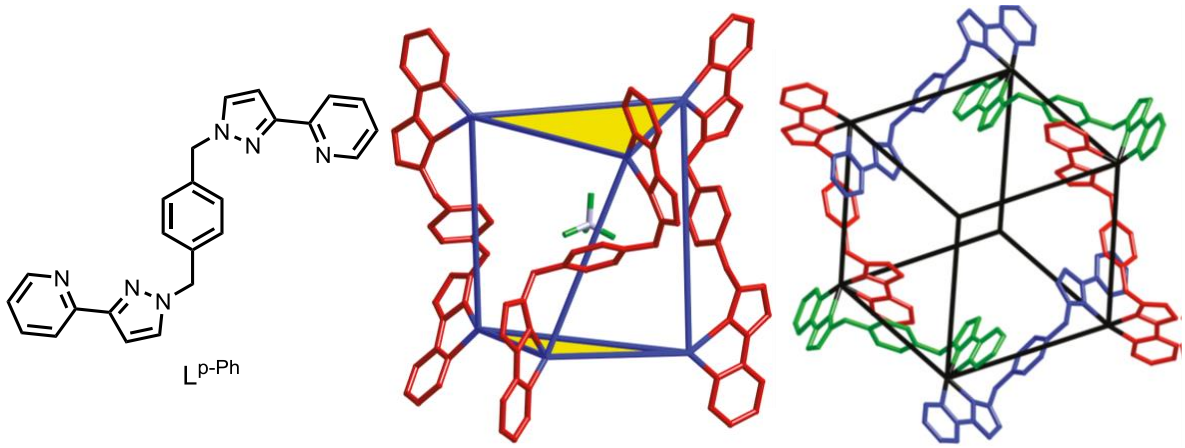

Figure 1.4.8 The bis-bidentate ligand $L^{p\text{-}Ph}$ (left), the twisted trigonal prism cation of $[Cu_6L_9](BF_4)_{12}$ (centre) showing only the three "pillar" ligands and the cubic cage cation of $[Ni_8L_{12}](BF_4)_{12}(SiF_6)_2$ (right) with the bridge-edging ligands shown. Adapted with permission from Ref. 98. Copyright 2010 American Chemical Society.

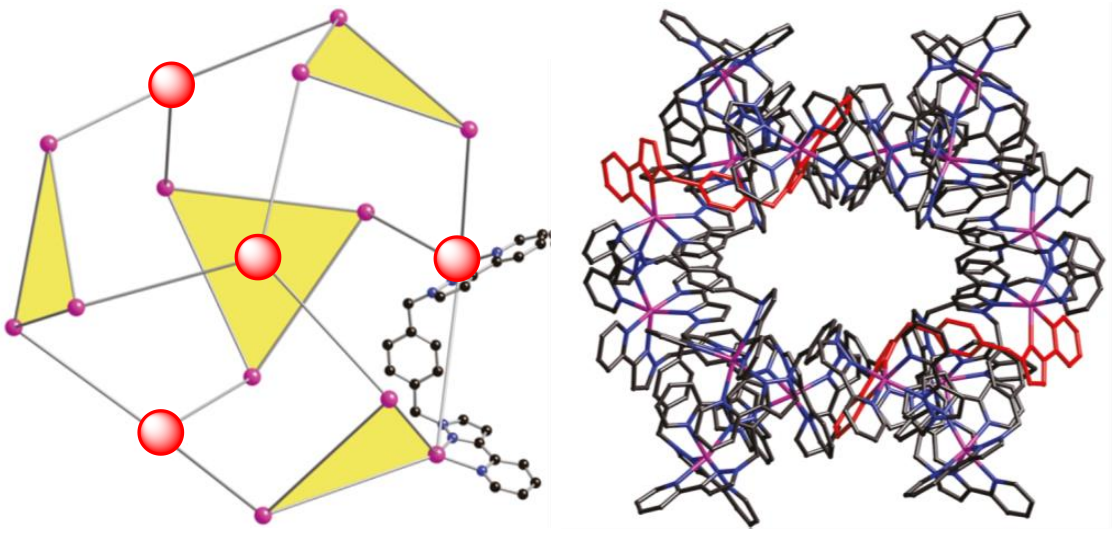

Figure 1.4.9 The tetra-capped truncated-tetrahedral array of metals in the complex cation of $[Cd_{16}(L^{p\text{-}Ph})_{24}](ClO_4)_{32}$ (left) showing only one bridging ligand and with the face-capping sites highlighted with a red circle, and a complete view of the complete cage cation (right). Adapted with permission from Ref. 98. Copyright 2010 American Chemical Society.

The structure of the $[M_{16}L_{24}]^{32+}$ cage is related to the truncated tetrahedral $[M_{12}L_{18}]^{24+}$ cage, except the four triangular faces are twisted, and then a capping atom is added to each of the four hexagonal faces (see Figure 1.4.9, highlighted with red circles). The four capping atoms have *fac* tris-chelate geometry,

whereas the twelve metal atoms occupying the triangular faces have *mer* tris-chelate geometry. If one were to control the geometry of the metal ions, the ability to select the geometry of the cage is made possible, and the unprecedented realm of the mixed-metal cage is a potential target for this.

Most recent work in the Ward group has involved the study of ligands with new functionality within the spacer unit. A new ligand class incorporating a furan or thiophene spacer has led to the isolation of a series of molecular squares, cubes and chains, in which the oxygen or sulphur atoms can become involved in interactions with the electron deficient coordinated pyrazole rings(see Figure 1.4.10, **a**).[99] A new benzophenone ligand reacts with silver(I) to yield an infinite triple helix composed of molecular double helicate subunits (see Figure 4.10, **b**).[100] Finally, a ligand with a routine 1,4 naphthalene spacer unit has led to an unprecedented coordination cage structure, a cuneane. This is the only possible 8-vertex polyhedron other than a cube that will form a cage in which each metal is connected to three others, i.e. a topological isomer of a cube.[101]

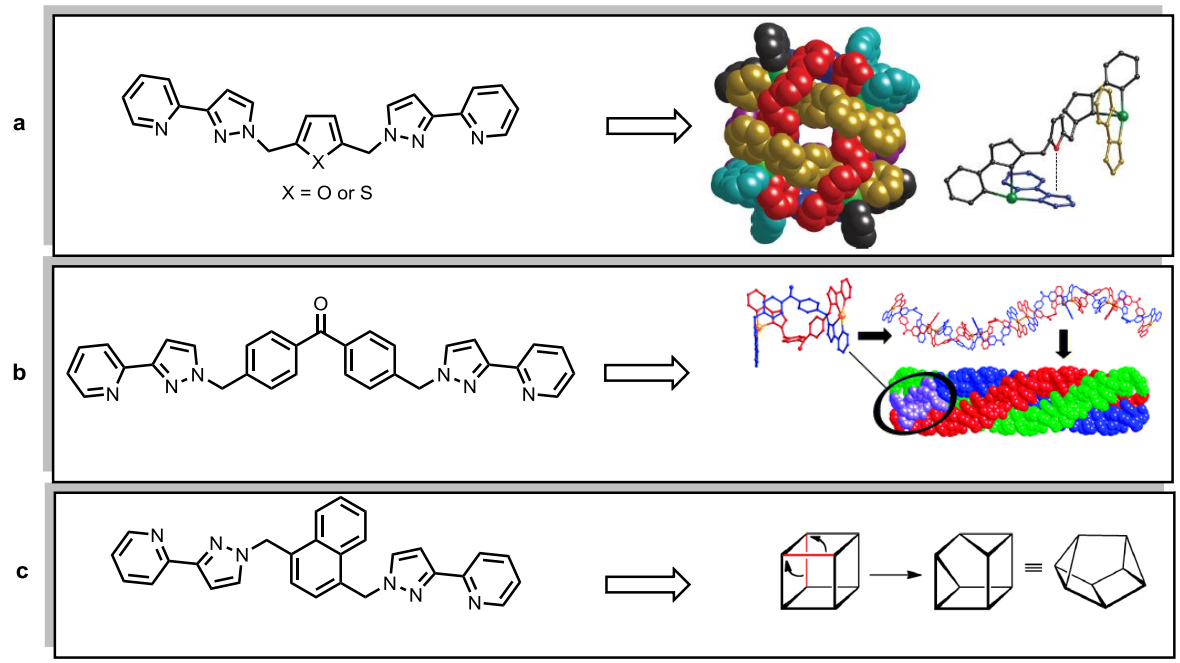

Figure 1.4.10 The furan or thiophene ligand and the cubic Cu_8L_{12} cage structure it forms, with an oxygen → pyrazole interaction highlighted (**a**); the benzophenone ligand and the hierarchical self-assembly of the triple helix of double helices (**b**), and; the 1,4-naphthalene ligand, and the derivation of a cuneane which describes the cage's core (**c**). Reproduced from Ref. 99-101 with permission from The Royal Society of Chemistry.

Efforts within the Ward group are now being directed towards rendering existing cages water soluble, as this will open up many new possibilities for host-guest chemistry. The water soluble ligand $L^{1,5\text{-nap-W}}$ was prepared, which forms cages isostructural to the M_8L_{12} cages prepared with $L^{1,5\text{-nap}}$ (see Figure 1.4.11).[94] This cage binds hydrophobic guests very strongly due to the hydrophobic effect particularly those which don't have to undergo significant conformational change upon encapsulation with the cavity. This has even enabled the determination of a host●guest crystal structure with cycloundecanone in the cage cavity.[102]

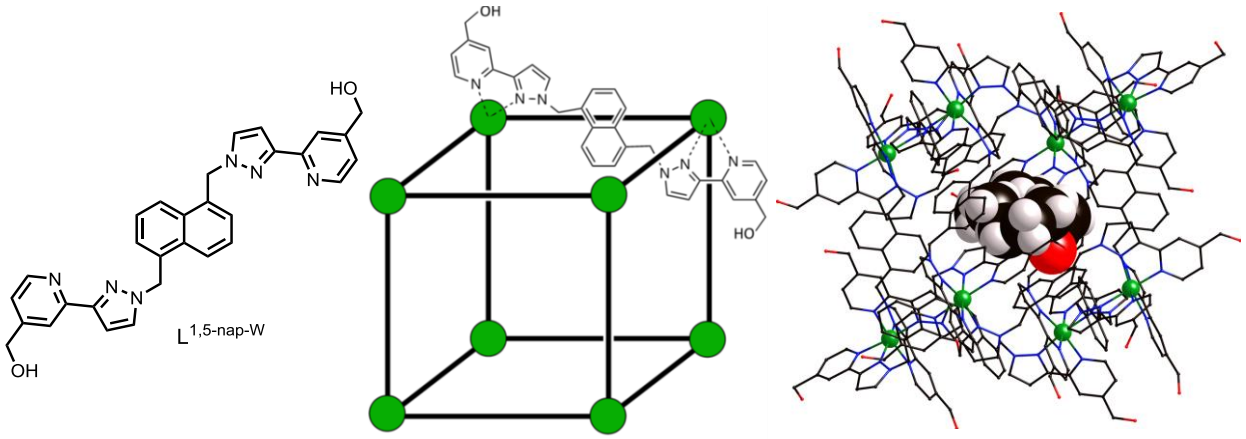

Figure 1.4.11 (Left) The water soluble ligand $L^{1,5\text{-nap-W}}$; (middle) schematic diagram of the cubic cage $[Co_8(L^{1,5\text{-nap-W}})_{12}]^{16+}$, emphasising the ligand connectivity; (right) crystal structure of the guest cycloundecanone inside the host $[Co_8(L^{1,5\text{-nap-W}})_{12}]^{16+}$. Adapted with permission from Ref. 102. Copyright 2010 American Chemical Society.

1.5 Mixed-metal coordination structures

Structures of increased complexity are highly desirable, as this may lead to increased functionality. The ability to create functional behaviour from controlled self-assembly is of course the ultimate challenge of the supramolecular chemist.[68] Two ways this may be achieved are by using more than one ligand so that heteroleptic structures are formed, or by using more than one metal so that heterometallic structures result. The use of more than one metal is particularly attractive because there is potential for variable magnetic, photochemical or electrochemical properties, or even synergistic catalysis.[103]

Two principal strategies can be applied for the synthesis of heterometallic coordination structures, and these are dependent on the kinetic stability of the metal ions in question. The first strategy is the **kinetic control approach**. This can be used when one of the metal ions in question is kinetically inert, for example Ru(II). By building a functionalisable framework around an inert $[Ru(N)_6]^{2+}$ scaffold, heterometallic structures can be formed by a stepwise synthesis without the worry of the ruthenium centre rearranging. This approach has been used within the Ward group, where the complex $[Ru(H_2bpp)_2]^{2+}$, which possesses functionalisable N-H groups, was alkylated to yield an inert $[Ru(N)_6]^{2+}$ core furnished with four pendant bidentate pyrazolyl-pyridyl sites.[104] In the presence of Ag(I) ions, a $[RuAg_2]^{4+}$ double helix results (see Figure 1.5.1). The post-coordination functionalisation of the ligand is important in being able to form a single product, as this precludes the ruthenium(II) ion from being scrambled across the different sites.

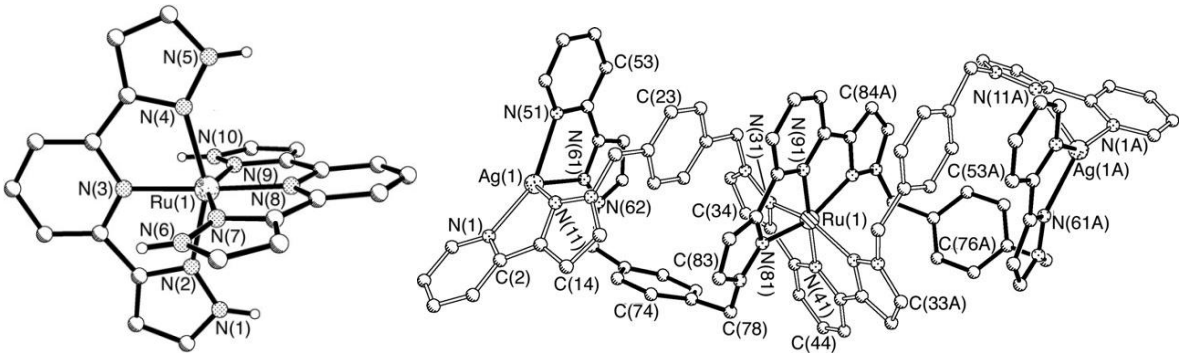

Figure 1.5.1 Crystal structure of the $[Ru(H_2bpp)_2]^{2+}$ cation (left), and the complex cation of the resulting $[RuAg_2L_2]^{4+}$ double helix. Reproduced from Ref. 104 with permission from The Royal Society of Chemistry.

Fletcher's group have also used ruthenium(II) cores as the basis of forming heterometallic structures. The group have taken the approach of isolating the facial (*fac*) isomer of substituted tris-bipyridine complexes of ruthenium(II).[105-107] Whilst this is not a trivial procedure, the C_3 symmetry of the *fac*-isomer of such complexes is necessary to form polynuclear structures such as helicates. In this instance, Fletcher's group used a tripodal ligand in which the tether could be removed once the ligand was coordinated to ruthenium(II). The resulting three bidentate ligands were functionalised with three pendant bipyridyl binding sites, and reaction with Fe(II) ions resulted in the formation of a $[RuFeL_3]^{4+}$ helicate (see Figure 1.5.2). Such a helicate could not be selectively formed without the initial isolation of the *fac* isomer; the kinetic control step.

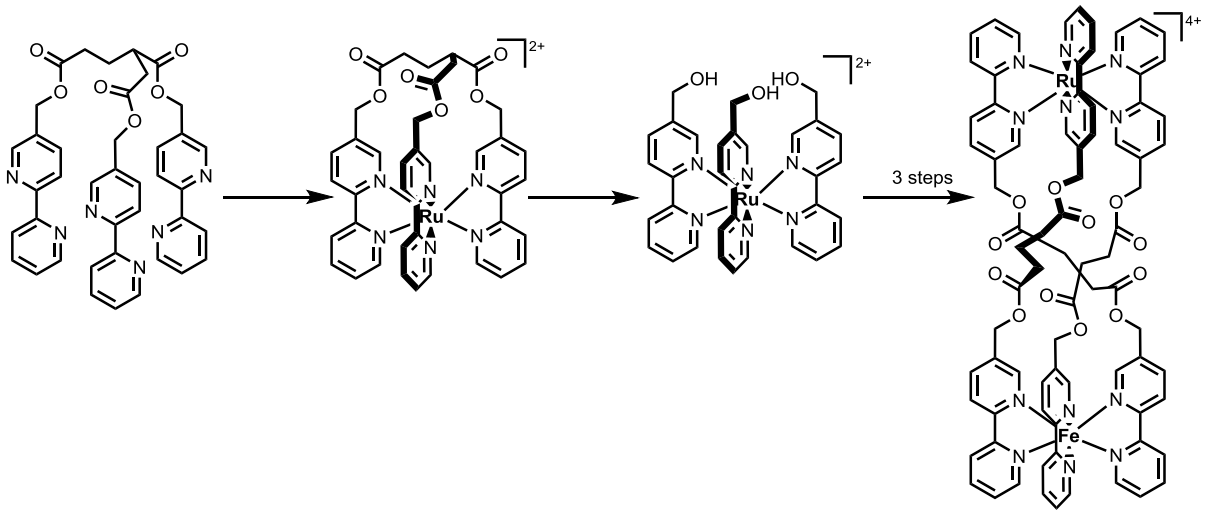

Figure 1.5.2 The tripodal ligand prepared by Fletcher's group and the reaction strategy for preparing the inert heterometallic helicate.[105]

The Thomas group has also used a similar approach, in what they term the 'complex as ligand' approach.[108] By preforming a protected ruthenium(II) complex to act as a divergent ligand, reaction with protected convergent metal centres resulted in the formation of a series of kinetically labile or inert heterometallic teteranuclear metallomacrocycles (see Figure 1.5.3). Host–guest studies carried out with the Ru_2Re_2 macrocyle reveals that the complex functions as a luminescent sensor for anions in organic solvents, and aromatic molecules in water.[108,109]

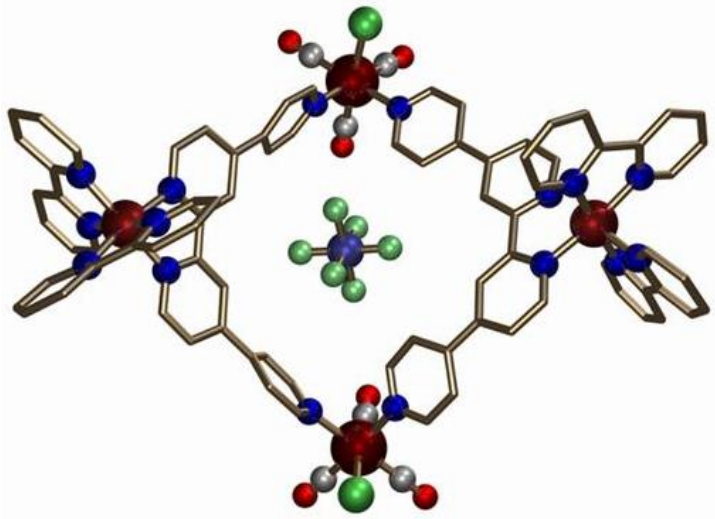

Figure 1.5.3 Crystal structure of the $[Ru_2Re_2]^{4+}$ macrocyclic sensor with a hexafluorophosphate anion residing in the central cavity. Reproduced with permission from Ref. 108. Copyright © 2006 WILEY-VCH Verlag GmbH & Co. KGaA, Weinheim.

The second strategy that will enable the designed synthesis of heterometallic coordination structures is the **thermodynamic control approach.** This strategy takes advantage of the different coordination preferences of different metal ions, and can be approximately explained by considering hard-soft acid-base (HSAB) theory: hard metals prefer hard ligand binding sites, and soft metals prefer soft ligand binding sites. Alongside this, one must also take into consideration the preferred binding geometry of each metal ion, and the corollary of this is that an unsymmetrical ligand is the main requirement for forming a heterometallic structure based on the thermodynamic control approach.

There have been many examples in the literature where asymmetric ligands have been used with hard and soft metal ions to create a complex heterometallic structure. Shionoya and co-workers have utilised

a ligand with a relatively soft pyridyl group and a relatively hard catecholate binding site to create a coordination cage with hard Ti(IV) ions and soft Pd(II) ions (see Figure 1.5.4).[110] Such systems have been shown to be interconvertable depending on stoichiometry and reaction conditions. For example, the $[Pd_3Ti_2L_6Cl_6]^{4-}$ cage shown in Figure 1.5.4 interconverts to a $[Pd_2Ti_2(HL_2)_2(acac)_2Cl_4]$ ring on addition of $TiO(acac)_2$ and trifluoroacetic acid. The $[TiL_3]^{2-}$ complex is the precursor to the cage, and it has been shown that one of the bidentate ligands can be replaced by a series of acetylacetonates and tropolonates, thus enabling site-selective ligand exchange as a facile route towards coordination cage interconversion.[111]

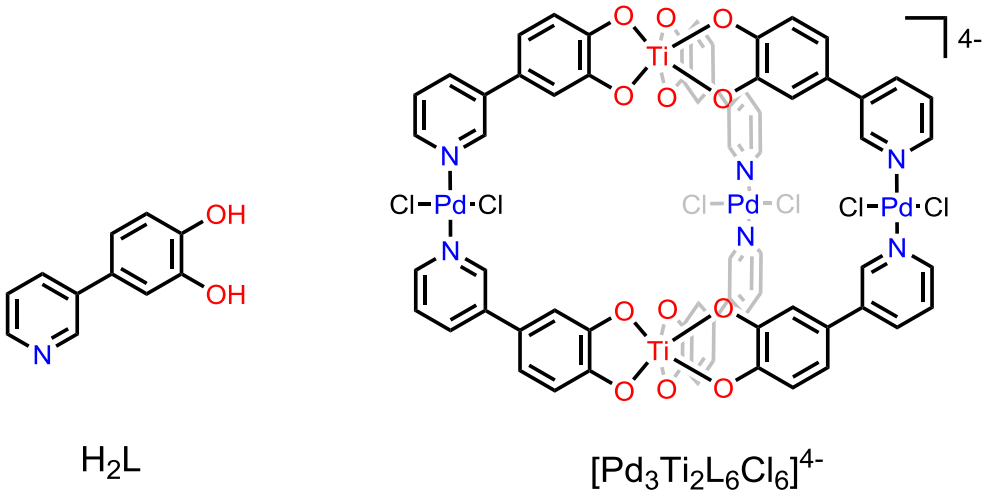

Figure 1.5.4 The asymmetric ligand prepared by Shionoya's group and the cage that results from reaction with Ti(IV) and Pd(II) ions.[110]

The method of using a hard metal tris-catecholate as a precursor to heterometallic coordination cages, in effect a metalloligand, has not been exclusively used by Shionoya's group. Wang and coworkers have used a ligand furnished with a pyridyl and acetylacetonate binding sites to create an aluminium(III) tris-catecholate metalloligand, which reacts with Pd(II) ions to form a $[Pd_6(AlL_3)_8](NO_3)_{12}$ cube (see Figure 1.5.5).[112] Reaction with $ZnBr_2$ yielded a trigonal pyramidal metallocage. In a collaboration with Stang's group, reaction of the metalloligand with a 60° diplatinum(II) acceptor yielded a structurally similar trigonal cage, in this case making use of the more inert Pt(II) ion to increase the solution stability of the cage once the desired product had been formed (see Figure 1.5.6).[113]

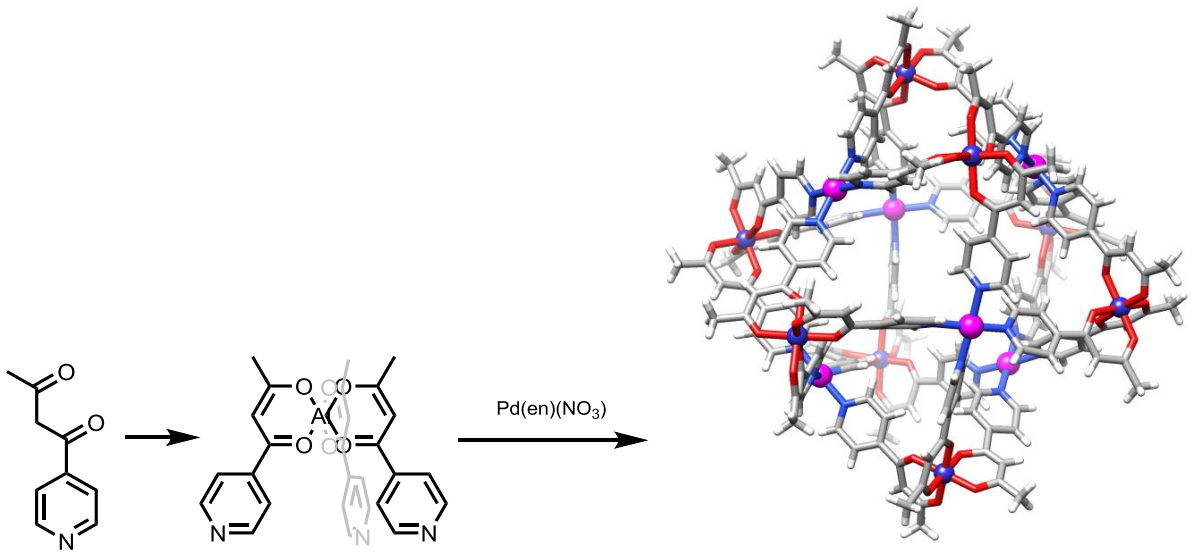

Figure 1.5.5 The asymmetric ligand used by Wang's group, and the metalloligand and cage that results from reaction with Al(III) and Pd(II) ions sequentially.[112]

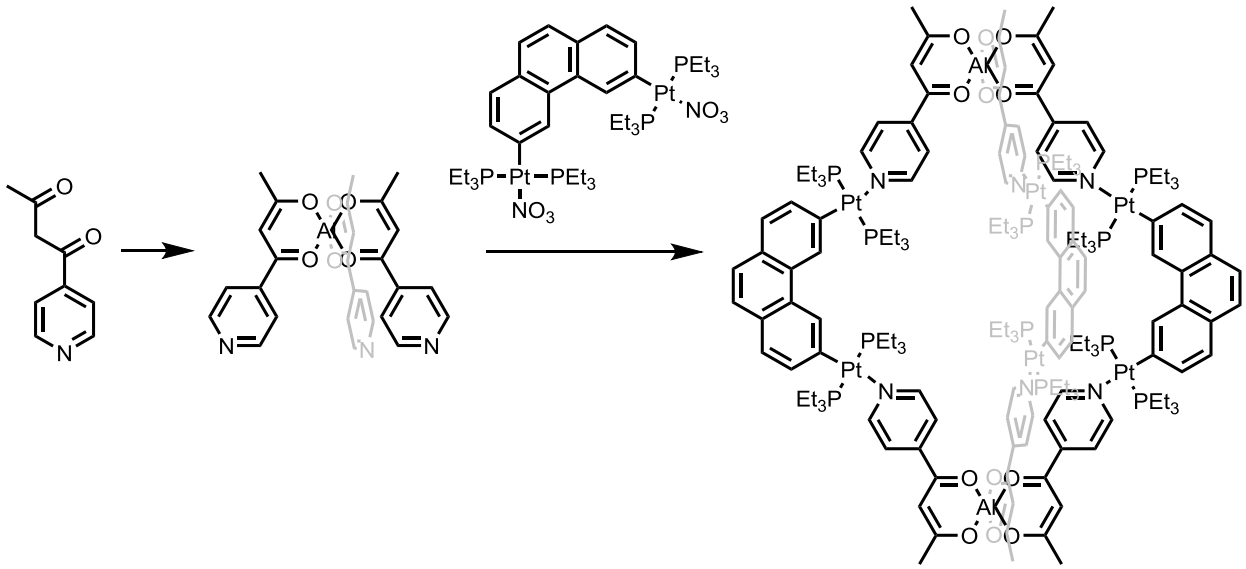

Figure 1.5.6 The metalloligand used by Wang and Stang's groups, and the cage that results from reaction with 60° Pt(II) ions.[113]

Nitschke's group has recently elaborated on the subcomponent self-assembly approach that has allowed them to synthesise a series of homonuclear cages with no preformed ligand.[54,58,60,64,114] In each of these cases the resulting ligand is symmetrical, with all metal ions having the same coordination mode (however in some cases, differing tris-chelate geometries). By modifying the components so that a symmetrical ligand cannot form, and introducing two metals that have differing coordination preferences, Nitschke was able to isolate a $Fe_8Pt_6L_{24}$ cubic cage from a one-pot synthesis in which 96 new bonds were formed.[115] This is a great demonstration of the power of the thermodynamic control approach, as such a complex structure can result from the one-pot reaction of such simple components.

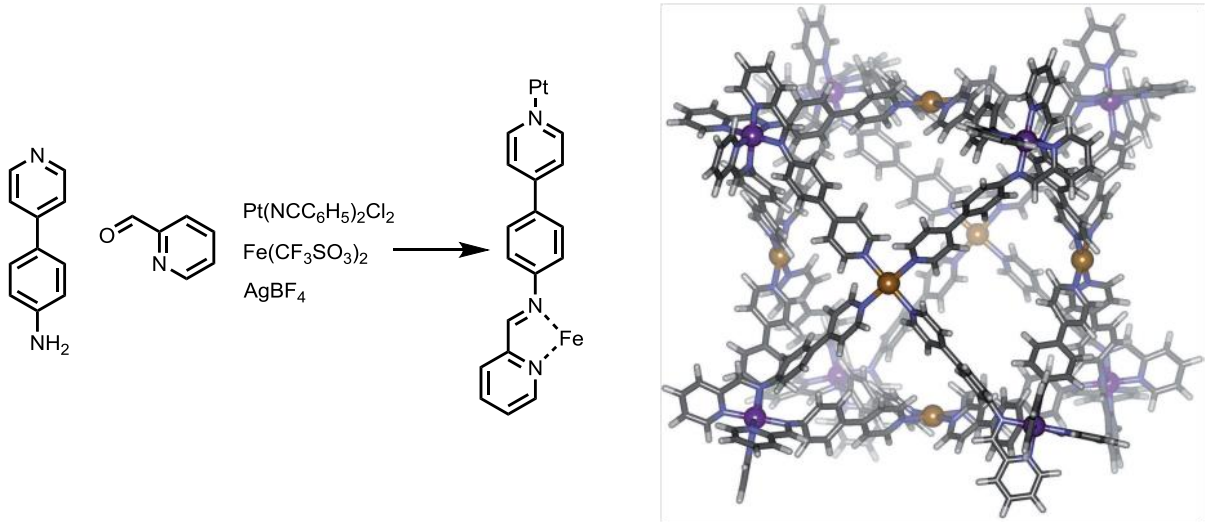

Figure 1.5.7 The $Fe_8Pt_6L_{24}$ cubic cage formed from subcomponent self-assembly, with one ligand indicating the coordination mode of each metal. Reproduced with permission from Ref. 115. Copyright © 2012 WILEY-VCH Verlag GmbH & Co. KGaA, Weinheim.

1.6 References

1. J. M. Lehn, *Angew. Chem. Int. Ed.*, 1988, **27**, 89.

2. G. R. Desiraju, *Nature*, 2001, **412**, 397.

3. C. T. Seto and G. M. Whitesides, *J. Am. Chem. Soc.*, 1993, **115**, 905.

4. C. A. Hunter and J. K. M. Sanders, *J. Am. Chem. Soc.*, 1990, **112**, 5525.

5. P. D. Beer, P. A. Gale and D. K. and Smith, *Supramolecular Chemistry*, Oxford University Press, Oxford, 1999.

6. J. W. Steed and J. L. Atwood, *Supramolecular Chemistry*, 2nd edn., Wiley, Chichester, 2009.

7. A. Klug, *Phil. Trans. R. Soc. Lond. B.*, 1999, **354**, 531.

8. J. S. Lindsey, *New J. Chem.*, 1991, **15**, 153.

9. D. Philp and J. F. Stoddart, *Angew. Chem. Int. Ed.*, 1996, **35**, 1155.

10. Y. Timsit and P. Varnai, *J. Mol. Recognit.*, 2011, **24**, 137.

11. C. J. Pedersen, *Angew. Chem. Int. Ed.*, 1988, **27**, 1021.

12. J. P. Sauvage and M. Ward, *Inorg. Chem.*, 1991, **30**, 3869.

13. J. P. Mathias, E. E. Simanek, J. A. Zerkowski, C. T. Seto and G. M. Whitesides, *J. Am. Chem. Soc.*, 1994, **116**, 4316.

14. M. Asakawa, P. R. Ashton, S. E. Boyd, C. L. Brown, S. Menzer, D. Pasini, J. F. Stoddart, M. S. Tolley, A. J. P. White, D. J. Williams and P. G. Wyatt, *Chem. - Eur. J.*, 1997, **3**, 463.

15. B. Dietrich, J. M. Lehn and J. P. Sauvage, *Tet. Lett.*, 1969, 2885.

16. J. M. Lehn, *Pure Appl. Chem.*, 1994, **66**, 1961.

17. J. M. Lehn, *Science*, 2002, **295**, 2400.

18. B. J. Holliday and C. A. Mirkin, *Angew. Chem. Int. Ed.*, 2001, **40**, 2022.

19. M. M. Safont-Sempere, G. Fernandez and F. Wuerthner, *Chem. Rev.*, 2011, **111**, 5784.

20. P. J. Stang and B. Olenyuk, *Acc. Chem. Res.*, 1997, **30**, 502.

21. S. R. Seidel and P. J. Stang, *Acc. Chem. Res.*, 2002, **35**, 972.

22. M. Fujita, J. Yazaki and K. Ogura, *J. Am. Chem. Soc.*, 1990, **112**, 5645.

23. M. Fujita, O. Sasaki, T. Mitsuhashi, T. Fujita, J. Yazaki, K. Yamaguchi and K. Ogura, *Chem. Commun.*, 1996, 1535.

24. M. Fujita, *Chem. Soc. Rev.*, 1998, **27**, 417.

25. R. W. Saalfrank, A. Stark, K. Peters and H. G. Vonschnering, *Angew. Chem. Int. Ed.*, 1988, **27**, 851.

26. R. W. Saalfrank, A. Stark, M. Bremer and H. U. Hummel, *Angew. Chem. Int. Ed.*, 1990, **29**, 311.

27. R. W. Saalfrank, B. Horner, D. Stalke and J. Salbeck, *Angew. Chem. Int. Ed.*, 1993, **32**, 1179.

28. M. Fujita, D. Oguro, M. Miyazawa, H. Oka, K. Yamaguchi and K. Ogura, *Nature*, 1995, **378**, 469.

29. M. Fujita, M. Tominaga, A. Hori and B. Therrien, *Acc. Chem. Res.*, 2005, **38**, 369.

30. T. Murase, S. Horiuchi and M. Fujita, *J. Am. Chem. Soc.*, 2010, **132**, 2866.

31. M. Yoshizawa, J. K. Klosterman and M. Fujita, *Angew. Chem. Int. Ed.*, 2009, **48**, 3418.

32. R. Chakrabarty, P. S. Mukherjee and P. J. Stang, *Chem. Rev.*, 2011, **111**, 6810.

33. M. Fujita, K. Umemoto, M. Yoshizawa, N. Fujita, T. Kusukawa and K. Biradha, *Chem. Commun.*, 2001, 509.

34. J. Bunzen, J. Iwasa, P. Bonakdarzadeh, E. Numata, K. Rissanen, S. Sato and M. Fujita, *Angew. Chem. Int. Ed.*, 2012, **51**, 3161.

35. K. Harris, D. Fujita and M. Fujita, *Chem. Commun.*, 2013, **49**, 6703.

36. T. Kikuchi, S. Sato, D. Fujita and M. Fujita, *Chem. Sci.*, 2014, **5**, 3257.

37. K. Suzuki, S. Sato and M. Fujita, *Nature Chem.*, 2010, **2**, 25.

38. D. L. Caulder and K. N. Raymond, *Acc. Chem. Res.*, 1999, **32**, 975.

39. B. Kersting, M. Meyer, R. E. Powers and K. N. Raymond, *J. Am. Chem. Soc.*, 1996, **118**, 7221.

40. T. Beissel, R. E. Powers and K. N. Raymond, *Angew. Chem. Int. Ed.*, 1996, **35**, 1084.

41. P. J. Steel, *Acc. Chem. Res.*, 2005, **38**, 243.

42. M. D. Ward, *Chem. Commun.*, 2009, 4487.

43. C. R. K. Glasson, G. V. Meehan, C. A. Motti, J. K. Clegg, P. Turner, P. Jensen and L. F. Lindoy, *Dalton Trans.*, 2011, **40**, 10481.

44. R. W. Saalfrank, H. Glaser, B. Demleitner, F. Hampel, M. M. Chowdhry, V. Schunemann, A. X. Trautwein, G. B. M. Vaughan, R. Yeh, A. V. Davis and K. N. Raymond, *Chem.-Eur. J.*, 2002, **8**, 493.

45. D. L. Caulder, R. E. Powers, T. N. Parac and K. N. Raymond, *Angew. Chem. Int. Ed.*, 1998, **37**, 1840.

46. C. J. Brown, G. M. Miller, M. W. Johnson, R. G. Bergman and K. N. Raymond, *J. Am. Chem. Soc.*, 2011, **133**, 11964.

47. C. J. Hastings, M. D. Pluth, R. G. Bergman and K. N. Raymond, *J. Am. Chem. Soc.*, 2010, **132**, 6938.

48. M. D. Pluth, R. G. Bergman and K. N. Raymond, *Angew. Chem. Int. Ed.*, 2007, **46**, 8587.

49. R. G. Bergman, D. Fiedler, D. H. Leung and K. N. Raymond, *Acc. Chem. Res*., 2005, **38**, 349.

50. D. Fiedler, R. G. Bergman and K. N. Raymond, *Angew. Chem. Int. Ed.*, 2004, **43**, 6748.

51. M. D. Pluth, R. G. Bergman and K. N. Raymond, *Acc. Chem. Res*., 2009, **42**, 1650.

52. Z. J. Wang, C. J. Brown, R. G. Bergman, K. N. Raymond and F. D. Toste, *J. Am. Chem. Soc*., 2011, **133**, 7358.

53. B. Breiner, J. K. Clegg and J. R. Nitschke, *Chem. Sci.*, 2011, **2**, 51.

54. R. A. Bilbeisi, J. K. Clegg, N. Elgrishi, X. d. Hatten, M. Devillard, B. Breiner, P. Mal and J. R. Nitschke, *J. Am. Chem. Soc*., 2012, **134**, 5110.

55. M. M. J. Smulders and J. R. Nitschke, *Chem. Sci.*, 2012, **3**, 785.

56. I. A. Riddell, M. M. J. Smulders, J. K. Clegg and J. R. Nitschke, *Chem. Commun*., 2011, **47**, 457.

57. V. E. Campbell, X. de Hatten, N. Delsuc, B. Kauffmann, I. Huc and J. R. Nitschke, *Nature Chem.*, 2010, **2**, 684.

58. P. Mal and J. R. Nitschke, *Chem. Commun.*, 2010, **46**, 2417.

59. P. Mal, B. Breiner, K. Rissanen and J. R. Nitschke, *Science*, 2009, **324**, 1697.

60. P. Mal, D. Schultz, K. Beyeh, K. Rissanen and J. R. Nitschke, *Angew. Chem. Int. Ed.*, 2008, **47**, 8297.

61. R. J. Sarma and J. R. Nitschke, *Angew. Chem. Int. Ed.*, 2008, **47**, 377.

62. J. R. Nitschke, *Acc. Chem. Res.*, 2007, **40**, 103.

63. T. K. Ronson, S. Zarra, S. P. Black and J. R. Nitschke, *Chem. Commun.*, 2013, **49**, 2476.

64. W. Meng, B. Breiner, K. Rissanen, J. D. Thoburn, J. K. Clegg and J. R. Nitschke, *Angew. Chem. Int. Ed.*, 2011, **50**, 3479.

65. W. Meng, J. K. Clegg and J. R. Nitschke, *Angew. Chem. Int. Ed.*, 2012, **51**, 1881.

66. P. P. Neelakandan, A. Jimenez and J. R. Nitschke, *Chem. Sci.*, 2014, **5**, 908.

67. I. A. Riddell, Y. R. Hristova, J. K. Clegg, C. S. Wood, B. Breiner and J. R. Nitschke, *J. Am. Chem. Soc.*, 2013, **135**, 2723.

68. M. D. Ward and P. R. Raithby, *Chem. Soc. Rev.*, 2013, **42**, 1619.

69. M. Yoshizawa, Y. Takeyama, T. Okano and M. Fujita, *J. Am. Chem. Soc.*, 2003, **125**, 3243.

70. M. Yamanaka, M. Kawaharada, Y. Nito, H. Takaya and K. Kobayashi, *J. Am. Chem. Soc.*, 2011, **133**, 16650.

71. M. M. Conn and J. Rebek, *Chem. Rev.*, 1997, **97**, 1647.

72. R. Custelcean, J. Bosano, P. V. Bonnesen, V. Kertesz and B. P. Hay, *Angew. Chem. Int. Ed.*, 2009, **48**, 4025.

73. R. Custelcean, P. V. Bonnesen, N. C. Duncan, X. Zhang, L. A. Watson, G. Van Berkel, W. B. Parson and B. P. Hay, *J. Am. Chem. Soc.*, 2012, **134**, 8525.

74. R. Custelcean, *Chem. Soc. Rev.*, 2014, **43**, 1813.

75. K. Warnmark, P. N. W. Baxter and J. M. Lehn, *Chem. Commun.*, 1998, 993.

76. C. R. K. Glasson, G. V. Meehan, J. K. Clegg, L. F. Lindoy, P. Turner, M. B. Duriska and R. Willis, *Chem. Commun.*, 2008, 1190.

77. C. R. K. Glasson, J. K. Clegg, J. C. McMurtrie, G. V. Meehan, L. F. Lindoy, C. A. Motti, B. Moubaraki, K. S. Murray and J. D. Cashion, *Chem. Sci.*, 2011, **2**, 540.

78. J. K. Clegg, F. Li, K. A. Jolliffe, G. V. Meehan and L. F. Lindoy, *Chem. Commun.*, 2011, **47**, 6042.

79. B. Therrien, G. Suess-Fink, P. Govindaswamy, A. K. Renfrew and P. J. Dyson, *Angew. Chem. Int. Ed.*, 2008, **47**, 3773.

80. B. Therrien, *Eur. J. Inorg. Chem.*, 2009, 2445.

81. S. Trofimenko, *J. of Chem. Edu.*, 2005, **82**, 1715.

82. R. L. Paul, A. J. Amoroso, P. L. Jones, S. M. Couchman, Z. R. Reeves, L. H. Rees, J. C. Jeffery, J. A. McCleverty and M. D. Ward, *J. Chem. Soc., Dalton Trans.*, 1999, 1563.

83. J. S. Fleming, K. L. V. Mann, S. M. Couchman, J. C. Jeffery, J. A. McCleverty and M. D. Ward, *J. Chem. Soc., Dalton Trans.*, 1998, 2047.

84. J. S. Fleming, K. L. V. Mann, C. A. Carraz, E. Psillakis, J. C. Jeffery, J. A. McCleverty and M. D. Ward, *Angew. Chem. Int. Ed.*, 1998, **37**, 1279.

85. R. L. Paul, Z. R. Bell, J. C. Jeffery, J. A. McCleverty and M. D. Ward, *Proc. Nat. Acad. Sci. of U. S. A.*, 2002, **99**, 4883.

86. R. L. Paul, Z. R. Bell, J. S. Fleming, J. C. Jeffery, J. A. McCleverty and M. D. Ward, *Heteroatom Chem.*, 2002, **13**, 567.

87. R. L. Paul, S. M. Couchman, J. C. Jeffery, J. A. McCleverty, Z. R. Reeves and M. D. Ward, *J. Chem. Soc., Dalton Trans.*, 2000, 845.

88. B. R. Hall, L. E. Manck, I. S. Tidmarsh, A. Stephenson, B. F. Taylor, E. J. Blaikie, D. A. Vander Griend and M. D. Ward, *Dalton Trans.*, 2011, **40**, 12132.

89. S. P. Argent, H. Adams, L. P. Harding and M. D. Ward, *Dalton Trans.*, 2006, 542.

90. A. M. Najar, I. S. Tidmarsh, H. Adams and M. D. Ward, *Inorg. Chem.*, 2009, **48**, 11871.

91. I. S. Tidmarsh, T. B. Faust, H. Adams, L. P. Harding, L. Russo, W. Clegg and M. D. Ward, *J. Am. Chem. Soc.*, 2008, **130**, 15167.

92. S. Turega, M. Whitehead, B. R. Hall, M. F. Haddow, C. A. Hunter and M. D. Ward, *Chem. Commun.*, 2012, **48**, 2752.

93. S. Turega, M. Whitehead, B. R. Hall, A. J. H. M. Meijer, C. A. Hunter and M. D. Ward, *Inorg. Chem.*, 2013, **52**, 1122.

94. M. Whitehead, S. Turega, A. Stephenson, C. A. Hunter and M. D. Ward, *Chem. Science*, 2013, **4**, 2744.

95. S. P. Argent, H. Adams, T. Riis-Johannessen, J. C. Jeffery, L. P. Harding, O. Mamula and M. D. Ward, *Inorg. Chem.*, 2006, **45**, 3905.

96. N. K. Al-Rasbi, H. Adams, L. P. Harding and M. D. Ward, *Eur. J. Inorg. Chem.*, 2007, 4770.

97. S. P. Argent, H. Adams, T. Riis-Johannessen, J. C. Jeffery, L. P. Harding and M. D. Ward, *J. Am. Chem. Soc.*, 2006, **128**, 72.

98. A. Stephenson, S. P. Argent, T. Riis-Johannessen, I. S. Tidmarsh and M. D. Ward, *J. Am. Chem. Soc.*, 2011, **133**, 858.

99. A. Stephenson and M. D. Ward, *Dalton Trans.*, 2011, **40**, 10360.

100. A. Stephenson and M. D. Ward, *Chem. Commun.*, 2012, **48**, 3605.

101. A. Stephenson and M. D. Ward, *Dalton Trans.*, 2011, **40**, 7824.

102. S. Turega, W. Cullen, M. Whitehead, C. A. Hunter and M. D. Ward, *J. Am. Chem. Soc.*, 2014, **136**, 8475.

103. M. M. J. Smulders, I. A. Riddell, C. Browne and J. R. Nitschke, *Chem. Soc. Rev.*, 2013, **42**, 1728.

104. Q.-H. Wei, S. P. Argent, H. Adams and M. D. Ward, *New J. Chem.*, 2008, **32**, 73.

105. N. C. Fletcher, R. T. Brown and A. P. Doherty, *Inorg. Chem.*, 2006, **45**, 6132.

106. N. C. Fletcher, M. Nieuwenhuyzen, R. Prabarahan and A. Wilson, *Chem. Commun.*, 2002, 1188.

107. R. T. Brown, N. C. Fletcher, M. Nieuwenhuyzen and T. E. Keyes, *Inorg. Chim. Acta*, 2005, **358**, 1079.

108. P. de Wolf, P. Waywell, M. Hanson, S. L. Heath, A. Meijer, S. J. Teat and J. A. Thomas, *Chem.-Eur. J.*, 2006, **12**, 2188.

109. P. de Wolf, S. L. Heath and J. A. Thomas, *Chem. Commun.*, 2002, 2540.

110. S. Hiraoka, Y. Sakata and M. Shionoya, *J. Am. Chem. Soc.*, 2008, **130**, 10058.

111. Y. Sakata, S. Hiraoka and M. Shionoya, *Chem.-Eur. J.*, 2010, **16**, 3318.

112. H. B. Wu and Q. M. Wang, *Angew. Chem. Int. Ed.*, 2009, **48**, 7343.

113. M. Wang, V. Vajpayee, S. Shanmugaraju, Y.-R. Zheng, Z. Zhao, H. Kim, P. S. Mukherjee, K.-W. Chi and P. J. Stang, *Inorg. Chem.*, 2011, **50**, 1506.

114. W. Meng, J. K. Clegg, J. D. Thoburn and J. R. Nitschke, *J. Am. Chem. Soc.*, 2011, **133**, 13652.

115. M. M. J. Smulders, A. Jimenez and J. R. Nitschke, *Angew. Chem. Int. Ed.*, 2012, **51**, 6681.

2. *Fac* and *mer* isomers of Ru(II) tris (pyrazolyl-pyridine) complexes as models for the vertices of coordination cages: structural characterisation and hydrogen-bonding characteristics

2.1 Introduction

Host–guest chemistry of hollow container molecules is an increasingly important field of study because of the fundamental insights it can offer into molecular recognition processes,[1-5] and because of potential applications in areas such as alterations of reactivity of bound guests which allows novel synthetic transformations;[6-9] catalysis;[10-12] and targeted drug delivery.[13,14] Of these, all rely on highly selective binding of specific guests, sometimes involving hydrogen-bond based recognition between the guest and the cavity of the host.[15-20]

In most examples where hydrogen-bonds are used in guest binding within a cage cavity, the hydrogen bond donor atoms are heteroatoms. Custelcean and co-workers have synthesised a series of ligands which contain a urea linkage between two 2,2'-bipyridyl units. Combination of three equivalents of ligand with two equivalents of nickel(II) or zinc(II) resulted in the formation of a tetrahedral cage with 12 endohedral urea protons; this provides an ideal binding environment for tetrahedral oxoanions such as sulfate (see Figure 2.1.1).[18] Computer-aided design has shown that each sulphate anion can accept up to 12 N–H···O hydrogen-bonds in its solvation shell, and this is indeed the case in the crystal structure of the $[M_4L_6]^{8+}$ cages with encapsulated sulphate anions. This is an example of how a binding pocket can be precisely tailored for a specific guest.

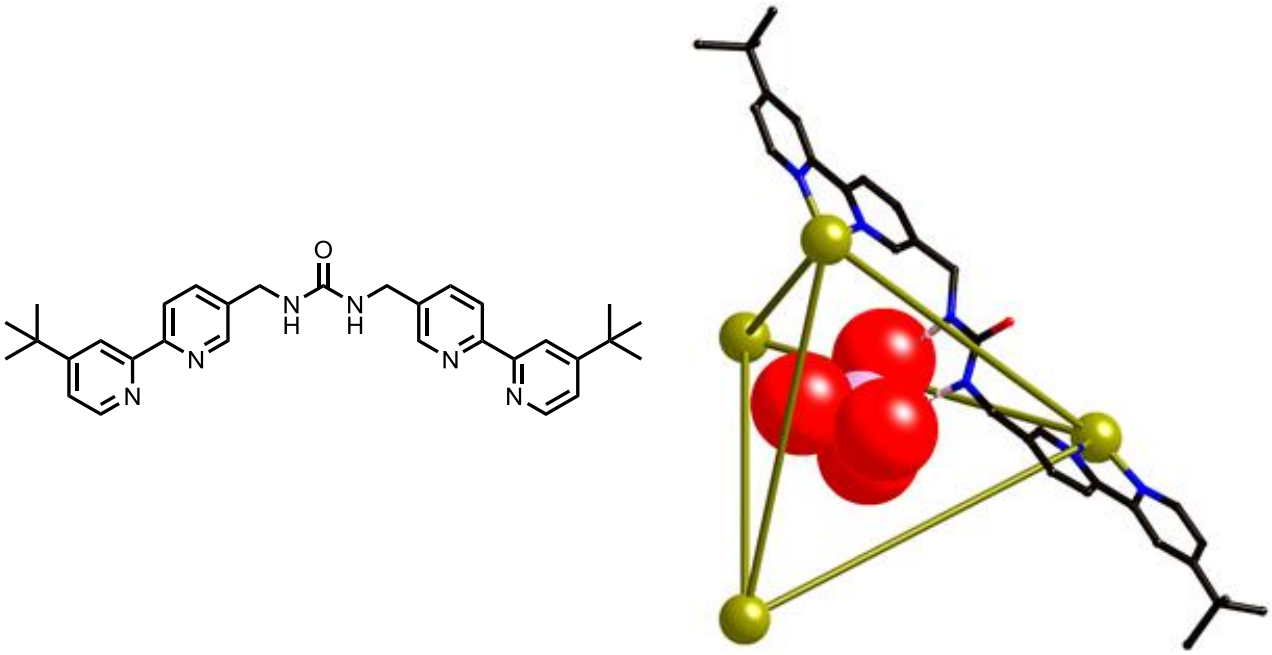

Figure 2.1.1 Left: The urea-functionalised ligand. Right: Custelcean's M_4L_6 cage with an ecapsulated SO_4^{2-} anion, emphasising the hydrogen-bonding interactions between the host and guest.

Amouri and co-workers have synthesised a Pd_2L_4 cage which also contains endohedral N-H protons, as well as unsaturated exposed faces of the square-planar palladium centres (see Figure 2.1.2).[20] These two properties combine to result in the encapsulation of the anionic guest $[Pt(NO_2)_4]^{2-}$ within the cage cavity, whereby the NO_2 groups of the anionic guest form hydrogen bonds with the amine groups of the host, and long metal-oxygen coordination bonds (Pd – O 2.964 Å) with the palladium centres.

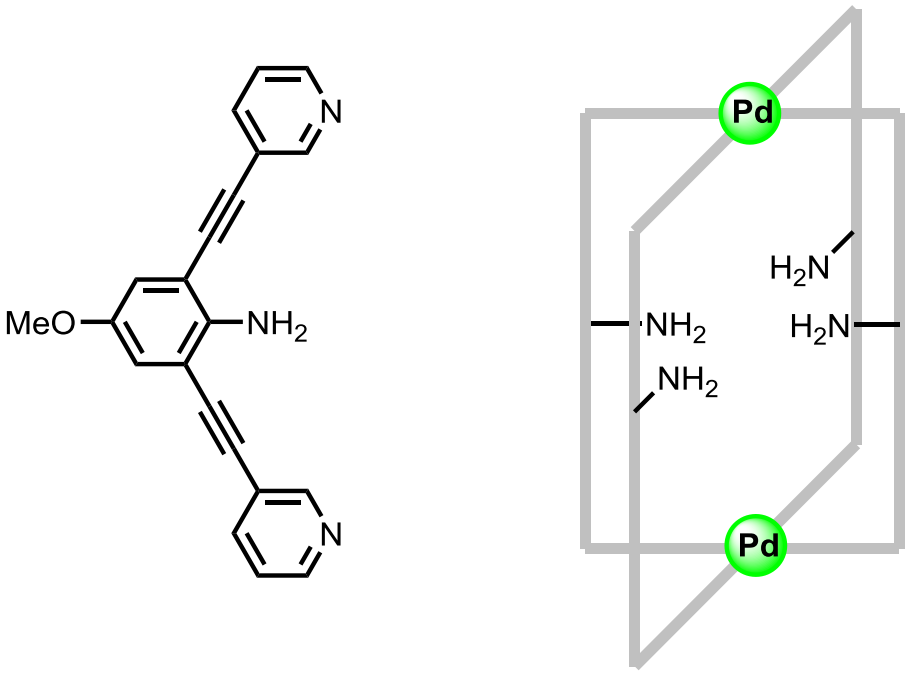

Figure 2.1.2 The ligand used by Amouri (left) to form the Pd_2L_4 cage with 4 sets of endohedral NH_2 protons (right).

Ward's group has recently described some detailed studies of guest binding in the cavity of a family of $[M_8(L^{1,5\text{-naph}})_{12}]^{16+}$ coordination cages[21-23] (see Figure 2.1.3) which have structures with a metal ion at each vertex of a cube and a bis-bidentate ligand, containing two chelating pyrazolyl-pyridine termini, spanning each edge.[24,25] Variation in external substituents has allowed these to be solubilised in different solvents without affecting the structure of the core cage and its central cavity. Importantly, the eight metal ions are not all in the same coordination environment: two of them (at either end of a long diagonal) have a *fac* tris-chelate coordination geometry whereas the other six have a *mer* geometry. Thus the cages are superficially 'cubic' due to the arrangement of metal ions, but the variation in *fac* or *mer* tris-chelate geometries at different sites results in S_6 molecular symmetry in solution.

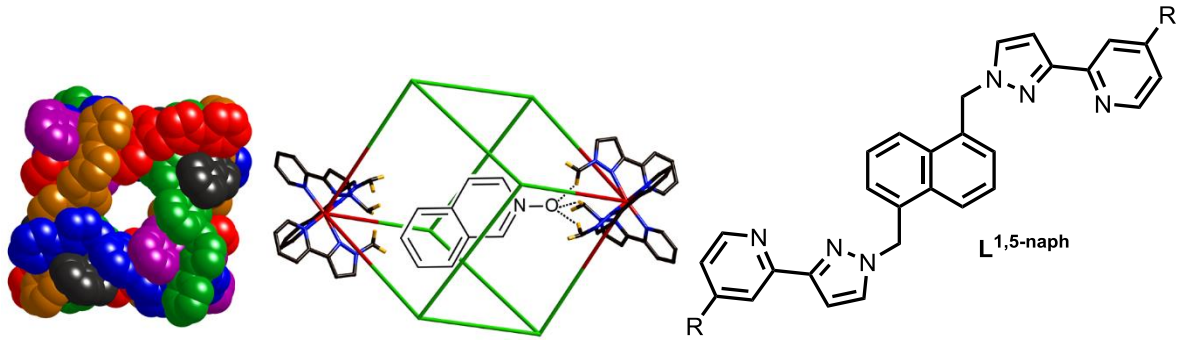

Figure 2.1.3 The general structure of the $[M_8(L^{1,5\text{-naph}})_{12}]^{16+}$ coordination cage, with ligands coloured differently for clarity (left); a sketch showing the likely mode of binding of hydrogen-bond accepting guests at one of the two *fac* tris-chelate metal vertices (middle); structure of the $L^{1,5\text{-naph}}$ family of ligands used to make cubic coordination cages (R' = H, CH_2OH) (right).

The formation of two *fac* tris-chelate sites results in assembly of convergent groups of inwardly-directed methylene protons, which lie quite close to the Co(II) centre and are therefore in a region of high electrostatic potential. This provides a binding pocket where electron-rich atoms can bind via a set of charge-assisted C–H···X hydrogen-bonds (see Figure 2.1.3). At the remaining six *mer* tris-chelate Co(II) centres there is no such convergent group of C–H protons, and additionally these metal ions are more sterically protected by the ligand substituents such that no close approach of an electron-rich guest atom to the metal centre is possible.[21]

These cages bind, with high shape and size selectivity, a range of hydrogen-bond-accepting bicyclic organic molecules such as coumarin and isoquinoline-*N*-oxide, in which the exocyclic O atom acts as the hydrogen-bond acceptor. ^{1}H NMR studies on numerous host/guest combinations in MeCN showed a strong correlation between guest binding strength and the hydrogen-bond acceptor ability of the guest, confirming that a hydrogen-bonding interaction with the interior surface of the cage makes an important contribution to complex formation.[21] Molecular modelling studies showed that the minimum-energy structures had the guests oriented such that their exocyclic oxygen atom did indeed lie in the pocket defined by the convergent set of methylene protons at one of the two *fac* tris-chelate vertices, in the regions of the cavity where electrostatic potential is most positive (*cf.* Figure 2.1.3, centre).

Up to the point at which this research was conducted, the Ward group have not been able to grow crystals of a host M_8L_{12} coordination cage containing a bound guest to confirm the binding mode.[26] It is important for this work however to have clear proof that the hypothesis – *viz.* that the *fac* tris-chelate sites in the cages provide preorganised binding sites for recognition of hydrogen-bond acceptors – is correct, particularly in the solution phase, as this knowledge will influence design and study of future generations of host cages. It is noted that there are several examples of simple tris-chelate complexes in which a convergent arrangement of three polar substituents such as amides or carboxylates on one face of the complex provides a binding site for interacting with anions[27-29] and even proteins.[30] Although the Ward group cage complexes only contain inwardly directed C–H groups as the hydrogen-bonding sites it might be expected to see the same geometric discrimination between *fac* (convergent set of hydrogen- bond donor atoms) and *mer* (non convergent hydrogen-bond donors) isomers.

The basis of this work therefore was to prepare simple, kinetically stable, mononuclear Ru(II) complexes based on pyrazolyl-pyridine type ligands, as either their *fac* or *mer* isomers, to use as models for the different metal vertices in the coordination cage. Structural characterisation of these has been used to confirm their similarity to the metal centres in the cage superstructure, and ^{1}H NMR spectroscopic titrations have been performed to see if the coordination geometry of the metal complex does influence how well a hydrogen-bonding guest interacts with it. From this has been found clear evidence that the *fac* tris-chelate metal complex units do act as better hydrogen-bond donors than the related *mer* tris-chelate complexes, and that this interaction is associated with the convergent group of methylene protons in the *fac* complexes. There is therefore good evidence (beyond molecular modelling) to support our understanding of how guest molecules interact with the interior surface of the cage hosts.

2.2 Results and Discussion

2.2.1 Initial attempts to isolate *fac*- and *mer*-$[Co(L^{bz})_3](BF_4)_2$ by crystallisation

The initial targets for investigation were *fac* and *mer* tris-chelate Co(II) complexes of the benzyl-substituted pyrazolyl-pyridine ligand L^{bz}, which is effectively half of the bridging ligand $L^{1,5\text{-naph}}$ and will provide a coordination environment around a single metal ion that is as close as possible to what is found in the $[Co_8(L^{1,5\text{-naph}})_{12}]^{16+}$ cages (see Figure 2.2.1).[25] The ligand L^{bz} is simply prepared by alkylation of the pyrazole ring of 3-(2-pyridyl)-1H-pyrazole with benzyl bromide. Reaction of L^{bz} with $Co(BF_4)_2$ afforded $[Co(L^{bz})_3](BF_4)_2$ as a mixture of *fac* and *mer* isomers as shown by ^{1}H NMR spectroscopy. Statistically these are expected to form in a 1 : 3 ratio in the absence of other factors which might favour one geometry over the other. In the *fac* isomer (expected C_3 symmetry) all three ligands will be equivalent. In the *mer* isomer (expected C_1 symmetry) all three ligands will be in different chemical environments. Thus a mixture of *fac* and *mer* isomers of $[Co(L^{bz})_3](BF_4)_2$ is expected to show in its ^{1}H NMR spectrum four different environment for the ligand L^{bz}, and if the statistical 1 : 3 ratio occurs this means that all four ligand environments will be present with equal likelihood. Bulky substituents which are too close to one another in the *fac* isomer would skew this equilibrium in favour of the *mer* isomer; at the other extreme, cooperative non-covalent interactions between ligands can strongly favour the *fac* isomer, as shown recently by Scott and co-workers.[31,32]

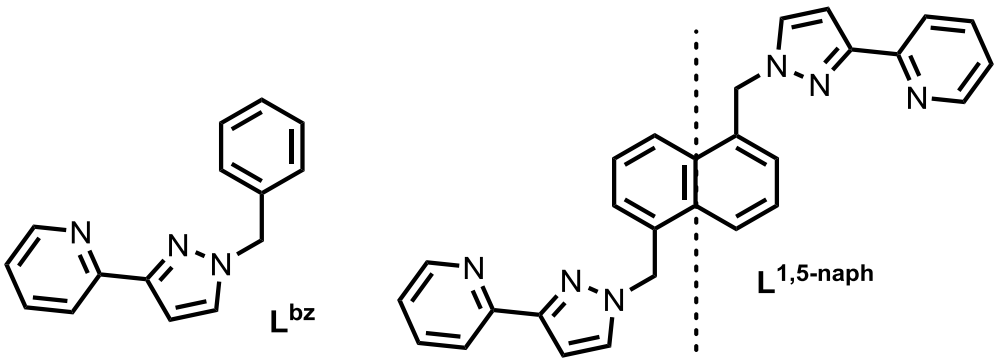

Figure 2.2.1 Structure of the ligand L^{bz}, and its relation to the ligand $L^{1,5\text{-naph}}$.

The ^{1}H NMR spectrum of $[Co(L^{bz})_3](BF_4)_2$ (see Figure 2.2.2) shows a statistical mix of *fac* and *mer* isomers with four ligand environments in equal abundance. As has been observed before the paramagnetism of high-spin Co(II) spreads out the signals over a wide chemical shift range making identification of the mixture of isomers straightforward.[24] Whilst all signals are not individually assigned, and some of the less shifted ones clearly overlap in the 0–10 ppm region, the presence of four independent ligand environments for the mixture of *fac* and *mer* isomers is obvious: some sets of four signals that are clearly the same proton (a–d) in four different environments are labelled on Figure 2.2.2.

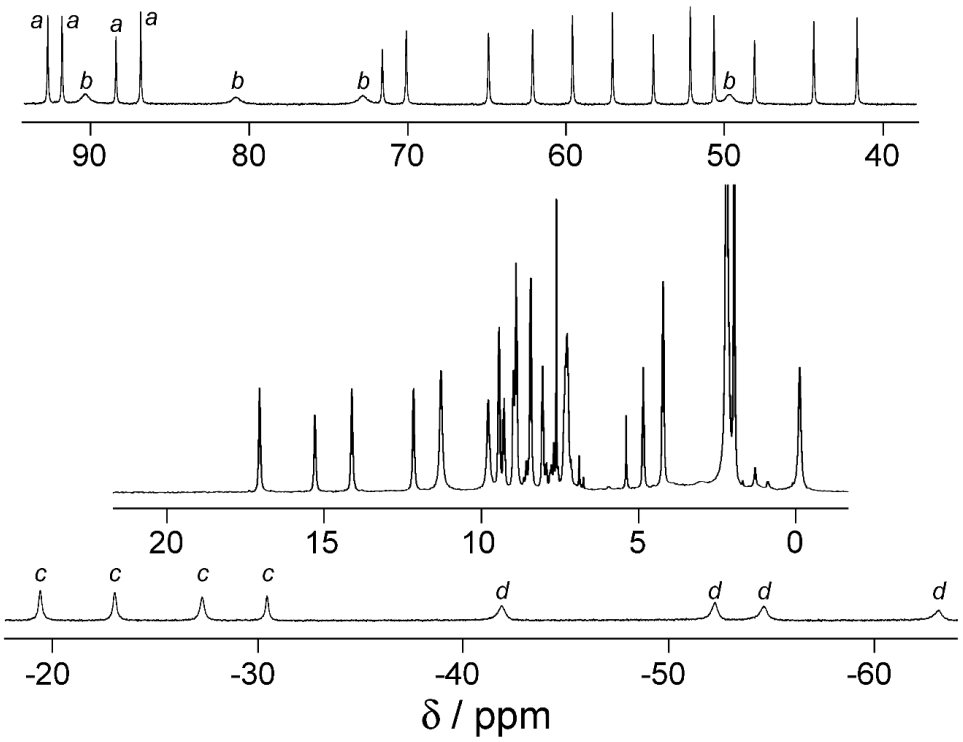

Figure 2.2.2 ^{1}H NMR spectrum of $[Co(L^{bz})_3](BF_4)_2$ (CD_3CN, 250 MHz), showing the mixture of *fac* and *mer* isomers with four independent ligand environments present in equal abundance.

Crystallisation of this mixture from $CHCl_3$ afforded X-ray quality crystals of what proved to be the *mer* isomer of $[Co(L^{bz})_3](BF_4)_2$ (see Figure 2.2.3). The quasi-octahedral coordination geometry and the Co–N distances (in the range 2.14–2.20 Å) are unremarkable and very similar to what is observed in the complete coordination cages. One of the pendant phenyl rings [C(31C)–C(36C)] lies stacked with a coordinated pyrazolyl-pyridine fragment from a different ligand within the same molecule. Importantly the three CH_2 groups are not convergent and do not form a clearly-defined binding pocket, although

three of them [H(26B), H(26D) and H(26F)] form close contacts with F atoms of the fluoroborate anions or the O atom of a water molecule (H···X separations involving these H atoms, 2.49–2.93 Å).

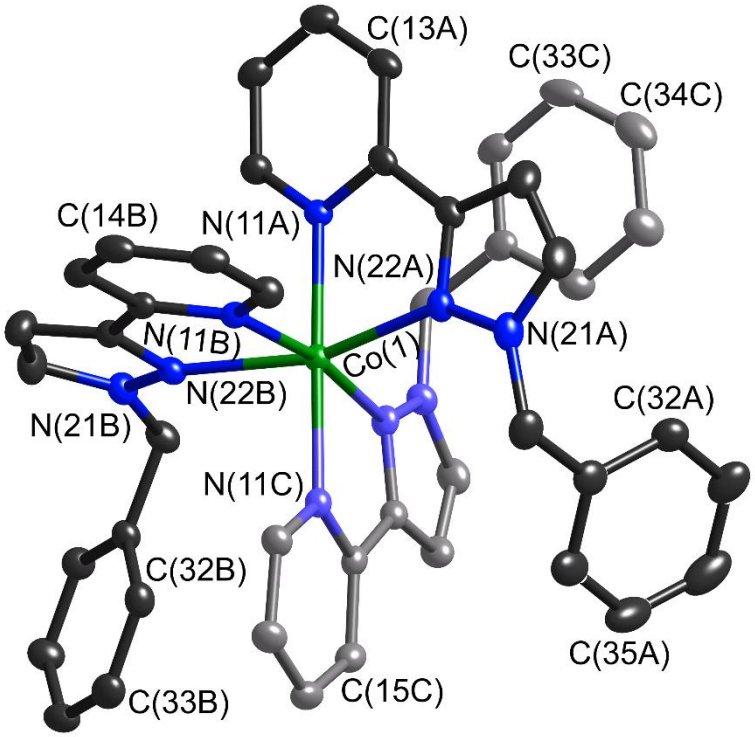

Figure 2.2.3 Structure of the complex cation of *mer*-$[Co(L^{bz})_3](BF_4)_2 \cdot CHCl_3 \cdot H_2O$ (thermal ellipsoids at 40% probability level). One ligand is shown with paler colours for clarity.

Attempts to crystallise the *fac* isomer of $[Co(L^{bz})_3](BF_4)_2$ for comparison purposes were unsuccessful. Only the *mer* isomer crystallised, and – given the kinetic lability of Co(II) – this likely resulted in re-establishment of the 3 : 1 *mer* : *fac* equilibrium ratio in solution, such that the amount of *fac* isomer present diminished as the crystallisation proceeded. This was confirmed by measuring the ^{1}H NMR spectrum of redissolved crystals of *mer*-$[Co(L^{bz})_3](BF_4)_2$ which was exactly the same as that in Figure 2.2.2: i.e. the pure *mer* isomer equilibrated to the 3 : 1 *mer* : *fac* equilibrium in the time it took to dissolve the crystals and record the NMR spectrum.

It was then attempted to see if the use of different anions may template the formation of the *fac* isomer. Thus, the reaction was repeated with tetraphenylborate, acetate and hexafluorophosphate salts of cobalt(II). Reaction of $Co(OAc)_2$ with L^{bz} followed by anion metathesis with sodium tetraphenylborate in acetonitrile resulted in the complex as its tetraphenylborate salt. Slow evaporation of solvent resulted

in X-ray quality crystals of what also proved to be the *mer* isomer of $[Co(L^{bz})_3](BPh_4)_2$ (see Figure 2.2.4). The structure of the complex cation is similar to that of the tetrafluoroborate salt, with a quasi-octahedral coordination geometry and similar Co–N distances (in the range 2.12–2.17 Å). The associated anions make numerous CH···π contacts with the associated anions, which effectively wrap around the complex cations (see Figure 2.2.4, bottom). Once formed, the crystals were extremely insoluble, only dissolving in d_6-dmso. This caused the dissociation of the complex, as the ^{1}H NMR spectrum was quite unlike that seen in Figure 2.2.2; the complex falls apart in very competitive solvents.

A deep purple solution of $Co(OAc)_2$ and L^{bz} in acetonitrile described above yielded X-ray quality crystals after slow evaporation of the solvent, even without additional anions being added. This proved to be an unexpected product (see Figure 2.2.5). The structure was revealed to be the linear trimer $[Co_3(L^{bz})_2(OAc)_6]$ in which the central cobalt(II) atom [Co(1)] lies on an inversion centre, such that half of the complex is crystallographically unique. Each pyridyl-pyrazolyl ligands chelate to one of the terminal Co(2) atoms, and the six acetate anions bridge the cobalt(II) cations in two distinct ways. The first acetate binding mode is a μ^2-1,3 bridging manner, in which each acetate oxygen [O(13B), O(14B), O(13D) and O(14D)] is singly bonded to a different cobalt(II) cation. The second type of bridging observed is slightly more unusual, in that the acetate acts as a chelating ligand for the terminal Co(2) atoms with one of the oxygen atoms [O(13C)] also bridging Co(1) and Co(2).

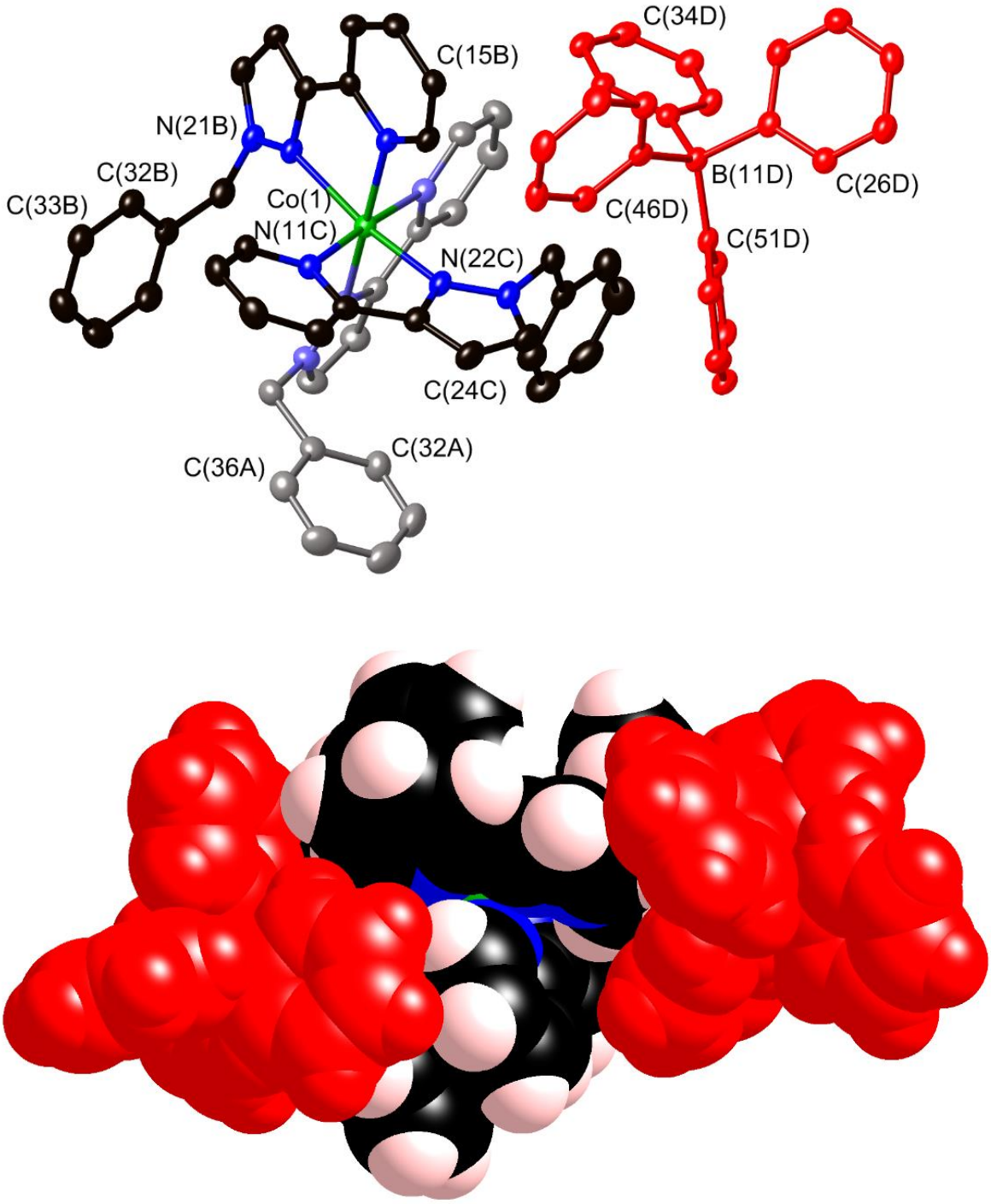

Figure 2.2.4 Top: Structure of the complex cation and one anion of *mer*-$[Co(L^{bz})_3](BPh_4)_2$ (thermal ellipsoids at 50% probability level). The anion is shown in red and one ligand is shown with paler colours for clarity. Bottom: Space-filling view of *mer*-$[Co(L^{bz})_3](BPh_4)_2$.

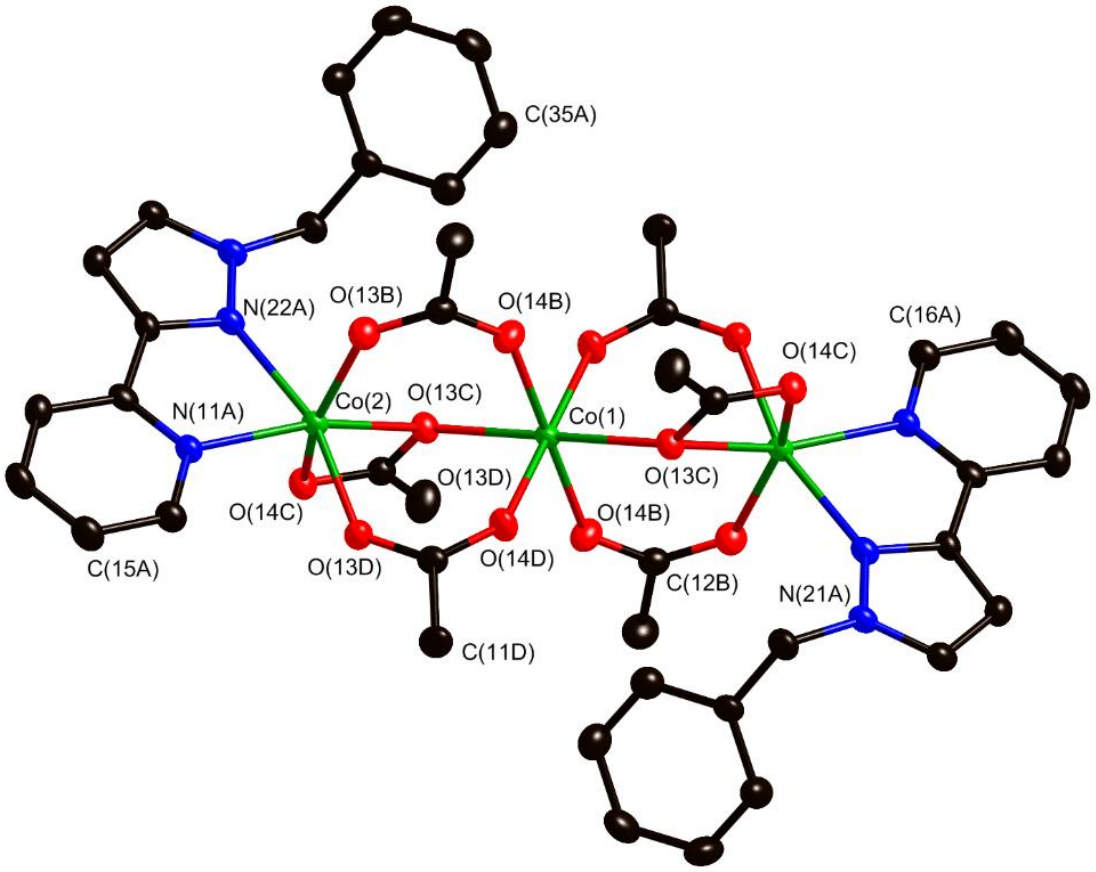

Figure 2.2.5 Structure of the complex of $[Co_3(L^{bz})_2(OAc)_6]\cdot 2MeCN$ (thermal ellipsoids at 50% probability level).

The result of these bridging interactions is a central cobalt(II) atom with pseudo-octahedral geometry as a result of six oxygen donor atoms provided by six different acetate anions (see Figure 2.2.6), with bond lengths in the region of 2.06 – 2.13 Å, and *cis*-bond angles in the region of 86.9 – 93.1 °. The terminal cobalt(II) atoms have a heavily distorted pseudo-octahedral geometry, with Co – O bond lengths in the range of 2.01 – 2.19 Å [O(13B) and O(14C), respectively], and Co – N bond lengths of 2.15 and 2.22 Å [N(11A) and N(22A)]. The cis-bond angles are heavily distorted from 90 °, ranging from 59.9 ° for the angle between the two oxygen atoms of the chelating acetate [O(13C) and O(14C)], and 104.4 ° between O(13C) and N(22A). A similar structure has been reported recently by Mukherjee and co-workers, in which two terminal cobalt(II) atoms with an N_2O_4 donor atom set and a central one with an O_6 donor set form a linear trimer.[33]

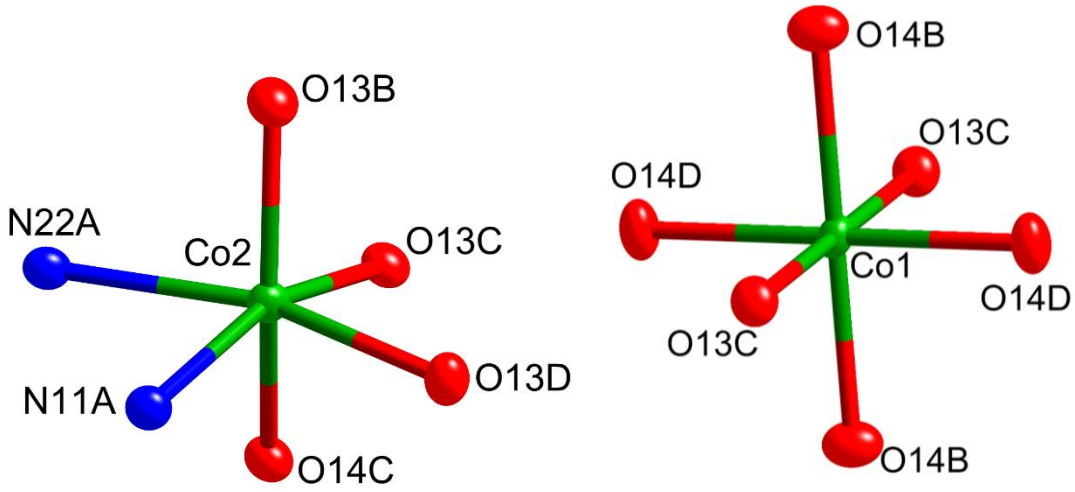

Figure 2.2.6 Coordination spheres of the crystallographically unique metal centres in the complex of $[Co_3(L^{bz})_2(OAc)_6]\cdot 2MeCN$ (thermal ellipsoids at 50% probability level).

The final attempt to isolate X-ray quality crystals of the *fac* isomer of $[Co(L^{bz})_3]^{2+}$ was co-crystallisation with a guest molecule, in an effort to template the formation of the convergent CH_2 binding pocket which is present in the *fac* isomer, but absent in the *mer* isomer. Thus, a sample of $[Co(L^{bz})_3](PF_6)_2$ was prepared by anion metathesis of a solution of $Co(OAc)_2$ with L^{bz} in acetonitrile with potassium hexafluorophosphate, and an excess of isoquinoline N-oxide was added to this in acetonitrile. Slow diffusion of di-isopropyl ether vapour into this acetonitrile solution resulted in the formation of X-ray quality crystals which proved, again, to be an unexpected structure (see Figure 2.2.7).

The formulation of the crystal structure is $[Co(L^{bz})_2(L^{N\text{-}ox})](PF_6)$. The guest molecule was indeed incorporated in complex crystal structure, but as a chelating ligand rather than a non-covalently bound guest. Isoquinoline N-oxide has been oxidised at the 1-position in order to form 1-hydroxyisoquinoline N-oxide, which forms a favourable 5-membered chelate ring when bound to Co(II). The mechanism of this oxidation is unclear, and there are no reported syntheses of this ligand in the literature.

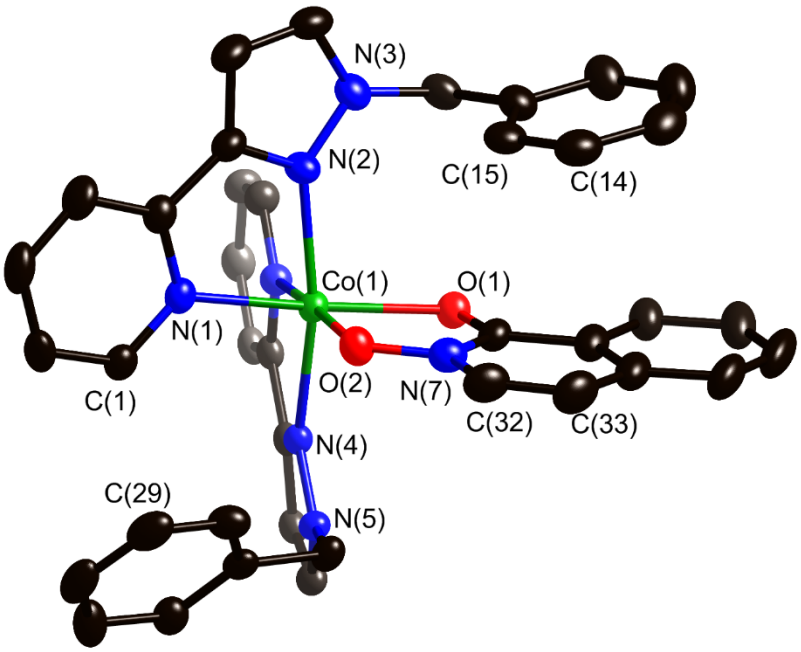

Figure 2.2.7 Structure of the complex cation of $[Co(L^{bz})_2(L^{N\text{-}ox})](PF_6)$ (thermal ellipsoids at 50% probability level). The anion is shown in red and one ligand is shown with paler colours for clarity.

Two ligands L^{bz} make up the rest of the coordination sphere of the cobalt(II) ion, resulting in a distorted quasi-octahedral geometry. The structure is stabilised by intramolecular π – π stacking between the electron-rich pendant phenyl ring of one ligand and the electron-deficient isoquinoline (see Figure 2.2.7). There are also pairs of intermolecular CH···π interactions between the CH_2 protons and phenyl rings of neighbouring complexes (see Figure 2.2.8). There are also numerous C–H···F hydrogen-bonds between the hexafluorophosphate anions and the coordinated and pendant aromatic rings, with H···F distances in the range of 2.35 – 2.85 Å.

It is clear from these efforts that trying to isolate and study separately the *fac* and *mer* isomers of $[Co(L^{bz})_3]X_2$ as models for the separate types of cage vertex is not feasible, and we therefore changed strategy to the use of a more kinetically inert metal centre.

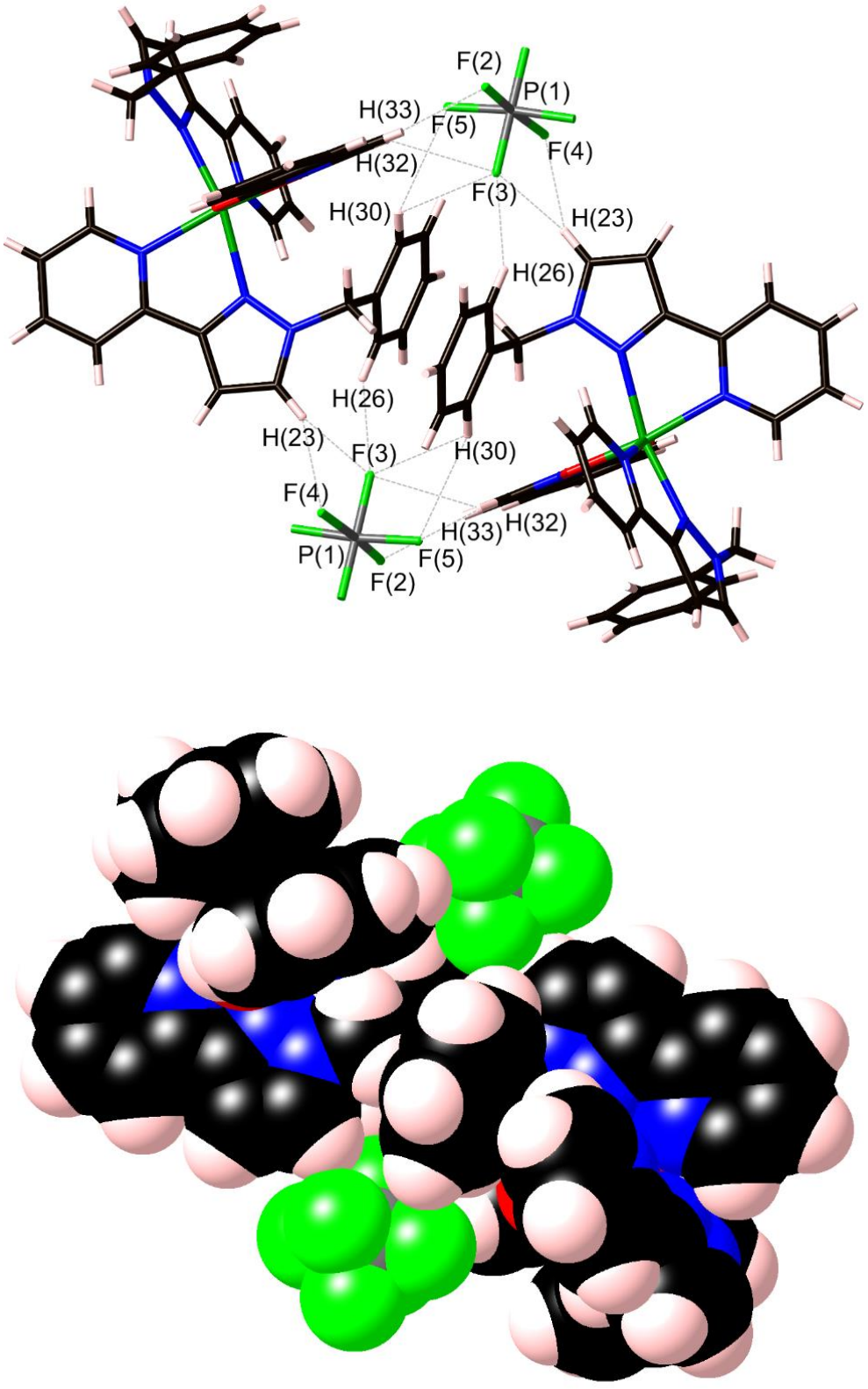

Figure 2.2.8 Top: Stick representation of $[Co(L^{bz})_2(L^{N\text{-}ox})](PF_6)$ emphasising the hydrogen-bonding interactions between the complex cations and anions. Bottom: Space-filling view from the same perspective.

2.2.2 Isolation and structural characterisation of *fac*- and *mer*-$[RuL_3](PF_6)_2$

We required a kinetically inert metal ion for which *fac* and *mer* tris-chelate complexes are sufficiently stable to be prepared at modest temperatures, purified by chromatography or fractional crystallisation, and studied in solution, without undergoing any significant isomerisation. To be an accurate model for the vertices of the cage, the metal ion must also have a 2+ charge and have metal–ligand bond distances similar to that of the Co(II) complexes. The obvious candidate is Ru(II), with which there are numerous well-studied examples of isolation and characterisation of *fac* and *mer* isomers of non-symmetric chelating ligands.[28-30,34-38]

Preparation of $[Ru(L^{bz})_3]^{2+}$ salts as a mixture of isomers is routine and the 3 : 1 *mer* : *fac* ratio was confirmed by ^{1}H NMR spectroscopy. However chromatographic separation was difficult. There are examples from Fletcher and co-workers of effective chromatographic separation of *fac* and *mer* isomers of Ru(II) complexes, but in those cases the large, polar substituents exaggerated the geometric and electronic differences between the isomers which may have facilitated the separation.[36] With relatively compact and non-polar benzyl substituents in $[Ru(L^{bz})_3]^{2+}$ salts the structural difference between the isomers did not appear to be enough to allow effective chromatographic separation under a range of conditions. Attempts at fractional crystallisation provided a few crystals of one isomer or the other but not on a sufficient scale or in a predictable way.

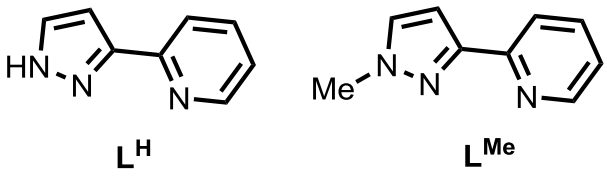

L^H L^{Me}

Figure 2.2.9 Structure of the ligands L^H and L^{Me}.

A different strategy was therefore adopted, which was to prepare the complex $[Ru(L^H)_3]^{2+}$ using unsubstituted 3-(2-pyridyl)-1H-pyrazole (see Figure 2.2.9, left), and then to separate the isomers according to their different ability to form adducts with other metal ions *via* the pendant pyrazolyl groups.[39] Reaction of $RuCl_3$ with excess L^H in ethylene glycol at reflux afforded a yellow solution from

which $[Ru(L^H)_3](PF_6)_2$ precipitated on addition of aqueous KPF_6. This was purified (without separation of the isomers) by column chromatography on silica using a MeCN– water–aqueous KNO_3 mixture, and the resulting sample of $[Ru(L^H)_3](PF_6)_2$ was shown by ^{1}H NMR spectroscopy to be the expected 3 : 1 mixture of *mer* and *fac* isomers with four independent ligand environments of equal abundance being present (see Figure 2.2.10a).

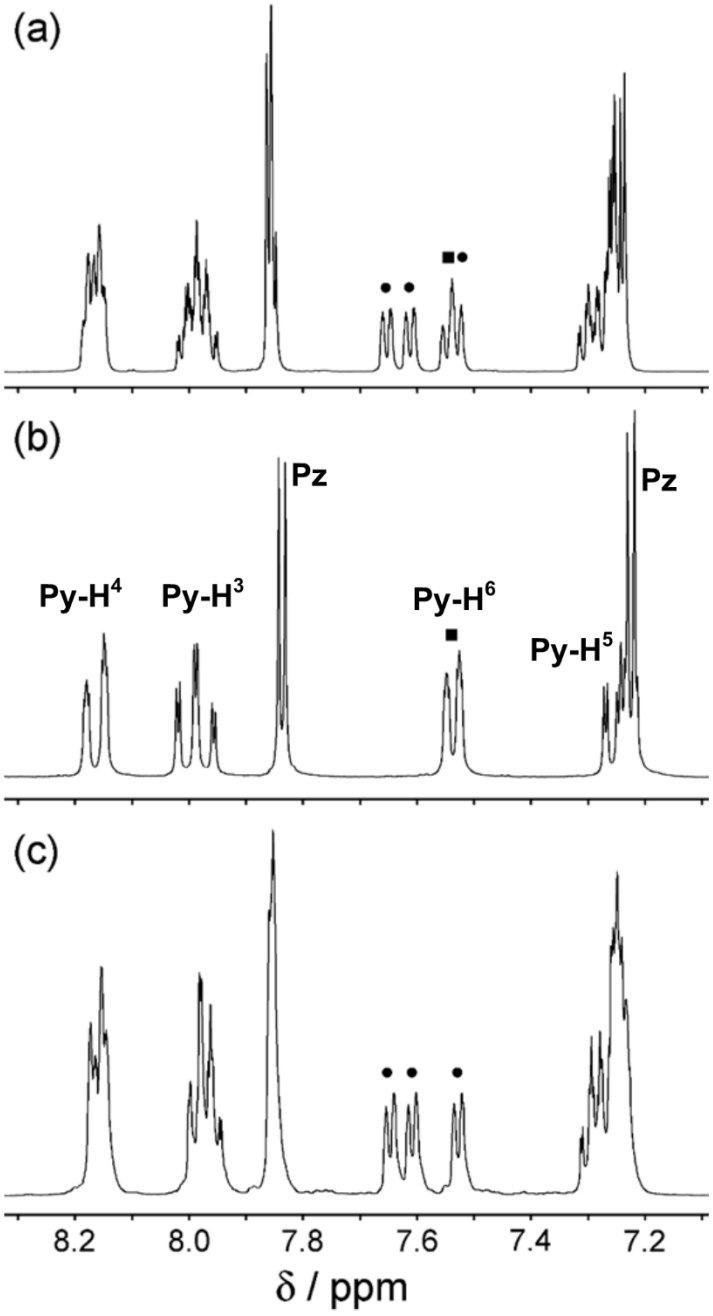

Figure 2.2.10 ^{1}H NMR spectra (CD_3CN, 400 MHz) of $[Ru(L^H)_3](PF_6)_2$: (a) the as-isolated statistical mixture of *fac* and *mer* isomers; (b) the pure *fac* isomer (Pz = pyrazole, Py = pyridine); (c) the pure *mer* isomer.

Separation of this into its geometric isomers was achieved quantitatively by reaction of $[Ru(L^H)_3](PF_6)_2$ with $Cu(BF_4)_2$ in MeOH containing Et_3N to give the pentanuclear complex $[\{Ru(L^-)_3\}_2Cu_3](PF_6)$ as previously reported by Lam and coworkers.[39] In this complex, two *fac*-$[Ru(L^H)_3]^{2+}$ units have had their pyrazolyl NH groups deprotonated by the Et_3N. The resulting *fac*-$[Ru(L^-)_3]^-$ unit has an array of three anionic pyrazolyl donors on the same face of the complex, and two of these *fac*-$[Ru(L^-)_3]^-$ units sandwich a triangle of three Cu(I) ions to give a stable Ru_2Cu_3 complex which has a triple helical structure and with each Cu(I) ion coordinated by two pyrazole anions, one from each Ru(II) unit. This complex precipitates from MeOH as it forms and is trivially separated by filtration.

In contrast *mer*-$[Ru(L^H)_3]^{2+}$ cannot form a stable Cu(I) adduct in this way as the three pyrazolyl *N*3 atoms are not convergent; so it remains in the reaction solution from which it may be separated and purified. Treatment of the precipitated $[\{Ru(L^-)_3\}_2Cu_3](PF_6)$ with CF_3CO_2H in CH_2Cl_2 re-protonates the pyrazole rings, to regenerate $[Ru(L^H)_3]^{2+}$ which is now (after a simple workup) the pure *fac* isomer. Figures 2.2.10(b) and 2.2.10(c) show the ^1H NMR spectra of *fac*- and *mer*-$[Ru(L^H)_3](PF_6)_2$ respectively, with one ligand environment and three ligand environments (6 proton environments and 18 proton environments respectively). The correspondence of these signals with the spectrum of the initially-isolated mixture of isomers in Figure 2.2.10a is obvious; note especially the set of three doublets at around 7.6 ppm for the *mer* isomer (Figure 2.2.10c, each labelled with a black circle), and the corresponding single doublet for the *fac* isomer (Figure 2.2.10b, labelled with a black square), which overlap in the spectrum of the mixture of isomers (Figure 2.2.10a). This separation *via* an intermediate Cu(I) adduct proved to be a simple and effective way to isolate pure *fac* and *mer* isomers.

X-Ray quality crystals of both isomers of the complex were readily obtained and the structures are shown in Figure 2.2.11 and 2.2.12. In the structure of *mer*-$[Ru(L^H)_3](PF_6)_2$ (Figure 2.2.11) the Ru–N distances lie in the range 2.04–2.09 Å, slightly shorter than in the Co(II) complexes but still sufficiently similar for the Ru(II) complexes to act as credible structural analogues of the Co(II) vertices in the $[Co_8(L^{1,5\text{-naph}})_{12}]^{16+}$ coordination cages.[21-23] The complex has a generally unremarkable structure with the expected pseudo-octahedral geometry and typical bond lengths and angles.

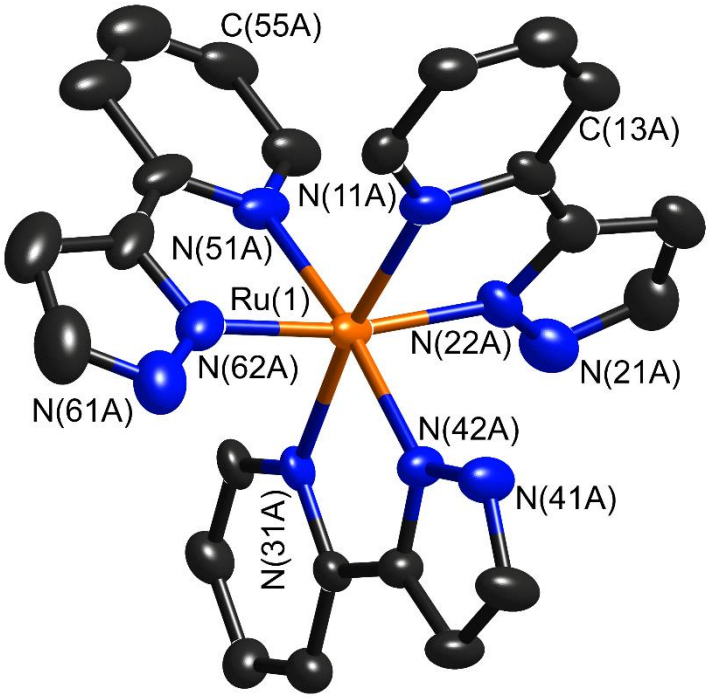

Figure 2.2.11 Structure of the complex cation of *mer*-$[Ru(L^H)_3](PF_6)_2 \cdot 2MeCN$ (thermal ellipsoids at 40% probability level).

The structure of the *fac* isomer (Figure 2.2.12) however reveals a surprise: the complex is partially deprotonated (at the pyrazolyl NH sites) to give the hydrogen-bonded dimer $[Ru(L^H)_3Ru(L^-)_3](PF_6)$. In this complex there are two independent complex fragments in the unit cell, both lying on a C_3 axis which passes through both metal ions such that one third of each complex is in the asymmetric unit. One complex is *fac*-$[Ru(L^H)_3]^{2+}$, containing Ru(1), and is the fully protonated dication, as expected. The other however is *fac*-$[Ru(L^-)_3]^-$, containing Ru(2), in which all three pyrazolyl rings are deprotonated. The protonated and deprotonated complex units are closely associated via three NH···N hydrogen bonds involving the pyrazolyl NH from the Ru(1) complex [N(21A)] and the deprotonated pyrazolyl ring from the Ru(2) complex [N(21B)]. As both units have the same chirality, the result – if a hydrogen-bonded pair of ligands pyridyl–pz–H···pz–pyridyl is taken as a single 'strand' spanning two metal ions – is a triple helical architecture similar to that of $[\{Ru(L^-)_3\}_2Cu_3](PF_6)$ reported earlier[39] but with H^+ ions replacing the Cu(I) ions in the centre. The N···N separations involved in the NH–N hydrogen bonds (all equivalent) are 2.66 Å, indicative of short, strong hydrogen-bonding interactions.

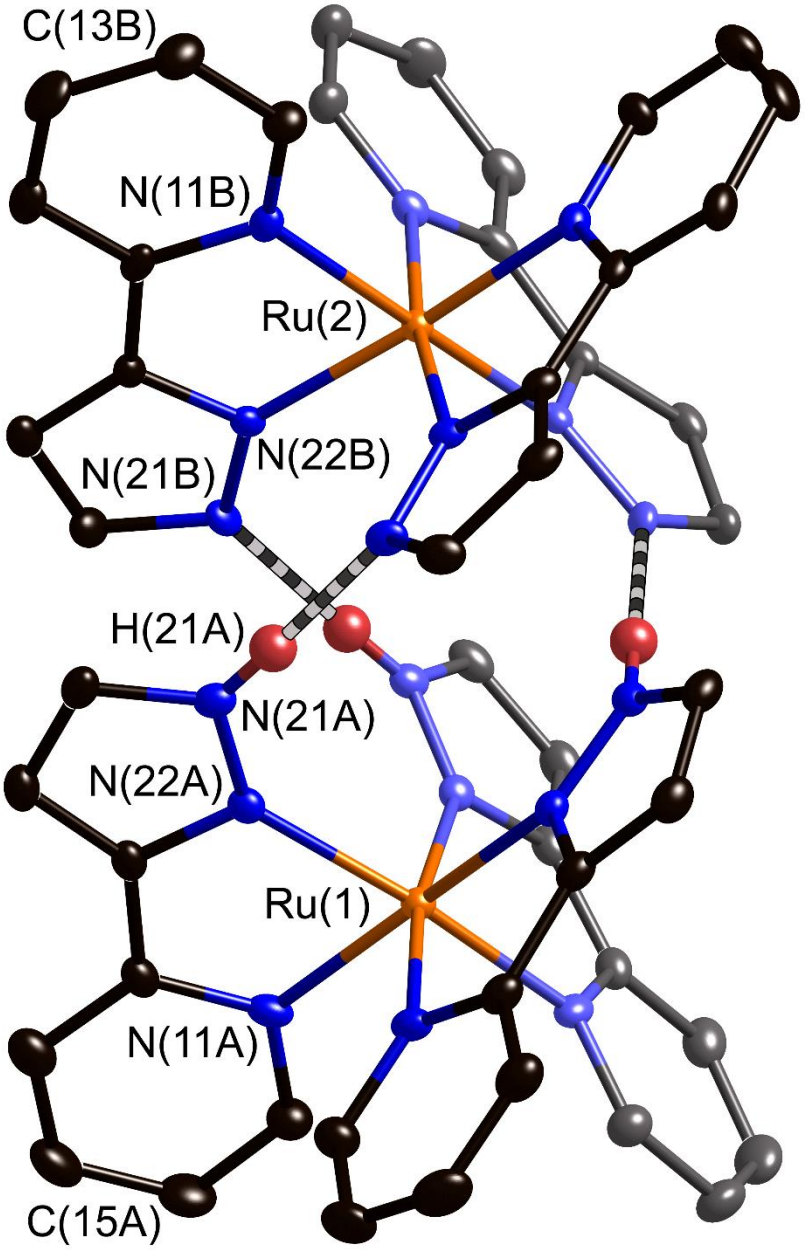

Figure 2.2.12 Structure of the hydrogen-bonded dinuclear complex cation of *fac*, *fac*-$[Ru(L^H)_3Ru(L^-)_3](PF_6)\cdot 3C_7H_8$ (thermal ellipsoids at 40% probability level). Some of the ligands are shown in paler colours for clarity; the hydrogen-bonds between the two complex units are indicated by the striped lines.

In addition this close association of the two complex units results in π-stacking between the pyrazolyl rings of each, with an average interplanar separation of ca. 3.3 Å between overlapping ligand fragments. This will be facilitated by the fact that one pyrazolyl ring in each stacked pair is deprotonated and therefore electron-rich compared to the other, so the stack involves a donor–acceptor interaction. These crystals grew from a solution containing fully protonated *fac*-$[Ru(L_H)_3]$- $(PF_6)_2$; presumably the loss of

three protons per two complex units is driven by the extra stability of the hydrogen-bonded and π-stacked pair of cationic and anionic complex units in the crystal. Telfer and co-workers have reported related examples of helicates formed from homochiral mononuclear units that assemble *via* inter-ligand hydrogen-bonding interactions in exactly the same way.[40]

With *fac*- and *mer*-$[Ru(L^{H})_3](PF_6)_2$ readily available by this route, conversion to the corresponding isomers of $[Ru(L^{bz})_3](PF_6)_2$ was carried out by alkylation of the pyrazole groups with benzyl bromide in CH_2Cl_2 at reflux, using solid Cs_2CO_3 as base and a catalytic amount of tetrabutylammonium iodide (Finkelstein reaction). This straightforward reaction works under a range of conditions but conditions as mild as possible were used to prevent any isomerisation of the Ru(II) complex which might be facilitated by high temperatures, and by use of good donor solvents which would facilitate ligand dissociation.

It was found that under these conditions conversion of $[Ru(L^{H})_3](PF_6)_2$ to $[Ru(L^{bz})_3](PF_6)_2$ proceeded cleanly and with no evidence (by NMR spectroscopy) of any of the alternate isomer forming (see Figures 2.2.13 and 2.2.14). Chromatographic purification afforded good yields of *fac*- and *mer*-$[Ru(L^{bz})_3](PF_6)_2$. By extrapolation we now have a potentially general method to prepare *fac* and *mer* isomers of any complex-$[Ru(L^{R})_3]^{2+}$ where 'R' denotes a group that can be attached to a pyrazole ring by alkylation, which is further demonstrated in Chapter 3.

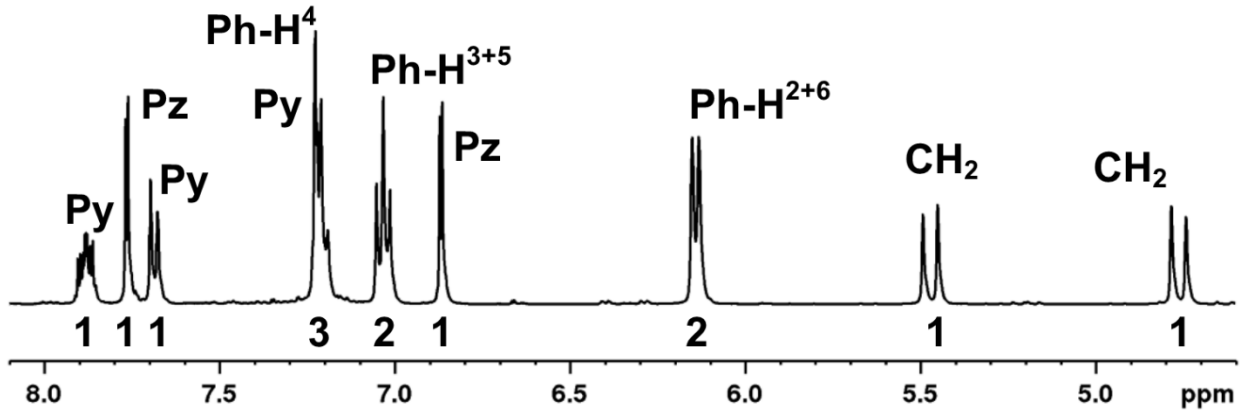

Figure 2.2.13 Assigned ^{1}H NMR spectrum (400 MHz, CD_3CN) of *fac*-$[Ru(L^{bz})_3](PF_6)_2$ (Pz = pyrazole, Py = pyridine, Ph = phenyl).

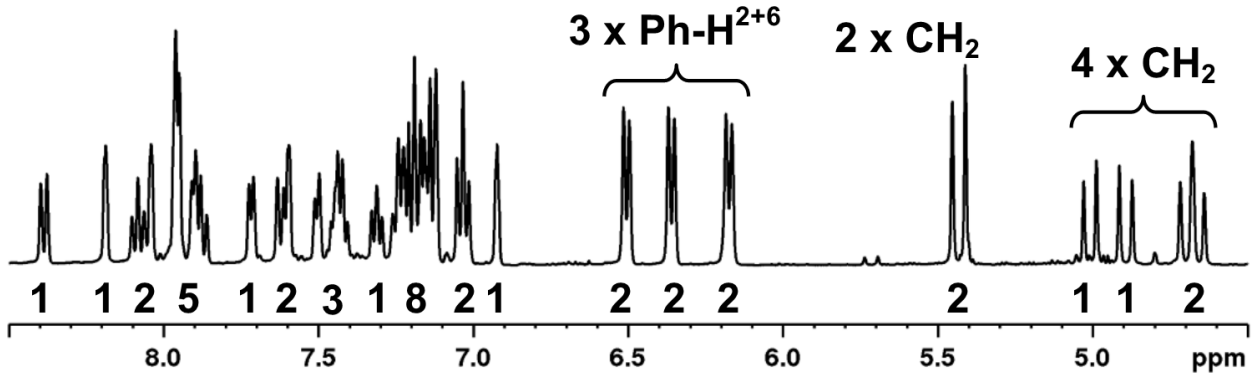

Figure 2.2.14 Partially assigned ^{1}H NMR spectrum (400 MHz, $(CD_3)_2CO$) of *mer*-$[Ru(L^{bz})_3](PF_6)_2$ (Ph = phenyl).

The X-ray crystal structure of *fac*-$[Ru(L^{bz})_3](PF_6)_2$ is shown in Figure 2.2.15. In the complex cation (Figure 2.2.15a) the Ru–N bond distances all lie in the range 2.07–2.09 Å. In each ligand the pendant phenyl ring lies stacked with the coordinated pyrazolyl-pyridine unit of another adjacent ligand, with a separation between near-parallel overlapping groups of ca. 3.4 Å, exactly as is seen in the *fac* tris-chelate vertices of the metal cages. This arrangement of ligands results in the formation of a set of three methylene groups close together on the same face of the complex. The 'inwardly' directed member of each pair [H(26A), H(26C) and H(26E)] lies ca. 3.3 Å from the Ru(II) centre and these are the closest H atoms to the metal centre apart from the pyridyl H^6 atoms (3.1–3.2 Å). This set of protons defines

what we believe to be the site where hydrogen-bonding to electron-rich atoms of guests occurs inside the cage cavities.[21]

Evidence for this comes from the presence of an acetone solvent molecule in the lattice (Figure 2.2.15b) which lies such that its oxygen atom is located in this pocket, where a guest would be expected to bind. The O atom is not exactly symmetrically located in the pocket in the solid state but lies closer to C26(B) and C26(C) (O···C non-bonded distances are 3.11 and 3.18 Å respectively, indicative of the presence of CH···O hydrogen bonding; these are indicated by dashed lines in Figure 2.2.15b) than it does to O(26C) (3.63 Å), with the result that there are four O···H–C hydrogen-bond separations in the range 2.51 to 2.80 Å. This solvent molecule rather nicely illustrates the presence of the binding site at the *fac* tris-chelate vertices of the cages.

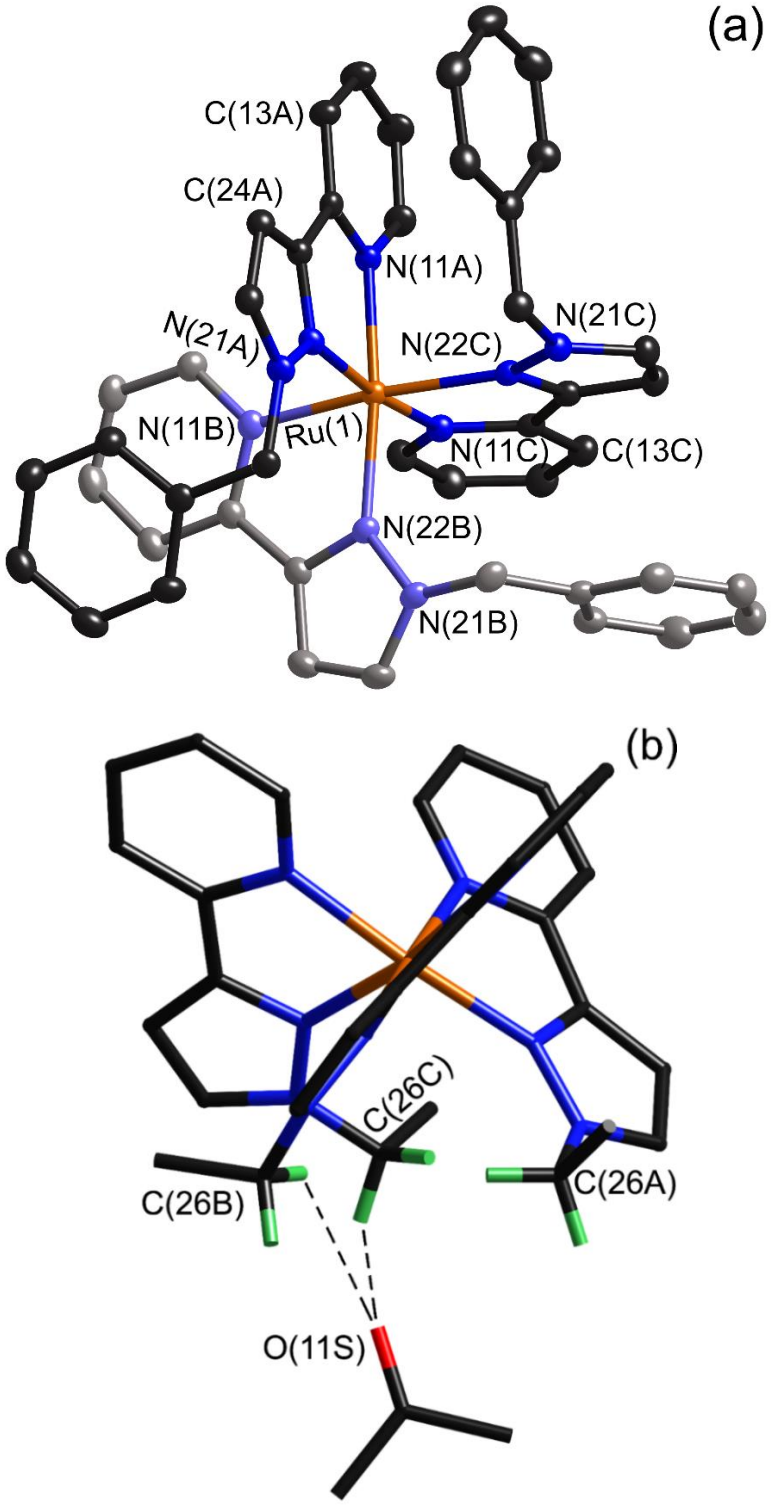

Figure 2.2.15 (a) Structure of the complex cation of *fac*-[Ru(L^{bz})$_3$](PF$_6$)$_2$·2Me$_2$CO (thermal ellipsoids at 40% probability level); one ligand is shown with paler colours for clarity. (b) Alternative view of the complex cation with the phenyl rings not shown, emphasising the convergent arrangement of methylene protons to form an hydrogen-bond donor site, and the presence of a hydrogen-bonded molecule of acetone at this site; the two shortest CH···O interactions are shown by dashed lines.

The X-ray crystal structure of *mer*-$[Ru(L^{bz})_3](PF_6)_2$ (Figure 2.2.16) shows that the structure of the complex cation is generally similar to that of *mer*-$[Co(L^{bz})_3](BF_4)_2$; the most obvious π-stacking interaction between ligands involves the pendant phenyl ring of ligand B (according to the numbering scheme of Figure 2.2.16) with the coordinated pyrazolyl-pyridine unit of ligand C. Compared to the *fac* isomer the divergent arrangement of the methylene protons no longer results in a specific hydrogen-bonding recognition site.

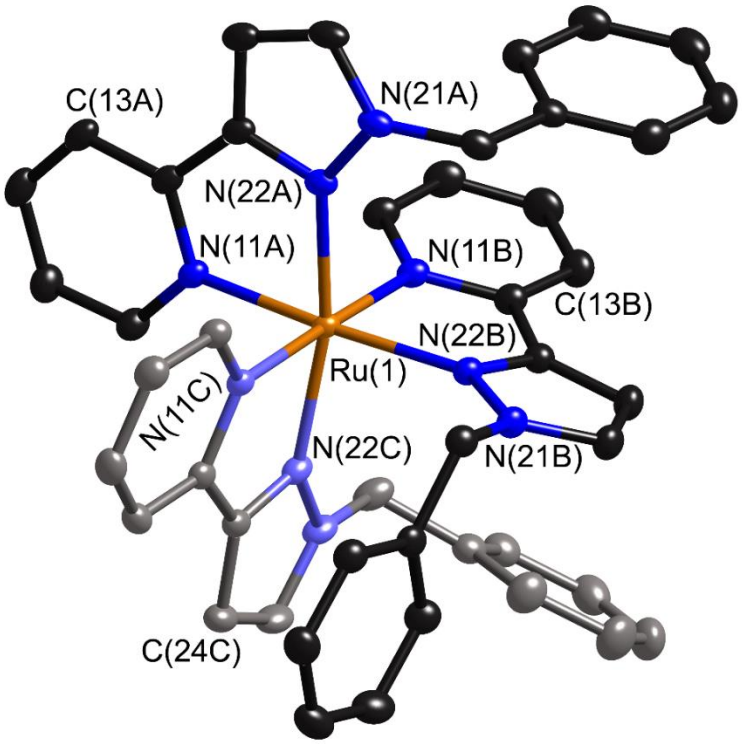

Figure 2.2.16 Structure of the complex cation of *mer*-$[Ru(L^{bz})_3](PF_6)_2 \cdot Me_2CO$ (thermal ellipsoids at 40% probability level); one ligand is shown with paler colours for clarity.

2.2.3 Measurement of guest binding to *fac*- and *mer*-$[Ru(L^{bz})_3](PF_6)_2$

To measure the differential abilities of *fac*- and *mer*-$[Ru(L^{bz})_3](PF_6)_2$ to act as a hydrogen-bond donor the equilibrium constant for adduct formation with isoquinoline- N-oxide was measured. On the basis of previous measurements using complete cages as hosts, this was identified as one of the strongest-binding guests in MeCN (K = 2100 M^{-1}, cf. Figure 2.1.3).[21] It was suggested that this is due to the high partial negative charge on the oxygen atom (high value of the hydrogen-bond acceptor parameter β), which interacts with the hydrogen-bond donor sites of the *fac* tris-chelate metal vertices of the cage, which have a combined hydrogen-bond donor ability comparable to that of phenol.[21]

A ^{1}H NMR titration (performed by Mr William Cullen) of *fac*-$[Ru(L^{bz})_3](PF_6)_2$ with isoquinoline- N-oxide in MeCN showed a steady shift in one of the signals from the diastereotopic CH_2 protons, but not the other which was essentially invariant (Figure 2.2.17). This is emphasised in Figure 2.2.17b which shows a series of superimposed ^{1}H NMR spectra recorded during the titration: the methylene doublet at 4.7 ppm does not move but the other signal at around 5.4 ppm shifts by ca. 0.1 ppm. No other proton signals moved significantly during the titration. The shift of one methylene proton signal but not the other is consistent with the O atom of the guest forming an hydrogen-bonding interaction with the inwardly-directed proton from each methylene group but not with the other proton which is externally directed. Free rotation about the C–C bonds of the benzyl substituents will be hindered by the aromatic stacking (*cf.* the crystal structure), which would prevent the 'inward' and 'outward' H atoms of each methylene group from exchanging position on the NMR timescale. The interaction with the isoquinoline-N-oxide necessarily involves one of these two protons more than the other – as is observed. Indeed the ^{1}H NMR spectrum confirms that the conformation observed in the crystal structure (Figure 2.2.15) is preserved in solution, as the signals for the coordinated pyrazolyl-pyridine ligand units of *fac*-$[Ru(L^{bz})_3](PF_6)_2$ are substantially shifted compared to those of *fac*-$[Ru(L^{H})_3](PF_6)_2$ and *fac*-$[Ru(L^{Me})_3](PF_6)_2$ by π-stacking with the pendant phenyl rings (see Experimental section for details).

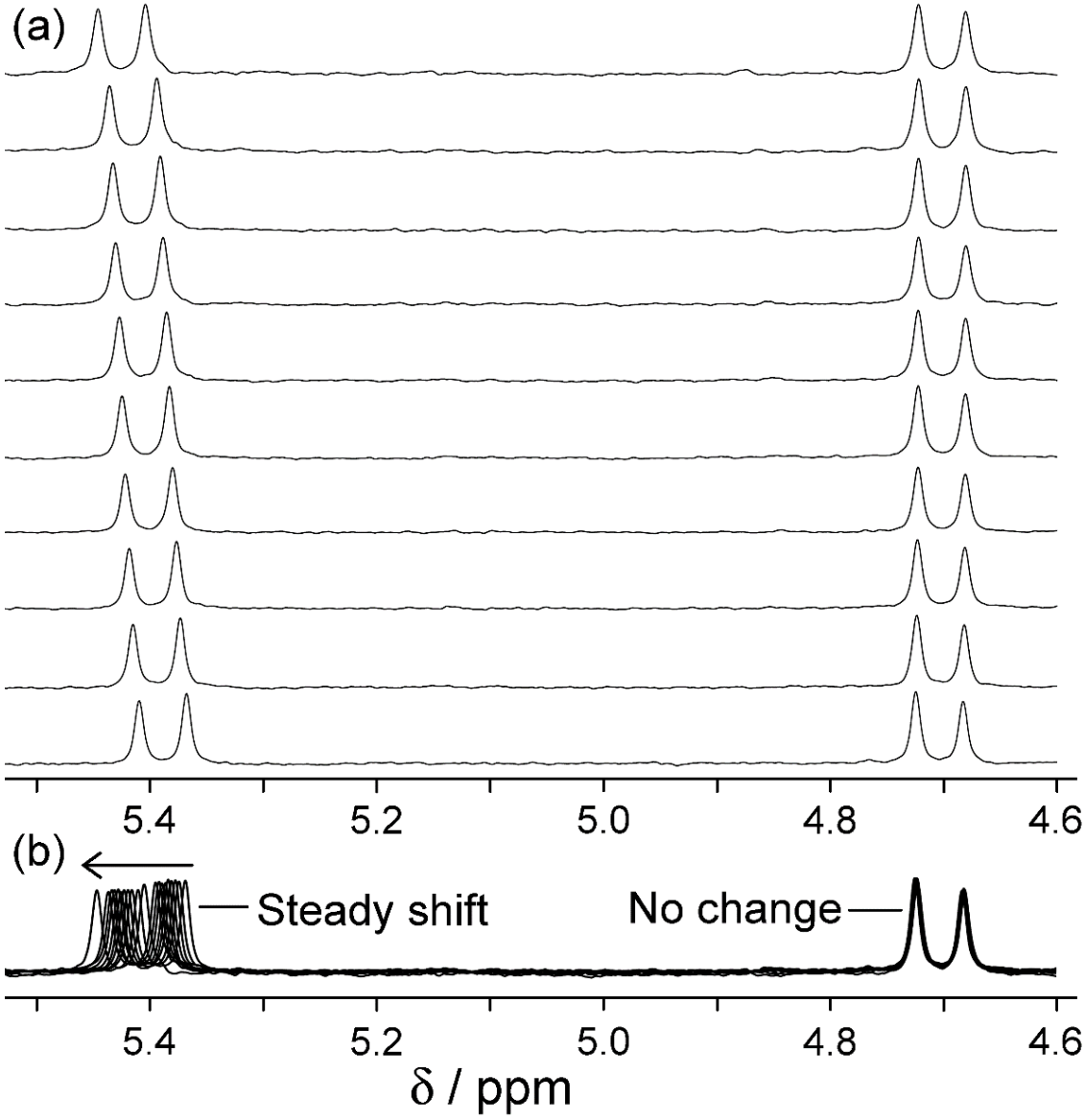

Figure 2.2.17 Changes in the ^{1}H NMR chemical shift of the two inequivalent methylene proton signals of *fac*-$[Ru(L^{bz})_3](PF_6)_2$ (0.23 mM) during titration with isoquinoline-N-oxide (up to 0.7 M) in CD_3CN. (a) Stacked plots; (b) overlaid plots to emphasise how one signal moves but the other does not.

It was apparent during the titration that complex formation was not complete even after a very large excess of isoquinoline- N-oxide was added, which is indicative of a low binding constant. The plot of chemical shift value for the methylene proton vs. (concentration of guest) gives a curve whose shape is consistent with 1 : 1 host/guest binding (Figure 2.2.18, data points shown as circles), and the calculated value of *K* from this is 1(±1) M^{-1}.[†] Thus an obvious interaction of *fac*-$[Ru(L^{bz})_3](PF_6)_2$ with isoquinoline-N-oxide that involves the methylene protons is seen, even if it is weak. Importantly however no such change in chemical shift of the methylene protons could be observed using the *mer* isomer; the change in chemical shift of a representative ^1H signal from a methylene proton is also shown in Figure 2.2.18 (data points shown as squares). Apart from the magnitude of the Δδ for this proton during the titration being much smaller, there is no significant curvature to the line, with the result that the association constant between *mer*-$[Ru(L^{bz})_3](PF_6)_2$ and isoquinoline-N-oxide in MeCN oxide is too weak even to estimate. There is therefore clear evidence that the convergent set of methylene protons associated with a *fac* tris-chelate site does act as an hydrogen-bond donor to isoquinoline- N-oxide, which supports our understanding of guest binding inside the complete cage cavities. However this binding constant is surprisingly low. Based on what was observed for binding inside the host cage (*K* = 2100 M^{-1}), this type of hydrogen-bonding interaction associated with mononuclear *fac*-$[Ru(L^{bz})_3](PF_6)_2$ – if it is similar to what happens inside a cage cavity – should give a much larger *K* value than was observed. For the $[Co_8(L^{1,5\text{-naph}})_{12}](BF_4)_{16}$/ isoquinoline-N-oxide complex that was reported earlier, the binding constant of *K* = 2100 M^{-1} gives ΔG = −19 kJ mol^{-1}.[21]

[†] Actually the curve-fitting software generates more precise values than these, of 0.8(±0.1) M^{-1} and 0.4(±0.1) M^{-1} for binding of isoquinoline-N-oxide to *fac*-$[Ru(L^{bz})_3](PF_6)_2$ and *fac*-$[Ru(L^{Me})_3](PF_6)_2$ respectively. However, as the binding is so weak, the curve fitting is based only on the early part of the binding curve, with <50% complex formation even in the presence of guest concentrations of up to 1 M. This means in practice that the errors are underestimated. Accordingly the value of K ≈ 1(±1) is quoted for both cases. Any difference in K between *fac*-$[Ru(L^{bz})_3](PF_6)_2$ and *fac*-$[Ru(L^{Me})_3](PF_6)_2$ is not significant for the purposes of this work; the important point is that the behaviour of the *fac* isomers is clearly distinct from that of the *mer* isomers.

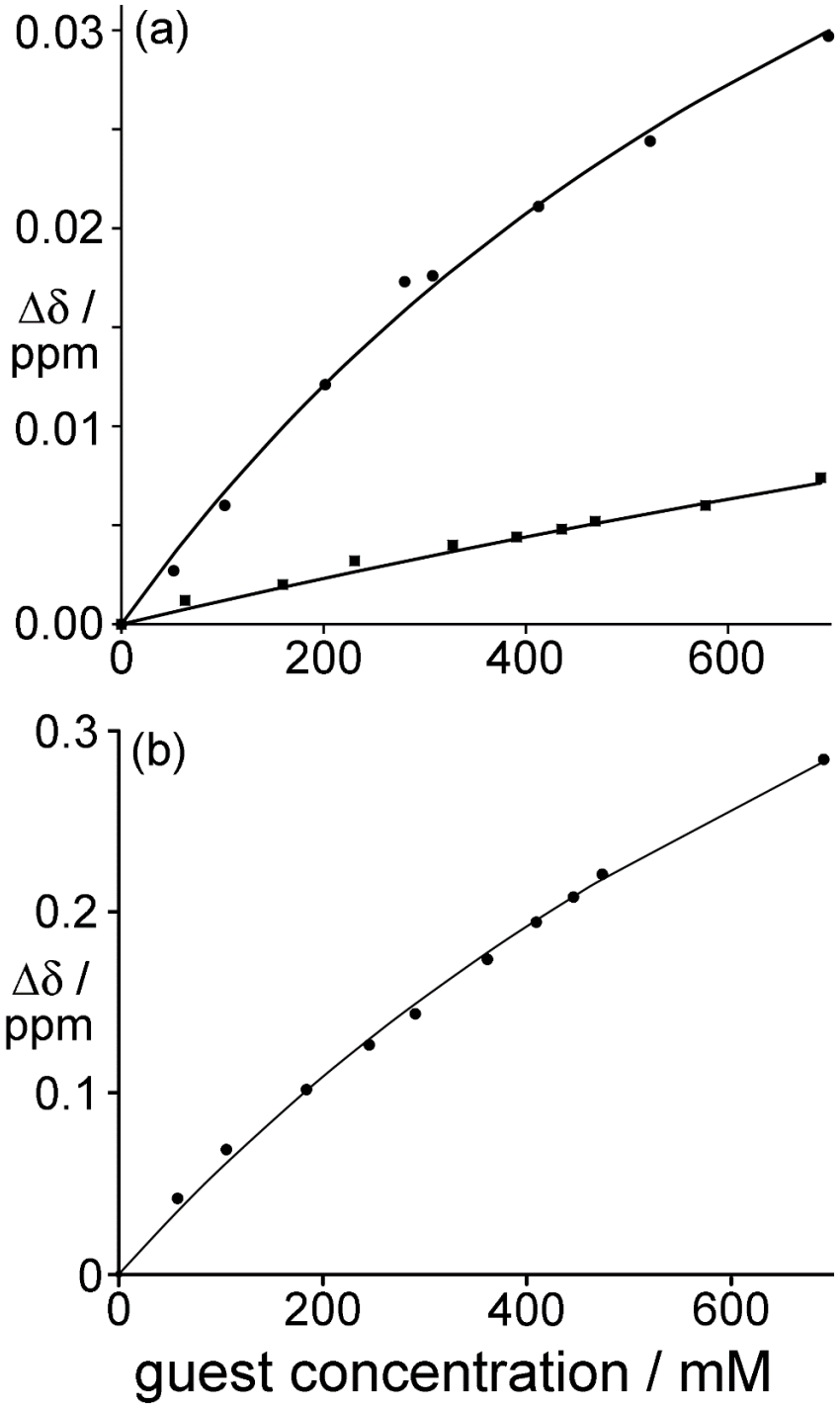

Figure 2.2.18 (a) ^{1}H NMR binding curves showing shift of the methylene proton signals in *fac*-[Ru(L^{bz})$_3$](PF$_6$)$_2$ (circles, upper line) and *mer*-[Ru(L^{bz})$_3$](PF$_6$)$_2$ (squares, lower line) during titration with isoquinoline- N-oxide. For *fac*-[Ru(L^{bz})$_3$](PF$_6$)$_2$ the data fit a 1 : 1 binding isotherm with $K \approx 1$ M^{-1}; for *mer*-[Ru(L^{bz})$_3$](PF$_6$)$_2$ the binding constant is too weak to measure. (b) ^{19}F NMR binding curve showing the change in environment of the [PF$_6$]$^-$ ion of *fac*-[Ru(L^{bz})$_3$](PF$_6$)$_2$ as it is displaced from the hydrogenbonding site when isoquinoline-N-oxide is added. Again the data fit a 1 : 1 binding isotherm with $K \approx 1$ M^{-1}.

Some of this arises from van der Waals interactions between the guest and the walls of the cage, and some from solvophobic effects, but even so the contribution from H-bonding alone was estimated to be several kJ mol^{-1} and it would be expected that this would be similar in the mononuclear model complex *fac*-$[Ru(L^{bz})_3](PF_6)_2$. Instead we see $K \approx 1\ M^{-1}$, giving ΔG for guest binding of more or less zero despite the same type of hydrogen-bonding interaction as occurs inside the cage cavity. One reason for this may be that competition for the hydrogen-bonding site from the hexafluorophosphate anions is occurring, which would weaken the *K* value for association with the neutral guest: but this competition of anions for the binding site does not occur in the complete cages for some reason. In mononuclear *fac*-$[Ru(L^{bz})_3](PF_6)_2$ the anions have free access to the relatively unhindered hydrogen-bonding site and could therefore be competing with binding of isoquinoline-N-oxide in solution. In contrast, in all structurally characterised examples of the $[M_8(L^{1,5\text{-naph}})_{12}]X_{16}$ cages, anions are located outside the cage cavities, with the H-bond donor sites occupied by small solvent molecules such as MeOH or water.[25] This suggests the possibility (but does not of course prove) that the anions may also be excluded from the cage cavity in solution. This would explain the much higher binding constants for guest binding in the cage, as competition from anions would be absent.

To check for competing anion-binding in *fac*-$[Ru(L^{bz})_3](PF_6)_2$, the titration between *fac*-$[Ru(L^{bz})_3](PF_6)_2$ and isoquinoline-N-oxide in MeCN was repeated but recording ^{19}F NMR spectra to see if there was any evidence for the hexafluorophosphate ion changing its environment. If there were no change it could be said that there was no significant cation/anion association in solution. In contrast, a shift of the ^{19}F NMR signal would suggest that the anion was being displaced from the hydrogen-bonding site by the added isoquinoline-N-oxide, and this is what is observed. The ^{19}F NMR signal of the $[PF_6]^-$ anion of *fac*-$[Ru(L^{bz})_3](PF_6)_2$ appeared as a doublet at −73.0 ppm which steadily shifted to −72.7 ppm as isoquinoline-N-oxide was titrated in. The resultant binding curve (Δδ vs. concentration of isoquinoline-N-oxide; Figure 2.2.18b) fitted well to a 1 : 1 isotherm with a value of *K* the same within error (≈1 M^{-1}) as that derived from the ^1H NMR titration (Figure 2.2.17 and 2.2.18).

Thus, binding of isoquinoline-N-oxide to the hydrogen-bond donor site of *fac*-$[Ru(L^{bz})_3](PF_6)_2$ is accompanied by displacement of $[PF_6]^-$. As a control experiment, the change in the ^{19}F NMR chemical

shift of the $[PF_6]^-$ anion of *mer*-$[Ru(L^{bz})_3](PF_6)_2$ during titration with isoquinoline-N-oxide was also measured; this resulted in a binding constant too small to measure accurately.

This confirms that there is ion-pairing between cation and anion in solution with PF_6^- interacting with the hydrogen- bond donor site of the *fac*-$[Ru(L^{bz})_3]^{2+}$ cation, and this competition provides one reason for the low value of *K* observed for binding of isoquinoline-N-oxide. An obvious experiment to try and mitigate this effect would be to use the anion tetraphenylborate which might be expected to form weaker ion pairs with the *fac*-$[Ru(L^{bz})_3]^{2+}$ cation; this experiment is described in the next section. A second contribution to the weak interaction between *fac*-$[Ru(L^{bz})_3](PF_6)_2$ and isoquinoline-N-oxide could be steric. The pendant benzyl groups of *fac*-$[Ru(L^{bz})_3](PF_6)_2$ may not be fully bent out of the way of the binding site in solution, but could move around blocking access to the hydrogen-bonding site. In the complete cages the hydrogen-bonding site is exposed because the bridging ligands have to stretch to an adjacent metal ion and are therefore stretched away from the binding site which is exposed to the cavity interior. However that may not be the case in *fac*-$[Ru(L^{bz})_3](PF_6)_2$ where steric interference from the pendant benzyl groups is possible. A control experiment to test this is to replace the pendant phenyl ring with an H atom which will remove any possible steric encumbrance, and this is also described in the next section.

2.2.4 Control experiment (1): measurement of guest binding to *fac*- and *mer*-$[Ru(L^{Me})_3](PF_6)_2$

Reaction of *fac*- or *mer*-$[Ru(L^{H})_3](PF_6)_2$ with MeI resulted in N-methylation of the pyrazolyl rings to give *fac*- or *mer*-$[Ru(L^{Me})_3](PF_6)_2$ respectively (see Figure 2.2.9 for ligand structure); again, by doing this reaction under mild conditions, the individual isomers retained their structural integrity with none of the alternate isomers forming (see Figure 2.2.19). Crystal structures are in Figure 2.2.20 and are as expected. In *fac*-$[Ru(L^{Me})_3](PF_6)_2$ there is no solvent molecule or other electron-rich atom occupying the hydrogen-bonding site, but the convergence of the methyl groups and the position of the hydrogen-bonding site is clear. Compared to *fac*-$[Ru(L^{bz})_3](PF_6)_2$, any possible steric hindrance to guest binding arising from the phenyl rings is now removed. Conversely, any possibly favourable effects – e.g. guest

binding being facilitated by π-stacking with the pendant phenyl rings around the binding pocket – will also be absent.

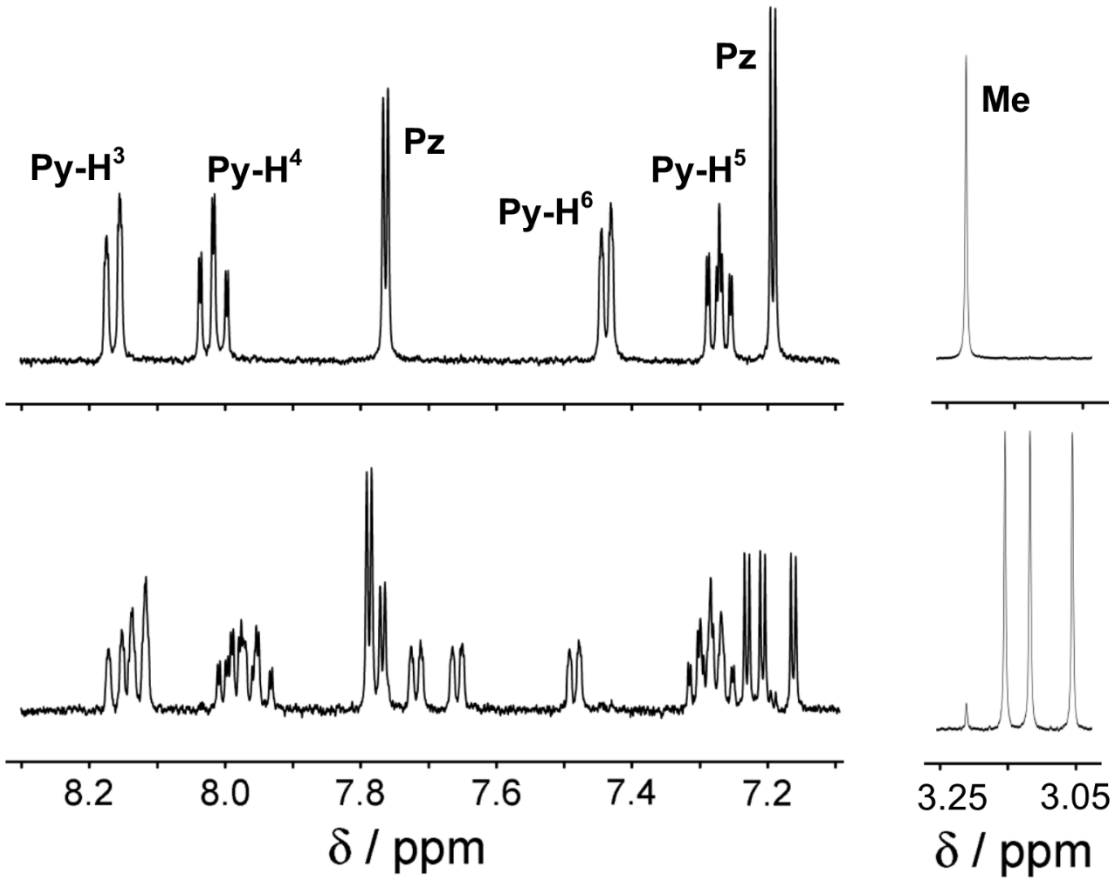

Figure 2.2.19 ^{1}H NMR spectra (CD_3CN, 400 MHz) of $[Ru(L^{Me})_3](PF_6)_2$: (top) *fac* isomer (Pz = pyrazole, Py = pyridine); (bottom) *mer* isomer.

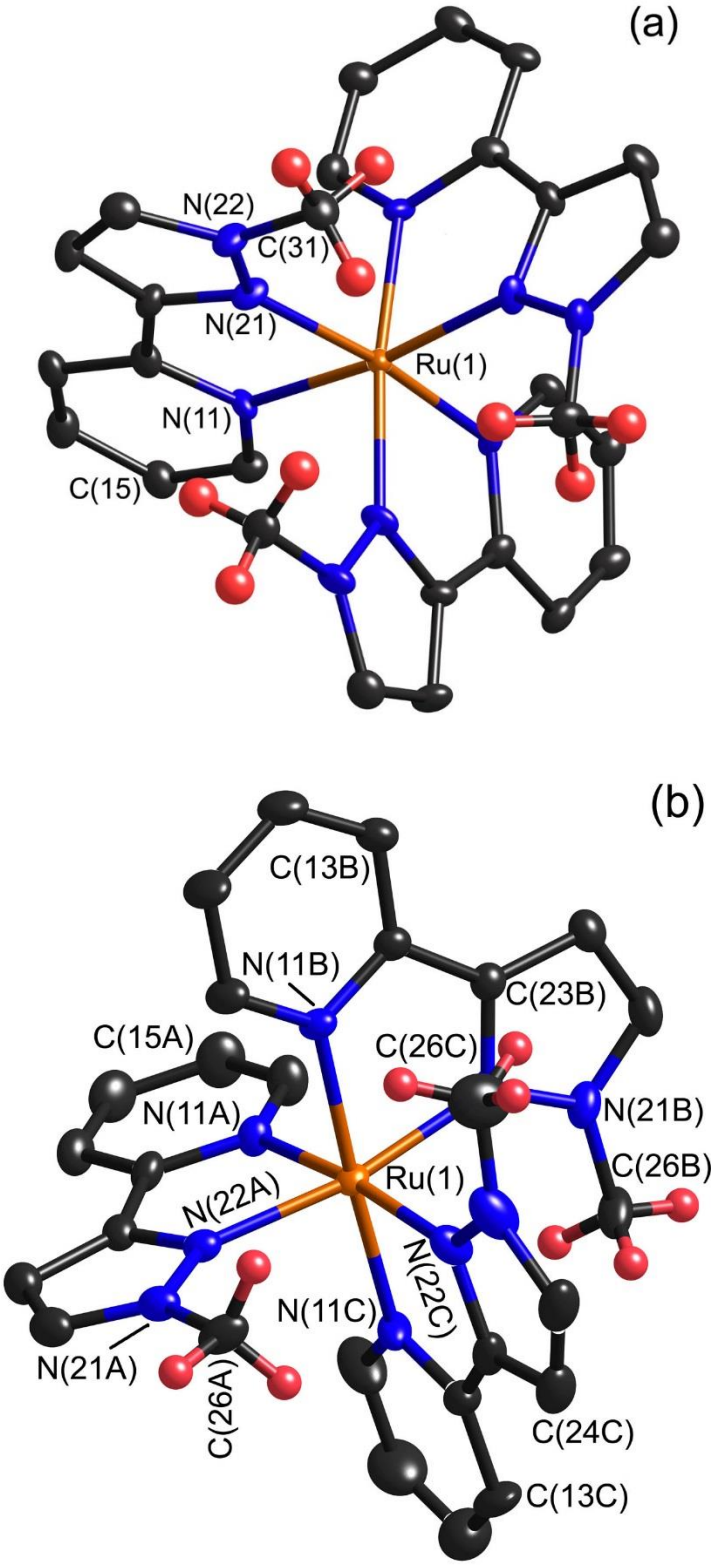

Figure 2.2.20 Structures of the complex cations of (a) *fac*-$[Ru(L^{Me})_3](PF_6)_2$ (thermal ellipsoids at 40% probability level) and (b) *mer*-$[Ru(L^{Me})_3](PF_6)_2$ (thermal ellipsoids at 30% probability level). H atoms of the methyl groups are shown in red to emphasise the binding pocket formed by convergence of the three methyl groups in the former case.

^{1}H NMR titrations (again performed by Mr William Cullen) of each isomer with isoquinoline-N-oxide in MeCN gave similar results to what was observed with *fac*- and *mer*-[Ru(L^{bz})$_3$](PF$_6$)$_2$. The *fac* isomer again demonstrated definite but weak binding with isoquinoline-N-oxide on the basis of a steady shift of the methyl protons (which are now all equivalent). The graph of Δδ vs. (concentration of guest) showed gentle curvature and could be fitted to a 1 : 1 binding isotherm (Figure 2.2.21) with, again, $K \approx 1(\pm 1)$ M^{-1}.[†] The interaction of *mer*-[Ru(L^{Me})$_3$](PF$_6$)$_2$ with isoquinoline-N-oxide in MeCN was insignificant, with much smaller Δδ for the methyl protons during the titration, and no detectable curvature in the graph. Again a clear difference is seen between the behaviour of the two geometric isomers, but the important point is that the weak binding observed for *fac*-[Ru(L^{bz})$_3$](PF$_6$)$_2$ is clearly not associated with any steric blocking of the binding site by the pendant phenyl rings. This leaves ion-pairing as the other possible culprit.

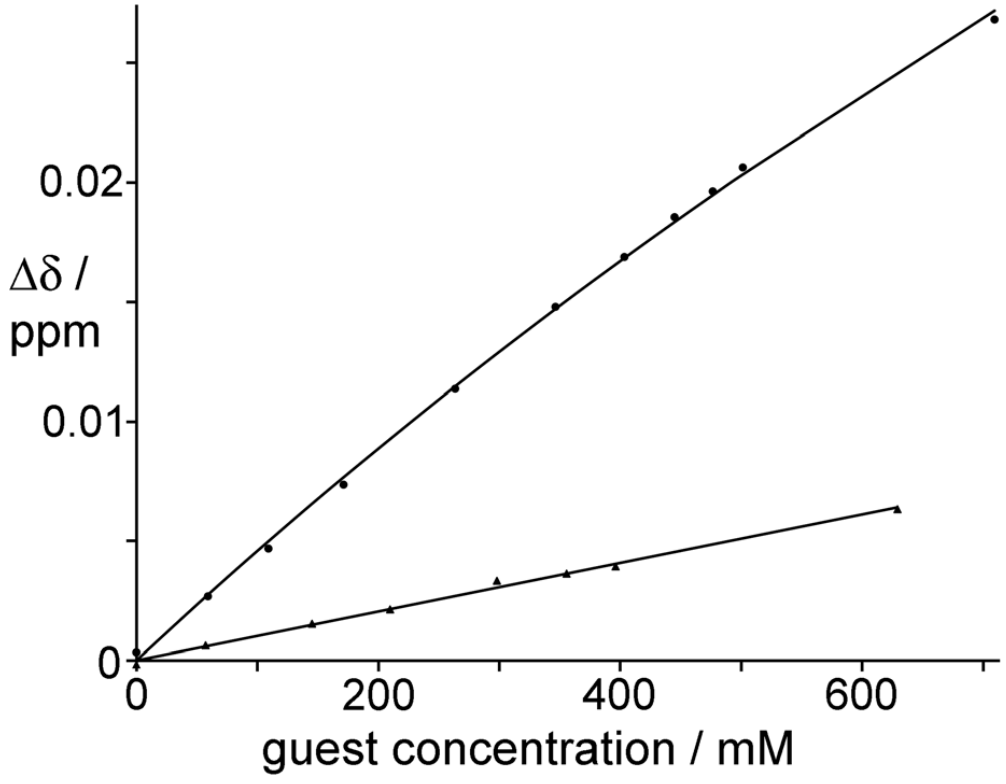

Figure 2.2.21 ^{1}H NMR binding curves showing shift of the methylene proton signals in *fac*-[Ru(L^{Me})$_3$](PF$_6$)$_2$ (circles, upper line) and *mer*-[Ru(L^{Me})$_3$](PF$_6$)$_2$ (triangles, lower line) during titration with isoquinoline-N-oxide. For *fac*-[Ru(L^{Me})$_3$](PF$_6$)$_2$ the data fit a 1 : 1 binding isotherm with $K \approx 1$ M−1; for *mer*-[Ru(L^{Me})$_3$](PF$_6$)$_2$ the binding constant is too weak to measure.

2.2.5 Control experiment (2): measurement of guest binding to *fac*-$[Ru(L^{bz})_3](BPh_4)_2$

For the second control experiment *fac*-$[Ru(L^{bz})_3]^{2+}$ was isolated as its tetraphenylborate salt, by simple anion metathesis starting from the hexafluorophosphate salt. The tetraphenylborate anion might be expected to result in less competition than the hexafluorophosphate ion for the hydrogen-bonding site of the cation. A ^{1}H NMR titration with isoquinoline-N-oxide resulted in a steady shift of the signals for one of the diastereotopic methylene protons of *fac*-$[Ru(L^{bz})_3]^{2+}$ but not the other, exactly as before (cf. Figure 2.2.17); again, the resulting binding curve fitted to a 1 : 1 binding isotherm with $K \approx 1(\pm 1)$ M^{-1}.[†] However, during the titration the ^{1}H NMR signals for the $[BPh_4]^-$ anion also shifted steadily, consistent with it being displaced as an ion-pair breaks up, in the same way as the $[PF_6]^-$ anion. The *K* value calculated from the shift of the most intense $[BPh_4]^-$ ^{1}H signal when it is displaced, is the same within experimental error as that derived from the shift of the methylene proton of the complex cation when the guest binds. Again, therefore, guest binding to the complex cation, and anion displacement, occur together (Figure 2.2.22).

This is somewhat surprising as the tetraphenylborate anion is not a hydrogen-bond acceptor. However ion-pairing with the *fac*-$[Ru(L^{bz})_3]^{2+}$ cation could occur in solution via charge-assisted π–π or CH–π interactions between electron-deficient pyrazolyl-pyridine groups that are coordinated to a 2+ metal centre, and the electron-rich phenyl rings of the anion (c.f. figure 2.2.4). Examples of such ion pairs involving tetraphenylborate as the anion are known.[41,42] Thus although hydrogen-bonding is not operative, the tetraphenylborate anion competes for binding to the complex cation just as much as does the hexafluorophosphate anion, which means that the interaction with isoquinoline- N-oxide remains weak.

The clear conclusion to be drawn from this is that the hydrogen-bonding recognition sites in the cubic coordination cage (Figure 2.1.3) are effective at facilitating guest binding in the cavity in MeCN because anions are excluded from the cavity which is consistent with all crystal structures of these cages with a

variety of anions and obtained from a variety of solvents.[21-23,25] Exclusion of anions from the binding site is therefore an important principle to take into account in design of new generations of cage hosts.

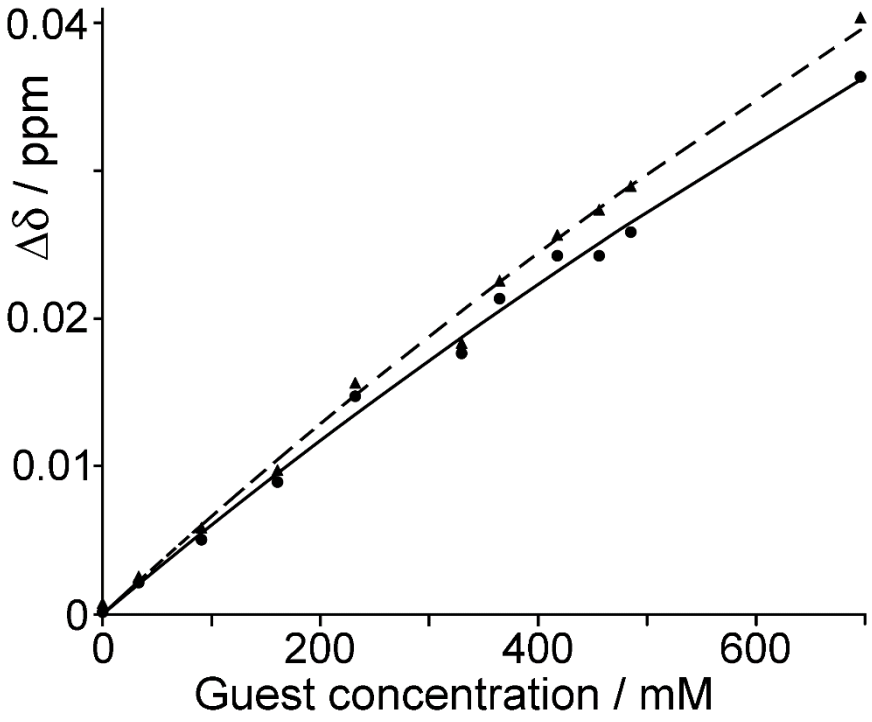

Figure 2.2.22 ^{1}H NMR binding curves obtained from titration of $[Ru(L^{Bz})_3](BPh_4)_2$ with isoquinoline-N-oxide in MeCN: the shift of the methylene proton signal at ca. 5.4 ppm due to hydrogen-bonding with the guest (black triangles/dashed line); (b) the shift of the most intense tetraphenylborate signal at 7.3 ppm as it is displaced from the complex cation by the competing guest (black circles/solid line). Both sets of data fit a 1 : 1 binding isotherm with $K \approx 1\ M^{-1}$.

2.3 Conclusion

There are three main conclusions from this work. Firstly, a simple and general synthetic procedure has been developed which will allow access to a wide range of substituted analogues of $[Ru(L^{H})_3]^{2+}$ as their pure *fac* and *mer* isomers without tedious chromatographic separation or relying on fractional crystallisation. The mixture of *fac*- and *mer*-$[Ru(L^{H})_3]^{2+}$ may be separated by reaction with a Cu(I) salt which allows the deprotonated *fac* isomer to precipitate as its Cu(I) adduct whilst the *mer* isomer remains in solution;[39] decomposition of the *fac*-$[Ru(L^{-})_3]^{-}$/Cu(I) adduct with acid liberates pure *fac*-

$[Ru(L^{H})_3]^{2+}$. Alkylation of the pyrazolyl *N*3 positions under mild conditions allows substituted analogues to be prepared with retention of isomeric integrity.

Secondly, it has been shown that *fac*-$[Ru(L^{bz})_3]^{2+}$ and *fac*-$[Ru(L^{Me})_3]^{2+}$ act as better hydrogen-bond donor sites to isoquinoline- N-oxide (*via* formation of C–H···O hydrogen bonds) than do their *mer* isomers, because of the convergent group of weakly δ+ methylene protons in the former cases. Absolute values of binding constants are low but the clear difference between the behaviour of the *fac* and *mer* isomers confirms our earlier supposition[21-23] that this specific recognition element – hydrogen bonding to methylene protons at a *fac* tris-chelate binding site – is involved in guest binding in coordination cages which incorporate metal complex vertices of this type.

Thirdly – and unexpectedly – in these simple mononuclear complexes the ability of the hydrogen-bond donor site of *fac*-$[Ru(L^{bz})_3]^{2+}$ or *fac*-$[Ru(L^{Me})_3]^{2+}$ to interact with the guest isoquinoline-N-oxide, which binds more strongly in the cavity of the cubic cage host in MeCN, is reduced by competition from anions – even those traditionally regarded as 'weakly interacting' such as hexafluorophosphate and tetraphenylborate. The effectiveness of the cubic cages as hosts for hydrogen-bond accepting guests therefore seems to rely not just on the presence of the two *fac* tris-chelate metal centres and their convergent group of CH protons, but also on the exclusion of anions from the cage cavity. All crystal structures of this family of cubic cages show that anions are located outside the cavity: although this does not prove that they cannot enter the cavity in solution, the difference in guest binding between the mononuclear model complexes reported in this work, and the same H-bonding site inside a cage cavity, does imply that in the latter case competition from anions is prevented. Thus we have two important design principles for future generations of host cages.

2.4 Experimental

3-(2-Pyridyl)pyrazole (L^H) was prepared by the literature method.[43] Metal salts and all organic reagents were purchased from Alfa or Sigma-Aldrich and used as received. NMR spectra were recorded on Bruker DRX 500 MHz, Bruker AV-III 400 MHz or AV-I 250 MHz instruments. Electrospray mass spectra were recorded on a Micromass LCT instrument. Calculation of 1 : 1 *K* values for guest binding from NMR titration data was performed using a program that has been reported previously.[44]

Synthesis of L^{bz}

A mixture of benzyl bromide (1.78 g, 10.4 mmol), 3-(2-pyridyl)-pyrazole (1.51 g, 10.4 mmol), THF (25 cm^3) and concentrated aqueous NaOH (20 M, 5 cm3) was stirred at 25 °C for 4 days. The organic layer was separated, dried over $MgSO_4$ and evaporated to dryness. The clear oil was washed with Et_2O resulting in precipitation of L^{bz} as a white solid. Yield: 1.55 g, 63%. ^{1}H NMR (250 MHz, $CDCl_3$): δ 8.65 (1H, ddd, *J* = 4.9, 1.9, 1.0 Hz; pyridyl H^6), 7.96 (1H, d, *J* = 7.8, 1.1 Hz; pyridyl H^3), 7.72 (1H, td, *J* = 7.8, 1.8 Hz; pyridyl H^4), 7.42 (1H, d, *J* = 2.3 Hz; pyrazolyl H^5), 7.39–7.24 (5H, m; ArH), 7.20 (1H, ddd, *J* = 7.6, 4.9, 1.1 Hz; pyridyl H^5), 6.92 (1H, d, *J* = 2.3 Hz; pyrazolyl H^4), 5.41 (2H, s; CH_2). ESMS: m/z 236.1 $[M + H]^+$. Found: C, 76.3; H, 5.4; N, 17.6%. Required for $C_{15}H_{13}N_3$: C, 76.6; H, 5.6; N, 17.9%. Data is in accordance with the literature.[45]

Synthesis of $[Co(L^{bz})_3](BF_4)_2$

A mixture of $Co(BF_4)_2$•$6H_2O$ (0.037 g, 0.11 mmol) in MeOH (5 cm^3) was added to a stirred solution of L^{bz} (0.077 g, 0.33 mmol) in CH_2Cl_2 (5 cm^3) and stirring was continued at temperature overnight. The solvent was removed under reduced pressure resulting in a pink residue. X-Ray quality crystals of the *mer* isomer were grown as orange blocks by dissolving the solid in the minimum amount of $CHCl_3$ followed by slow evaporation of the solvent. Yield: 0.11 g, 0.10 mmol, 93 %. ESMS: m/z 382 $\{[Co(L^{bz})_3]\}^{2+}$; 264 $\{[Co(L^{bz})_2]\}^{2+}$. Found: C, 57.7; H, 4.4; N, 13.2 %. Required for $[Co(L^{bz})_3](BF_4)_2$: C, 57.6; H. 4.2; N, 13.4 %. For ^{1}H NMR data, see main text.

Synthesis of $[Co(L^{bz})_2(OAc)_6]$

A mixture of $Co(OAc)_2 \cdot 4H_2O$ (0.073 g, 0.29 mmol) in MeOH (5 cm^3) was added to a stirred solution of L^{bz} (0.210 g, 0.89 mmol) in CH_2Cl_2 (5 cm^3) and stirring was continued at temperature overnight. The solvent was removed under reduced pressure resulting in a purple residue. X-Ray quality crystals were grown by slow evaporation of a solution of the residue in acetonitrile. Yield: 0.25 g (crude).

Synthesis of $[Ru(L^H)_3](PF_6)_2$

A mixture of $RuCl_3$ (1.00 g, 4.82 mmol), 3-(2-pyridyl)-pyrazole (2.24 g, 15.43 mmol, 3.2 equiv.) and ethylene glycol (40 cm^3) was heated to reflux with stirring for 48 h. After cooling the red mixture, excess ligand was removed by washing with chloroform. Saturated aqueous KPF_6 was added to precipitate the complex which was extracted from the suspension with several portions of CH_2Cl_2. The combined organic extracts were dried over Na_2SO_4, and the solvent removed in vacuo to yield a golden yellow solid (3.71 g, 93 %). ESMS: m/z 682 $(M - PF_6)^+$, 268 $(M - 2PF_6)^{2+}$. The ^1H NMR spectrum revealed a statistical (3:1) mixture of *mer* and *fac* isomers (see main text). Slow diffusion of diisopropyl ether or toluene vapour into a solution of the complex in acetonitrile over a few weeks afforded a mixture of yellow crystals of *mer*-$[Ru(L^H)_3](PF_6)_2$ and red crystals of *fac*,*fac*-$[Ru(L^H)_3Ru(L^-)_3](PF_6)$.

Separation of $[Ru(L^H)_3](PF_6)_2$ into *fac* and *mer* isomers

Step (i): precipitation of the *fac* isomer as its Cu(I) adduct. A mixture of $[Ru(L^H)_3](PF_6)_2$ (mixture of isomers from previous preparation; 0.87 g, 1.05 mmol), Et_3N (0.6 cm^3, 4.33 mmol), $Cu(BF_4)_2 \cdot 6H_2O$ (1.43 g, 4.14 mmol) and methanol (75 cm^3) was heated to reflux with stirring for 16 h. After cooling to room temperature, the orange precipitate of crude $[\{Ru(L^-)_3\}_2Cu_3](PF_6)$ was filtered off and washed with methanol and diethyl ether. This complex was dissolved in dichloromethane and some green precipitate [unreacted Cu(II) starting material] filtered off, before removing the solvent in vacuo to leave an orange solid which was pure $[\{Ru(L^-)_3\}_2Cu_3](PF_6)$. Yield: 0.11 g, 0.08 mmol, 15 % (60 % with respect to the *fac* isomer). ESMS: m/z 1258.1 $(M - PF_6)^+$. The ^1H NMR spectrum was consistent with the reported one.[39]

Step (ii): isolation and purification of *mer*-[Ru(L^H)$_3$](PF$_6$)$_2$. The remaining filtrate after precipitation of [Ru$_2$Cu$_3$(PyPz)$_6$](PF$_6$) [step (i), above] contains *mer*-[Ru(L^H)$_3$](PF$_6$)$_2$ which did not precipitate. This solution was evaporated to dryness. The residue was redissolved in with CH_2Cl_2 (100 cm^3) and a green solid by-product was filtered off and discarded. To the filtrate was added trifluoroacetic acid (2 cm^3, 1.44 mmol) to neutralise the Et_3N and ensure that the *mer*-[Ru(L^H)$_3$](PF$_6$)$_2$ remained fully protonated at the pyrazolyl *N*3 positions. Excess trifluoroacetic acid was removed by repeatedly dissolving the mixture in methanol/dichloromethane (1 : 1) and evaporation to dryness. The residue was then dissolved in dichloromethane; aqueous KPF_6 was added and the mixture shaken vigorously. The organic layer was separated, dried over $MgSO_4$, and the solvent removed in vacuo. Chromatography on silica eluting with MeCN/water/saturated $KNO_{3(aq)}$ (100 : 10 : 1) on a silica column resulted in a yellow band which was collected. After removing acetonitrile by rotary evaporation, excess saturated aqueous KPF_6 was added and the product was extracted into dichloromethane. The organic layer was separated, dried over $MgSO_4$, and the solvent removed in vacuo to yield *mer*-[Ru(L^H)$_3$](PF$_6$)$_2$ as a yellow solid (Yield: 0.51 g, 59 %). ^{1}H NMR (400 MHz, $(CD_3)_2CO$): δ 8.47 – 8.32 (3H, m; 3 x pyridyl H^4), 8.18 – 8.01 (6H, m; 3 x pyridyl H^6 and 3 x pyrazolyl H^5), 7.92 - 7.79 (3H, m; 3 x pyridyl H^3), 7.53 – 7.31 (6H, m; 3 x pyrazolyl H^4 and 3 x pyridyl H^5). ESMS: m/z 682 $(M - PF_6)^+$, 268 $(M - 2PF_6)^{2+}$.

Step (iii): isolation and purification of *fac*-[Ru(L^H)$_3$](PF$_6$)$_2$. To a solution of [{Ru(L^-)$_3$}$_2$Cu$_3$](PF$_6$) (0.11 g, 0.08 mmol) in CH_2Cl_2 (10 cm^3) was added trifluoroacetic acid (1 cm^3, 0.72 mmol), causing an immediate colour change from deep orange to yellow. Excess trifluoroacetic acid was removed by repeatedly dissolving the mixture in methanol/dichloromethane (1 : 1) and evaporation to dryness. The residue was then dissolved in dichloromethane; aqueous KPF_6 was added and the mixture shaken vigorously. The organic layer was separated, dried over $MgSO_4$, and the solvent removed in vacuo to leave pure *fac*-[Ru(L^H)$_3$](PF$_6$)$_2$ as a yellow solid. Yield: 0.14 g, 99 %. ^{1}H NMR (400 MHz, $(CD_3)_2CO$): δ 8.41 (1H, ddd, *J* = 8.0, 1.6, 0.8 Hz; pyridyl H^4), 8.12 (1H, td, *J* = 7.9, 1.5 Hz; pyridyl H^6), 8.07 (1H, d, *J* = 2.9 Hz; pyrazolyl H^5), 7.83 (1H, ddd, *J* = 5.7, 1.5, 0.8 Hz; pyridyl H^3), 7.44

(1H, d, J = 2.9 Hz; pyrazolyl H^4), 7.42 (1H, ddd, J = 7.9, 5.7, 1.5; pyridyl H^5). ESMS: m/z 682 $(M - PF_6)^+$, 268 $(M - 2PF_6)^{2+}$.

Synthesis of *fac*-[Ru(L^{bz})$_3$](PF$_6$)$_2$

A mixture of *fac*-[Ru(L^H)$_3$](PF$_6$)$_2$ (0.06 g, 0.07 mmol), benzyl bromide (0.1 cm^3, 0.82 mmol), Cs_2CO_3 (0.33 g, 1.00 mmol), Bu_4NI (0.12 g, 0.33 mmol) and CH_2Cl_2 (25 cm^3) was heated to reflux in the dark with stirring for 24 h. After cooling to room temperature, excess Cs_2CO_3 was filtered off and the solvent removed by rotary evaporation, before purification of the yellow solid by column chromatography on silica. Elution with MeCN/water/saturated aqueous KNO_3 (100 : 10 : 2) resulted in a single yellow band moving down the column which was collected. After removing acetonitrile by rotary evaporation, excess saturated aqueous KPF_6 was added and the product was extracted from the suspension into dichloromethane. The organic layer was separated, dried over $MgSO_4$, and the solvent removed in vacuo to yield *fac*-[Ru(L^{bz})$_3$](PF$_6$)$_2$ as a yellow solid. Slow diffusion of di-isopropyl ether vapour into a solution of the complex in acetone afforded the product as yellow needles. Yield: 0.01 g, 85 %. ^{1}H NMR (400 MHz, $(CD_3)_2CO$): δ 8.10 (1H, d, J = 2.9 Hz; pyrazolyl), 8.05 (1H, td, J = 7.8, 1.5 Hz; pyridyl H^4), 7.95 (1H, d, J = 8.0 Hz; pyridyl H), 7.52 (1H, d, J = 5.4 Hz; pyridyl H), 7.41 (1H, ddd, J = 7.4, 5.6, 1.5 Hz; pyridyl H), 7.21 (1H, t, J = 7.5 Hz; phenyl H^4), 7.14 (1H, d, J = 2.9 Hz; pyrazolyl), 7.05 (2H, t, J = 7.8 Hz; phenyl H^3/H^5), 6.22 (2H, d, J = 7.8 Hz; phenyl H^2/H^6), 5.73 (1H, d, J = 17.0 Hz; CH_2), 5.06 (1H, d, J = 17.0 Hz; CH_2). ESMS: m/z 952.2 $(M - PF_6)^+$, 403.6 $(M - 2PF_6)^{2+}$. Found: C, 48.1; H, 3.6; N, 11.0. $C_{45}H_{39}F_{12}N_9P_2Ru$•$2H_2O$ requires C, 47.7; H, 3.8; N, 11.1%. UV/Vis in MeCN [λ_{max}/nm (10^{-3} ε/M^{-1} cm^{-1})]: 399 (15.4), 284 (52.0), 241 (41.6).

Synthesis of *mer*-[Ru(L^{bz})$_3$](PF$_6$)$_2$

This was prepared according to the method above for *fac*-[Ru(L^{bz})$_3$](PF$_6$)$_2$, but using *mer*-[Ru(L^H)$_3$](PF$_6$)$_2$ (0.23 g, 0.27 mmol), benzyl bromide (0.5 cm^3, 4.21 mmol), Cs_2CO_3 (0.49 g, 1.52 mmol) and acetonitrile (50 cm^3). Yield: 81%. Slow diffusion of di-isopropyl ether vapour into a solution of the complex in acetone after two weeks affords the product as yellow blocks. ^{1}H NMR (400 MHz, $(CD_3)_2CO$): δ 8.42 (1H, d, J = 8.0 Hz), 8.22 (1H, d, J = 2.9 Hz), 8.11 (1H, td, J = 7.9, 1.5 Hz), 8.07 (1H,

d, *J* = 2.9 Hz), 8.02 – 7.97 (3H, m), 7.94 (1H, d, *J* = 5.6 Hz), 7.91 (1H, td, *J* = 7.9, 1.5 Hz), 7.75 (1H, d, *J* = 5.6 Hz) 7.66 (1H, d, *J* = 8.0 Hz), 7.63 (1H, d, *J* = 2.9 Hz), 7.55 (1H, d, *J* = 5.6 Hz), 7.49 – 7.42 (2H, m), 7.34 (1H, ddd, *J* = 7.9, 5.6, 1.5 Hz), 7.30 – 7.12 (8H, m), 7.05 (2H, t, *J* = 7.7 Hz), 6.96 (1H, d, *J* = 2.9 Hz), 6.53 (2H, d, *J* = 7.4 Hz), 6.39 (2H, d, *J* = 7.4 Hz), 6.21 (2H, d, *J* = 7.4 Hz), 5.44 (2H, d, *J* = 16.7 Hz), 5.03 (1H, d, *J* = 16.7 Hz), 4.91 (1H, d, *J* = 16.7 Hz), 4.71 (2H, m). ESMS: m/z 952.2 $(M - PF_6)^+$, 403.6 $(M - 2PF_6)^{2+}$. Found: C, 48.8; H, 3.8; N, 10.7. $C_{45}H_{39}F_{12}N_9P_2Ru \cdot H_2O \cdot (acetone)_{0.5}$ requires C, 48.8; H, 3.9; N, 11.0%. UV/Vis in MeCN [λ_{max}/nm (10^{-3} ε/M^{-1} cm^{-1})]: 396 (13.9), 282 (49.8), 241 (38.5).

Synthesis of *fac*-[Ru(L^{Me})$_3$](PF$_6$)$_2$

A mixture of *fac*-[Ru(L^{H})$_3$](PF$_6$)$_2$ (0.06 g, 0.07 mmol), methyl iodide (0.2 cm^3, 3.9 mmol), Cs_2CO_3 (0.16 g, 0.49 mmol) and CH_2Cl_2 (30 cm^3) was heated to reflux in the dark with stirring for 14 h. Subsequent workup and purification was as described above for *fac*-[Ru(L^{bz})$_3$](PF$_6$)$_2$. Yield: 0.05 g, 73%. Slow diffusion of di-isopropyl ether vapour into a solution of the complex in acetone afforded the product as yellow blocks. ^{1}H NMR (400 MHz, $(CD_3)_2CO$): δ 8.43 (1H, ddd, *J* = 8.1, 5.0, 0.7 Hz; pyridyl H^6), 8.15 (1H, td, *J* = 7.8, 1.4 Hz; pyridyl H^4), 8.10 (1H, d, *J* = 2.8 Hz; pyrazolyl H^5), 7.74 (1H, ddd, *J* = 5.6, 1.5, 0.7 Hz; pyridyl H^3), 7.48 (1H, d, *J* = 2.8 Hz; pyrazolyl H^4), 7.45 (1H, ddd, *J* = 7.8, 5.6, 1.5 Hz; pyridyl H^5), 3.52 (3H, s; CH_3). ESMS: m/z 724 $(M - PF_6)^+$, 290 $(M - 2PF_6)^{2+}$. Found: C, 37.4; H, 3.1; N, 14.3. $C_{27}H_{27}F_{12}N_9P_2Ru$ requires C, 37.3; H, 3.1; N, 14.5%. UV/Vis in MeCN [λ_{max}/nm (10^{-3} ε/M^{-1} cm^{-1})]: 400 (15.5), 281 (49.2), 238 (40.4).

Synthesis of *mer*-[Ru(L^{Me})$_3$](PF$_6$)$_2$

This was prepared using *mer*-[Ru(L^{H})$_3$](PF$_6$)$_2$ (0.06 g, 0.07 mmol), methyl iodide (0.2 cm^3, 3.9 mmol), Cs_2CO_3 (0.16 g, 0.49 mmol) and CH_2Cl_2 (30 cm^3) exactly as described above for the *fac* isomer. Yield: 0.05 g, 73%. Slow diffusion of di-isopropyl ether vapour into a solution of the complex in acetone afforded the product as yellow blocks. ^{1}H NMR (400 MHz, $(CD_3)_2CO$): δ 8.47 – 8.35 (3H, m), 8.16 – 8.06 (6H, m), 8.04 (1H, d, *J* = 5.6 Hz), 7.98 (1H, d, *J* = 5.6 Hz), 7.79 (1H, d, *J* = 5.6 Hz), 7.53 (1H, d, *J* = 7.53 Hz), 7.51 – 7.40 (5H, m), 3.47 (3H, s; CH_3), 3.41 (3H, s; CH_3), 3.35 (3H, s; CH_3). ESMS: m/z

724 $(M - PF_6)^+$, 290 $(M - 2PF_6)^{2+}$. Found: C, 37.4; H, 3.1; N, 14.3. $C_{27}H_{27}F_{12}N_9P_2Ru$ requires C, 37.3; H, 3.1; N, 14.5%. UV/Vis in MeCN [λ_{max}/nm (10^{-3} ε/M^{-1} cm^{-1})]: 397 (15.8), 281 (54.2), 239 (41.8).

2.5 X-ray crystallography

Crystals were removed from the mother liquor, coated with oil, and transferred rapidly to a stream of cold N_2 on the diffractometer (Bruker APEX-2) to prevent any decomposition due to solvent loss. In all cases, after integration of the raw data, and before merging, an empirical absorption correction was applied (SADABS)[46] based on comparison of multiple symmetry-equivalent measurements. The structures were solved by direct methods and refined by full-matrix least squares on weighted F^2 values for all reflections using the SHELX suite of programs.[47]

Most of the structural determinations were straightforward; the only problems were that *mer*-$[Ru(L^H)_3](PF_6)_2 \cdot 2MeCN$ and *mer*-$[Ru(L^{Me})_3](PF_6)_2$ required a large number of restraints to assist with the refinement. Crystals of *mer*-$[Ru(L^H)_3](PF_6)_2 \cdot 2MeCN$ diffracted weakly and only data with $2\theta < 46°$ were used for the final refinement; global restraints (SIMU and DELU on all ligand C and N atoms) were used to keep the displacement parameters reasonable. In *mer*-$[Ru(L^{Me})_3](PF_6)_2$ one of the hexafluorophosphate anions was disordered over two sites. Weak diffraction meant that global restraints (SIMU and DELU on all C, F and N atoms) were used to keep the displacement parameters reasonable, and in addition geometric restraints were applied to some of the ligand rings to prevent the geometries from becoming too eccentric.

Summary of crystallographic data for the new crystal structures:

Complex	*mer*-$[Co(L^{bz})_3](BF_4)_2 \cdot CHCl_3 \cdot H_2O$	*mer*-$[Co(L^{bz})_3](BPh_4)_2$	$[Co_3(L^{bz})_2(OAc)_6]\cdot 2MeCN$
Formula	$C_{46}H_{42}B_2Cl_3CoF_8N_9O$	$C_{93}H_{79}B_2CoN_9$	$C_{46}H_{50}Co_3N_8O_{12}$
Molecular weight	1075.79	1403.20	1083.73
T, K	100(2)	100(2)	100(2)
Crystal system	Monoclinic	Monoclinic	Triclinic
Space group	*P*2(1)/c	*P*2(1)/n	*P*-1
a, Å	12.2347(3)	13.3398(5)	9.1527(5)
b, Å	31.6797(9)	22.8481(8)	10.6804(5)
c, Å	13.5802(4)	24.3691(8)	13.7357(7)
α,°	90	90	72.134(2)
β,°	115.6540(10)	97.701(2)	73.533(2)
γ,°	90	90	72.657(2)
V, $Å^3$	4744.7(2)	7360.4(4)	1192.32(11)
Z	4	4	1
ρ, g cm^{-3}	1.503	1.266	1.509
Crystal size, mm^3	0.25 x 0.30 x 0.40	0.50 x 0.20 x 0.20	0.40 x 0.40 x 0.20
μ, mm^{-1}	0.610	0.289	1.102
Data, restraints, parameters	10912, 0, 619	16875 / 0 / 946	5284 / 0 / 317
Final *R*1, *wR2*[a]	0.0628, 0.1655	0.0467, 0.1435	0.0551, 0.1721

$[Co(L^{bz})_2(L^{N\text{-}ox})](PF_6)$	*fac,fac*-$[Ru(L^H)_3Ru(L^-)_3](PF_6)\cdot 3C_7H_8$	*mer*-$[Ru(L^H)_3](PF_6)_2 \cdot 2MeCN$
$C_{39}H_{32}CoF_6N_7O_2P$	$C_{69}H_{63}F_6N_{18}PRu_2$	$C_{28}H_{27}F_{12}N_{11}P_2Ru$
834.62	1491.5	908.62
100(2)	100(2)	100(2)
Triclinic	Trigonal	Monoclinic
P-1	*P*–3	*P*2(1)/c
10.8745(6)	14.1604(10)	14.3036(9)
11.9720(7)	14.1604(10)	13.2235(8)
17.0547(9)	19.0761(14)	23.5081(16)
72.081(3)	90	90
78.303(4)	90	121.776(4)
68.771(3)	120	90
1958.81(19)	3312.6(4)	3779.9(4)
2	2	4
1.415	1.495	1.597
0.30 x 0.24 x 0.09	0.02 x 0.02 x 0.03	0.25 x 0.30 x 0.40
0.551	0.555	0.596
9457 / 35 / 502	5090, 0, 292	5413, 327, 491
0.0782, 0.2369	0.0506, 0.1594	0.0858, 0.2955

fac-$[Ru(L^{bz})_3](PF_6)_2$ •$2Me_2CO$	*mer*-$[Ru(L^{bz})_3](PF_6)_2$ •Me_2CO	*fac*-$[Ru(L^{Me})_3](PF_6)_2$	*mer*-$[Ru(L^{Me})_3](PF_6)_2$
$C_{51}H_{51}F_{12}N_9O_2P_2Ru_2$	$C_{48}H_{45}F_{12}N_9OP_2Ru$	$C_{27}H_{27}F_{12}N_9P_2Ru_2$	$C_{27}H_{27}F_{12}N_9P_2Ru_2$
1213.02	1154.94	868.59	868.59
100(2)	100(2)	100(2)	100(2)
Triclinic	Triclinic	Trigonal	Monoclinic
P–1	*P*–1	*P*3*c*1	$P2_1/c$
11.1447(2)	11.7741(3)	10.3032(3)	13.8161(5)
12.2542(3)	12.1017(3)	10.3032(3)	13.2773(5)
20.6452(4)	17.9981(4)	17.0022(5)	20.7149(7)
93.7290(10)	99.8650(10)	90	90
95.9190(10)	96.3270(10)	90	117.692(2)
111.0040(10)	107.5040(10)	120	90
2602.28(9)	2373.61(10)	1563.08(8)	3364.7(2)
2	2	2	4
1.548	1.616	1.845	1.715
0.20 x 0.20 x 0.50	0.30 x 0.18 x 0.12	0.18 x 0.19 x 0.25	0.05 x 0.31 x 0.35
0.456	0.494	0.714	0.664
11756, 0, 698	10838, 0, 660	2421, 1, 156	7735, 391, 503
0.0465, 0.1346	0.0260, 0.0680	0.0464, 0.1263	0.0634, 0.1538

[a] The value of R1 is based on 'observed' data with $I>2\sigma(I)$; the value of wR2 is based on all data.

2.6 References

1. B. Breiner, J. K. Clegg and J. R. Nitschke, *Chem. Sci.*, 2011, **2**, 51.

2. D. Ajami and J. Rebek, Jr., *Acc. Chem. Res.*, 2013, **46**, 990.

3. L. Adriaenssens and P. Ballester, *Chem. Soc. Rev.*, 2013, **42**, 3261.

4. M. Yoshizawa, J. K. Klosterman and M. Fujita, *Angew. Chem. Int. Ed.*, 2009, **48**, 3418.

5. S. Ma, M. M. J. Smulders, Y. R. Hristova, J. K. Clegg, T. K. Ronson, S. Zarra and J. R. Nitschke, *J. Am. Chem. Soc.*, 2013, **135**, 5678.

6. Y. Fang, T. Murase and M. Fujita, *Chem.-As. J.*, 2014, **9**, 1321.

7. S. Horiuchi, T. Murase and M. Fujita, *Chem.-As. J.*, 2011, **6**, 1839.

8. T. Murase, S. Horiuchi and M. Fujita, *J. Am. Chem. Soc.*, 2010, **132**, 2866.

9. S. Horiuchi, Y. Nishioka, T. Murase and M. Fujita, *Chem. Commun.*, 2010, **46**, 3460.

10. C. J. Hastings, R. G. Bergman and K. N. Raymond, *Chem.-Eur. J.*, 2014, **20**, 3966.

11. Z. J. Wang, K. N. Clary, R. G. Bergman, K. N. Raymond and F. D. Toste, *Nat. Chem.*, 2013, **5**, 100.

12. C. J. Brown, G. M. Miller, M. W. Johnson, R. G. Bergman and K. N. Raymond, *J. Am. Chem. Soc.*, 2011, **133**, 11964.

13. J. E. M. Lewis, E. L. Gavey, S. A. Cameron and J. D. Crowley, *Chem. Sci.*, 2012, **3**, 778.

14. B. Therrien, G. Suess-Fink, P. Govindaswamy, A. K. Renfrew and P. J. Dyson, *Angew. Chem. Int. Ed.*, 2008, **47**, 3773.

15. R. Custelcean, *Chem. Soc. Rev.*, 2014, **43**, 1813.

16. R. Custelcean, *Chem. Commun.*, 2013, **49**, 2173.

17. R. Custelcean, P. V. Bonnesen, N. C. Duncan, X. Zhang, L. A. Watson, G. Van Berkel, W. B. Parson and B. P. Hay, *J. Am. Chem. Soc.*, 2012, **134**, 8525.

18. R. Custelcean, J. Bosano, P. V. Bonnesen, V. Kertesz and B. P. Hay, *Angew. Chem. Int. Ed.*, 2009, **48**, 4025.

19. S. Yi, V. Brega, B. Captain and A. E. Kaifer, *Chem. Commun.*, 2012, **48**, 10295.

20. C. Desmarets, G. Gontard, A. L. Cooksy, M. N. Rager and H. Amouri, *Inorg. Chem.*, 2014, **53**, 4287.

21. S. Turega, M. Whitehead, B. R. Hall, A. J. H. M. Meijer, C. A. Hunter and M. D. Ward, *Inorg. Chem.*, 2013, **52**, 1122.

22. M. Whitehead, S. Turega, A. Stephenson, C. A. Hunter and M. D. Ward, *Chem. Sci.*, 2013, **4**, 2744.

23. S. Turega, M. Whitehead, B. R. Hall, M. F. Haddow, C. A. Hunter and M. D. Ward, *Chem. Commun.*, 2012, **48**, 2752.

24. M. D. Ward, *Chem. Commun.*, 2009, 4487.

25. I. S. Tidmarsh, T. B. Faust, H. Adams, L. P. Harding, L. Russo, W. Clegg and M. D. Ward, *J. Am. Chem. Soc.*, 2008, **130**, 15167.

26. S. Turega, W. Cullen, M. Whitehead, C. A. Hunter and M. D. Ward, *J. Am. Chem. Soc.*, 2014, **136**, 8475.

27. S. G. Telfer, G. Bernardinelli and A. F. Williams, *Dalton Trans.*, 2003, 435.

28. E. A. P. Armstrong, R. T. Brown, M. S. Sekwale, N. C. Fletcher, X. Q. Gong and P. Hu, *Inorg. Chem.*, 2004, **43**, 1714.

29. N. C. Fletcher, M. Nieuwenhuyzen and S. Rainey, *J. Chem. Soc., Dalton Trans.*, 2001, 2641.

30. M. H. Filby, J. Muldoon, S. Dabb, N. C. Fletcher, A. E. Ashcroft and A. J. Wilson, *Chem. Commun.*, 2011, **47**, 559.

31. C. P. Sebli, S. E. Howson, G. J. Clarkson and P. Scott, *Dalton Trans.*, 2010, **39**, 4447.

32. S. E. Howson, L. E. N. Allan, N. P. Chmel, G. J. Clarkson, R. van Gorkum and P. Scott, *Chem. Commun.*, 2009, 1727.

33. A. K. Sharma, F. Lloret and R. Mukherjee, *Inorg. Chem.*, 2013, **52**, 4825.

34. N. C. A. Baker, N. McGaughey, N. C. Fletcher, A. V. Chernikov, P. N. Hortonb and M. B. Hursthouse, *Dalton Trans.*, 2009, 965.

35. N. C. Fletcher, R. T. Brown and A. P. Doherty, *Inorg. Chem.*, 2006, **45**, 6132.

36. R. T. Brown, N. C. Fletcher, M. Nieuwenhuyzen and T. E. Keyes, *Inorg. Chim. Acta*, 2005, **358**, 1079.

37. N. C. Fletcher, M. Nieuwenhuyzen, R. Prabarahan and A. Wilson, *Chem. Commun.*, 2002, 1188.

38. B. A. Wu, J. Yang, X. J. Huang, S. G. Li, C. D. Jia, X. J. Yang, N. Tang and C. Janiak, *Dalton Trans.*, 2011, **40**, 5687.

39. M. H. W. Lam, S. T. C. Cheung, K. M. Fung and W. T. Wong, *Inorg. Chem.*, 1997, **36**, 4618.

40. S. G. Telfer, T. Sato and R. Kuroda, *Angew. Chem. Int. Ed.*, 2004, **43**, 581.

41. E. Solari, F. Musso, E. Gallo, C. Floriani, N. Re, A. Chiesivilla and C. Rizzoli, *Organometallics*, 1995, **14**, 2265.

42. P. A. W. Dean, M. Jennings, U. Rajalingam, D. C. Craig, M. L. Scudder and I. G. Dance, *Crystengcomm*, 2002.

43. A. J. Amoroso, A. M. C. Thompson, J. C. Jeffery, P. L. Jones, J. A. McCleverty and M. D. Ward, *J. Chem. Soc.-Chem. Commun.*, 1994, 2751.

44. A. P. Bisson, C. A. Hunter, J. C. Morales and K. Young, *Chem.-Eur. J.*, 1998, **4**, 845.

45. X.-S. Shi, C.-S. Liu, J.-R. Li, Y. Guo, J.-N. Zhou, X.-H. Bu, *J. Mol. Struct.*, 2005, **754**, 71.

46. G. M. Sheldrick, *SADABS: A program for absorption correction with the Siemens SMART system*, University of Göttingen, Germany, 1996.

47. G. M. Sheldrick, *Acta Cryst. Sect. A*, 2008, **64**, 112.

3. Stepwise synthesis of heterometallic coordination cages using inert and labile subcomponents

3.1 Introduction

The synthesis of heterometallic coordination complexes is currently the subject of intense research.[1-5] Despite recent progress in this field, most cage complexes are based on just two types of component, i.e. one type of metal ion and one type of bridging ligand. This limits the structural and functional and complexity that may be achievable. Given that the metal ions which form the basis of cage assemblies provide both structural information (*via* their preferences for specific coordination geometries) and possible functionality properties (such as redox activity, magnetism, colour or luminescence),[6-8] efforts directed at assembling heterometallic cages – with control of which metal ions occupy which sites – are surprisingly limited.

In order to construct heterometallic structures, one must consider the coordination preferences of each metal, and particularly their kinetic labilities. When one does this, two options become evident. If both metals are kinetically labile, then a one-pot synthesis becomes viable. When mixed with an unsymmetrical ligand, the combination of metal ions and ligand will be able to rearrange, assembling and disassembling in such a way that initial 'mistakes' are 'corrected', eventually resulting in a structure that represents the thermodynamic minimum (see Figure 3.1.1). Such a method can be described as the **thermodynamic control approach** towards forming heterometallic structures. The crucial aspect of this approach is that the ligand contains binding sites which will be able to differentiate between the two types of metal, based on the coordination preference of the metals. For example, the use of unsymmetrical ligands possessing both hard and soft binding sites which will selectively bind to hard

and soft metals, respectively.[9-13] Another example is the use of ligands with unsymmetrical denticity in combination with metals with differing geometric preferences.[14-17]

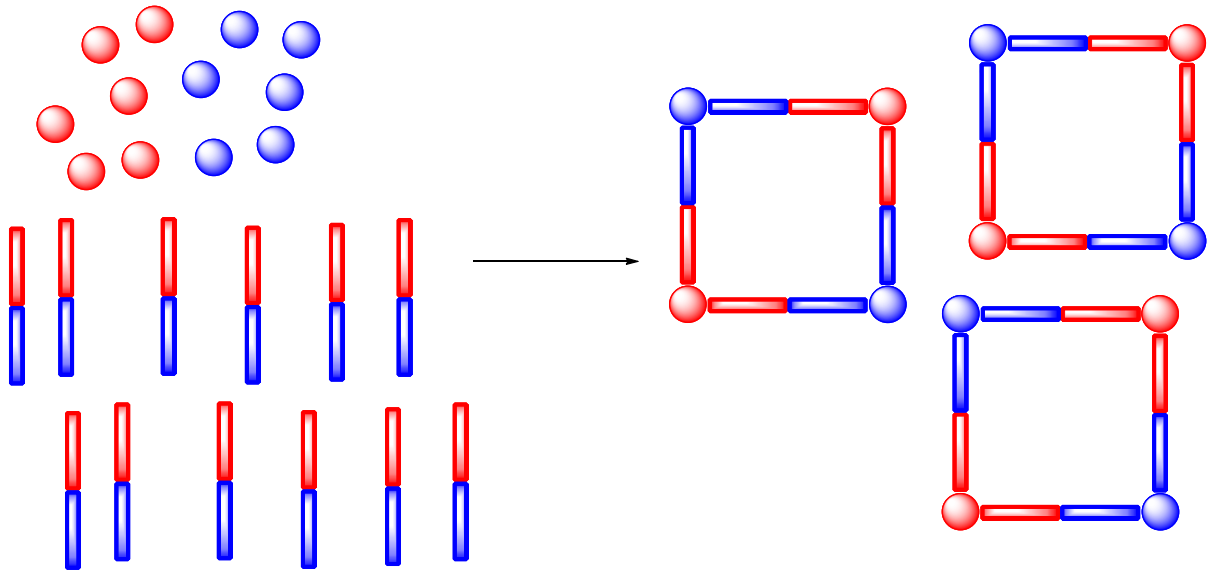

Figure 3.1.1 A schematic representation of heterometallic self-assembly using the thermodynamic control approach. Red and blue spheres depict kinetically labile metal ions. Red and blue rectangles represent bridging ligands.

When one of the metals is kinetically inert, a different strategy must be applied, a strategy that can be referred to as the **kinetic control approach**. Instead of a one pot-synthesis under overall thermodynamic control, a stepwise approach must be used in which an inert complex with pendant binding sites is formed initially under kinetic control, and this fragment is then mixed with the labile components under self-assembly conditions as demonstrated in Figure 3.1.2. In this case, the green spheres represent kinetically inert metal ions which are reacted with an unsymmetrical ligand to form a complex with pendant binding sites, which are saturated upon addition of a labile metal ion. Such an approach has also been termed the 'complex as ligand' approach, due to the way that the metal complex behaves as a rigid preorganised ligand in many cases.[18]

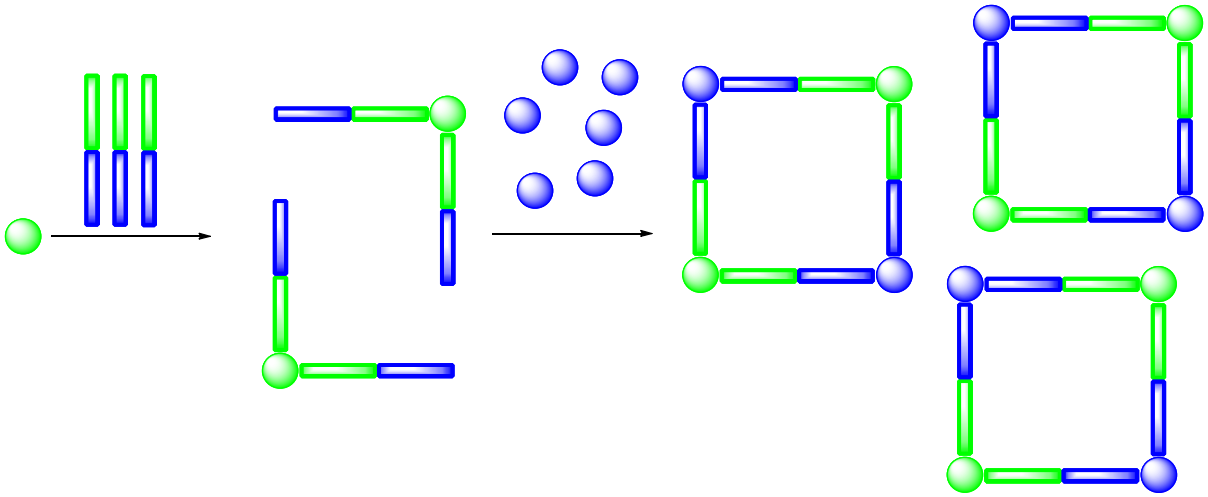

Figure 3.1.2 A schematic representation of heterometallic self-assembly using the kinetic control approach. Green spheres represent kinetically inert metal ions, blue spheres depict kinetically labile metal ions. Green and blue rectangles represent bridging ligands.

Ruthenium(II) is an ideal candidate for use in an inert metal ion based scaffold, given its tractable synthetic chemistry: modestly high temperatures suffice for preparation of N,N'-donor tris-chelate complexes but the complexes are generally inert at room temperature. In addition incorporation of Ru^{2+} centres allows inclusion of a type of functional behaviour (redox activity) that is not normally associated with such cages. If an unsymmetrical ligand were used it should then be possible to separate the meridional (*mer*) and facial (*fac*) isomers of a Ru(II) tris-chelate complex (see Figure 3.1.3), a necessary property of the inert metal, as will be explained later. Many examples have been described in the literature where such separation is achievable.[19-26]

The extensive family of polyhedral cage complexes described by Ward and co-workers generally contain an octahedral tris-chelate metal ion at each vertex, and a bis-bidentate bridging ligand (containing two pyrazolyl-pyridine chelating termini) along each edge (see Chapter 1 for examples of Ward group ligands and cages).[27] In these complexes the geometric isomerism (*fac* vs. *mer*) of the metal centres turns out to play a crucial role in the nature of the assembly that forms. In some complexes, such as a family of M_4L_6 tetrahedra, all four metal centres have a fac tris-chelate geometry;[28-30] in contrast, in a series of $M_{12}L_{18}$ truncated tetrahedra, all metal centres have a mer tris-chelate geometry.[31] In several

other types of cage assembly however there is a 3:1 mixture of *mer* : *fac* tris-chelate vertices – these include M_4L_6 tetrahedra, M_8L_{12} cubes and $M_{16}L_{24}$ tetra-capped truncated tetrahedra.[32-35] Therefore, the ability to control the self-assembly of such cages – particularly mixed-metal versions – relies on the ability to prepare kinetically stable, geometrically pure *fac* or *mer* tris-chelate subcomponents as starting points to propagate a specific assembly.

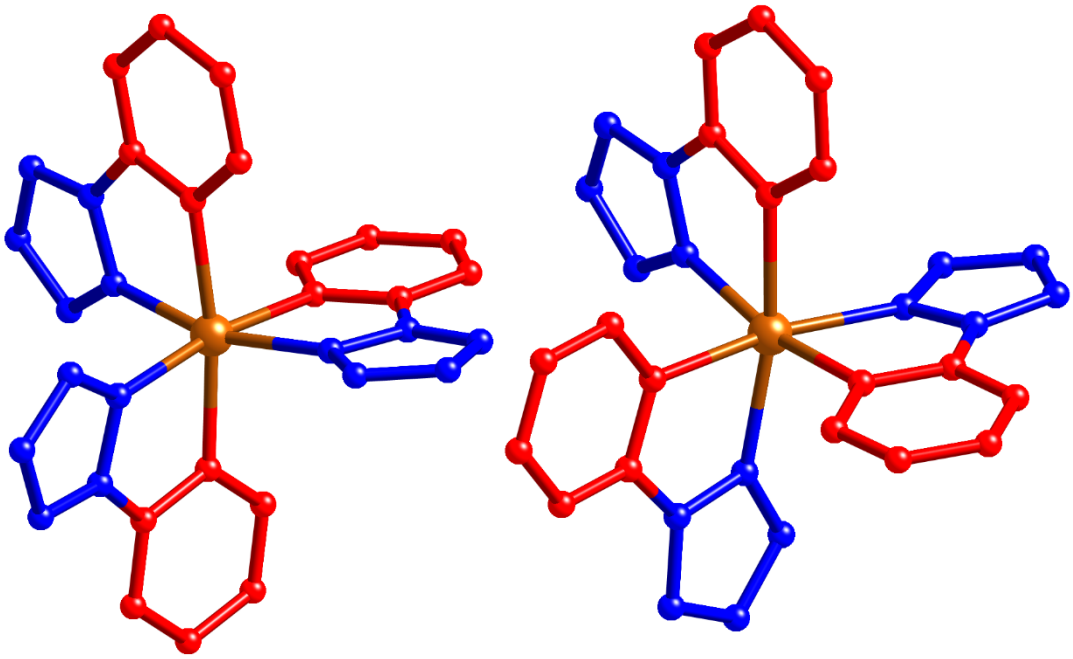

Figure 3.1.3 Diagrams for the *mer* (left) and *fac* (right) isomers of a Ru(II) tris-chelate complex with pyrazolyl-pyridine ligands.

There are examples in the literature where kinetically inert metal ions have been used as the basis of a heterometallic structure, frequently resulting in helical or cyclic structures.[22,36-40] However, the examples where hollow heterometallic coordination cages with a defined cavity have resulted are very scarce.[14] Two methodologies have been used to achieve these types of structures; i) separation of *fac*-ML_3 tris chelates from a mixture of *mer* and *fac* isomers, and ii) functionalisation of an inert $Ru(N)_6$ core to furnish it with pendant binding sites.

Piguet's group has demonstrated the ability to separate *fac*-ML_3 tris chelates possessing three pendant binding sites by ion exchange chromatography when M = Cr(III), Os(II) or Ru(II).[26,38,41] These *fac*-ML_3 units have enabled the synthesis of a series of heterobimetallic d-f triple-stranded helicates when mixed

with lanthanide ions, which have led to some interesting functional behaviour such as Cr-Ln energy transfer.

Fletcher's group has been concerned with the separation of the *fac*-isomer of a series of Ru(II) tris-bipyridines. Although having experienced successful separations by ion exchange chromatography, the use of a tripodal ligand allowed the formation of a cage-like Ru(II) complex with *fac* tris-chelate geometry. The tether could subsequently be removed, allowing functionalisation of the ligands in order to introduce three pendant binding sites, and upon reaction with Fe(II) ions a $RuFeL_3$ helicate was formed.[22]

Previous work in the Ward group has also made use of the post-coordination functionalisation of ligands.[36] The complex $[Ru(H_2bpp)_2]^{2+}$ (H_2bpp = 2,6-bis(pyrazol-3-yl)pyridine), which possesses four functionalisable N-H groups, can be synthesised as a single product with no geometrical isomerism possible. This can then be alkylated to form an inert $[Ru(N)_6]^{2+}$ core furnished with four pendant bidentate pyrazolyl-pyridyl sites. In the presence of Ag(I) ions, a $[RuAg_2]^{4+}$ double helix results. Reaction of Ru(II) ions with the preformed multidentate ligand would not allow the formation of a discrete trinuclear helicate.

The objective of this work is to synthesise heteronuclear coordination cages incorporating inert Ru(II) tris-chelate complexes as either the pure *fac*- isomer or as a controlled mixture of the *mer*- and *fac*-isomers at specific sites within heterometallic cage complexes, thus creating the potential for redox-based switching of guest binding.[42] The cages will be studied by ^1H NMR spectroscopy, ESMS, X-ray crystallography and electrochemical methods.

3.2 Results and discussion

3.2.1 Preparation of mononuclear Ru(II) subcomponents

The initial aim was for the synthesis of tris-chelates of Ru(II) in which the metal ion is coordinated to one end of a bis-bidentate ligand (see Figure 3.2.1), such that there are three pendant bidentate groups. These $[RuL_3]^{2+}$ complexes should then be isolated as either purely the *fac* isomer or as a statistical 3:1 mixture of the *mer* and *fac* isomers as starting points to propagate a specific assembly.

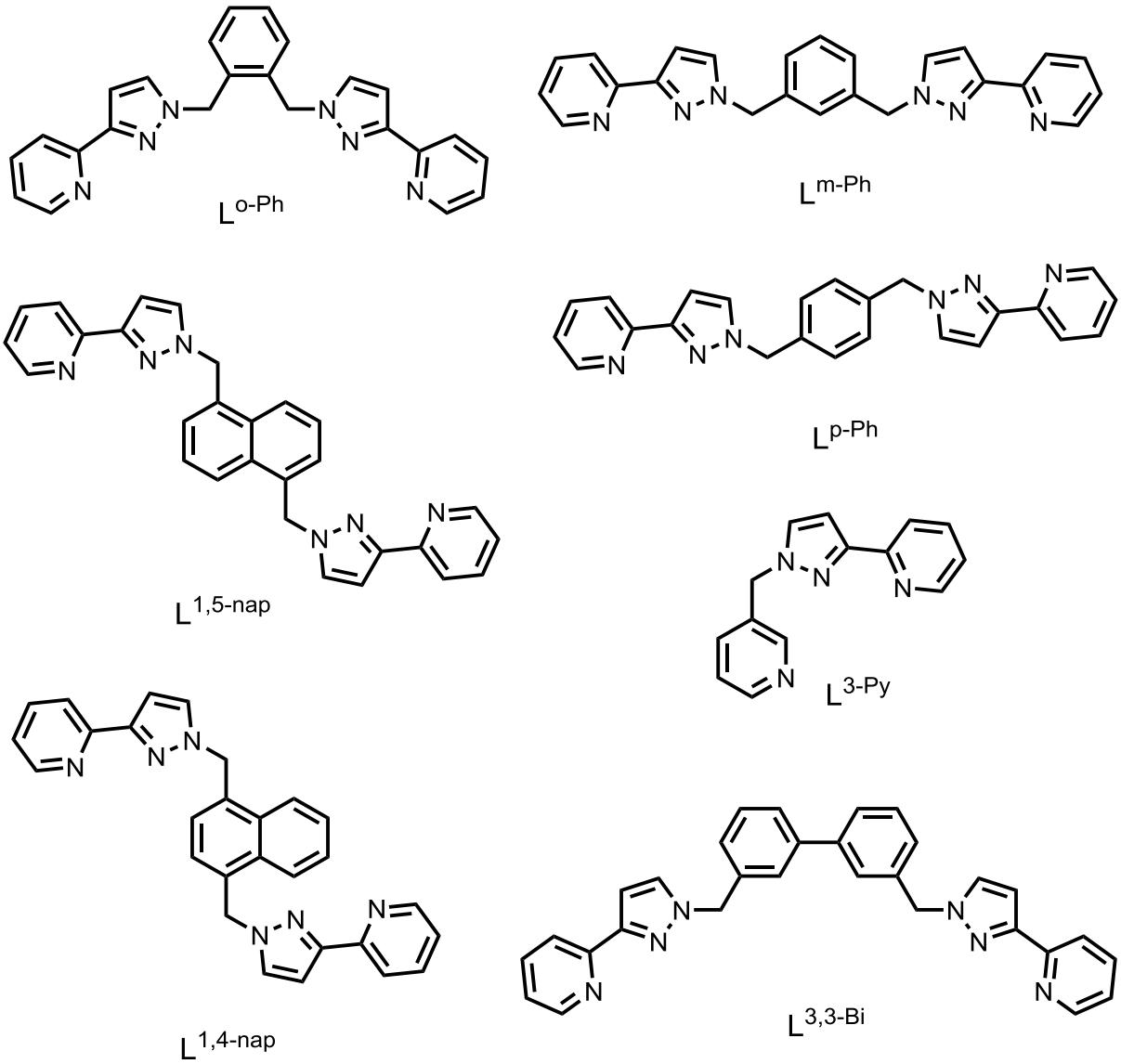

Figure 3.2.1 The ligands used in this work.

3.2.1.1 $[Ru(L^{1,5\text{-nap}})_3](PF_6)_2$

The first mononuclear complex studied was $[Ru(L^{1,5\text{-nap}})_3](PF_6)_2$, which uses a 1,5-substituted naphthalene ligand (see Figure 3.2.1 for ligand structure). Previous work in the Ward group has shown that reaction of $L^{1,5\text{-nap}}$ with a variety of transition metal dications in a 3 : 2 ratio leads to the formation of cubic M_8L_{12} coordination cages, in which two of the metal ions (at either end of the long diagonal) have a *fac* tris-chelate geometry with the three pyridyl donors on one face of the octahedron and the three pyrazolyl donors on the other. In contrast, the other six metal ions have a *mer* tris-chelate geometry.[32] Therefore, $[Ru(L^{1,5\text{-nap}})_3](PF_6)_2$ can be introduced into the cage either as purely the *fac*-isomer at opposite corners, or as a 3 : 1 mixture of the *mer* and *fac* isomers at alternating sites (see Figure 3.2.2).

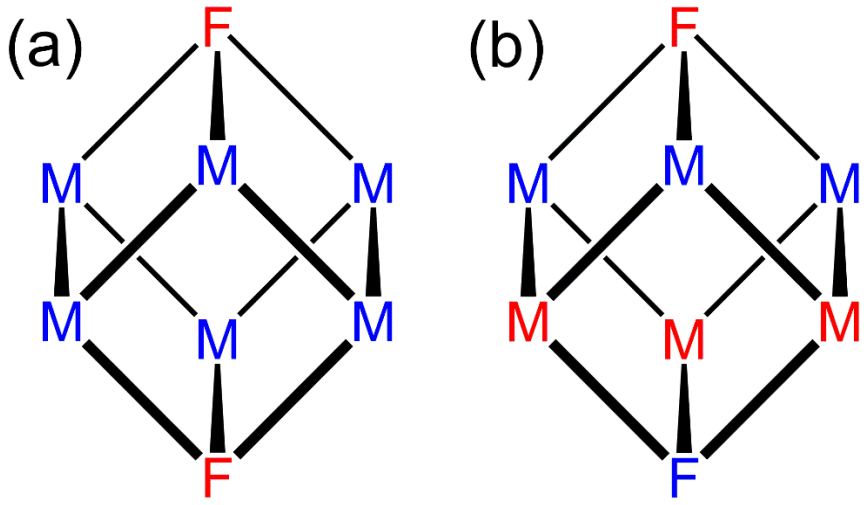

Figure 3.2.2 Schematic diagram of the cubic cage, showing the positions of the two *fac* (F) and six *mer* (M) metal centres. In the homonuclear cages all metal ions are the same; in a heteronuclear cage the two types of metal ion are split over the red [Ru(II)] and blue [M(II)] sites. (a) Ru_2M_6 arrangement, with Ru(II) occupying the two *fac* centres and the other metal occupying all six *mer* centres. (b) Ru_4M_4 arrangement, with each ion type occupying one *fac* and three *mer* centres.

$[Ru(L^{1,5\text{-nap}})_3](PF_6)_2$ was prepared by reaction of $RuCl_2(dmso)_4$ with > 3 equiv. $L^{1,5\text{-nap}}$ in refluxing ethylene glycol, and after work-up a yellow solid was isolated which analysed as $[Ru(L^{1,5\text{-nap}})_3](PF_6)_2$ by elemental analysis and ESMS (see Figure 3.2.3). Given the non-symmetrical nature of the pyrazolyl-

pyridine chelates this course forms as a mixture of *fac* and *mer* isomers. If there is no specific factor resulting in preference for one isomer over the other, a *fac*:*mer* ratio of 1:3 is expected. The ^{1}H NMR spectrum of $[Ru(L^{1,5\text{-nap}})_3](PF_6)_2$ is consistent with this, showing four independent ligand environments in equal abundance (see Figures 3.2.4 and 3.2.5). The *mer* isomer has no symmetry with all three ligands inequivalent; the *fac* isomer provides the fourth ligand environment with all three ligands equivalent due to the threefold symmetry but is only one-third as abundant. Hence we see signals for four independent ligand environments in equal abundance. In the $[Ru(L^{1,5\text{-nap}})_3]^{2+}$ complex cation, each ligand uses only one of its two chelating sites so there are three pendant pyrazolyl-pyridine binding sites.

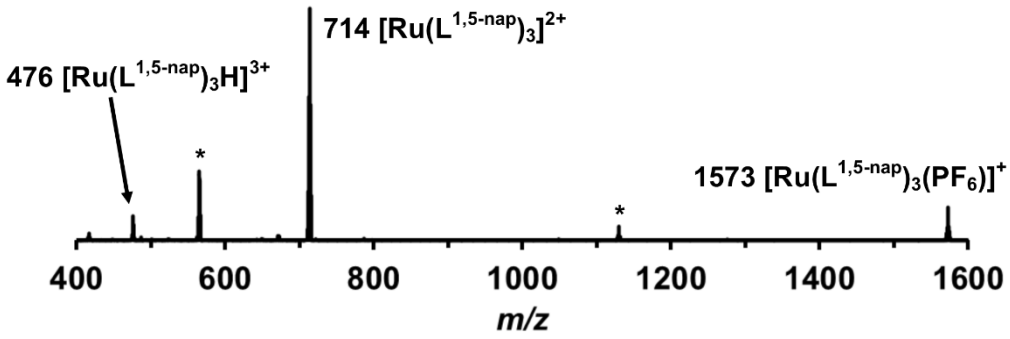

Figure 3.2.3 ESMS+ spectrum of $[Ru(L^{1,5\text{-nap}})_3][PF_6]_2$. Peaks at 566 and 1130 (marked with an asterisk, *) are due to fragmentation in the mass spectral conditions.

Conveniently for our purposes, this 1:3 *fac*:*mer* ratio of $[Ru(L^{1,5\text{-nap}})_3](PF_6)_2$ isomers is precisely what is required in the cage if every alternate site is occupied by a Ru(II) centre. This is not generally true of other members of the cage family, which contains examples in which the metal tris-chelate centres are all *fac* and other examples in which the metal centres are all *mer*.[27] Thus, no separation of isomers of $[Ru(L^{1,5\text{-nap}})_3](PF_6)_2$ is needed: the as-prepared mixture can be used as it stands to provide the necessary cage subcomponents in the correct proportions.

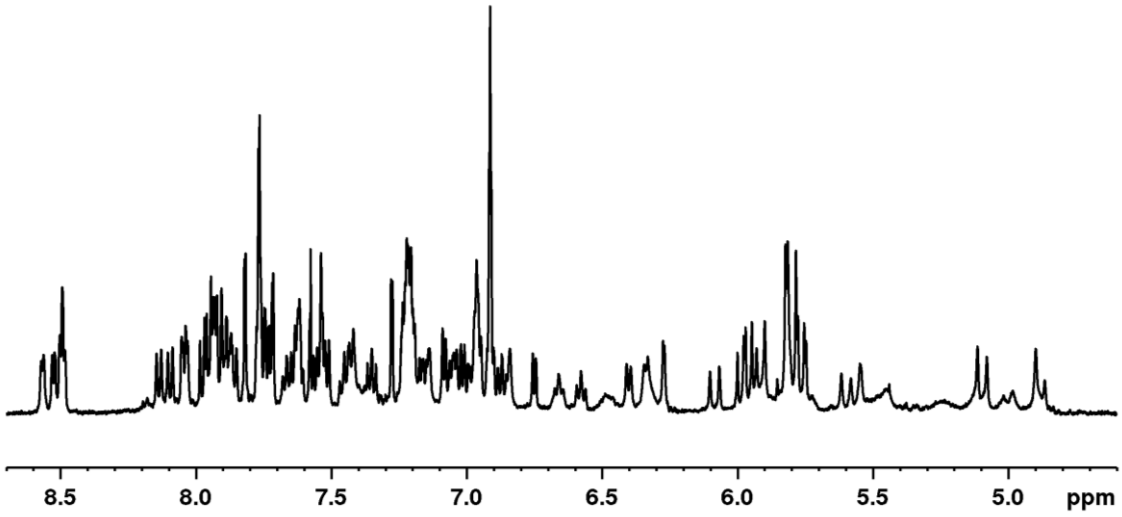

Figure 3.2.4 ^{1}H NMR spectrum (500 MHz, CD_3CN) of $[Ru(L^{1,5\text{-nap}})_3](PF_6)_2$.

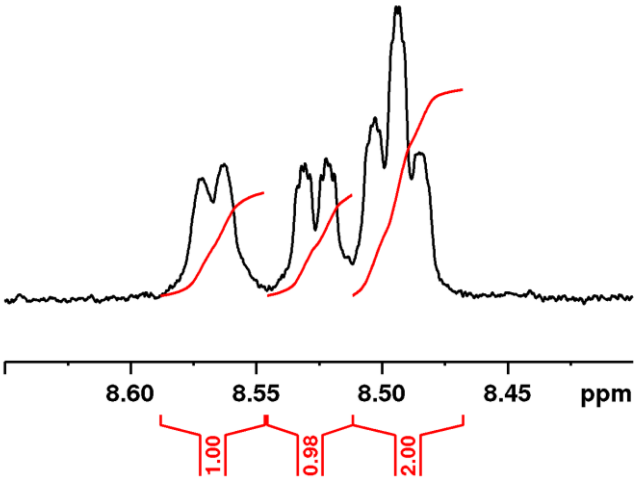

Figure 3.2.5 Expansion of ^{1}H NMR spectrum (500 MHz, CD_3CN) of $[Ru(L^{1,5\text{-nap}})_3](PF_6)_2$ showing the presence of four signals in an approximately 1 : 1 : 1 : 1 ratio for one of the pyridyl-H^6 protons, consistent with a 3:1 ratio of *mer* to *fac* isomers.

3.2.1.2 $[Ru(L^{m\text{-}Ph})_3](PF_6)_2$

Another ligand used by the Ward group to form cubic M_8L_{12} cages is the meta-phenylene substituted ligand $L^{m\text{-}Ph}$ (see Figure 3.2.1).[33] The reaction of $L^{m\text{-}Ph}$ with transition metal dications in a 3:2 ratio leads to cages with the same type of S_6-symmetric metal framework as seen with $L^{1,5\text{-}nap}$ based cages (see Figure 3.2.2). Therefore, $[Ru(L^{m\text{-}Ph})_3](PF_6)_2$ can be introduced into the cage in exactly the same way; either as purely the *fac*- isomer at two of the eight vertices (either end of a cube diagonal), or as a 3:1 mixture of the *mer* and *fac* isomers at four (alternating) vertices.

Thus, $[Ru(L^{m\text{-}Ph})_3](PF_6)_2$ was prepared by reaction of $RuCl_2(dmso)_4$ with > 3 equiv. $L^{m\text{-}Ph}$ in a refluxing ethanol/water mixture, and after work-up a yellow solid was isolated which analysed as $[Ru(L^{m\text{-}Ph})_3](PF_6)_2$ by elemental analysis and ESMS (*m/z* 714, $[Ru(L^{m\text{-}Ph})_3]^{2+}$). Interestingly, ^{1}H NMR analysis revealed that the mixture was not isolated as the purely statistical 3:1 *mer*/*fac* mixture of isomers; instead, the mixture contained an approximately 6.8:1 *mer*/*fac* ratio (see Figure 3.2.6). This was determined by comparing the integrals of a series of isolated peaks, and it was found that one set of peaks has a relative integral value of (approximately) 1.00, and a less abundant set of peaks has a relative integral value of 0.44. As one of the *fac* protons is in three different environments for the *mer* isomer, this gives the ratio 3:0.44, or 6.8:1. Clearly, some separation of the isomers would be needed to cleanly form a heterometallic structure; this will be addressed later in the chapter.

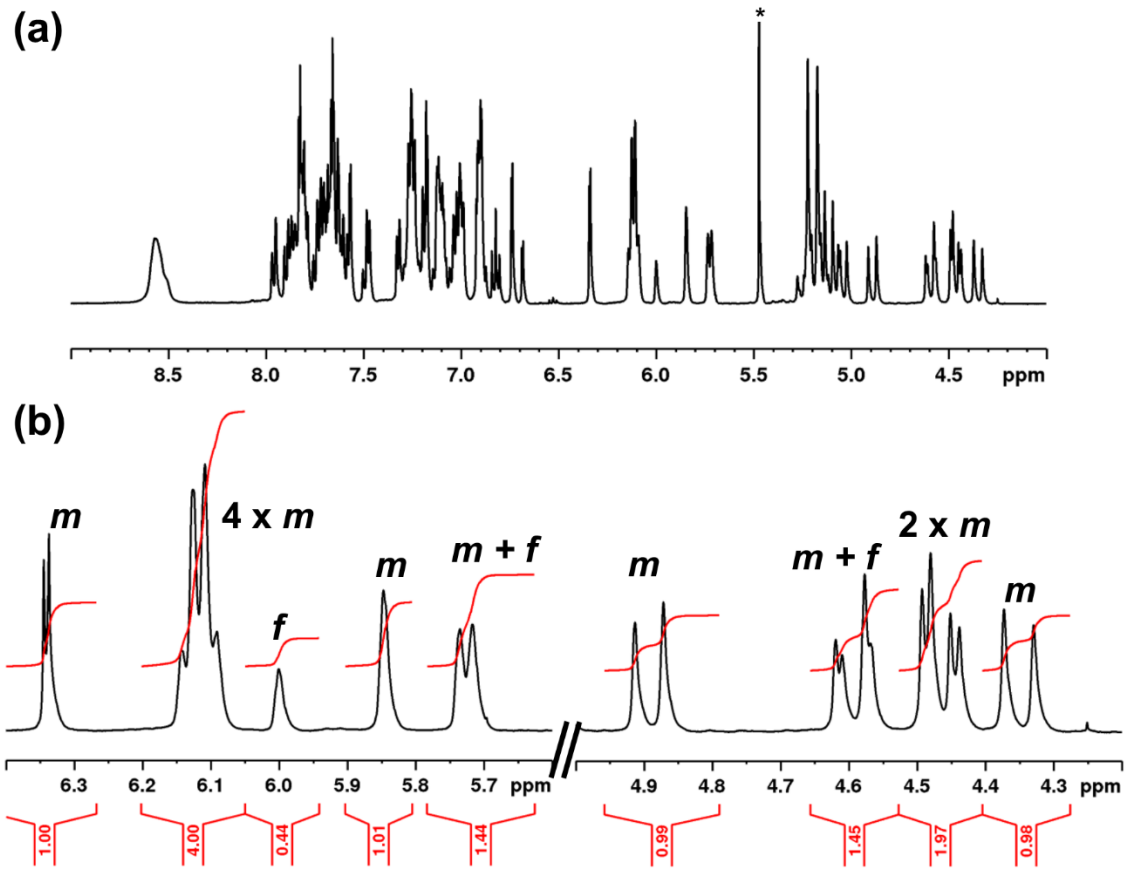

Figure 3.2.6 (a) ^{1}H NMR (CD_3CN, 400 MHz) spectrum of $[Ru(L^{m\text{-}Ph})_3](PF_6)_2$ (the peak marked with an asterisk, *, is a trace of protanted solvent); (b) expansion in two regions showing the mixture of *mer* and *fac* peaks in a 6.8:1 ratio.

3.2.1.3 $[Ru(L^{o\text{-}Ph})_2](PF_6)_2$

The ortho-phenylene substituted ligand $L^{o\text{-}Ph}$ (see Figure 3.2.1) has been shown to form M_4L_6 tetrahedral cages when mixed with Co(II) salts in the appropriate ratio.[28] All metal ions in this structure have a *fac* tris chelate geometry. Consequently, it may not be possible to precisely locate the different metal ions if *fac*-$[Ru(L^{o\text{-}Ph})_3](PF_6)_2$ were introduced into a $RuCo_3$ heterometallic tetrahedron as each site in the cage is equivalent, so we would expect disorder of the Ru(II) centre over all four metal sites in a crystal structure. Nevertheless, the synthesis of the mononuclear complex $[Ru(L^{o\text{-}Ph})_3](PF_6)_2$ was carried out in order to determine if the tetrahedral cage $[RuCo_3(L^{o\text{-}Ph})_6]^{8+}$ could be formed from more than two components.

Reaction of $RuCl_2(dmso)_4$ with > 3 equiv. $L^{o\text{-}Ph}$ in a refluxing ethanol/water mixture gave, after work-up, a yellow solid which did *not* analyse as the expected $[Ru(L^{o\text{-}Ph})_3](PF_6)_2$ by elemental analysis or ESMS. Instead, the bis-ligand species $[Ru(L^{o\text{-}Ph})_2](PF_6)_2$ was the only product observed by mass spectrometry (see Figure 3.2.7). The ^1H NMR spectrum of the recrystallized material revealed that there were two independent ligand environments (see Figure 3.2.8); for example, 8 CH_2 protons can be identified in the COSY spectrum (see Figure 3.2.9). One of the CH_2 groups appears as a singlet at 4.8 ppm with relative intensity 2H, whereas all other groups appear as 1H doublets (diastereotopic due to coordination of the ligand to a chiral metal centre), with one proton remarkably shielded at 2.5 ppm.

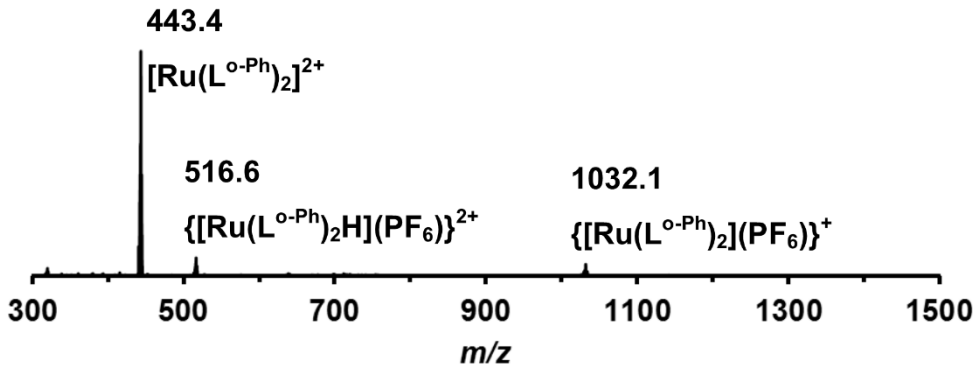

Figure 3.2.7 ESMS+ spectrum of $[Ru(L^{o\text{-}Ph})_2][PF_6]_2$.

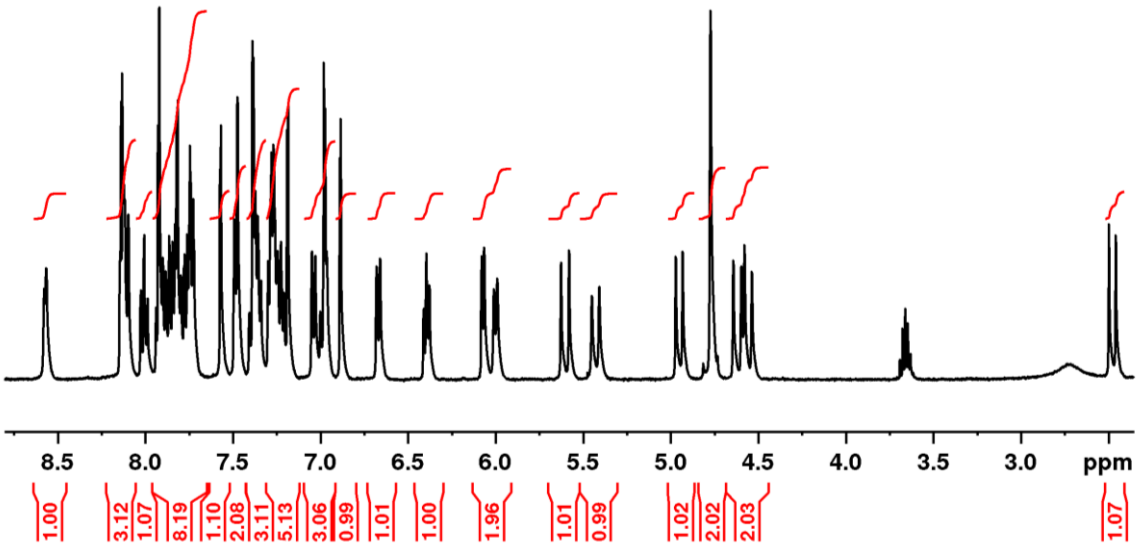

Figure 3.2.8 ^1H NMR spectrum (CD_3CN, 400 MHz) of $[Ru(L^{o\text{-}Ph})_2][PF_6]_2$.

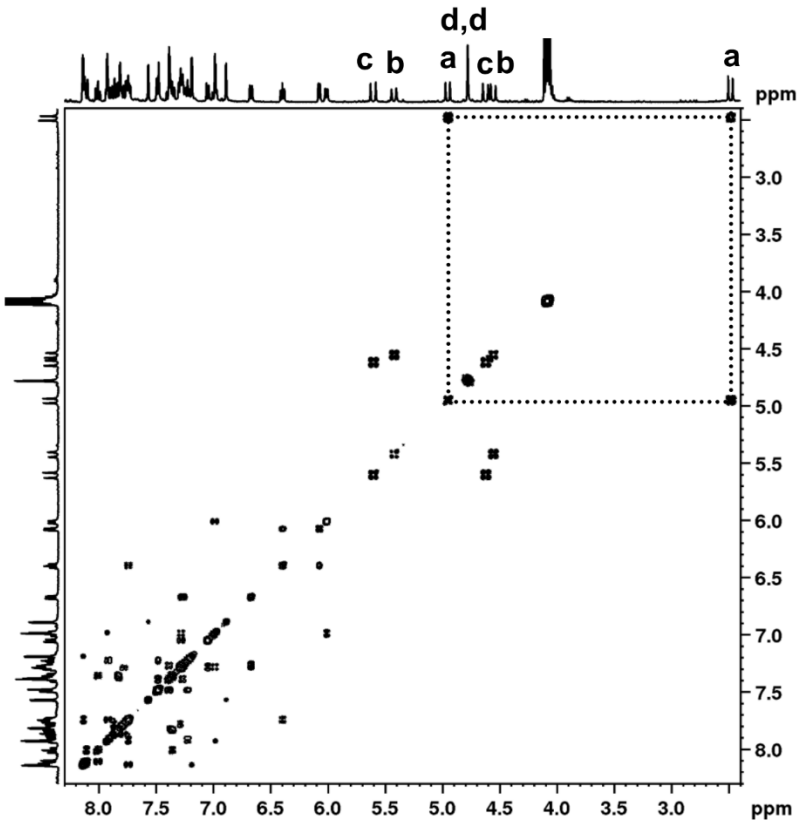

Figure 3.2.9 $^{1}H - {}^{1}H$ COSY spectrum (CD_3CN, 400 MHz) of $[Ru(L^{o\text{-}Ph})_2][PF_6]_2$ (CH_2 pairs are labelled a – d).

Given the complex formula and the fact there are the two independent ligand environments, the connectivity of the ligands to the metal centre can be guessed with a reasonable degree of confidence. Given that the ligand $L^{o\text{-}Ph}$ has been shown to act as a tetradentate chelate for metals with a smaller ionic radius than Co(II) [e.g. Ni(II)],[43] it is quite likely that the ligand is acting as a tetradentate chelate here, with another ligand filling the coordination sphere of Ru(II) and leaving a pendant pyrazolyl-pyridine terminus. However, this does not explain the extremely shielded proton (2.5 ppm), therefore a crystal structure was collected to elucidate the situation.

Slow diffusion of diethyl ether vapour into a solution of the complex in acetone/nitromethane afforded X-ray quality yellow crystals of $[Ru(L^{o\text{-}Ph})_2](PF_6)_2 \bullet 0.5MeNO_2$ (see Figure 3.2.10). The asymmetric unit contains two complete complex cations (and their respective anions) which have opposite optical configurations. As predicted, one of the ligands acts as a tetradentate chelate, and the other as a mono-bidentate ligand with a pendant pyrazolyl-pyridine terminus. The metal-nitrogen bond distances are unremarkable, with all Ru-N distances in the range of 2.04 – 2.10 Å.

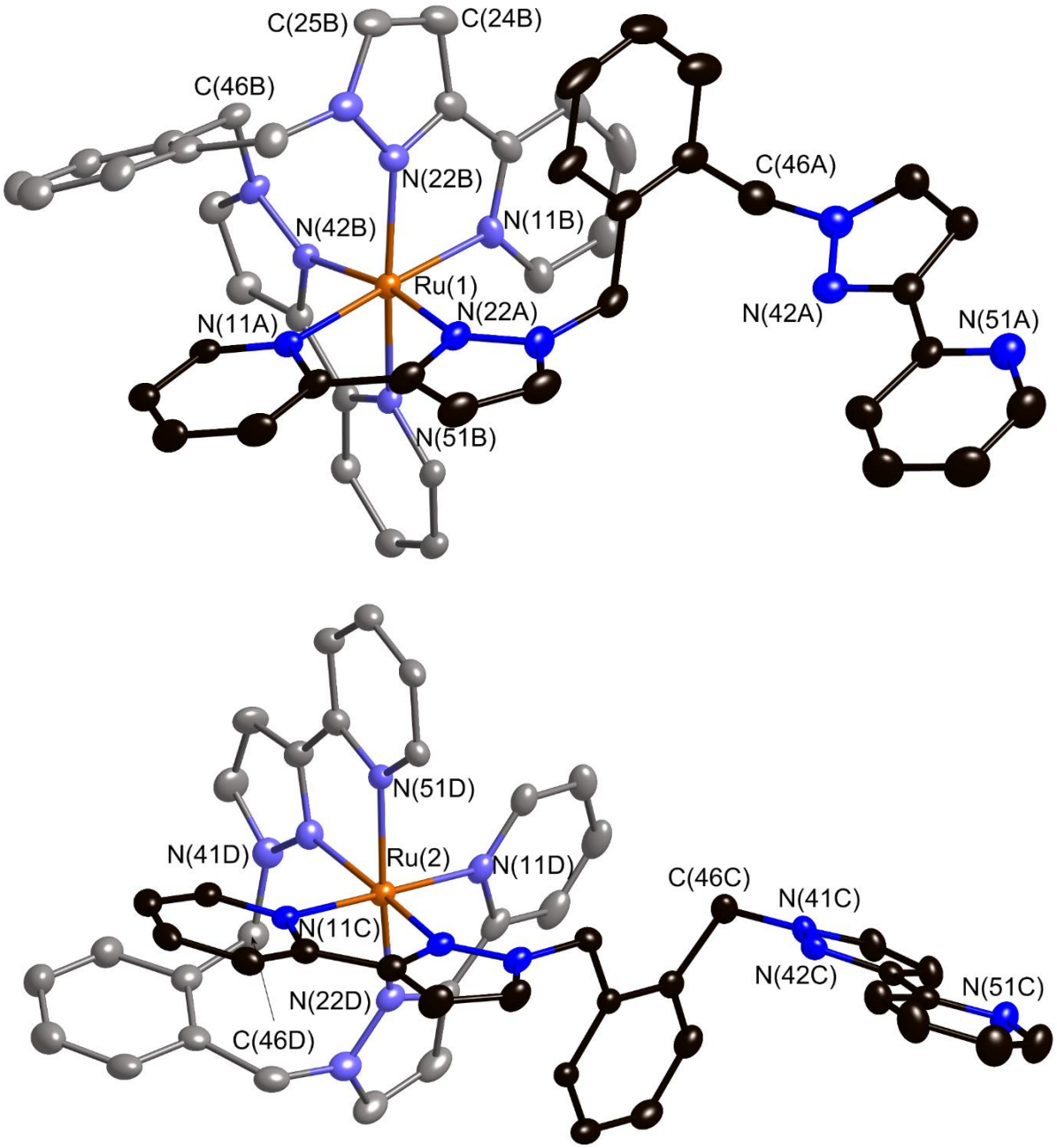

Figure 3.2.10 Crystal structures of the two independent complex cations found in the asymmetric unit of $[Ru(L^{o\text{-}Ph})_2](PF_6)_2$. Thermal ellipsoids for all non-hydrogen atoms shown at 40 % probability (tetradentate ligand shown in paler colours in each case for clarity).

It is clear from the crystal structure how one of the CH_2 groups gives rise to a singlet in the ^1H NMR spectrum – this is the methylene hinge connecting the pendant terminus to the phenylene spacer [C(46A) and C(46C)], relatively unaffected by the chirality of the metal centre. A space-filling view of one of the complexes reveals the highly shielded proton as one of the methylene protons of the tetradentate

ligand (see figure 3.2.11). The proton H(46G) is directed towards the centre of one of the coordinated pyrazolyl groups (average separation from the atoms of the ring: 2.44 Å) due to the rigid organisation required for the ligand to bind in a tetradentate manner. The proton is consequently shielded (2.5 ppm) from the external magnetic field in the ^{1}H NMR experiment due to the ring-current effect.

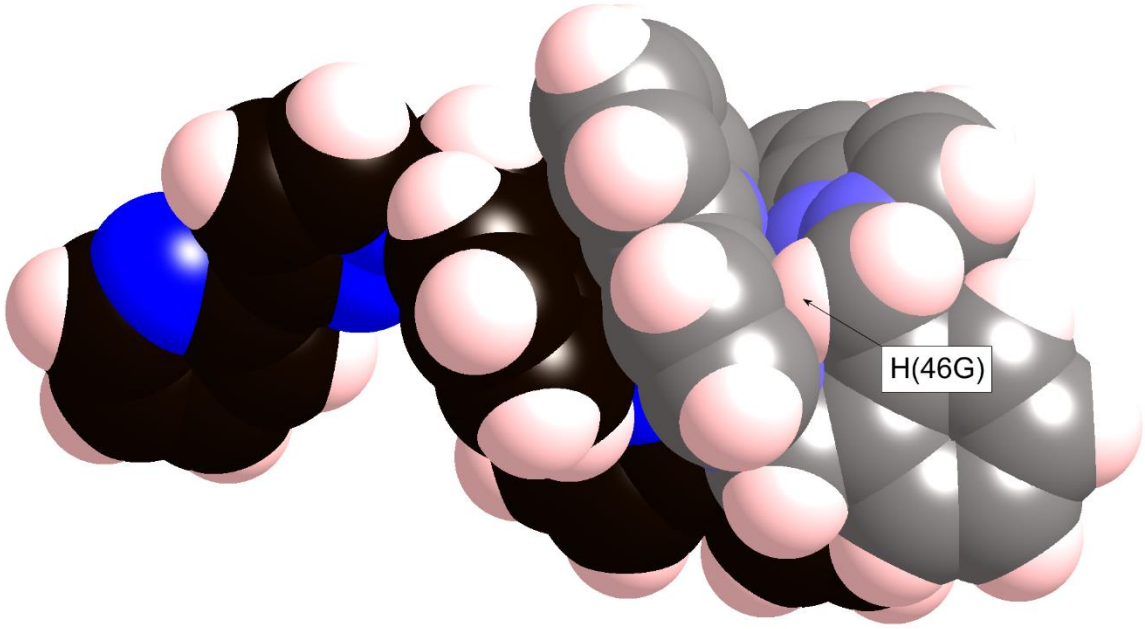

Figure 3.2.11 Space-filling view of one of the cations in the crystal structure of $[Ru(L^{o\text{-}Ph})_2](PF_6)_2$, emphasising the C-H ●●● π interaction of one of the methylene protons and a coordinated pyrazolyl ring.

Whilst the desired complex $[Ru(L^{o\text{-}Ph})_3](PF_6)_2$ could not be synthesised, the product $[Ru(L^{o\text{-}Ph})_2](PF_6)_2$, with one pendant binding site instead of three, may prove useful as a test-case for assembly of simple heteronuclear complexes with pyrazolyl-pyridyl ligands.

3.2.1.4 $[Ru(L^{p\text{-}Ph})_3](PF_6)_2$

The para-phenylene substituted ligand $L^{p\text{-}Ph}$ (see Figure 3.2.1) displays quite interesting supramolecular chemistry when mixed with a range of transition metal dications.[35] With Ni(II), it forms a M_8L_{12} cube structurally similar to the ones described previously; with Cu(II), a M_6L_9 trigonal prism is formed, in which all metals have a *mer* tris-chelate geometry; with Cd(II) and Zn(II), a $M_{16}L_{24}$ tetra-capped truncated tetrahedron is formed, in which four triangles of three metals with *mer* tris-chelate geometry (which define the truncated tetrahedron) are face-capped by four metals with *fac* tris-chelate geometry. As the largest cage prepared so far in the Ward group, a heterometallic version of this is quite a tantalising prospect. However, this will require the isolation of *fac*-$[Ru(L^{p\text{-}Ph})_3](PF_6)_2$.

$[Ru(L^{p\text{-}Ph})_3](PF_6)_2$ was prepared by reaction of $RuCl_2(dmso)_4$ with > 3 equiv. $L^{p\text{-}Ph}$ in a refluxing ethanol/water mixture, and after work-up a yellow solid was isolated which analysed as $[Ru(L^{p\text{-}Ph})_3](PF_6)_2$ by elemental analysis and ESMS (*m/z* 714, $[Ru(L^{p\text{-}Ph})_3]^{2+}$). As when $L^{m\text{-}Ph}$ was used, ^{1}H NMR analysis revealed that the mixture was not isolated as the purely statistical 3 : 1 *mer*/*fac* mixture of isomers; instead, the mixture was isolated as an approximately 5 : 1 *mer*/*fac* mixture (see Figure 3.2.12), as determined by the same method mentioned previously. It is clear at this point that isomeric purification of these types of complexes is necessary in order to isolate the pure *fac* isomer or the 3 : 1 *mer*:*fac* ratio of isomers required to cleanly form the heterometallic structures, and this is when significant efforts were devoted to separating the isomers, using $[Ru(L^{p\text{-}Ph})_3](PF_6)_2$ as the test-case to devise a strategy.

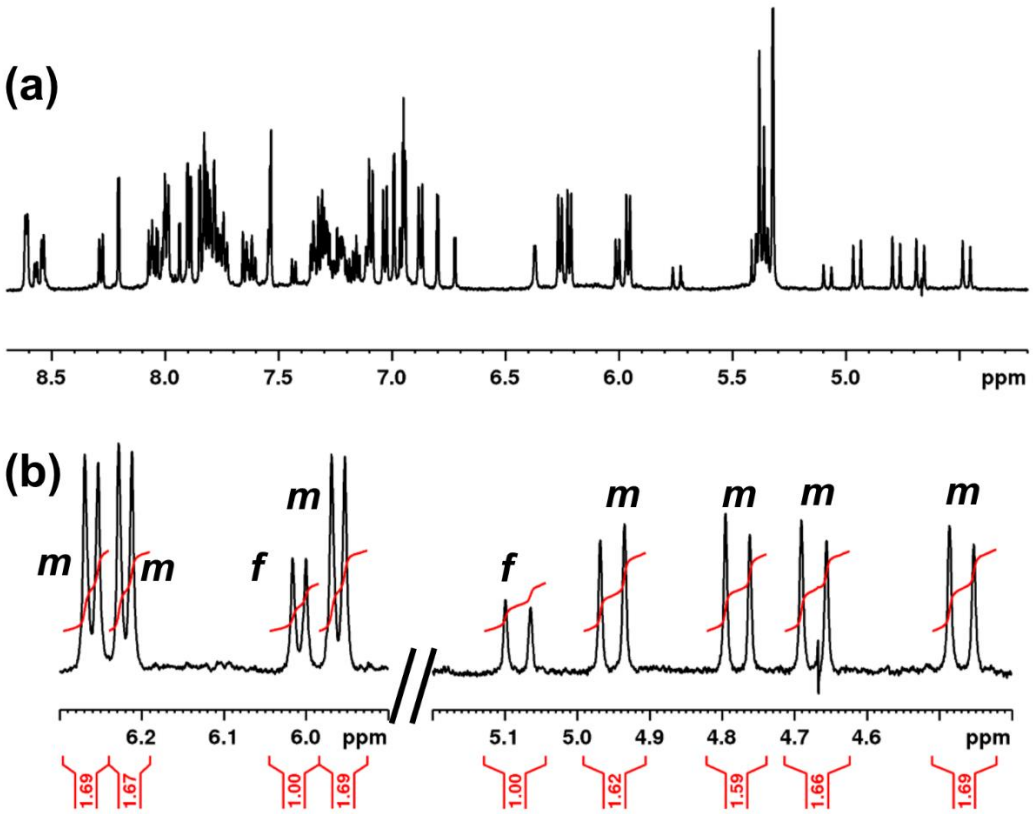

Figure 3.2.12 (a) ^{1}H NMR spectrum (500 MHz, $(CD_3)_2CO$) of *stat*-$[Ru(L^{p\text{-}Ph})_3](PF_6)_2$, showing the 80 proton resonances for 4 inequivalent ligand environments for a mixture of *mer* and *fac* isomer; (b) Expansions of the regions used to determine the approximate 5 : 1 ratio of *mer*/*fac*.

There exist many examples in the literature where a mixture of *mer* and *fac* isomers of unsymmetrical bipyridine containing complexes have been separated into their geometrically pure forms. One of the crudest methods is by fractional crystallisation; i.e. recrystallizing the mixture of isomers so that one isomer crystallises out preferentially, and then manually separating the crystals.[23, 24] This method is not entirely reliable, as it is extremely dependent on the solvent and ambient conditions, and yielded no separation of $[Ru(L^{p\text{-}Ph})_3](PF_6)_2$ after trying a range of crystallisation conditions. High-performance liquid chromatography (HPLC) has been used by Ishida and co-workers to achieve the isomeric separation of Ru(II) complexes with 5'-amino-2,2'-bipyridine-5-carboxylic acid derivatives, but their method did not work for purifying $[Ru(L^{p\text{-}Ph})_3](PF_6)_2$.[25]

Fletcher's group have reported many examples of isomeric separation of complexes with ester or amide functionalised ligands by preparative thin-layer chromatography (TLC) or column chromatography on

silica eluting with dimethylformamide/ ethanol (4 : 1) saturated with ammonium chloride.[21,44] The group has also successfully separated a series of unsymmetrical Ru(II) tris-bipyridine complexes into their respective *mer* and *fac* isomers on the basis of their interaction with the anion in ion exchange-chromatography using SP C-25 Sephadex.[45,46] Fletcher has reported that the chirality of the Sephadex support has made it possible to separate Λ and Δ optical isomers, but in some instances this has interfered with the separation of the geometrical isomers.[45] Attempts to separate the isomers of $[Ru(L^{p\text{-}Ph})_3](PF_6)_2$ were completely unsuccessful, so it is of course a possibility that this effect is preventing separation of the *mer* and *fac* isomers in this instance. Piguet and co-workers have used similar methodologies to separate the isomers of unsymmetrical Ru(II) and Os(II) tris-(benzimidazol-2-yl)-pyridine complexes.[26,38]

Previous work in the Ward group has shown that alkylation is achievable on the symmetrical complex $[Ru(H_2bpp)_2]^{2+}$ (see chapter one, Figure 1.51), furnishing a RuN_6^{2+} core with pendant binding sites.[36] Importantly, Fletcher has demonstrated that post-coordination functionalisation with retention of isomeric integrity is possible.[20-22] Therefore, this is the approach which was adopted, starting from *fac*-$[Ru(PyPzH)_3]^{2+}$ [see Figure 3.2.13; PyPzH = 3-(2-pyridyl)-pyrazole] which can be readily separated from the *mer* isomer using the method detailed in Chapter 2.[47] In *fac*-$[Ru(PyPzH)_3]^{2+}$ the three pyrazole rings, with their acidic NH protons, lie of course on the same face of the complex. Alkylation of these with the bromomethyl compound $Int^{p\text{-}Ph}$ completed the formation of the $L^{p\text{-}Ph}$ ligands coordinated to the metal centre at one end, to give *fac*-$[Ru(L^{p\text{-}Ph})_3]^{2+}$ which was isolated as the hexafluorophosphate salt, as confirmed by elemental analysis and ESMS (see Figure 3.2.14). The ^1H NMR spectrum showed 20 ^1H environments confirming the threefold symmetry with all three ligands equivalent (see Figure 3.2.15). Assignments (given with experimental details) were made on the basis of the COSY spectrum. Notably the CH_2 protons close to the Ru(II) chiral centre are diastereotopic, giving a coupled pair of doublets at 5.5 and 4.8 ppm whereas the CH_2 protons more remote from the Ru(II) centre give a singlet at 5.3 ppm.

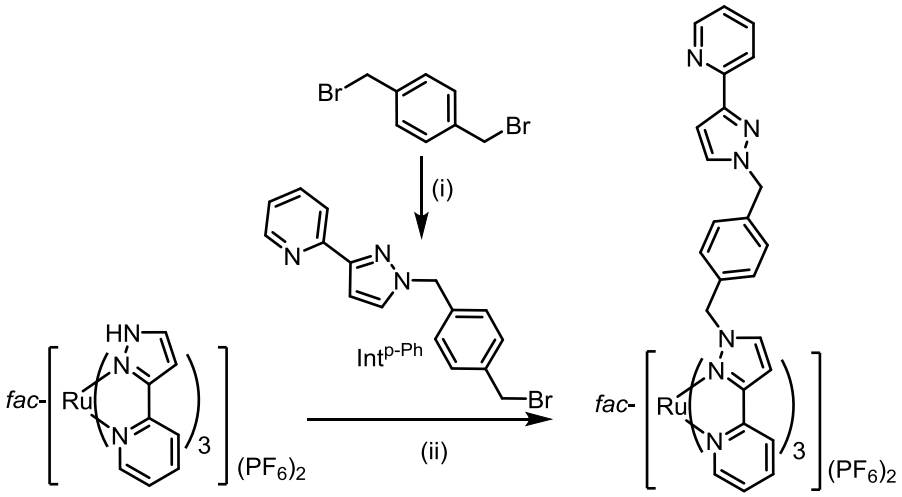

Figure 3.2.13 Preparation of *fac*-[Ru($L^{p\text{-}Ph}$)$_3$][PF_6]$_2$ (i) PyPzH, THF, NaOH (2 M), 40 ^oC, 1 hr; (ii) Cs_2CO_3, Bu_4NI, CH_2Cl_2, 40 ^oC, 5 days.

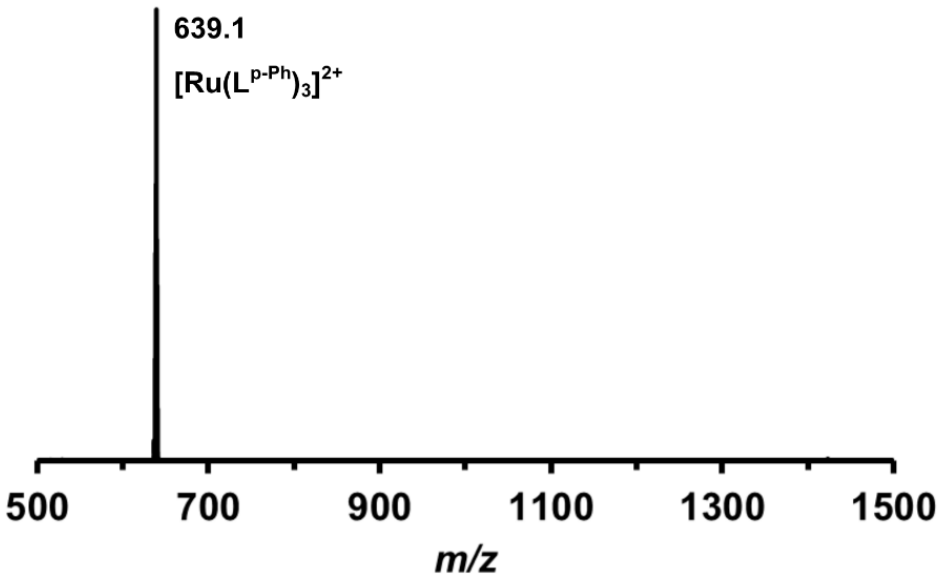

Figure 3.2.14 ESMS+ spectrum of *fac*-[Ru($L^{p\text{-}Ph}$)$_3$][PF_6]$_2$.

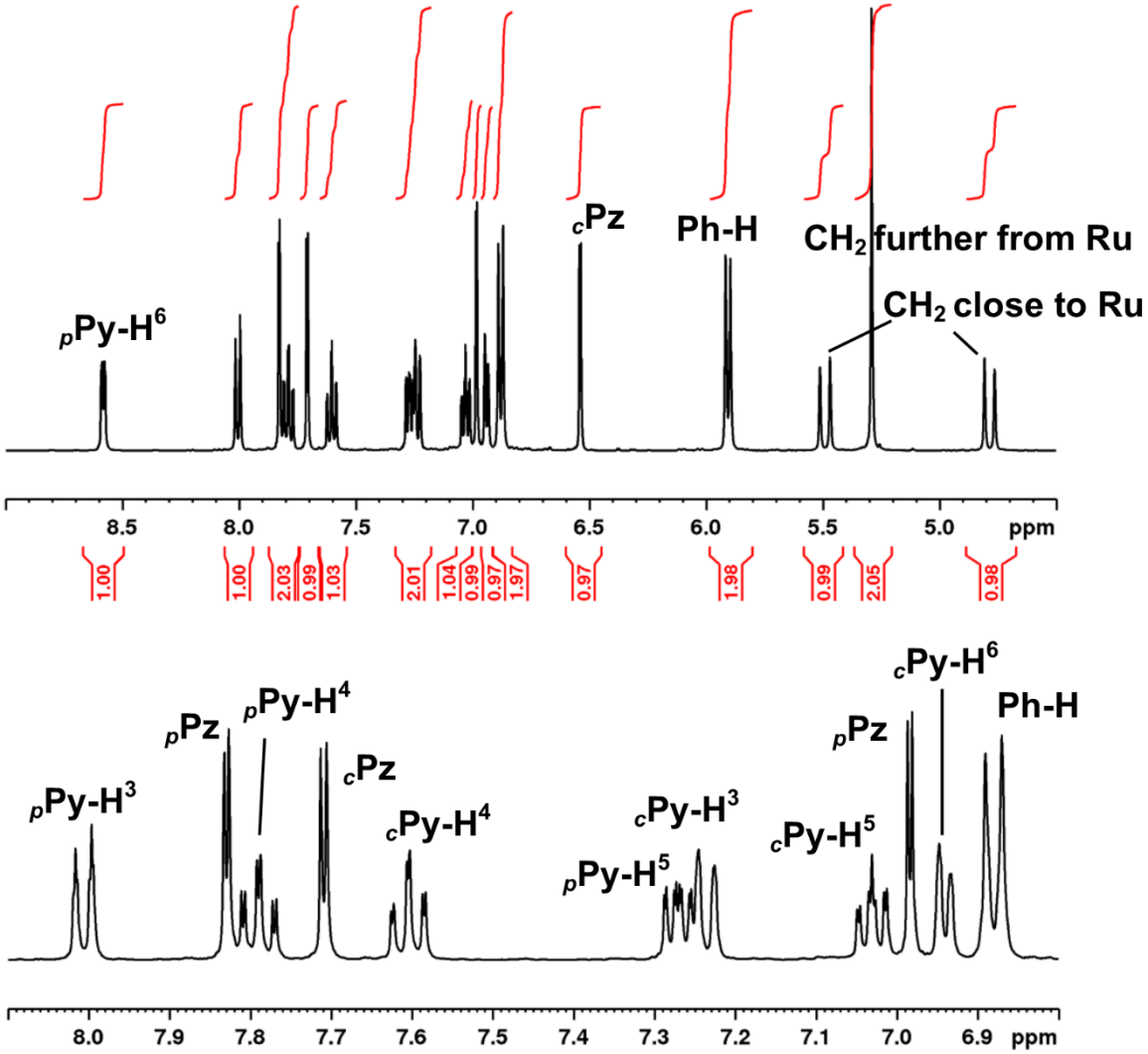

Figure 3.2.15 ^{1}H NMR spectrum of *fac*–[Ru($L^{p\text{-}Ph}$)$_3$][PF$_6$]$_2$ (CD_3CN, 400 MHz). Top: complete spectrum. Bottom: expansion of central region. (Py = pyridine, Pz = pyrazole, Ph = phenyl, *p* = pendant ring, *c* = coordinated ring).

The crystal structure of the complex cation of *fac*-[Ru($L^{p\text{-}Ph}$)$_3$][PF$_6$]$_2$•acetone is shown in Figure 3.2.16. The small crystals were weakly diffracting, and this dataset is the best of numerous attempts, but it is clear how the three pendant pyrazolyl-pyridine arms are directed to the same face of the complex. The phenyl group of each pendant arm forms a π-stacking interaction with a coordinated pyrazolyl-pyridine group from another ligand, as we have observed in related complexes.

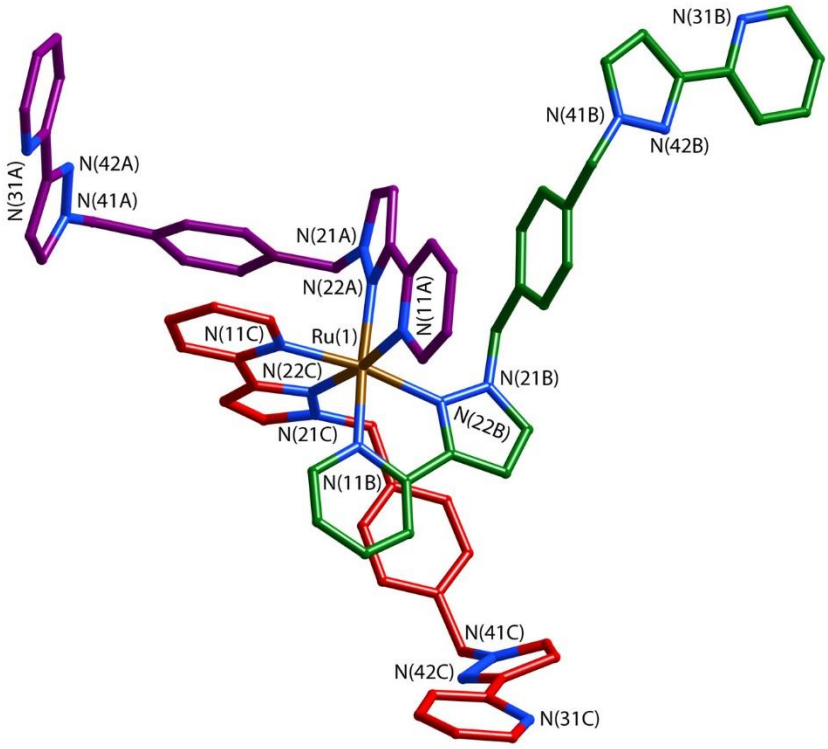

Figure 3.2.16 Structure of the complex cation of *fac*-$[Ru(L^{p\text{-}Ph})_3][PF_6]_2$•acetone with the three ligands coloured differently for clarity.

The same alkylation strategy was also applied using *mer*-$[Ru(PyPzH)_3]^{2+}$ as the starting material resulting in the isolation of pure *mer*-$[Ru(L^{p\text{-}Ph})_3][PF_6]_2$, as determined by ESMS and ^{1}H NMR spectroscopy (see Figure 3.2.17). The three inequivalent ligand arms are evidenced in the ^{1}H NMR spectrum by 60 ^{1}H environments. Within these peaks, sets of three can be seen for comparable protons on different arms. For example, three phenyl doublets are observed in the region of 6.2 – 5.9 ppm (labelled **A** in Figure 3.2.17), between 5.8 – 5.0 ppm the three diastereotopic CH_2 groups and three homotopic CH_2 groups can be found (labelled **a** and **b**, respectively, in Figure 3.2.17), and three pyrazolyl doublets are observed between 6.9 – 6.6 ppm.

Therefore, a method which can potentially be used to form any $[RuL_3]^{2+}$ complex based on a Ru(II) tris-pyrazolyl-pyridine core with isomeric purity, providing the appropriate alkyl bromide can be readily synthesised. Unfortunately, only the para-phenylene intermediate has been synthesised up to this point, as the other intermediate alkyl bromides required have been found to decompose readily. Consequently,

$[Ru(L^{p\text{-}Ph})_3]^{2+}$ is the only member of this series which has been isolated in an isomerically pure form thus far.

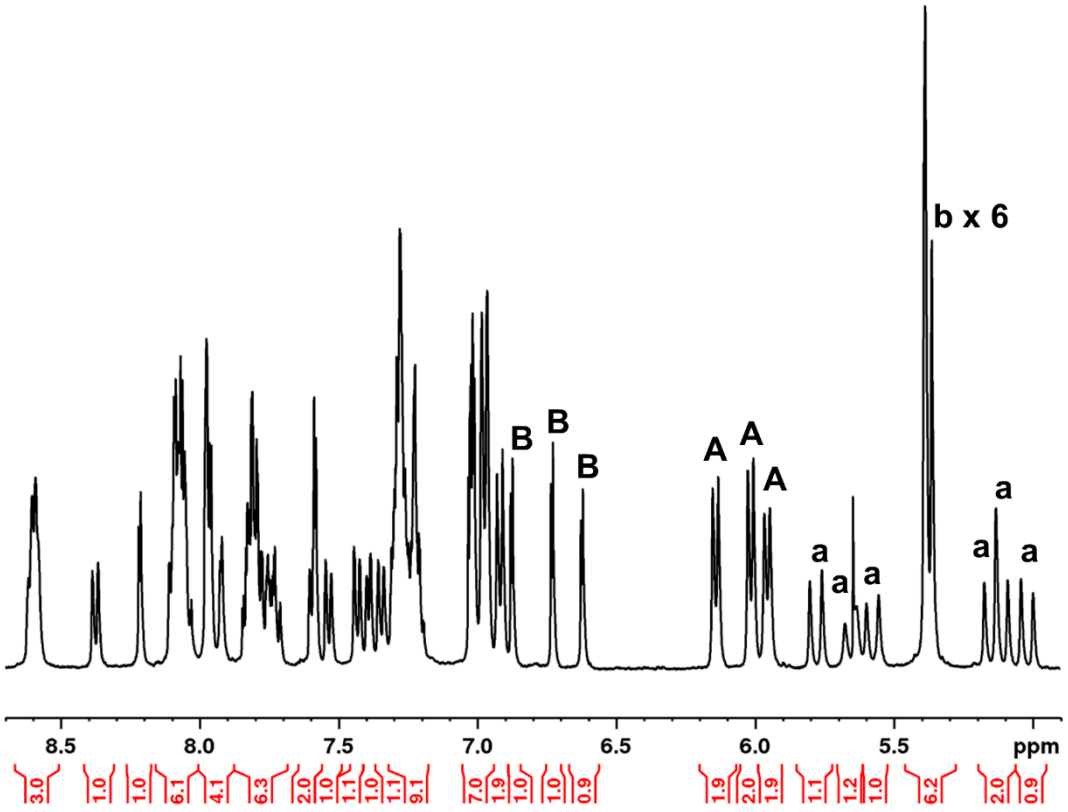

Figure 3.2.17 ^{1}H NMR spectrum (acetone-d_6, 400 MHz) of *mer*–$[Ru(L^{p\text{-}Ph})_3][PF_6]_2$. Labelled are three sets of CH_2 doublets (a), CH_2 singlets (b), phenyl doublets (A), and pyrazolyl doublets (B).

3.2.1.5 $[Ru(L^{3\text{-}Py})_3](PF_6)_2$

Using the same method as described for *fac*-$[Ru(L^{p\text{-}Ph})_3][PF_6]_2$, but using 3-(bromomethyl) pyridine hydrobromide instead of $Int^{p\text{-}Ph}$, resulted in the formation of the geometrically pure *fac*-$[Ru(L^{3\text{-}Py})_3]$-$[PF_6]_2$ with three pendant pyridyl groups (see Figure 3.2.1 for ligand structure). The ^{1}H NMR spectrum of the isolated yellow solid revealed twelve unique ^{1}H resonances, consistent with a C_3 symmetrical structure in which all ligands are equivalent (see Figure 3.2.18). Assignments (given in the experimental section) are made on the basis of the COSY spectrum. As observed in the ^{1}H NMR spectrum of *fac*-$[Ru(L^{p\text{-}Ph})_3][PF_6]_2$, the CH_2 protons are diastereotopic due to their close proximity to the Ru(II) chiral

centre and appear as a coupled pair of doublets at 5.9 and 5.1 ppm. Crystals of X-ray quality were grown, and the solid-state structure shows how the three pendant pyridyl groups are arranged on the same face of the complex (see Figure 3.2.19). Redissolved crystals of the complex gave a satisfactory mass spectrum (see Figure 3.2.20).

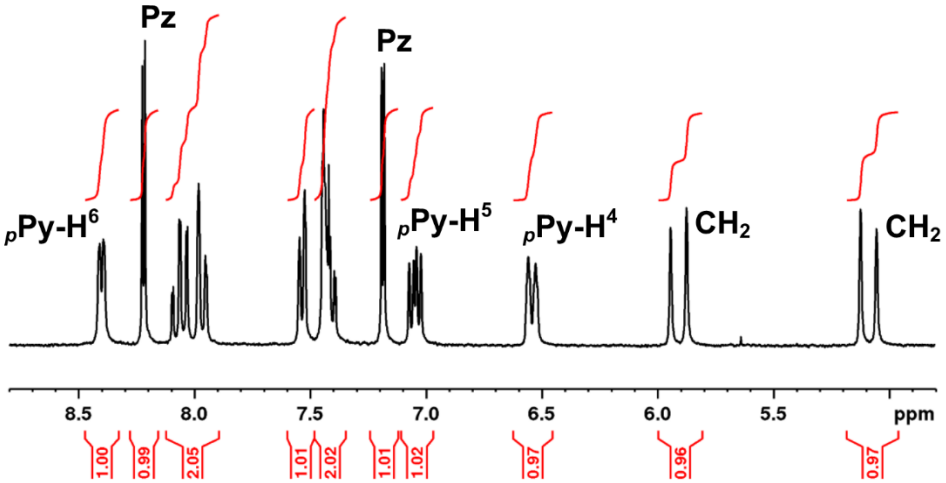

Figure 3.2.18 ^{1}H NMR spectrum (acetone-d_6, 250 MHz) of *fac*-[Ru($L^{3\text{-Py}}$)]$(PF_6)_2$ with partial assignment (Py = pyridine, Pz = pyrazole, Ph = phenyl, *p* = pendant ring; remaining assignment given in experimental section).

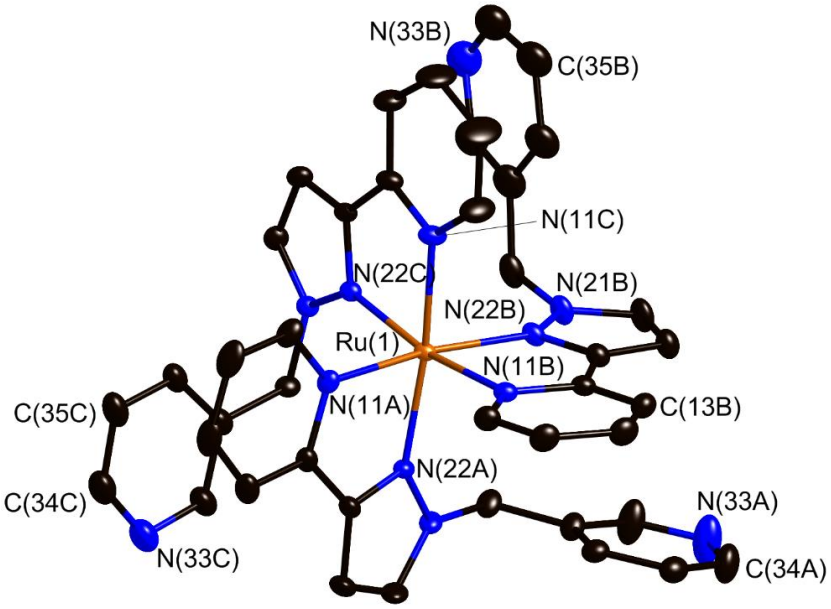

Figure 3.2.19 Crystal structure of the complex cation of *fac*-[Ru($L^{3\text{-Py}}$)]$(PF_6)_2$. Thermal ellipsoids of non-hydrogen atoms shown at 30 % probability.

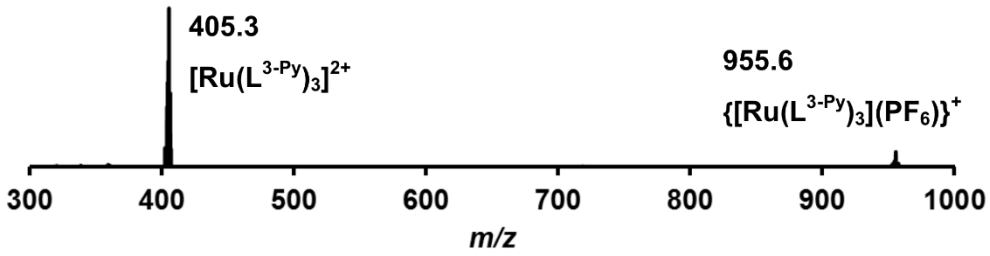

Figure 3.2.20 ESMS+ spectrum of redissolved crystals of *fac*-$[Ru(L^{3\text{-}Py})_3][PF_6]_2$.

The ligand $L^{3\text{-}Py}$ has not been previously studied within the Ward group, so there is no basis to predict which heterometallic complexes may be formed upon mixing *fac*-$[Ru(L^{3\text{-}Py})_3][PF_6]_2$ with labile transition metal cations. It is conceivable that upon reaction of the tris-monodentate 'complex-ligand' with 1.5 equivalents of a metal ion which can be 2-coordinate [e.g. Ag(I) or $\{Pd(en)\}^{2+}$; en = ethylenediamine], a heterometallic capsule may be formed (see Figure 3.2.21). However as discussed later, no crystals of heterometallic complexes were obtained to confirm this hypothesis; nonetheless, this could be a useful building block for heterometallic supramolecular assemblies.

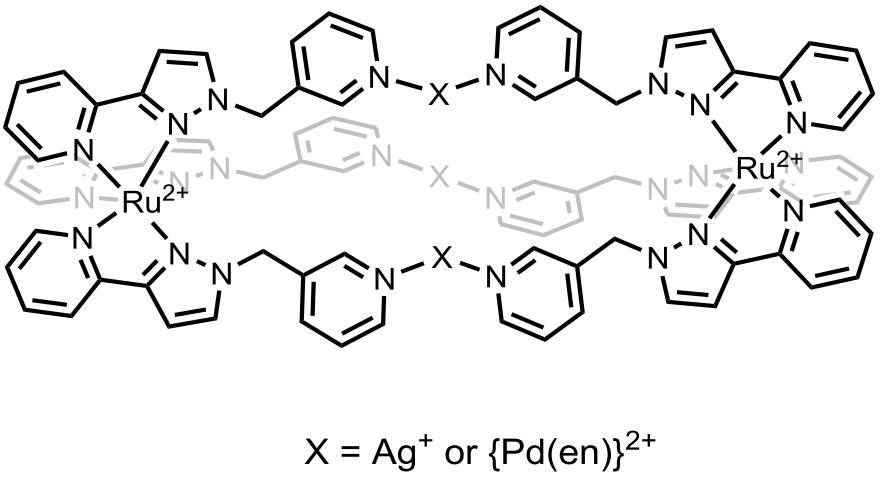

Figure 3.2.21 Possible structure of heterometallic capsules incorporating *fac*-$[Ru(L^{3\text{-}Py})_3]^{2+}$ units.

3.2.2 Stepwise synthesis of heterometallic cubic coordination cages

Having described the synthesis of a series of mononuclear complexes, our attention is now turned to the preparation of heterometallic coordination cages which, in the first instance, are based upon existing cages prepared by the Ward group. The cage family first studied is the $[M_8(L^{1,5\text{-nap}})_{12}]X_{16}$ octanuclear 'cube' [M = Co, Cd; X = a mono-anion such as BF_4^-, ClO_4^- or BPh_4^-]. There are several examples of such cages; all are based on a metal ion at each vertex of an approximate cube with the bridging ligand $L^{1,5\text{-nap}}$ spanning each of the twelve edges, giving each metal ion a tris(pyrazolyl-pyridine) coordination environment.[32,42,48,49] Importantly, the assembly requires that two of the metal ions (at either end of the long diagonal) have a *fac* tris-chelate geometry with the three pyridyl donors on one face of the octahedron and the three pyrazolyl donors on the other; whereas the other six metal ions have a *mer* tris-chelate geometry. With an inversion centre in the cage, this results in molecular S_6 symmetry with the C_3/S_6 axis through the two *fac* tris-chelate metal centres (see Figure 3.2.2).

The target of this work are the heterometallic analogues $[Ru_4M_4(L^{1,5\text{-nap}})_{12}](X)_{16}$ in which the Ru(II) and M(II) centres alternate. Each type of metal ion occupies strictly one *fac* and three *mer* tris-chelate sites in the cage superstructure. The *fac* / *mer* geometric isomerism could add another layer of complexity to the problem of controlled preparation of a heterometallic cage, but in this particular case, it works advantageously.

By starting with an inert $[Ru(L^{1,5\text{-nap}})_3]^{2+}$ unit as a pre-formed vertex, with three pendant sites at which cage assembly can be propagated by binding to labile Cd^{2+} ions, it follows that it will not be possible to have two Ru^{2+} ions adjacent to one another along one edge of the cube. The same is clearly true for the Cd^{2+} ions. The result must be strict alternation of the metal sites around the cube: this can be achieved in two ways which, due to the S_6 symmetry of the cube, are degenerate (see Figure 3.2.2). Consequently, a 3:1 mixture of *mer*:*fac* $[Ru(L^{1,5\text{-nap}})_3]^{2+}$ isomers would provide four pre-formed corners of the cube as the correct isomers, as well as all twelve ligands necessary to complete the assembly. Addition of four equivalents of a labile metal ion that forms octahedral tris-chelate complexes will complete the cube assembly with each type of ion in predictable positions (see Figure 3.2.22).

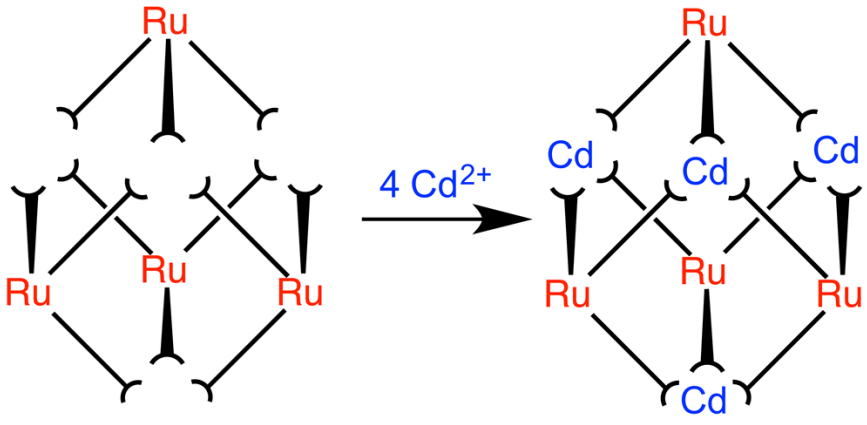

Figure 3.2.22 Schematic diagram of the reaction between four pre-formed $[Ru(L^{1,5\text{-nap}})_3]^{2+}$ complex units (each with three pendant binding sites) and four Cd^{2+} ions to complete assembly of the $[Ru_4Cd_4(L^{1,5\text{-nap}})_{12}]^{16+}$ cage. Arrangement of *fac* and *mer* centres is as shown in Figure 3.2.2.

The first step was the isolation of the kinetically inert mononuclear complex $[Ru(L^{1,5\text{-nap}})_3](PF_6)_2$ as a 1:3 mixture of *fac* and *mer* isomers; this has been described above (Section 3.2.1.1). The second step was to complete the assembly of the $[Ru_4Cd_4(L^{1,5\text{-nap}})_{12}]^{16+}$ cage by combining $[Ru(L^{1,5\text{-nap}})_3](PF_6)_2$ with labile Cd^{2+} ions in a 1:1 ratio, i.e. four of each type of unit as the cage requires (see Figure 3.2.22). The twelve pendant bidentate binding sites from four $[Ru(L^{1,5\text{-nap}})_3]^{2+}$ cations are exactly sufficient to combine with four Cd^{2+} ions ($4\ [Ru(L^{1,5\text{-nap}})_3]^{2+} + 4\ Cd^{2+} \rightarrow [Ru_4Cd_4(L^{1,5\text{-nap}})_{12}]^{16+}$), and the only way in which cage assembly can be completed is if the Cd^{2+} and Ru^{2+} centres are strictly alternating, as shown in Figure 3.2.22.

Reaction of $[Ru(L^{1,5\text{-nap}})_3](PF_6)_2$ (3:1 mixture of *mer* and *fac* isomers) with excess $Cd(ClO_4)_2$ in $MeNO_2$ at room temperature, followed by diffusion of di-isopropyl ether vapour into the solution, afforded a crop of small orange crystals. X-ray crystallographic analysis revealed the structure of the expected octanuclear cage (see Figure 3.2.23), which has been described before.[32,42,48,49] The key issue is crystallographic location of the Ru^{2+} and Cd^{2+} ions at different sites in the cage, which is non-trivial given their similar electron density and size which could lead either to disorder or to mis-identification.

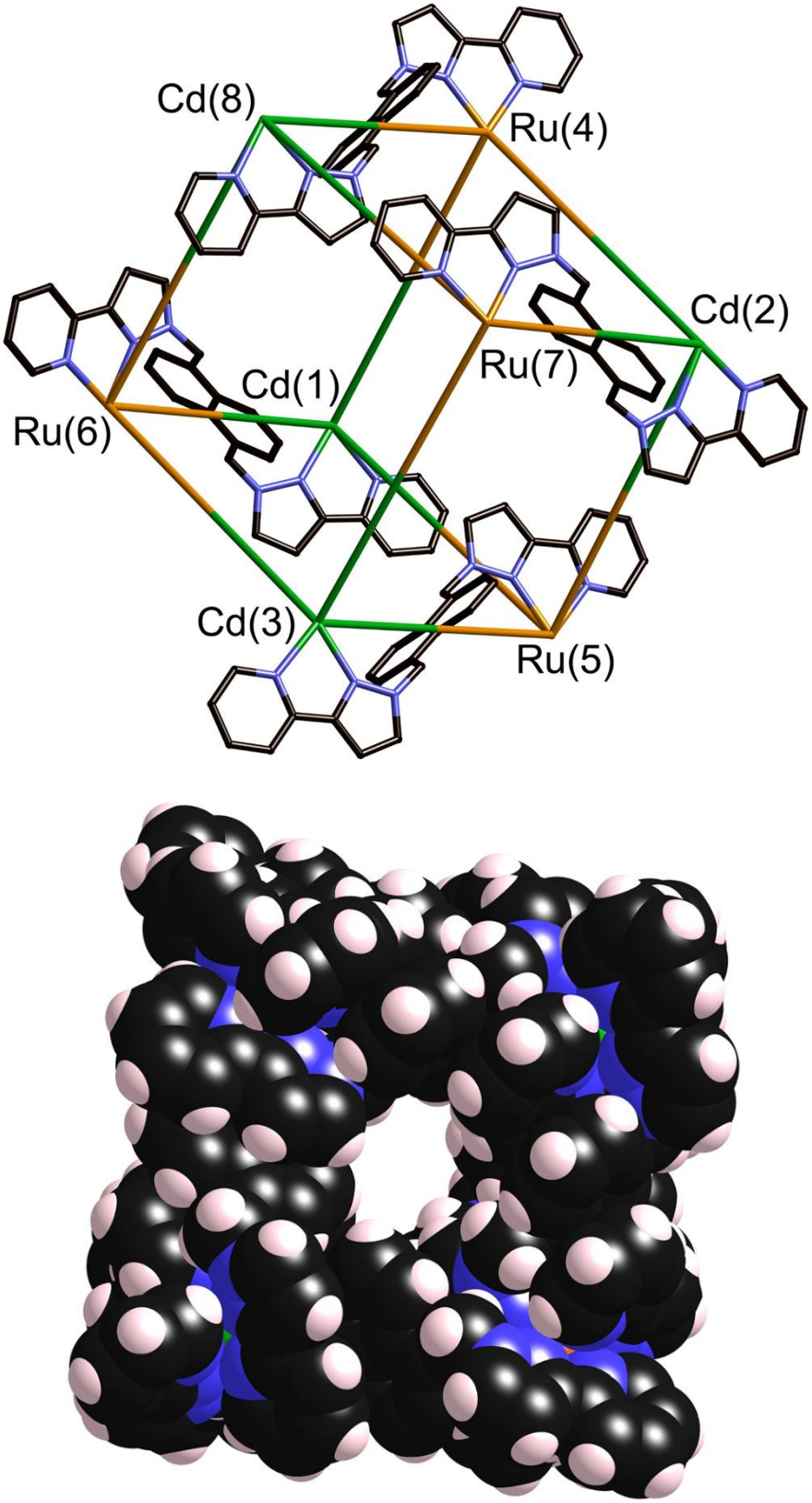

Figure 3.2.23 Two views of the cage complex cation in the structure of $[Ru_4Cd_4(L^{1,5\text{-nap}})_{12}](ClO_4)_{16}$. Top: a view emphasizing the approximately cubic array of metal ions with four of the bridging ligands included; Bottom, a space-filling view of the complete cage.

Two distinct pieces of crystallographic evidence confirmed the presence of four Ru^{2+} and four Cd^{2+} ions in the desired alternating arrangement. Firstly, these two ions should have different average M—N distances, with Ru—N distances shorter than Cd—N. The four metal positions identified as Ru^{2+} consistently had significantly shorter bond distances (average, 2.17 Å; see Figure 3.2.24) than the four positions identified as Cd^{2+} (average, 2.23 Å; see Figure 3.2.4). Secondly, correct assignment of Ru / Cd positions resulted in all eight metal ions having comparable and reasonable isotropic displacement parameters; inversion of the assignment, i.e. deliberately mis-labelling Ru as Cd and vice versa, resulted in one set of displacement parameters being anomalously large and the other set being anomalously small, as expected.

Cd(1)	2.22 Å	Ru(4)	2.18 Å
Cd(3)	2.24 Å	Ru(5)	2.17 Å
Cd(2)	2.22 Å	Ru(6)	2.19 Å
Cd(8)	2.22 Å	Ru(7)	2.16 Å

Figure 3.2.24 Average M—N bond distances around each metal centre in the complex cation of $[Ru_4Cd_4(L^{1,5\text{-nap}})_{12}](ClO_4)_{16}$.

The crystalline product was further analysed by ES mass spectrometry and ^{1}H NMR spectroscopy. The ES mass spectrum reveals a series of peaks at *m/z* $[Ru_4Cd_4(L^{1,5\text{-nap}})_{12}(ClO_4)_{16-z}]^{z+}$ (z = 4 – 9) corresponding to the intact complex cation associated with varying numbers of anions (see Figure 3.2.25). High-resolution ES spectra give sets of peak clusters for the ions with z = 5, 6, 7 that match exactly what is expected (see Figure 3.2.26). A ^{1}H NMR spectrum of $[Ru_4Cd_4(L^{1,5\text{-nap}})_{12}](ClO_4)_{16}$ in CD_3NO_2 was not very informative as it contains 88 independent proton environments in the region 4.7 – 8.4 ppm;[†] even at 800 MHz the signals overlap too much for meaningful assignment (see Figure

[†] The homonuclear cages $[M_8L_{12}]X_{16}$ contain 44 proton environments because the two different ligand environments (connecting *fac*/*mer* and *mer*/*mer* metal centres, with six ligands in each environment) have no internal symmetry.[31] In this heterometallic complex the symmetry is reduced by a further factor of two due to loss of the inversion centre.

3.2.27). However, a DOSY spectrum showed that all of the signals have the same diffusion constant, confirming the presence of a single large assembly in solution (see Figure 3.2.28).

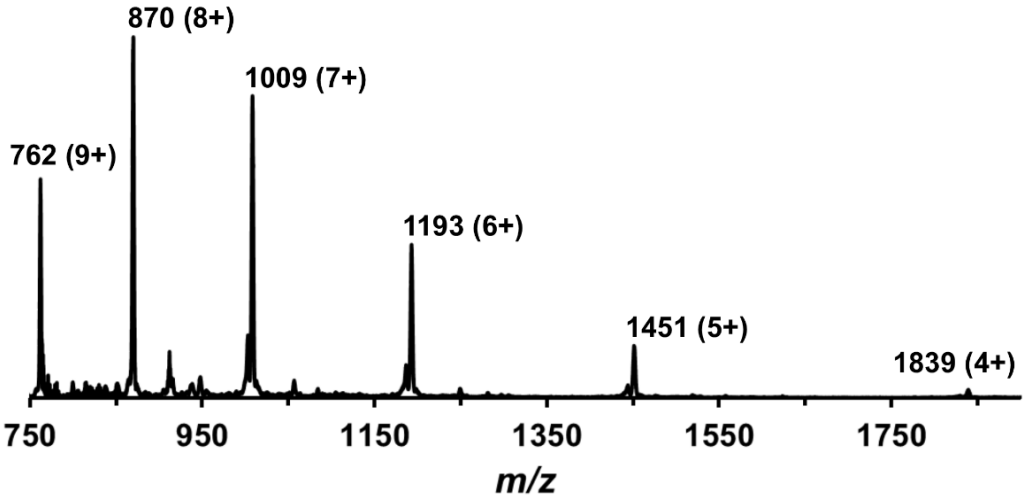

Figure 3.2.25 Electrospray mass spectrum of $[Ru_4Cd_4(L^{1,5\text{-nap}})_{12}](ClO_4)_{16}$ showing a sequence of peaks corresponding to $[Ru_4Cd_4(L^{1,5\text{-nap}})_{12}(ClO_4)_{16\text{-}z}]^{z+}$, i.e. loss of 4 – 9 perchlorate anions from the complete complex.

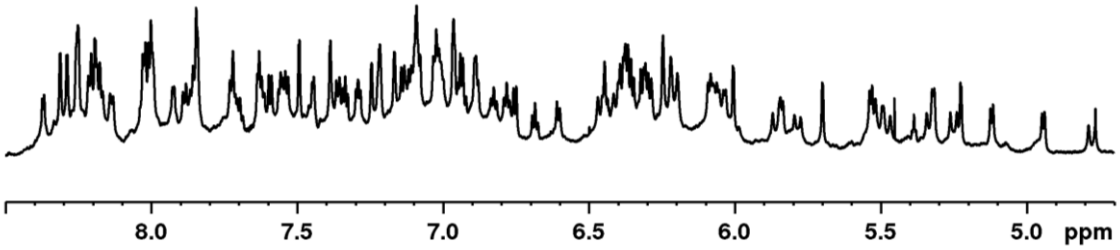

Figure 3.2.27 ^1H NMR spectrum (800 MHz, CD_3NO_2) of redissolved crystals of $[Ru_4Cd_4(L^{1,5\text{-nap}})_{12}](ClO_4)_{16}$.

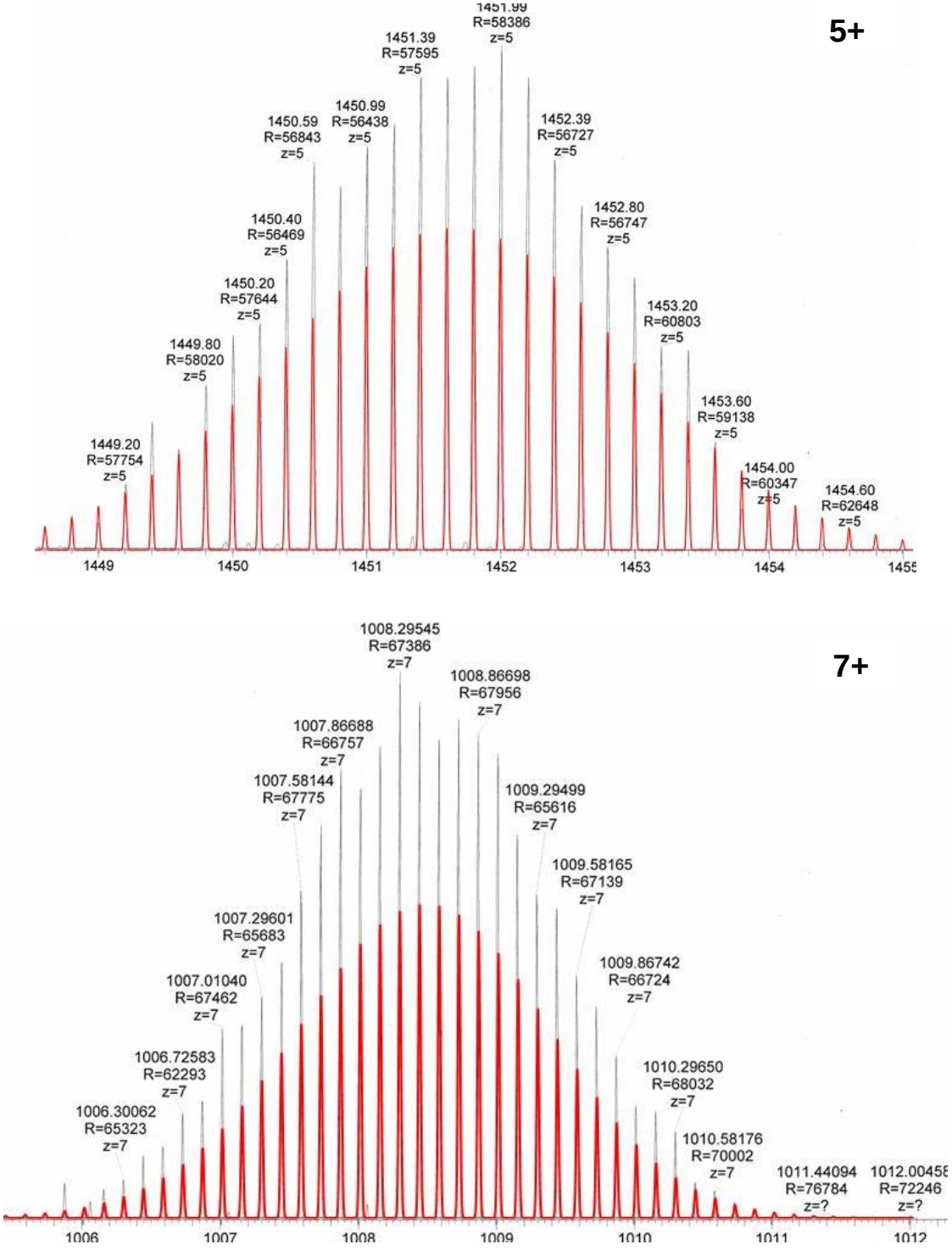

Figure 3.2.26 Expansions of high-resolution ESMS+ mass spectra of redissolved crystals of $[Ru_4Cd_4(L^{1,5\text{-nap}})_{12}](ClO_4)_{16}$, showing theoretical (red) and experimental (grey) isotope patterns and accurate masses for the 5 and 7+ peak clusters.

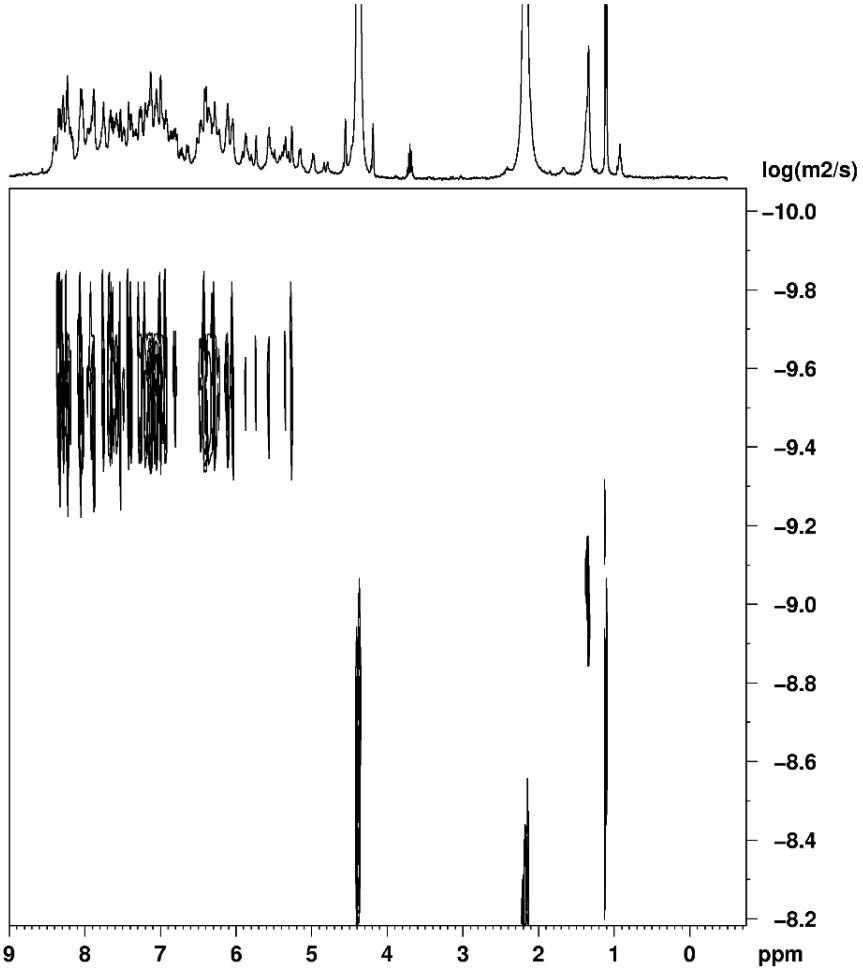

Figure 3.2.28 ^{1}H 2D DOSY NMR spectrum (400 MHz, CD_3NO_2) of redissolved crystals of $[Ru_4Cd_4(L^{1,5\text{-nap}})_{12}](ClO_4)_{16}$ emphasising how all of the signals associated with the cage have the same diffusion constant within experimental uncertainty.

Finally the electrochemical behaviour of the cage was investigated. The model complex $[Ru(L^{Me})_3](PF_6)_2$ (synthesis described in Chapter 2)[47] shows a reversible Ru^{2+}/Ru^{3+} couple at +0.95 V vs. ferrocene / ferrocenium (Fc/Fc+) for the *fac* isomer, and +0.92 V for the *mer* isomer – a difference of only 30 mV between the isomeric forms [see Figure 3.2.29, (a) and (b)]. For $[Ru_4Cd_4(L^{1,5\text{-nap}})_{12}](ClO_4)_{16}$ a single symmetric wave at +0.96 V vs. Fc/Fc^+ is observed, which is ascribed to all four Ru^{2+}/Ru^{3+} couples that are coincident because of the absence of electronic coupling between the Ru centres [see Figure 3.2.29, (c)]. The separate processes for the *fac* and *mer* centres are not resolved, but the wave is slightly broadened (ΔEp = 120 mV).

An important consequence of this redox activity is that the charge on the cage can be switched reversibly between charges of 16+ and 20+. Given that recent work in the Ward group has demonstrated how binding of electron-rich organic guests involves a substantial contribution from charge-assisted hydrogen-bonding to the internal surface of the cage, at the position where the electrostatic potential is most positive,[42] a reversible redox swing should affect the strength of the host/guest interaction and may provide a mechanism for controlling uptake and release of bound guests. Redox changes also offer the possibility of reversible changes in luminescence[6,40] or chromic[8] properties of the cage.

This work has shown how the rational design and synthesis of a heterometallic Ru_4Cd_4 coordination cage is possible *via* a combination of kinetically inert and labile metal ions, in which the four Ru^{2+} and four Cd^{2+} ions occupy specific sites in the array. The synthesis of this cage was facilitated by the 3:1 ratio of *mer*/*fac* isomers present in the $[Ru(L^{1,5\text{-nap}})_3]^{2+}$ subcomponent. The next piece of work investigated whether using a subcomponent with a 'non-ideal' ratio of isomers (i.e. not 3:1 *mer*/*fac*) would lead to the expected heteronuclear cage product.

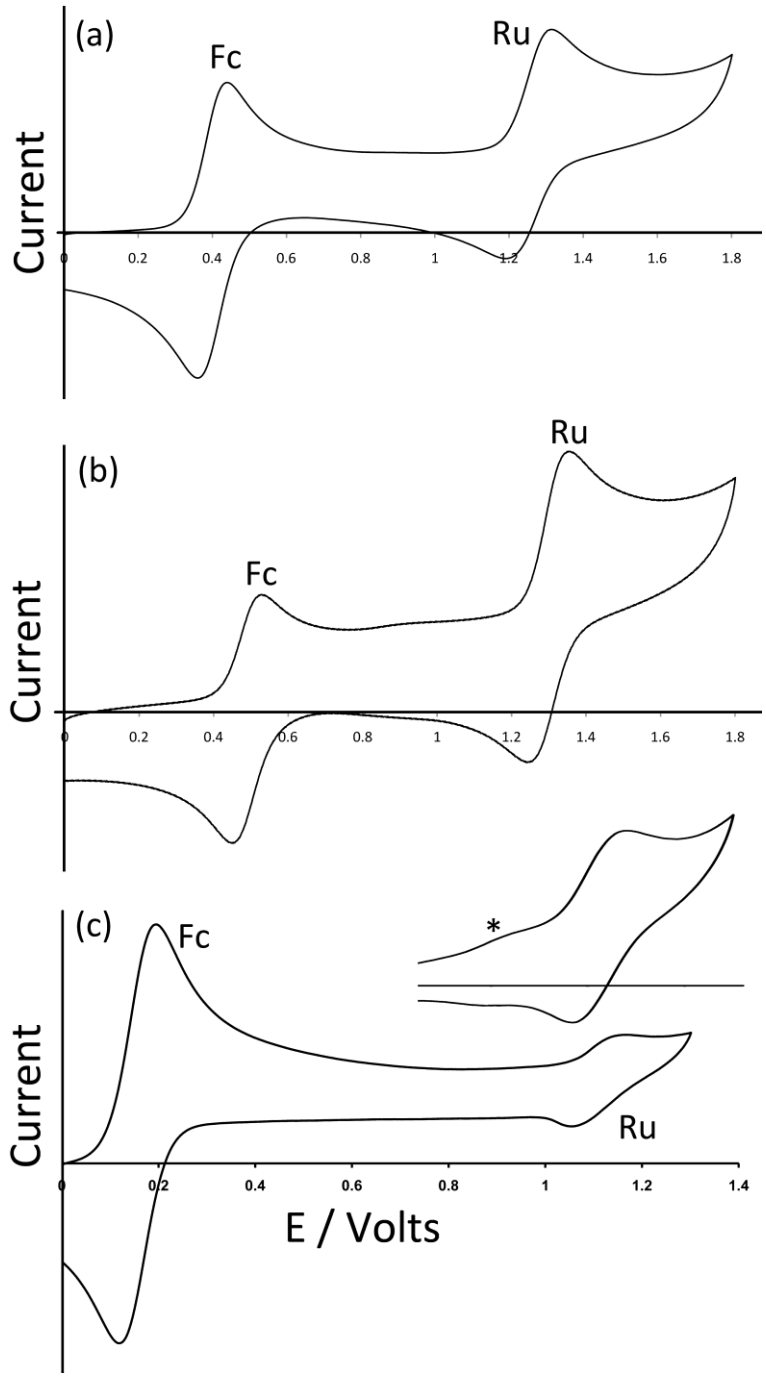

Figure 3.2.29 Cyclic voltammograms (MeCN / Bu_4NPF_6, Pt working electrode, scan rate 200 mV/sec) of (a) *fac*-$[Ru(L^{Me})_3](PF_6)_2$; (b) *mer*-$[Ru(L^{Me})_3](PF_6)_2$; (c) $[Ru_4Cd_4(L^{1,5\text{-nap}})_{12}](ClO_4)_{16}$. The reference electrode was a silver wire pseudo-reference, hence ferrocene was used as in internal standard (wave labelled 'Fc') and the potential of this is taken as zero in each case. The resulting calculated potentials for the Ru(II)/Ru(III) processes (labelled 'Ru') are in the main text. On trace (c), the small shoulder before the Ru(II)/Ru(III) wave (labelled * in the expansion) probably arises from the naphthyl groups in the ligands L as a similar feature occurs in the CV of the free ligand.

As described in Section 3.2.1.2, cubic M_8L_{12} cages are also formed with the ligand $L^{m\text{-}Ph}$, possessing an identical metal framework as seen with $L^{1,5\text{-}nap}$ based cages with identical S_6 symmetry.[33] Therefore, a synthesis analogous to that of $[Ru_4Cd_4(L^{1,5\text{-}nap})_{12}](ClO_4)_{16}$ could be performed with the subcomponent $[Ru(L^{m\text{-}Ph})_3]^{2+}$. However, the synthesis of $[Ru(L^{m\text{-}Ph})_3](PF_6)_2$ gave the product not in the desired isomeric ratio, but as an approximately 6.8:1 *mer*/*fac* mixture. With no method to separate the isomers, assembly of a heterometallic cage was performed using the as-isolated 6.8:1 *mer*/*fac* mixture of the Ru(II) components, in the hope that the self-assembly process would select the components necessary to complete a stable cage structure.

Thus, a combination of $[Ru(L^{m\text{-}Ph})_3](PF_6)_2$ and 1 equivalent of $Co(BF_4)_2$ in dichloromethane/methanol was mixed at room temperature overnight. After workup, a yellow solid was collected which was slowly recrystallized from nitromethane by vapour diffusion with THF. The mixture was monitored by ESMS over the course of two months whilst the recrystallization was occurring, revealing an interesting product evolution. Initially the spectrum was dominated by a dinuclear species $\{[CoRu(L^{m\text{-}Ph})_3]X_2\}^{2+}$ peaks [*m/z* 751, 785, 814; X = PF_6, BF_4 or F; see Figure 3.2.30(a)], but after a week a series of peaks corresponding to the tetranuclear $\{[Co_2Ru_2(L^{m\text{-}Ph})_6]X_5\}^{3+}$ grew in [*m/z* 1036, 1055, 1075, 1094; see Figure 3.2.30(b)]. Finally, after several months, a series of peaks corresponding to the octanuclear $\{[Co_4Ru_4(L^{m\text{-}Ph})_{12}]X_{16\text{-}n}\}^{n+}$ had grown in [e.g. *m/z* 806, 942, 1123, 1377, 1757 for n = 8 – 4, respectively; see Figure 3.2.30(c) and Figure 3.2.31].

After several months, the recrystallization mixture yielded a crop of yellow blocks and orange shards. The yellow blocks were more abundant and of excellent X-ray quality, and therefore a crystal structure was determined. The structure revealed an octanuclear coordination cage cation, as expected on the basis of the mass spectrum, but with the formulation $[Ru_4Co_4(L^{m\text{-}Ph})_{12}\{Na(BF_4)_4\}](PF_6)_5(BF_4)_8$ (see Figures 3.2.32 and 3.2.33). The metal framework was approximately cubic, with alternating Ru(II) and Co(II) ions at each metal site, as expected (Ru – Co separations along the edges lying in the range 9.79 – 10.63 Å; M – M – M angles between 80.0 º – 103.0 º). However, the structure revealed two surprises.

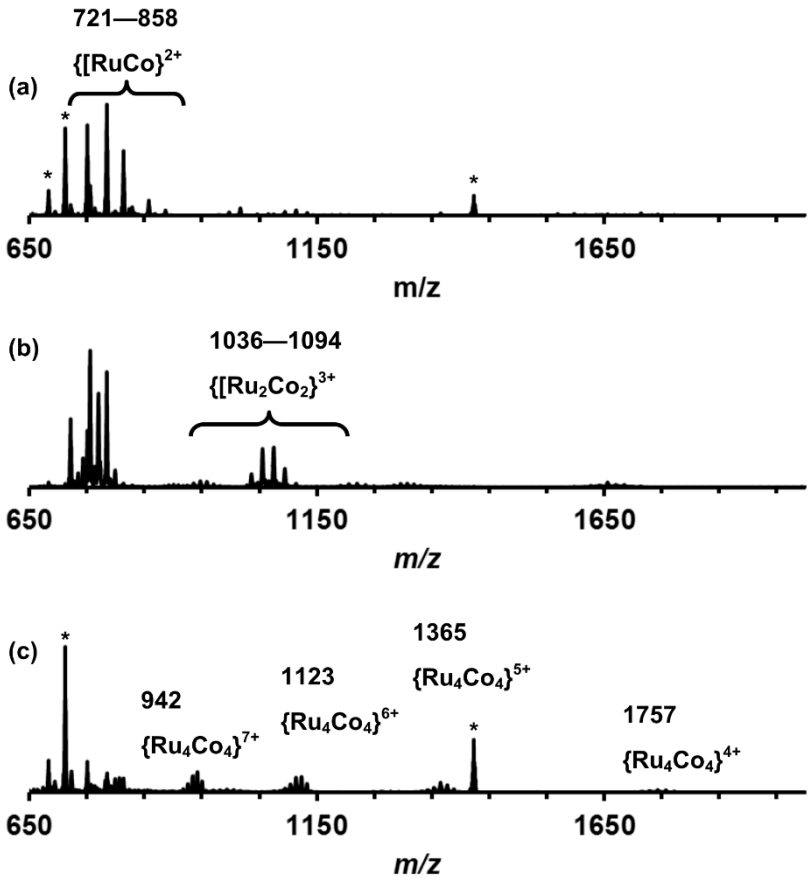

Figure 3.2.30 Series of electrospray mass spectra following the evolution of the product mixture of $[Co_nRu_n(L^{m\text{-}Ph})_{3n}]X_{4n}$. (a) Product mixture after 1 day; (b) product mixture after 1 week; (c) product mixture after 2 months. Peaks labelled with an asterisk, *, are due to $[Ru(L^{m\text{-}Ph})_3]^{2+}$, presumably arising from fragmentation of the complete complexes.

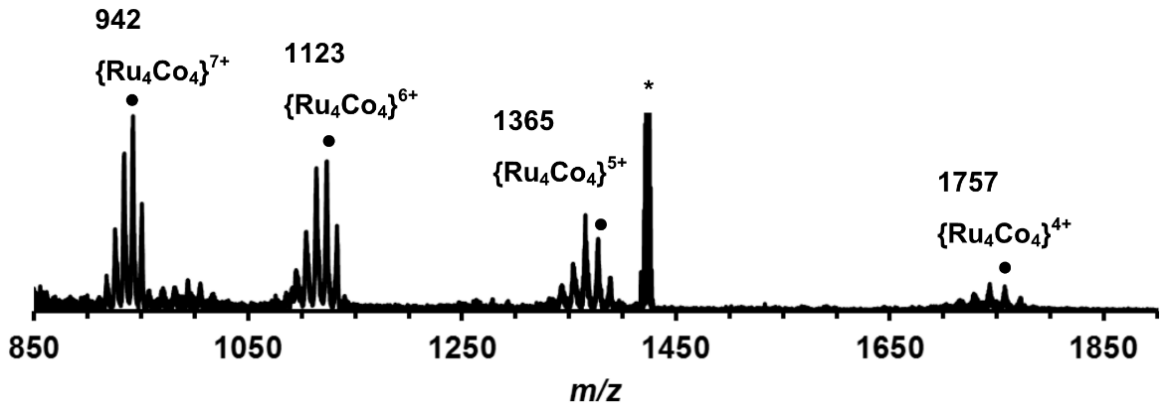

Figure 3.2.31 Expansion of the ES mass spectrum of $[Co_4Ru_4(L^{m\text{-}Ph})_{12}]X_{16}$. A cluster of peaks is observed at each member of the series, due to differing anion formulations. The *m/z* values given for the peaks labelled with a dot, ●, where $X_{16\text{-}n} = \{(PF_6)_{15}(BF_4)\} - nPF_6$.

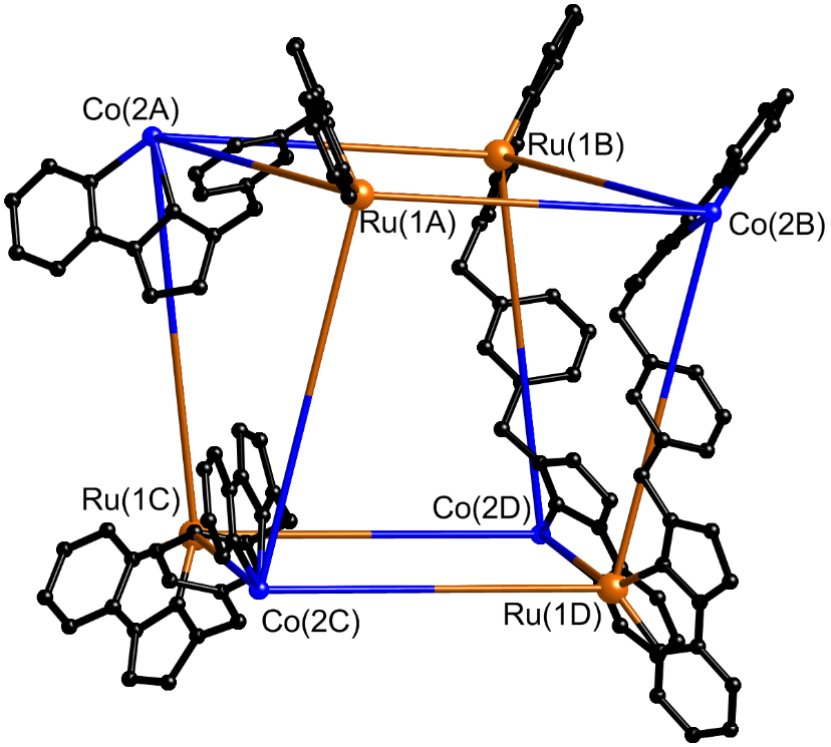

Figure 3.2.32 Partial view of the complex cation of $[Ru_4Co_4(L^{m\text{-}Ph})_{12}\{Na(BF_4)_4\}](PF_6)_5(BF_4)_8$. All Ru and all Co atoms are crystallographically equivalent, and are labelled differently for clarity. Only four (crystallographically equivalent) ligands are shown.

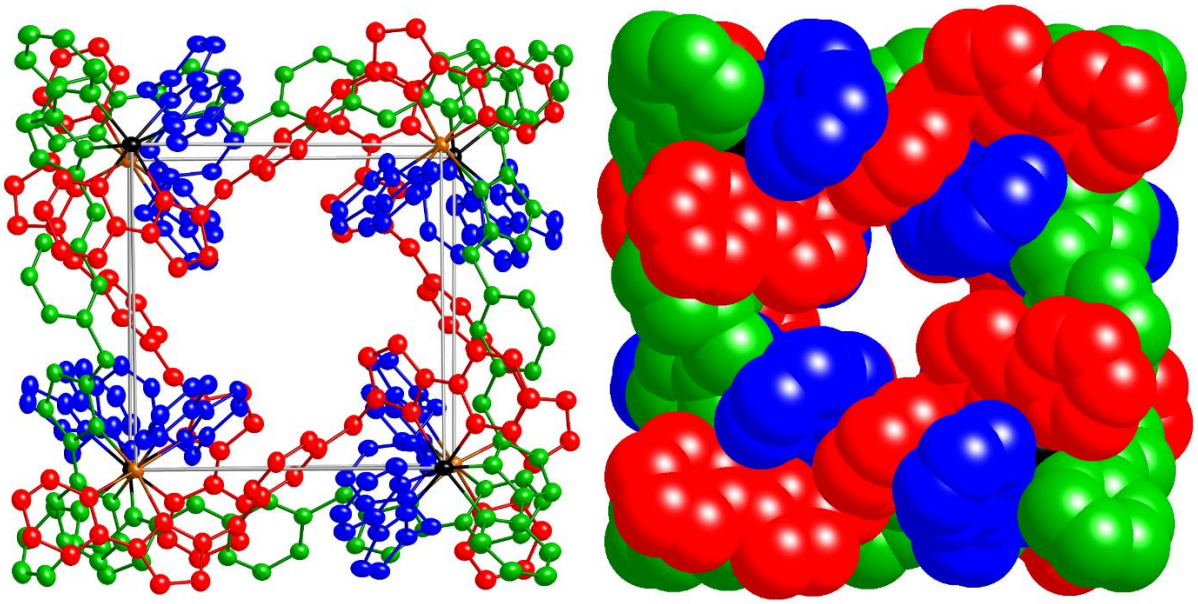

Figure 3.2.33 Left: View of the complete complex cation of $[Ru_4Co_4(L^{m\text{-}Ph})_{12}\{Na(BF_4)_4\}](PF_6)_5(BF_4)_8$. Thermal ellipsoids shown at 40 % probability, and crystallographically equivalent ligands are coloured the same. Right: Space-filling view of the complex cation from the same perspective.

The octanuclear cage crystallised in the tetragonal space group P-42_1m, with S_4 symmetry (axis through the centre of the face of the cube), such that one quarter of the complex cation is in the asymmetric unit, comprising one metal centre with a *fac* tris-chelate geometry and the second with a *mer* tris-chelate geometry. This has the consequence of the symmetry-expanded cube having alternating *fac* and *mer* metal sites around the framework, an arrangement which has not occurred in any previous cages of this family, even in the homonuclear analogues.[33,50,51] Thus, the cubic cage is of a new structural type.

Identification of the metal at each site turned out to be trivial; widely different M – N bond lengths [average 2.07 Å (*mer*) and 2.13 Å (*fac*)] and physically unreasonable thermal parameters upon mislabelling reveal that the *mer* site is occupied by Ru, and the *fac* site by Co (see Figure 3.2.34). That this product should crystallise out with exclusively *mer*-$[Ru(L^{m\text{-}Ph})_3](PF_6)_2$ can be rationalised on the basis that a large excess of this isomer was used in the cage-forming reaction. It is possible that the less-abundant orange shards contained *fac*-$[Ru(L^{m\text{-}Ph})_3](PF_6)_2$ in the more usual S_6 cubic cage, with one Ru(II) ion in the *fac* site and the other three at alternating *mer* positions (see Figure 3.2.2), in what would be an eloquent display of self-sorting. Unfortunately, at the time of writing a crystal structure has not been determined for the orange shards, so this hypothesis remains unproved, although the mass spectrum is consistent with a $[Co_4Ru_4(L^{m\text{-}Ph})_{12}]^{16+}$ cage.

Site	Label	Isotropic thermal parameter, U (Å^2)	Average M-N bond length (Å)
mer	Ru	0.033	2.07*
fac	Co	0.038	2.14
mer	Co	0.003	2.06**
fac	Ru	0.086	2.14

Figure 3.2.34 Table summarising the key crystallographic information for correct* and deliberate mis-assignment** of the different metal sites.

* Correct assignment of metals gives sensible thermal parameters.
** Deliberate mis-assignment of metals with physically unreasonable thermal parameters.

The new geometry for an M_8L_{12} cubic cage is interesting in itself, but equally interesting was what lay inside the cavity. Usually with this family of cages, a solvent molecule or anion is found directed at the convergent methylene protons surrounding the *fac* vertices. As there are four *fac* vertices in this structure, one might assume that there could be four guest molecules within the cavity, one occupying the binding pocket at each *fac* tris-chelate vertex, and this is what is observed. Within the cavity there lie four tetrafluoroborate anions, one directed towards each *fac* vertex. The organisation of these four anions into a tetrahedral array – dictated by the positioning of the four *fac* tris-chelate sites in the cube – results in formation of a central space surrounded by these four anions - a 'cavity within a cavity', within which is bound a sodium anion, presumably arising from sodium in the glassware (see Figures 3.2.35 and 3.2.36). Again, two key pieces of evidence support this identification; the bond length between the nearest fluorine and the encapsulated atom is consistent with a Na-F bond [Na(1) – F(32) distance 2.46 Å; Na(1) – F(31) distance 2.82 Å],[52] and the thermal parameters become nonsensical when the atom is labelled differently. The close proximity of the four anions is stabilised by coordination to sodium(I), and numerous CH•••F close contacts between the coordinated ligand and the anions, the shortest of which is 2.23 Å between H(25C) and F(32).

This 'complex within a complex' requires three layers in the self-assembly; a sodium cation binds to four tetrafluoroborate anions in an approximate tetrahedral array, around which eight metal cations and twelve ligands assemble into a cubic coordination cage. There is a remarkable degree of complexity in such an arrangement, one which draws parallels with the metallacrowns first reported by Pecoraro and co-workers.[53-56] In their discovery, they found that four salicylhydroximate molecules and four Mn(III) ions self-assemble around a Mn(II) ion in an inorganic analogue of a M^{2+}(12-crown-4) complex.[53] This is similar to the arrangement of fluorine atoms around the sodium atom in this structure, whose arrangement further templates the formation of a cubic coordination cage.

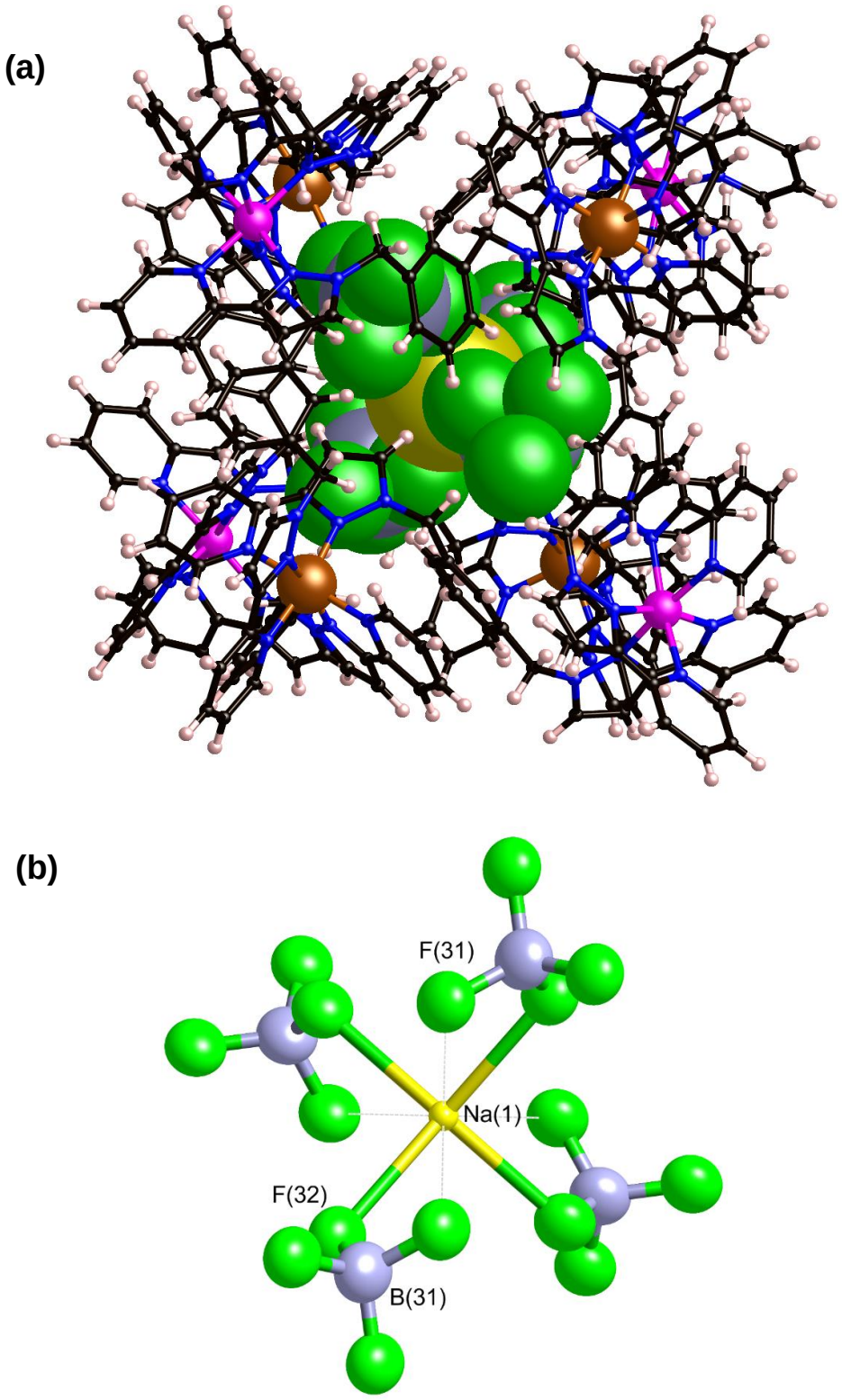

Figure 3.2.35 Two views of the complex and bound guests of $[Ru_4Co_4(L^{m\text{-}Ph})_{12}\{Na(BF_4)_4\}](PF_6)_5(BF_4)_8$. (a) View of the host-guest complex, with the guest $[Na(BF_4)_4]^{3-}$ shown in space-filling mode, and the cage shown in ball-and-stick mode. (b) Thermal ellipsoid plot of the bound guest $\{Na(BF_4)_4\}^{3-}$, ellipsoids shown at 40 % probability.

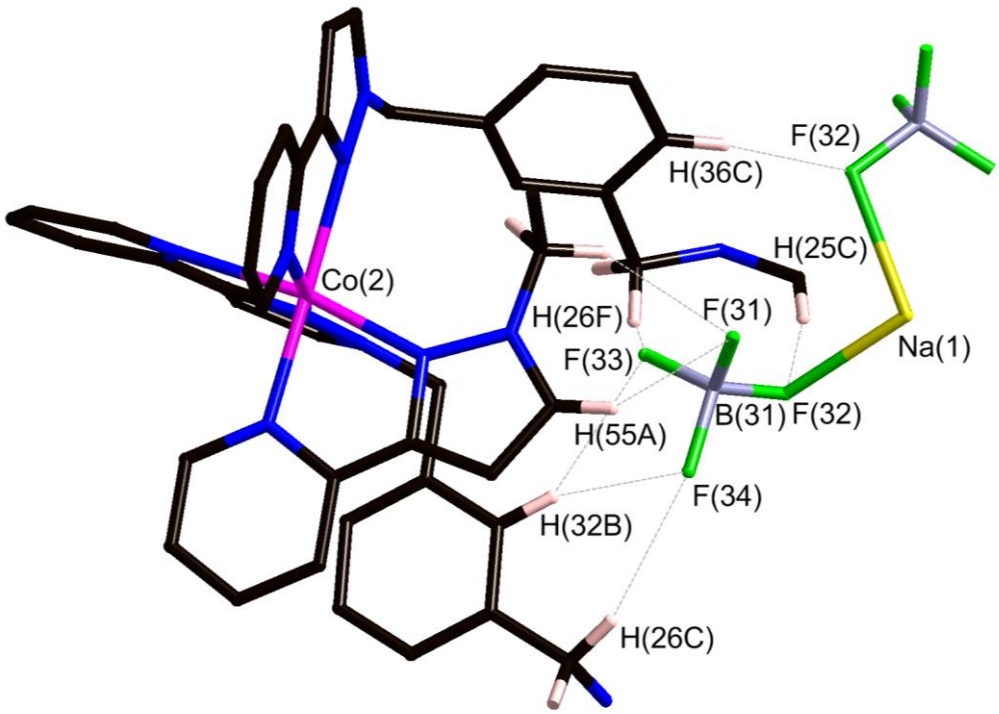

Figure 3.2.36 Partial view of one of the *fac*-$[Co(L^{m\text{-}Ph})_3]^{2+}$ vertices in the $[Ru_4Co_4(L^{m\text{-}Ph})_{12}]^{16+}$ complex cation, with numerous CH•••F interactions between coordinated ligands and the $[Na(BF_4)_4]^{3-}$ anion indicated by dashed lines.

We have therefore shown how the rational design and synthesis of a heterometallic Ru_4Cd_4 coordination cage is possible *via* a combination of kinetically inert and labile metal ions, in which the four Ru^{2+} and four Cd^{2+} ions occupy specific sites in the array. We have also shown how an unexpected product can arise from the self-assembly process when a 'non-ideal' ratio of isomers (i.e. not 3:1 *mer*/*fac*) in the $[RuL_3]^{2+}$ subcomponent is used. It follows from this that the structure of the resultant coordination cage can be possibly tailored by the isomeric identity of the $[RuL_3]^{2+}$ subcomponent, and further studies are being carried out within the group to examine this.

3.2.3 Stepwise assembly of an adamantoid Ru_4Ag_6 cage by control of metal coordination geometry at specific sites

As mentioned in Section 3.1, many of the cages described by the Ward group have a metal centre with *fac* tris-chelate geometry at specific sites in the cage.[32-35] By controlling geometric isomerism at specific sites in a cage, one might be able to direct formation of specific assemblies. For example, a mixed-metal hexadecanuclear $[Ru_4M_{12}L_{24}]^{32+}$ cage might be synthesised by combination of *fac*–$[Ru(L^{p\text{-}Ph})_3][PF_6]_2$ with the M(II) ions and additional ligand required to form the assembly, in which all Ru(II) ions would occupy the face-capping *fac* tris-chelate sites (this is described in more detail later).

In order to test this theory of controlling geometric isomerism at specific sites in a cage, a simple reaction was set up with the isomerically pure subcomponent *fac*–$[Ru(L^{p\text{-}Ph})_3][PF_6]_2$ and Ag(I) ions. Ag(I) generally forms four-coordinate bis-chelate complexes with pyrazolyl-pyridine ligands of this type, which have been shown to form high-quality crystals and thus facilitate X-ray analysis.[57,58] On the basis that three pendant bidentate sites are available for coordination in *fac*–$[Ru(L^{p\text{-}Ph})_3][PF_6]_2$, we combined *fac*–$[Ru(L^{p\text{-}Ph})_3][PF_6]_2$ with 1.5 equivalents of $AgPF_6$ to maximise the likelihood of a structure forming that conforms to the principle of maximum site occupancy, with all metal ions coordinatively saturated and all ligands fully coordinated.[59] If each pendant ligand fragment coordinates to a different Ag(I) ion, as is likely on steric grounds given the distance between the pendant pyrazolyl-pyridine units, we expect a mixed-metal cage in which each $[Ru(L^{p\text{-}Ph})_3]^{2+}$ unit caps a triangular array of Ag(I) ions.

Slow crystallisation of the reaction mixture afforded X-ray quality crystals of what proved to be a decanuclear Ru_4Ag_6 cage $[\{Ru(L^{p\text{-}Ph})_3\}_4Ag_6](PF_6)_{14}$ (see Figures 3.2.37 – 3.2.39). The cage has an adamantane-like structure, with a Ru(II) tris-chelate unit at each of the four three-connected vertices which are arranged in an approximate tetrahedron. An Ag(I) bis-chelate unit occupies each of the six two-connected vertices. Thus the structure can be described as a tetrahedral array of Ru(II) ions with an Ag(I) ion lying in the centre of each Ru•••Ru edge (see Figure 3.2.37), with every adjacent Ru(II)/Ag(I) pair connected by a bis-bidentate bridging ligand $L^{p\text{-}Ph}$.

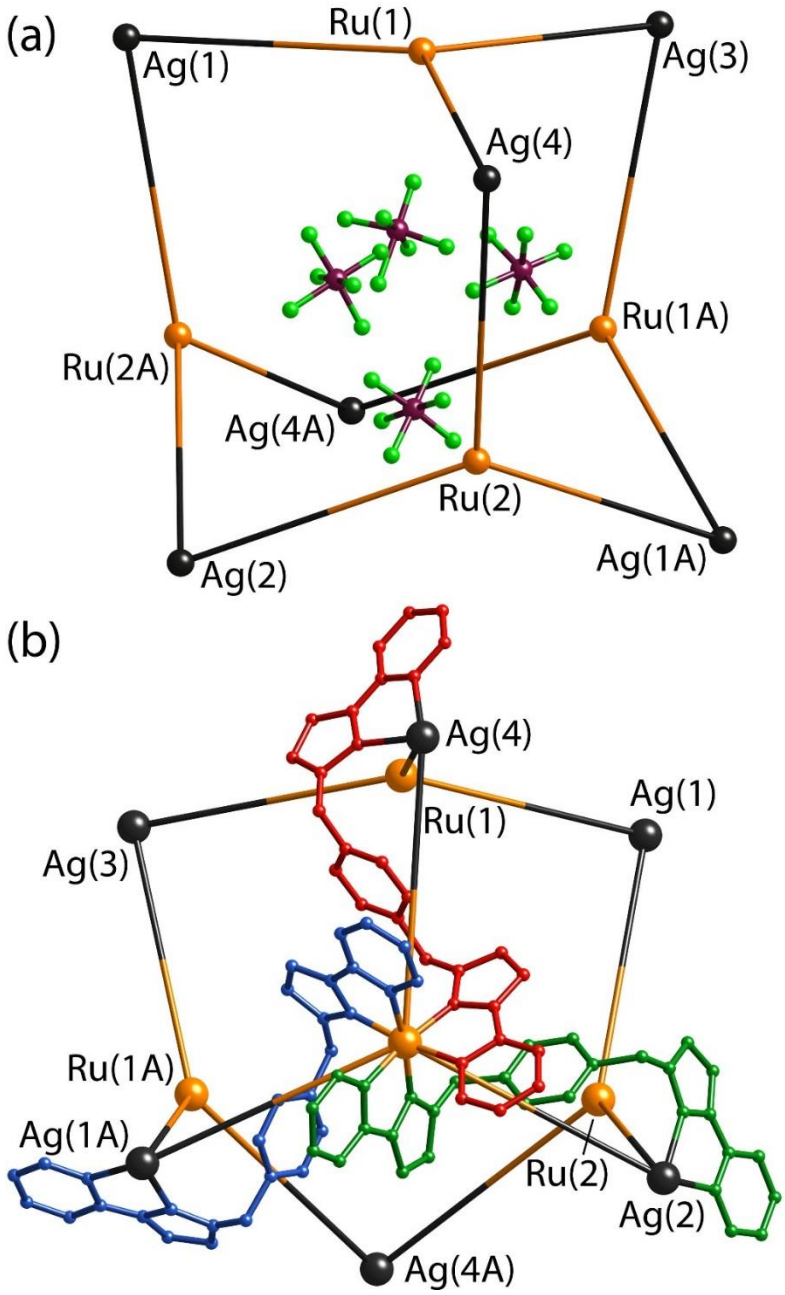

Figure 3.2.37 Two views of the structure of $[\{Ru(L^{p\text{-}Ph})_3\}_4Ag_6](PF_6)_{14}$: (a) the adamantane-like arrangement of metal ions, with the four anions that lie within the cavity also shown; (b) the metal superstructure with three of the bridging ligands included (coloured differently for clarity).

The molecule lies astride a crystallographic C_2 axis such that half of it is unique. This axis passes through Ag(2) and Ag(3) such that these lie on special positions with 50% occupancy in the asymmetric unit, whereas Ag(1) and Ag(4) are in general positions. There is a (non-crystallographic) C_3 axis through each Ru(II) tris-chelate vertex, with all four being homochiral; thus the complex belongs to the pure

rotation symmetry point group *T* which is a common consequence of removing mirror planes from high-symmetry polyhedra.[60]

The six Ag(I) ions lie on the three C_2 axes associated with *T* symmetry of which one [the Ag(2)•••Ag(3) axis, as mentioned above] occurs in the crystal structure; necessarily, all six Ag(I) ions have the same chirality associated with their two non-symmetrical chelating ligands. The nearest-neighbour Ru•••Ag separations (i.e. along an edge spanned by a bridging ligand) lie in the range 8.86 – 9.32 Å, averaging 9.06 Å.

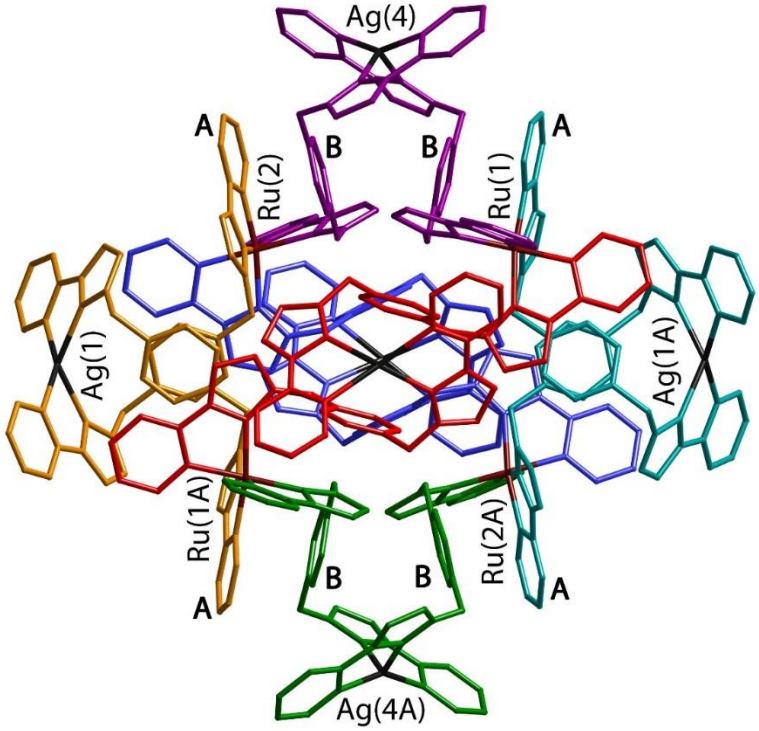

Figure 3.2.38 A view of the complex cation of $[\{Ru(L^{p\text{-}Ph})_3\}_4Ag_6](PF_6)_{14}$. The two ligands coordinated to each Ag(I) have the same colour. Labels A and B denote the electron-deficient (pyrazolyl-pyridine) and electron-rich (phenyl) units involved in the pairwise π-stacking interactions.

The flexibility of the ligands associated with the CH_2 'hinges' allows them to adopt a conformation which maximises inter-ligand π-stacking – a key driver for assembly of such cages.[27,61] This can be seen in the view shown in Figure 3.2.38, in which the octahedral disposition of the six Ag(I) ions is emphasised with these being placed top/bottom, left/right and front/back with each pair of Ag(I) ions lying on a C_2 axis. In this view, Ag(4)/Ag(4A) form the 'vertical' C_2 axis. The two ligands attached to

each Ag(I) ion have the same colour (i.e. the twelve ligands are coloured in six sets of two). The ligands are disposed such that a central phenyl ring of a bridging ligand (denoted 'B' in Figure 3.2.38) lies parallel to, and overlapping with, a pyrazolyl-pyridine unit of another ligand coordinated to the adjacent Ru(II) ion (denoted 'A' in Figure 3.2.38), forming a charge-assisted π-stack between electron-rich (phenyl) and electron-deficient (coordinated pyrazolyl-pyridine) ligands. In the view in Figure 3.2.38 there can be seen four such A/B stacked pairs; there are necessarily, therefore, twelve such interactions overall – involving every phenyl group – as the orientations with Ag(1)/Ag(1A) and Ag(2)/Ag(3) as the 'vertical' axis are equivalent.

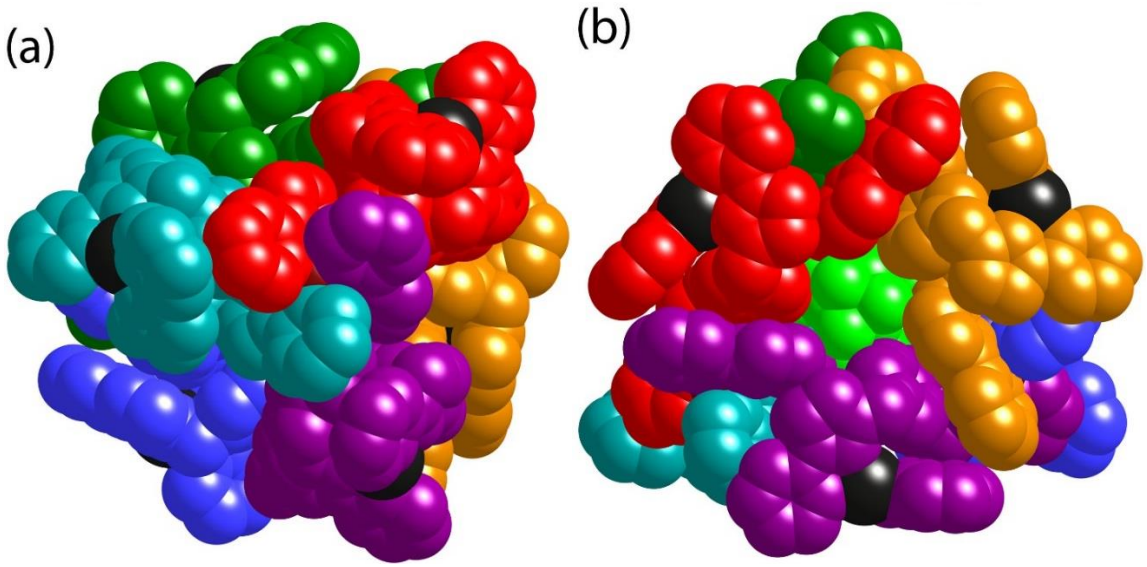

Figure 3.2.39 Space-filling views of the complex cation of $[\{Ru(L^{p\text{-}Ph})_3\}_4Ag_6](PF_6)_{14}$. (a) A view down one of the threefold axes, through a Ru(II) tris-chelate centre; (b) a view from the opposite side of the complex looking at one of the Ru_3Ag_3 faces, with one of the encapsulated $[PF_6]^-$ anions (F atoms in green) visible through the portal.

An alternative space-filling view, looking down one of the C_3 axes associated with a Ru(II) tris-chelate centre, is in Figure 3.2.39(a). The cage complex has an approximate cavity size of 178 $Å^3$ (calculated assuming that the windows are blocked; see Figure 3.2.40).[62] The cavity is occupied by a tetrahedral array of four $[PF_6]^-$ anions (see Figure 3.2.37a), each one blocking the window in one of the Ru_3Ag_3 faces of the cage, as shown in Figure 3.2.39(b) in which three of the F atoms of the $[PF_6]^-$ anion in that window can be clearly seen. The P•••P separations between the four encapsulated anions are in the

range of 5.44 – 5.61 Å, resulting in peripheral F•••F contacts between anions of ≈ 3Å, which is the sum of the van der Waals' radii of two F atoms. Each anion is involved in a range of CH•••F interactions with ligand H atoms. Figure 3.2.41(a) shows one of the anions embedded in the window in one of the Ru_3Ag_3 faces, with dotted lines indicating some of the short non-bonded C•••F contacts (≤ 3.15 Å) which are indicative of weak hydrogen-bonding interactions between anion and ligand. This view also nicely shows how the array of six ligands around each Ru_3Ag_3 face forms a cyclic helicate with every ligand in the cycle having the same sense of 'under and over' around the ring. Figure 3.2.41(b) shows how the four anions fill the cavity.

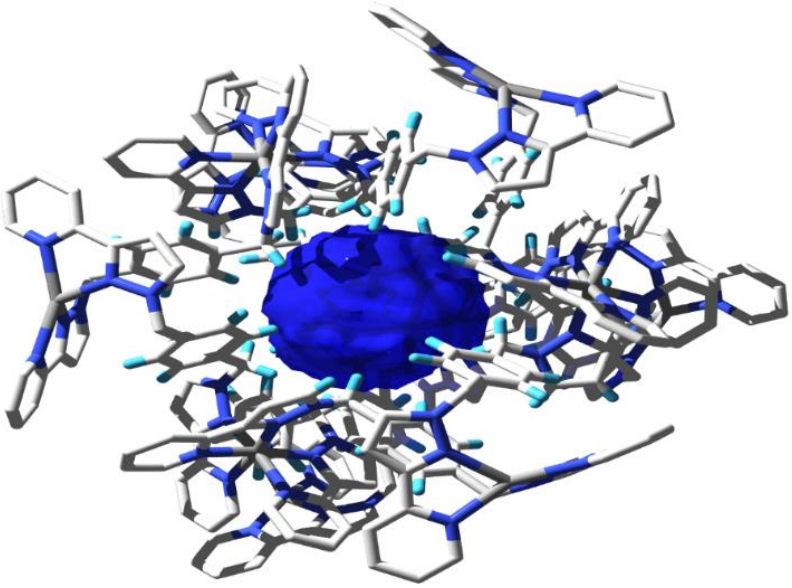

Figure 3.2.40 A view of the cavity in the centre of $[\{Ru(L^{p\text{-}Ph})_3\}_4Ag_6](PF_6)_{14}$, shown in blue (generated with Swiss-PDB viewer).[62]

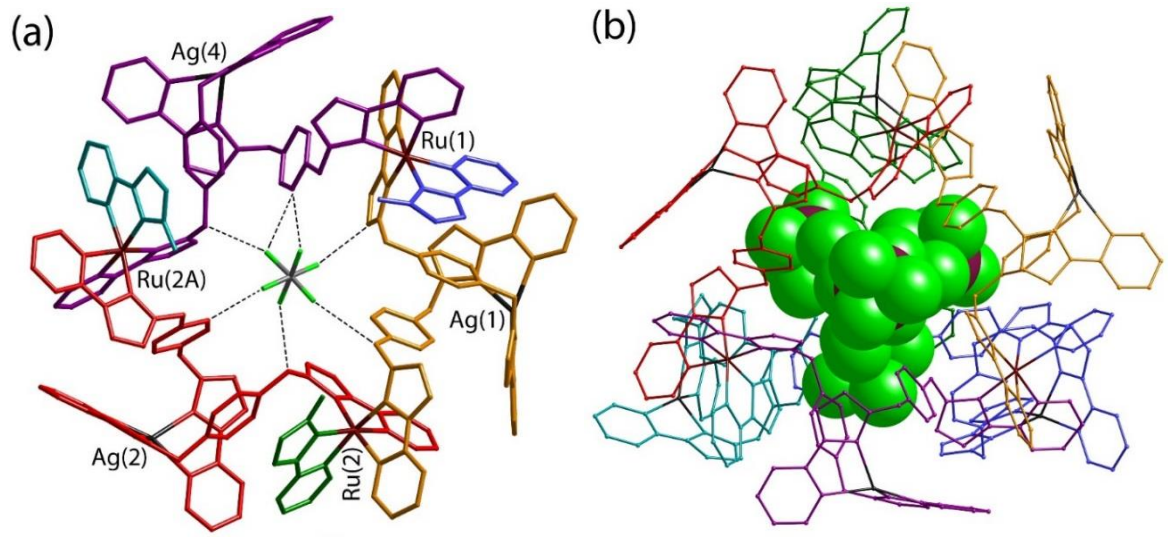

Figure 3.2.41 Two illustrations of how the encapsulated $[PF_6]^-$ anions interact with the cavity of the cage of $[\{Ru(L^{p\text{-}Ph})_3\}_4Ag_6](PF_6)_{14}$. (a) Location of one of the anions in the window in the centre of a Ru_3Ag_3 face with some of the shorter CH•••F interactions (C•••F separation ≤ 3.15 Å) shown by dotted lines; (b) a view of the cage (in wireframe mode) with the four anions shown in space-filling mode.

The structural integrity of the complex in solution was confirmed by ES mass spectrometry, which showed peaks corresponding to the species $[\{Ru_4Ag_6(L^{p\text{-}Ph})_{12}\}(PF_6)_{14\text{-}n}]^{n+}$ (n = 3, 4, 6), and also by ^{1}H NMR spectroscopy. The ^{1}H NMR spectrum at room temperature is very broad, indicative of molecular motions [possibly associated with the highly flexible Ag(I) centres] at a rate comparable to the ^{1}H NMR timescale. However at 75˚C the spectrum sharpened satisfactorily and showed the expected 20 independent ^{1}H signals associated with one environment for $L^{p\text{-}Ph}$ with no internal symmetry (see Figures 3.2.42 and 3.2.43); this spectrum is considerably different from that of *fac*–$[Ru(L^{p\text{-}Ph})_3][PF_6]_2$. Significantly, the chirality associated with the $\{Ag(NN)_2\}^+$ centres ensures that both independent sets of CH_2 protons are now diastereotopic, giving two pairs of coupled doublets in the 4.5 – 5.5 ppm region (see Figure 3.2.42). That this species is a large assembly is confirmed by its DOSY spectrum which clearly shows that all of its ^{1}H signals belong to a single species which has a much lower diffusion rate [log D(m^2 s^{-1}) = –9.2] than *fac*–$[Ru(L^{p\text{-}Ph})_3][PF_6]_2$ [log D(m^2 s^{-1}) = –8.4] (see Figure 3.2.44).

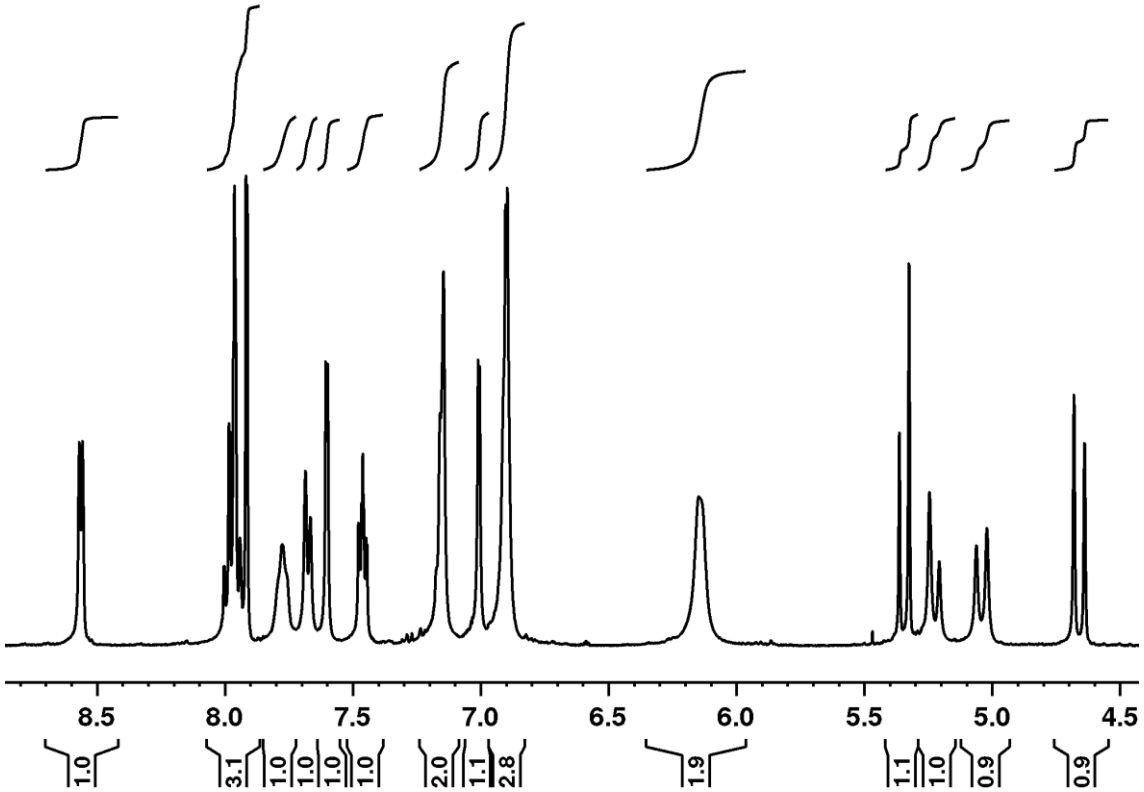

Figure 3.2.42 ^{1}H NMR spectrum of [{Ru($L^{p\text{-}Ph}$)$_3$}$_4$Ag$_6$](PF$_6$)$_{14}$ (CD_3CN, 400 MHz, 75 ˚C).

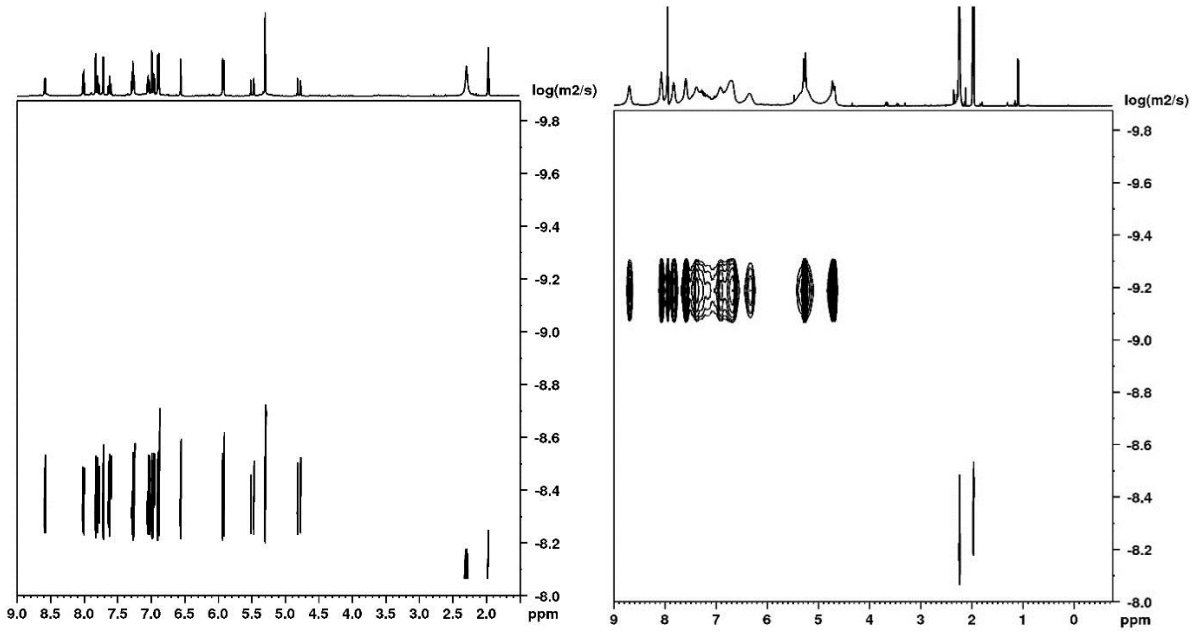

Figure 3.2.44 DOSY ^{1}H NMR spectra (400 MHz, CD_3CN, 25 ºC) of *fac*–[Ru($L^{p\text{-}Ph}$)$_3$][PF$_6$]$_2$ (left) and [{Ru($L^{p\text{-}Ph}$)$_3$}$_4$Ag$_6$](PF$_6$)$_{14}$ (right).

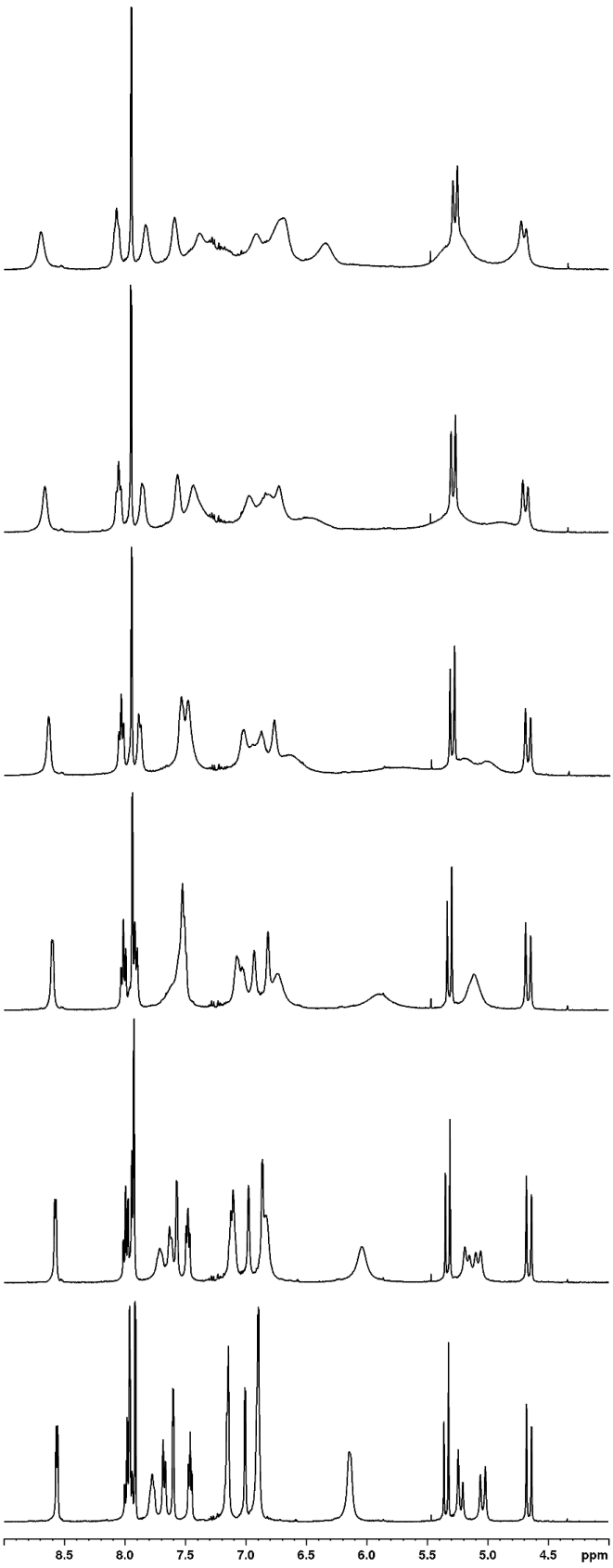

Figure 3.2.43 Series of ^{1}H NMR spectra of $[\{Ru(L^{p\text{-}Ph})_3\}_4Ag_6](PF_6)_{14}$ (CD_3CN, 400 MHz) at (from top down) 25, 35, 45, 55, 65, 75˚C showing the sharpening at higher temperatures.

Assembly of this cage with its adamantane-like structure thus relies on two different types of geometric control at specific metal sites. Firstly it requires the appropriate combination of metal vertices that are three-connected [each tris-chelate, Ru(II) ion is connected to three Ag(I) ions] and two connected [each bis-chelate Ag(I) ion is connected to two Ru(II) ions]. This is achieved by using metal ions with different stereoelectronic preference, i.e. a combination of 6-coordinate Ru(II) and 4-coordinate Ag(I) ions at alternating sites. Secondly, the structure relies on exclusive use of pre-formed, kinetically inert *fac* isomers of the $[Ru(L^{p\text{-}Ph})_3]^{2+}$ unit. It is noted that there are a few other examples of mixed-metal $M_6M'_4(\mu\text{–}L)_{10}$ complexes with an adamantane-like core structure,[63-66] several of which (from Ishio and co-workers) use cyanide bridges along the M–M' edges.[65,66]

3.2.4 Three component assembly of a heterometallic tetra-capped truncated tetrahedron

With satisfactory evidence that isomerically pure *fac*–$[Ru(L^{p\text{-}Ph})_3][PF_6]_2$ subcomponents can be used to propagate formation of a heterometallic array, efforts were directed towards preparing more elaborate structures that incorporate more than one component. As with the heterometallic cubes detailed in Section 3.2.2, such structures can be rationally designed based on the existing homonuclear versions. For example, if *fac*–$[Ru(L^{3,3\text{-}Bi})_3][PF_6]_2$ were to be isolated (see Figure 3.2.1 for ligand structure), then the synthesis of a heterometallic $[RuM_3(L^{3,3\text{-}Bi})_3]X_8$ tetrahedron could be achieved with Ru(II) located exclusively at the *fac* position, with labile metal dications occupying the remaining three *mer* vertices.[67] However, this cage has a relatively small cavity, which may limit its useful host-guest chemistry.[68] Consequently, the largest cage in this series, the $M_{16}L_{24}$ tetra-capped truncated tetrahedron, was targeted.[35,61]

The $M_{16}L_{24}$ structure consists of three triangles of *mer* tris-chelate metals capped by four *fac* tris-chelate metals, with either $L^{p\text{-}Ph}$ or $L^{1,4\text{-}nap}$ as the 24 bridging ligands. Importantly, the *fac* positions are not connected by the same edge. It follows therefore that four equivalents of *fac*–$[Ru(L^{p\text{-}Ph})_3][PF_6]_2$ will provide the four *fac* face-capping metal centres and twelve of the ligands required for the assembly. In

addition, twelve equivalents of ligand ($L^{p\text{-}Ph}$ or $L^{1,4\text{-}nap}$) and twelve equivalents of a labile transition metal dication [e.g. Cd(II) or Zn(II)] will be needed to complete the assembly (see Figure 3.2.45). The result of this would be a structure in which each Ru(II) 'complex-ligand' provides a bidentate binding site to three different M(II) ions.

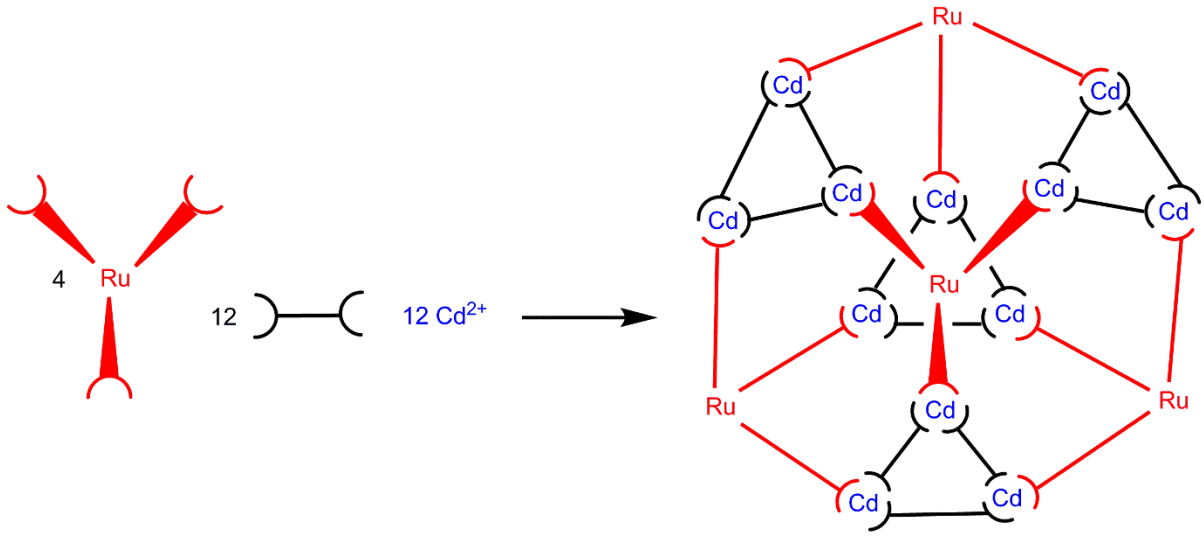

Figure 3.2.45 Schematic diagram of the reaction between four pre-formed *fac*-$[Ru(L^{p\text{-}Ph})_3]^{2+}$ complex units (each with three pendant binding sites), twelve Cd^{2+} ions and twelve additional ligands ($L^{p\text{-}Ph}$ or $L^{1,4\text{-}nap}$) to complete assembly of the $[Ru_4Cd_{12}L_{24}]^{32+}$ cage.

Thus, a reaction of *fac*–$[Ru(L^{p\text{-}Ph})_3][PF_6]_2$ and $[Cd_3(L^{1,4\text{-}nap})_3](BF_4)_6$ was dissolved in nitromethane at 90 ^oC and subsequently kept at room temperature (note: the additional ligand and metal dication was introduced as a 1 : 1 ratio pre-isolated solid[61] for ease of synthesis). The ^1H NMR spectrum of the mixture was recorded daily and the electrospray mass spectrum every week to detect any assemblies taking form. After 1 day the ^1H NMR spectrum was very poorly resolved, consistent with a slowly equilibrating mixture of assemblies (see Figure 3.2.46a), and the mass spectrum showed no signs of any large assemblies having already formed. After 1 month had passed, the ^1H NMR spectrum was considerably sharpened (see Figure 3.2.46b), although still too poorly resolved to distinguish all the individual peaks[ϕ]; the mass spectrum recorded at the same time however revealed that this was the ^1H

[ϕ] If the heterometallic assembly has the same symmetry as the homonuclear $M_{16}L_{24}$ cage, as expected, then there will be 2 independent ligand environments with no internal symmetry, and consequently 42 ^1H environments in the ^1H NMR spectrum.

NMR spectrum of the complete assembly $[Ru_4Cd_{12}(L^{p\text{-}Ph})_{12}(L^{1,4\text{-}nap})_{12}]X_{32}$ (X = BF_4 or PF_6; see Figure 3.2.47).

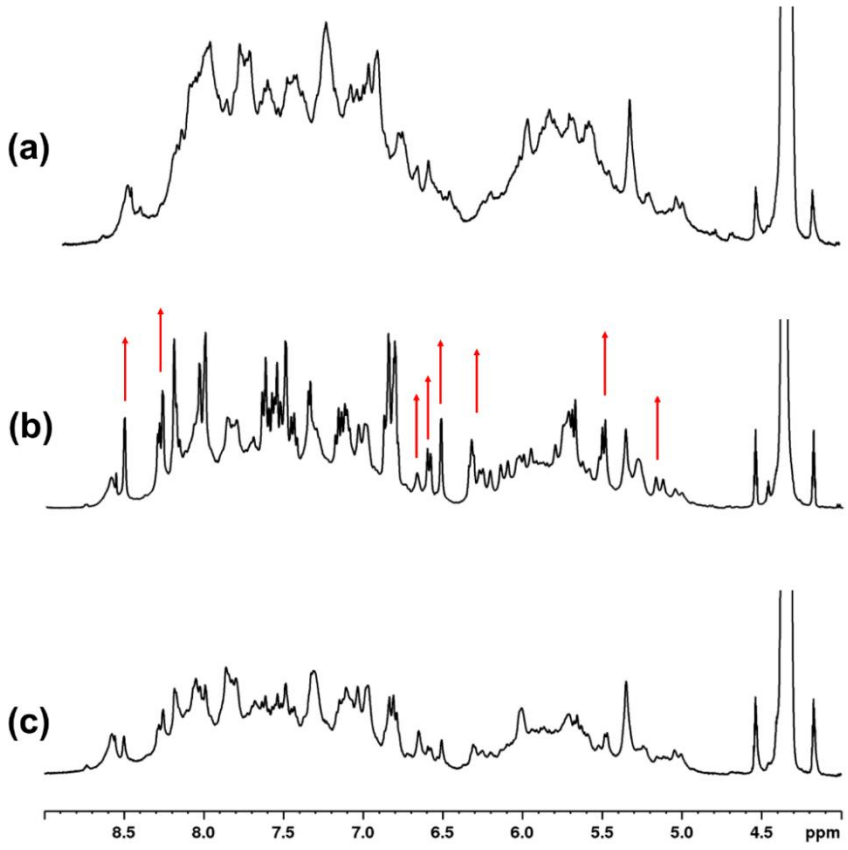

Figure 3.2.46 Series of ^{1}H NMR spectra (400 MHz, CD_3NO_2) of the mixture of *fac*-$[Ru(L^{p\text{-}Ph})_3](PF_6)_2$ and $[Cd_3(L^{1,4\text{-}nap})_3](BF_4)_6$: (a) 1 day after mixing; (b) 1 month after mixing (new peaks growing in are shown with red arrows); (c) after 5 months.

As is typical of cages of this type, the mass spectrum displayed a series of peaks for sequential loss of anions from the complete complex (i.e. $\{[Ru_4Cd_{12}(L^{p\text{-}Ph})_{12}(L^{1,4\text{-}nap})_{12}]X_{32\text{-}n}\}^{n+}$; n = 5 - 11; see Figure 3.2.47a). Within each member of this series was a cluster of peaks due to varying anion composition (see Figure 3.2.47b). The mass spectrum also contained mononuclear peaks due to fragmentation in the mass spectral conditions, as is common with cages of this type despite the low cone voltage used. No other large assemblies were detected in the mass spectrum. The spectra remained generally unchanged for several weeks afterwards, but after approximately 5 months the solution became turbid and a white

precipitate formed, presumably CdF_2.[35] The ^1H NMR spectrum had become noticeably less sharp at this point (see figure 3.2.45c), so it is assumed that the complex had decomposed.

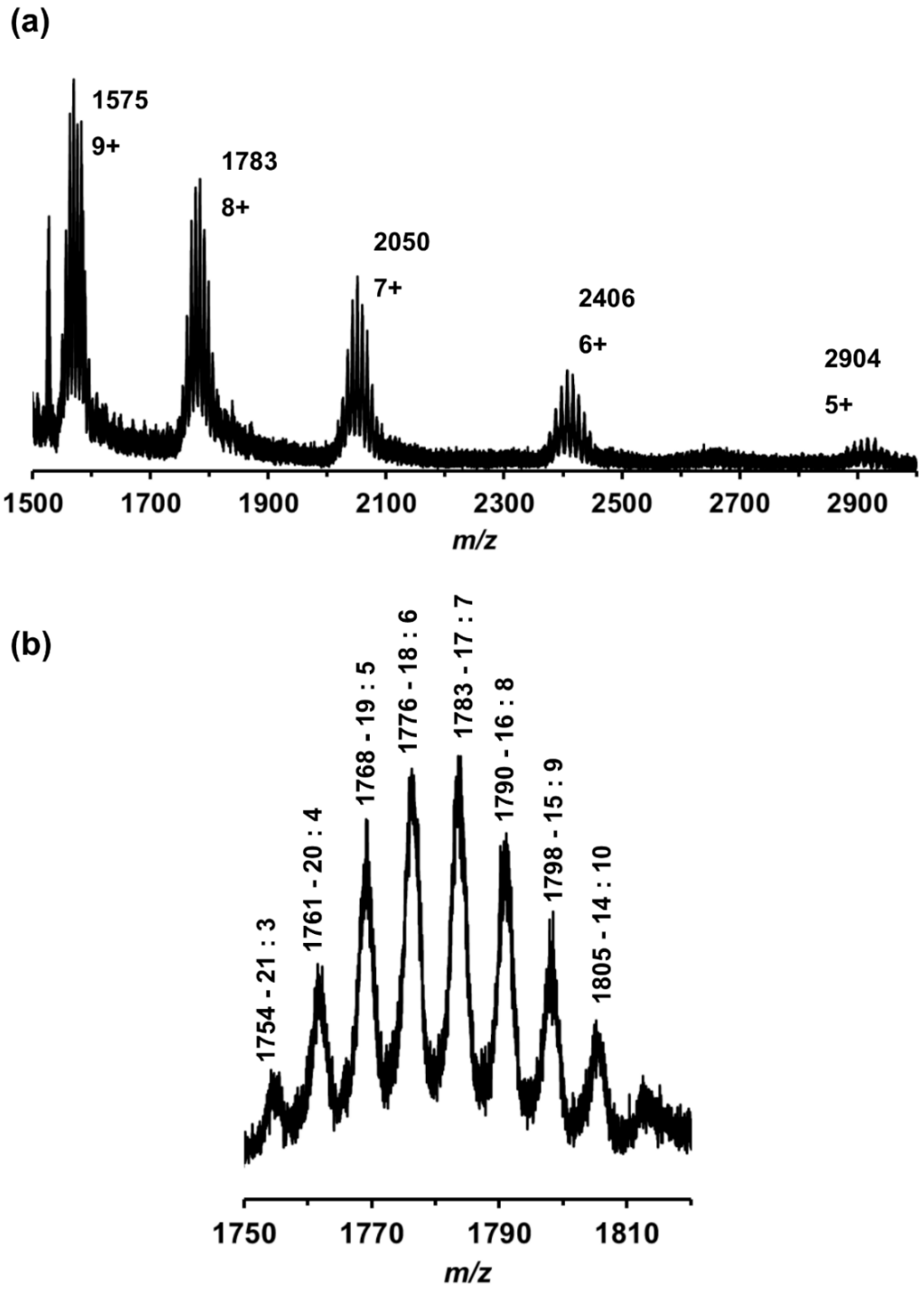

Figure 3.2.47 (a) Partial electrospray mass spectrum of $[Ru_4Cd_{12}(L^{p\text{-}Ph})_{12}(L^{1,4\text{-}nap})_{12}]X_{32}$, showing a series of peaks corresponding to $\{[Ru_4Cd_{12}(L^{p\text{-}Ph})_{12}(L^{1,4\text{-}nap})_{12}]X_{32\text{-}n}\}^{n+}$; i.e. loss of 5-9 anions from the complete complex (X = BF_4 or PF_6). (b) Expansion of the $\{[Ru_4Cd_{12}(L^{p\text{-}Ph})_{12}(L^{1,4\text{-}nap})_{12}]X_{24}\}^{8+}$ cluster of peaks; labels show the *m/z* value and BF_4 : PF_6 composition - e.g. *m/z* 1783, $\{[Ru_4Cd_{12}(L^{p\text{-}Ph})_{12}(L^{1,4\text{-}nap})_{12}](BF_4)_{21}(PF_6)_3\}^{8+}$.

Due to the considerable length of the equilibration time of the mixture, and the eventual decomposition of the formed cage, further studies have not been possible on this system. Additionally, crystals formed from this mixture were very small, and despite use of synchrotron radiation no suitable dataset could be collected. However, the unit cell determined is of comparable size to a previously reported crystal structure of $[Zn_{16}(L^{p\text{-}Ph})_{24}](BF_4)_{32}$, and as such is consistent with a large assembly (see Figure 3.2.48).

Compound	**$[Zn_{16}(L^{p\text{-}Ph})_{24}](BF_4)_{32}$**	**"$[Ru_4Cd_{12}(L^{p\text{-}Ph})_{12}(L^{1,4\text{-}nap})_{12}]X_{32}$"**
Crystal system	monoclinic	monoclinic
Space group	*C*2/*c*	?
a / Å	31.117(3)	32.223
b / Å	51.828(3)	46.906
c / Å	48.797(3)	51.533
α / °	90	90
β / °	99.950(2)	93.448
γ / °	90	90
V / Å^3	77 513(9)	77748

Figure 3.2.48 Previously reported unit cell for a homonuclear $M_{16}L_{24}$ compound (left), and the unit cell of the heteronuclear Ru_4Cd_{16} analogue (right).[35]

Further attempts are being made currently to prepare the heterometallic cage from the related subcomponent *fac*–$[Ru(L^{1,4\text{-}nap})_3][PF_6]_2$, which will hopefully add added solution stability to the cage due to the additional π-stacking associated with the naphthalene groups.[61]

3.2.5 Two heterometallic assemblies using preformed Ru(II) species and Ag(I) ions

The mononuclear complex $[Ru(L^{o\text{-}Ph})_2](PF_6)_2$, described in Section 3.2.13, contains one pendant bidentate binding site. This would theoretically preclude the formation of a hollow heterometallic array using labile octahedral dications, which requires all of the bridging lignads to span the cage edges. For example, $[Ru(L^{o\text{-}Ph})_2](PF_6)_2$ might react with Co(II) to form the heteronuclear species $[\{Ru(L^{o\text{-}Ph})_2\}_3Co]^{8+}$, in which all ligands and metal ions will be coordinatively saturated. However, the use of the more coordinatively flexible Ag(I) may allow the synthesis of some unexpected products, particularly due to the propensity of Ag(I) to form argentophilic interactions when ligands of this type are used.[57,58]

Reaction of $[Ru(L^{o\text{-}Ph})_2](PF_6)_2$ with $AgPF_6$ or $AgClO_4$ in methanol/dichloromethane solution gave in both cases a yellow powder. These were expected to have the formulation $[\{Ru(L^{o\text{-}Ph})_3\}_2Ag]X_5$, in which two mononuclear Ru(II) subcomponents are bound to a 4-coordinate Ag(I) ion; the ^{1}H NMR spectrum of each was consistent with this with the complexes giving nearly identical spectra, as expected since they differ only in the type of anions (see Figure 3.2.49). Each spectrum shows 40 ^{1}H resonances (two full independent ligand environments), as was the case with the mononuclear complex, due to the C_2 symmetry about the Ag(I) ion. Several of the peaks have shifted with respect to the starting material, due to coordination to the Ag(I) centre and additonal π-stacking, but the key difference between these spectra and the mononuclear complex is the splitting of the 'pendant' CH_2 singlet at 4.78 ppm into an approximate doublet (see Figure 3.2.50), highlighting the chirality imposed on the ligand by coordination to Ag(I) – the $\{Ag(NN)_2\}^+$ unit is inherently chiral if the NN donors are asymmetric.

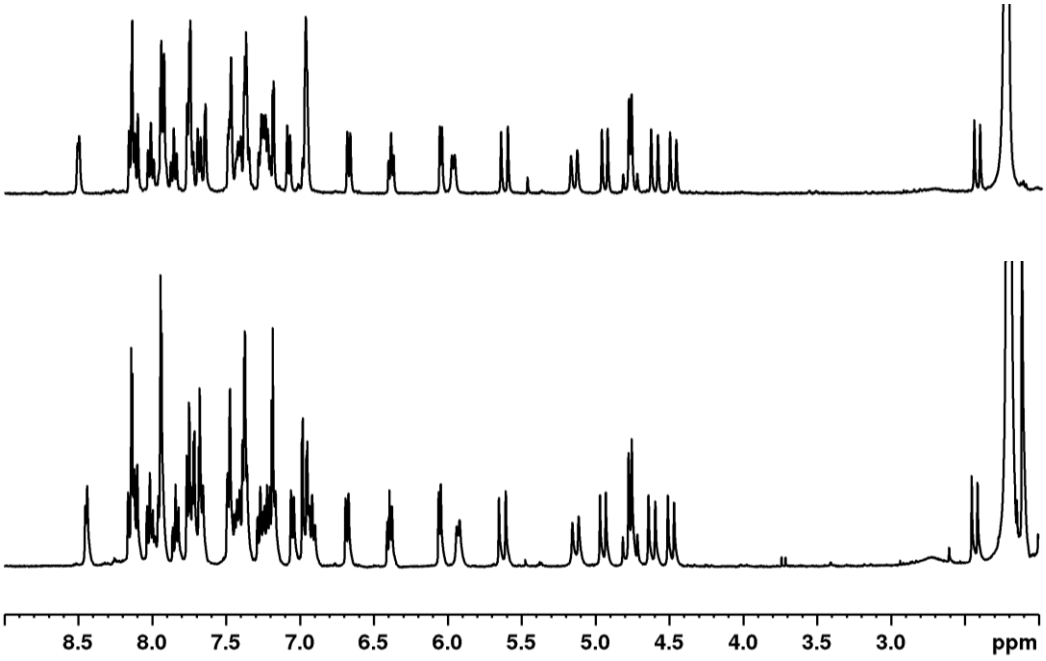

Figure 3.2.49 Full ^{1}H NMR spectra (CD_3CN, 400 MHz) of $[\{Ru(L^{o\text{-}Ph})_3\}_2Ag](PF_6)_5$ (top) and $[\{Ru(L^{o\text{-}Ph})_3\}_2Ag](ClO_4)(PF_6)_4$ (bottom).

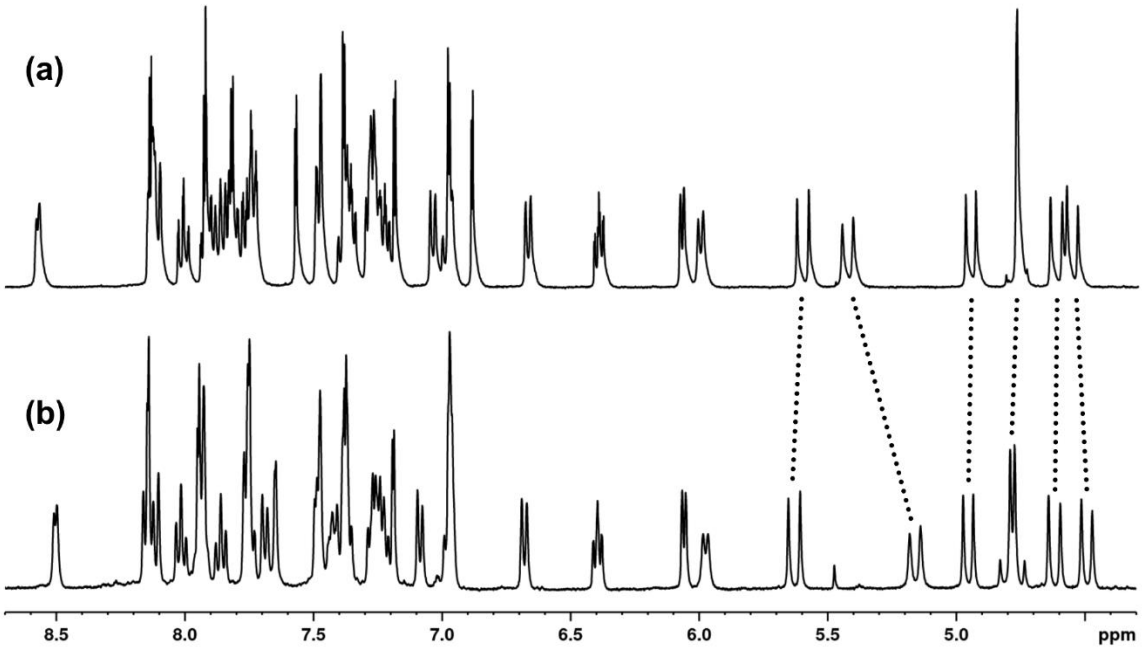

Figure 3.2.50 Comparison of the ^{1}H NMR spectra (CD_3CN, 400 MHz) of (a) $[Ru(L^{o\text{-}Ph})_2](PF_6)_2$, and (b) $[\{Ru(L^{o\text{-}Ph})_3\}_2Ag](PF_6)_5$. Note the splitting of the CH_2 singlet (a) at 4.78 ppm into a doublet (b).

To confirm the structure of the complex, X-ray quality crystals were grown by slow diffusion of toluene vapour into a solution of the complex $[\{Ru(L^{o\text{-}Ph})_3\}_2Ag](PF_6)_5$ in acetonitrile. Despite being well-formed the crystals diffracted fairly poorly. The crystal structure was indeed that of the expected $[\{Ru(L^{o\text{-}Ph})_3\}_2Ag](PF_6)_5 \bullet 2C_7H_8$, with half of the complex cation found in the asymmetric unit (see Figure 3.2.51). It is apparent that one face of Ag(3) is exposed, so the packing behaviour of the complex was studied in order to determine if any argentophilic interactions were present.

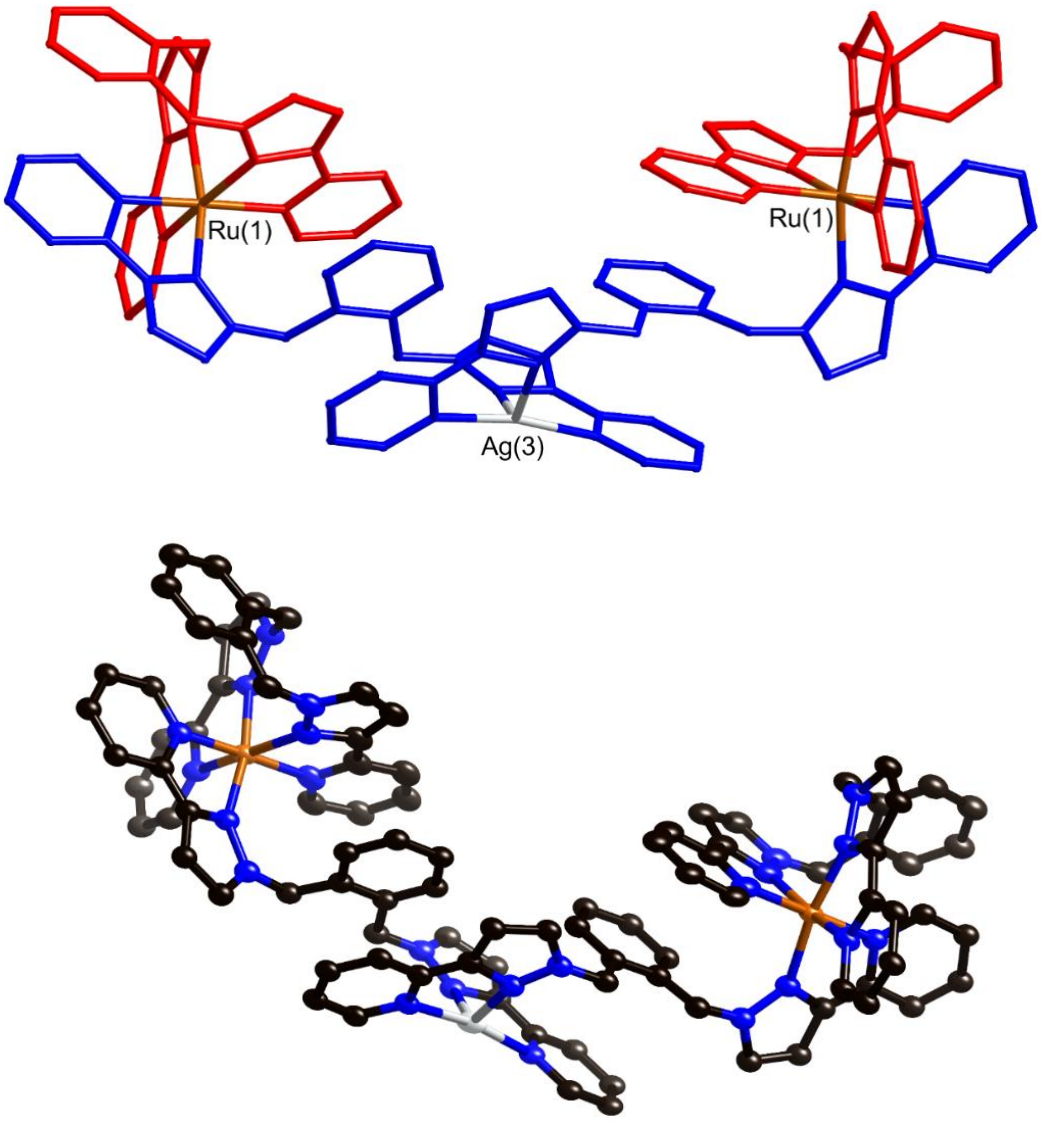

Figure 3.2.51 Crystal structure of the complex cation of $[\{Ru(L^{o\text{-}Ph})_2\}_2Ag](PF_6)_5$. Top: Stick model of the complex cation, with crystallographically independent ligands coloured differently. Bottom: Thermal ellipsoid plot of the complex cation (30 % probability level).

The trinuclear complex is found to assemble into a nonanuclear structure in the solid state, in which three separate complexes are closely packed together, stabilised by three six-tiered π-stacks lining the exterior of the assembly made up of PyPz and phenylene groups (see Figure 3.2.52). The Ag•••Ag separation between each of the three strands is 4.85 Å, a distance much larger than the sum of the van der Waals' radii for two Ag(I) ions, so there is clearly no argentophilic interaction present in this structure. However, the metal ions are still held quite closely together, so it should be likely that there is another stabilising factor in the formation of this assembly; this is provided by CH•••F hydrogen-bonding interactions between the complex and two disordered PF_6^- anions [closest contact F(53')•••H(15A) = 2.19 Å], which bind in the 'pockets' provided by the hourglass shaped assembly in close proximity to the metal centres [F(51) – Ag(3) separation 5.34 Å] (see Figure 3.2.53). A view down the c-axis emphasises the three-fold rotational symmetry of the complex and the anions which lie on the axis (see Figure 3.2.54).

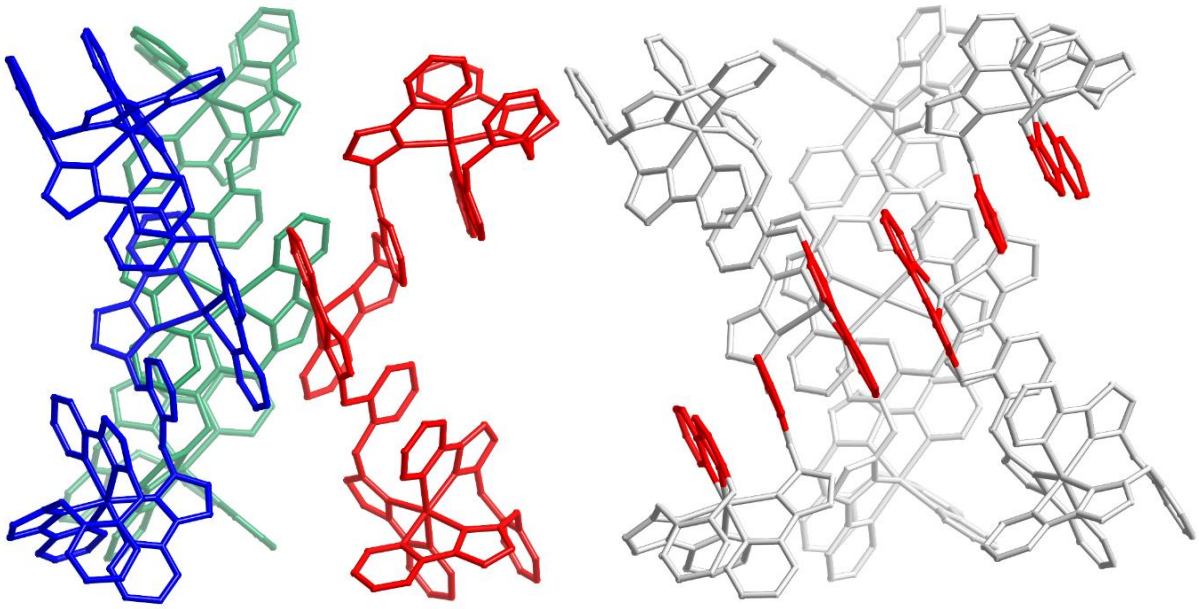

Figure 3.2.52 Two views of the second level of self-assembly within the crystal structure of $[\{Ru(L^{o\text{-}Ph})_2\}_2Ag](PF_6)_5$. Left: Three $[\{Ru(L^{o\text{-}Ph})_2\}_2Ag]^{5+}$ strands (coloured differently) closely assemble. Right: View from a similar perspective showing one of the three 6-tiered π-stacks which stabilise the close proximity of the three strands.

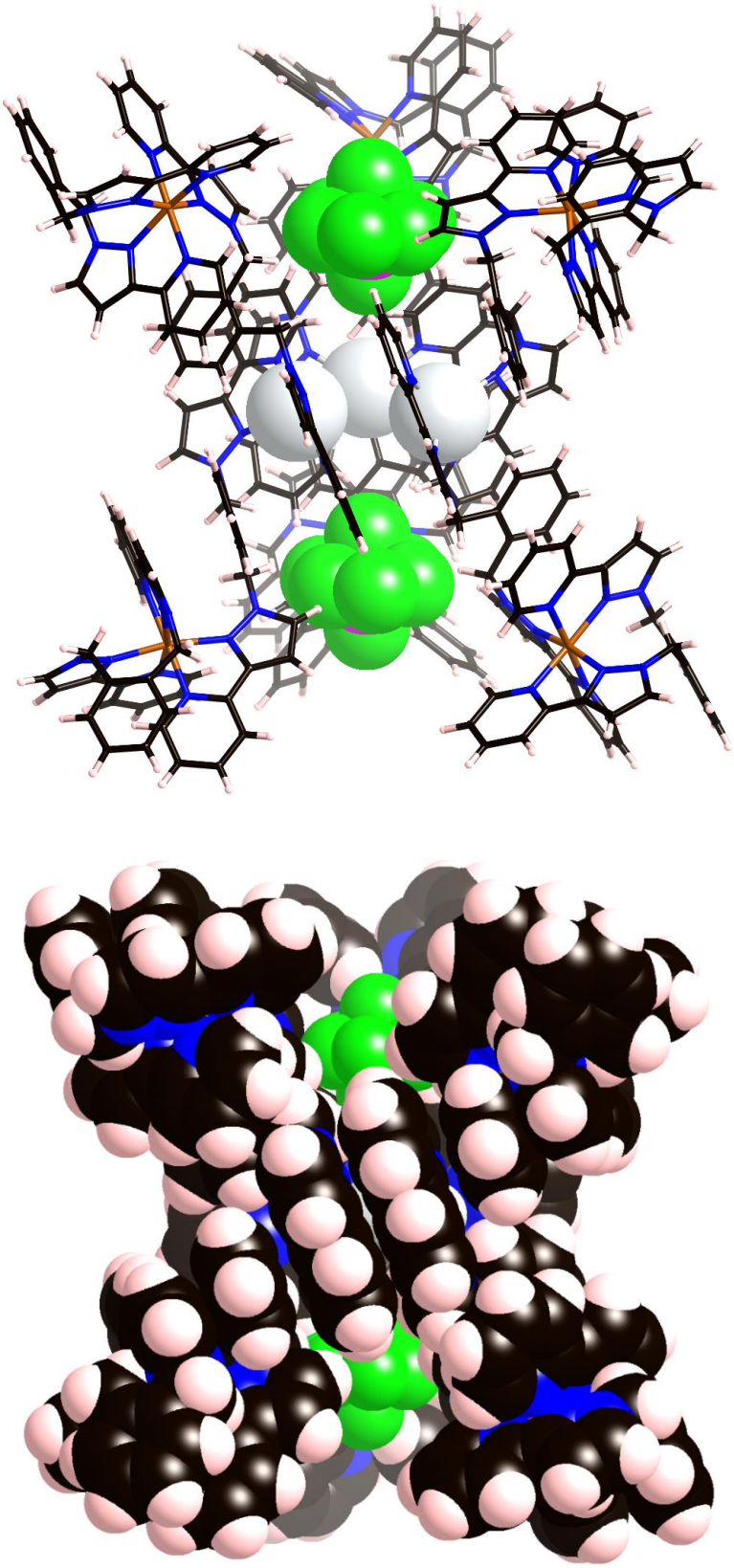

Figure 3.2.53 Two views of the crystal structure of $[\{Ru(L^{o\text{-}Ph})_2\}_2Ag](PF_6)_5$. Top: A view highlighting the interaction of two PF_6 molecules with the nonanuclear array, with the PF_6 molecules and silver atoms shown in space-filling mode; (bottom) space-filling mode view from the same perspective.

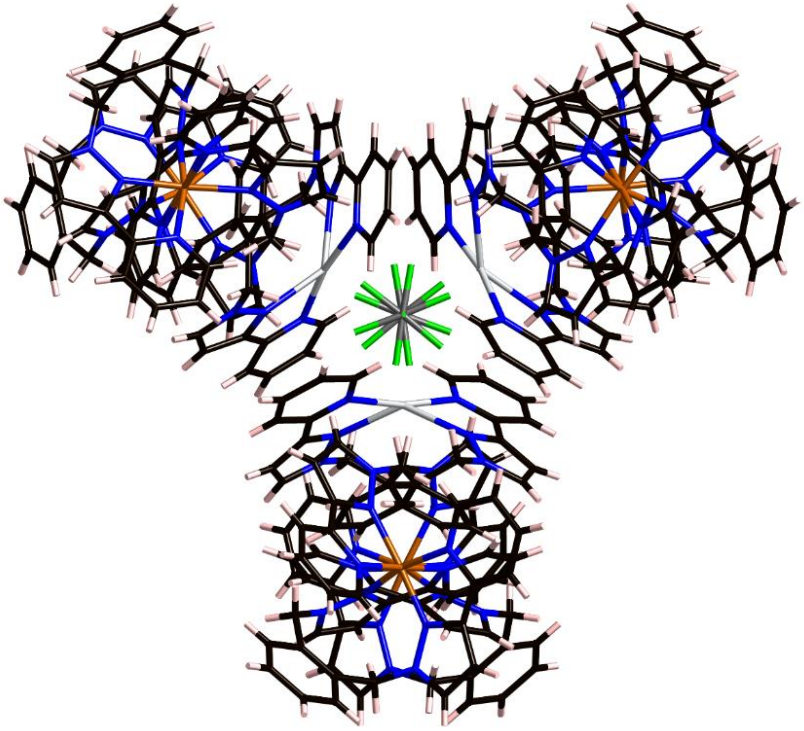

Figure 3.2.54 View down the c axis in the crystal structure of $[\{Ru(L^{o\text{-}Ph})_2\}_2Ag](PF_6)_5$, emphasising the three-fold rotational symmetry of the complex and guest anions.

Evidence that this nonanuclear assembly persists in solution to some extent was provided by the electrospray mass spectrum (see Figure 3.2.55). The spectrum is dominated by peaks for the mononuclear $[Ru(L^{o\text{-}Ph})_2(PF_6)]^+$ (*m/z* 1031) and the trinuclear $\{[\{Ru(L^{o\text{-}Ph})_2\}_2Ag](PF_6)_{5\text{-}n}\}^{n+}$ (*m/z* 723, 1157; n = 3 and 2, respectively). A peak at *m/z* 2460 can be attributable to either the trinuclear or nonanuclear assemblies, but the peak at *m/z* 1809 can only be attributed to $\{[\{Ru(L^{o\text{-}Ph})_2\}_6Ag_3](PF_6)_{11}\}^{4+}$ (see Figure 3.2.55c). Thus the π-stacking and interactions of the anions with the well-matched pockets in the structure observed in the solid state are strong enough to allow the assembly to be held together in solution, without any coordinative interactions.

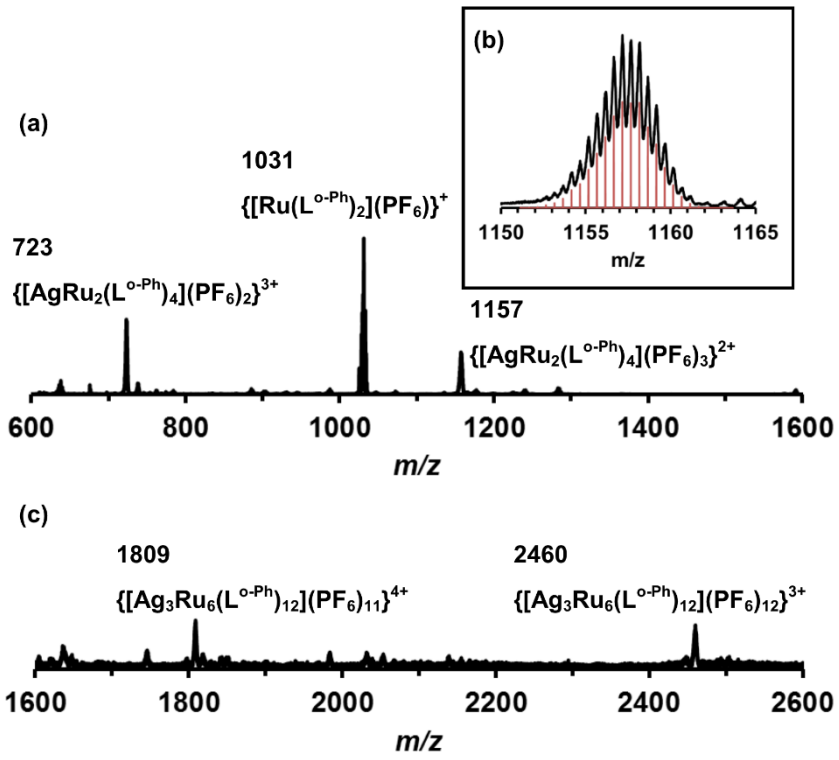

Figure 3.2.55 (a) Partial Electrospray mass spectrum of $[\{Ru(L^{o\text{-}Ph})_2\}_2Ag](PF_6)_5$; (b) Experimental (black) and theoretical (red) isotope spacing overlay for the peak at *m/z* 1157; (c) Expansion in the large *m/z* region of the mass spectrum, highlighting the solution integrity of the self-assembled nonanuclear structure.

The complex *fac*–$[Ru(L^{3\text{-}Py})_3][PF_6]_2$ is furnished with three pendant pyridyl groups which allow it to act as a tris-monodentate 'complex-ligand'. Reaction of the complex with 1.5 equivalents of Ag(I) would theoretically result in a structure in which the principle of maximum-site occupancy is fulfilled, potentially resulting in a capsule type structure (see Figure 3.2.21 in Section 3.2.1.5). Thus, *fac*–$[Ru(L^{3\text{-}Py})_3](PF_6)_2$ and $AgPF_6$ were mixed together in a 2 : 3 ratio in CD_3CN and the ^1H NMR spectrum recorded, which revealed a structure which has retained the C_3 symmetry present in the starting material (see Figure 3.2.56). Comparison of this spectrum with that of the *fac*–$[Ru(L^{3\text{-}Py})_3](PF_6)_2$ subcomponent shows that only the resonances for the pendant pyridyl protons have been significantly shifted (as confirmed by ^1H – ^1H COSY spectroscopy), consistent with coordination of the pyridyl groups to a Ag(I) centre (see Figure 3.2.57). The simplest product to explain these observations is the pentanuclear $[\{Ru(L^{3\text{-}Py})_3\}_2Ag_3](PF_6)_7$, in which all ligands will remain chemically equivalent. Unfortunately, the complex was not stable under mass spectral conditions, with the only evidence of a

heterometallic complex being a weak peak at *m/z* 1208 corresponding to $\{[\{Ru(L^{3\text{-}Py})_3\}_2Ag_2](PF_6)_4\}^{2+}$, and no crystals have been grown of X-ray quality, so the absolute structure of the product has not been determined.

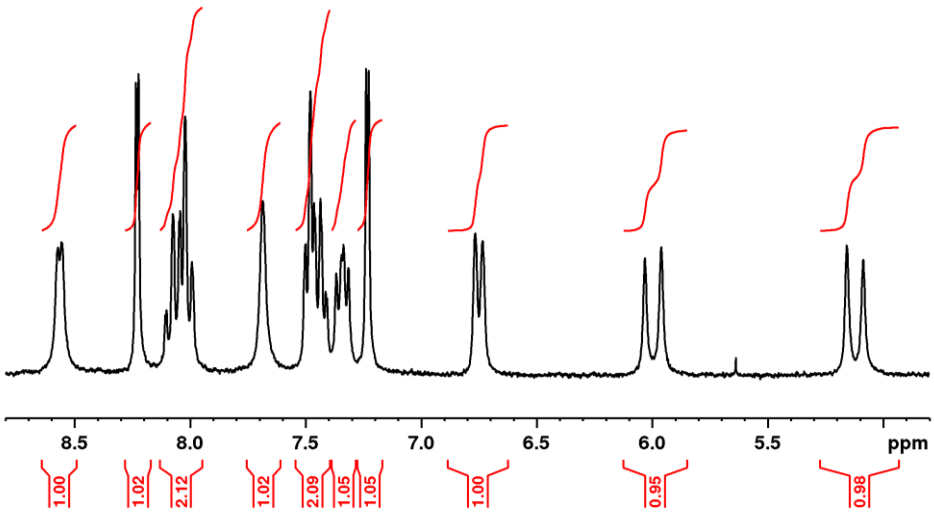

Figure 3.2.56 ^{1}H NMR spectrum (acetone-d_6, 250 MHz) of $[\{Ru(L^{3\text{-}Py})_3\}_2Ag_3](PF_6)_7$.

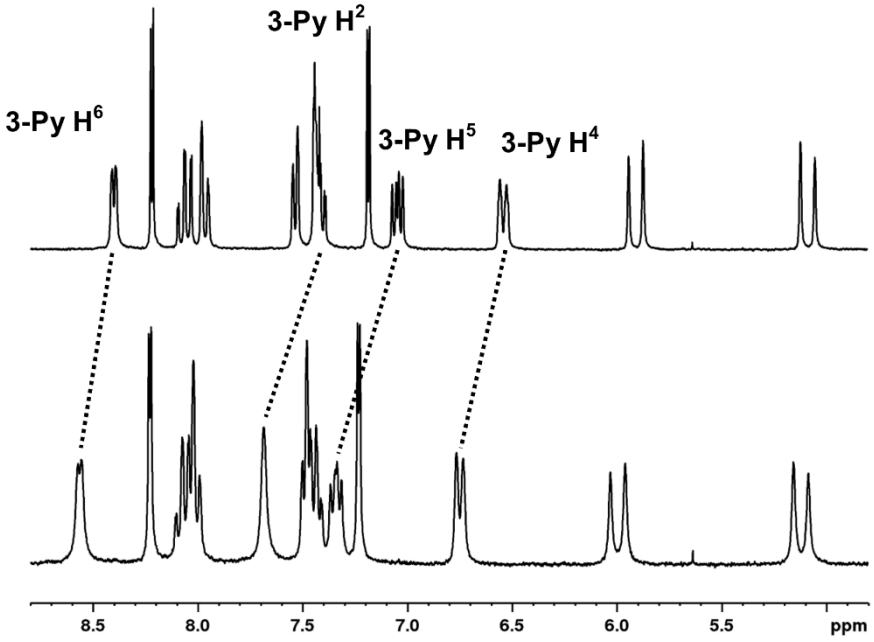

Figure 3.2.57 ^{1}H NMR spectra (acetone-d_6, 250 MHz) of $[Ru(L^{3\text{-}Py})_3](PF_6)_2$ (top) and $[\{Ru(L^{3\text{-}Py})_3\}_2Ag_3](PF_6)_7$ (bottom). Assignments are given for the 'pendant' 3-pyridyl ring, the peaks of which shift upon coordination to Ag(I).

3.3 Conclusion

A series of mononuclear Ru(II) complexes with pendant binding sites have been synthesised, either as a mixture of *mer*/*fac* isomers or purely the *fac* isomer, and these have been used to propagate the formation of supramolecular heterometallic arrays by combination with secondary metal ions.

The kinetically inert mononuclear complex $[Ru(L^{1,5\text{-nap}})_3](PF_6)_2$ (1 : 3 mixture of *fac* and *mer* isomers), with three pendant binding sites, reacts with labile Cd(II) ions to complete the assembly of a Ru_4Cd_4 cubic coordination cage in which reversible redox behaviour has been introduced at the Ru(II) sites. The complex $[Ru(L^{m\text{-Ph}})_3](PF_6)_2$ (1 : 7 mixture of *fac* and *mer* isomers) reacts with labile Co(II) ions to complete the assembly of a Ru_4Co_4 cubic coordination cage which exhibits a metal framework that is different from that of the homonuclear cage, and is one that has not been seen previously. The crystal structure revealed that this cage forms around a $[Na(BF_4)_4]^{3-}$ self-assembled core, such that the self-assembly requires three 'layers'.

The geometrically pure 'complex ligand' *fac*-$[Ru(L^{p\text{-Ph}})_3]^{2+}$, in which the three pendant bidentate binding sites are located on one face of the complex, reacts with Ag(I) ions to form the adamantoid decanuclear cage $[\{Ru(L^{p\text{-Ph}})_3\}_4Ag_6](PF_6)_{14}$ which contains a 6-coordinate Ru(II) ion at each vertex of a large tetrahedron and a 4-coordinate Ag(I) ion along each edge. The complex ligand also reacts with Cd(II) and additional $L^{1,4\text{-nap}}$ to form a $Ru_4Cd_{12}L_{24}$ assembly over a period of two months, which is stable under mass spectral conditions.

The mono-bidentate 'complex ligand' $[Ru(L^{o\text{-Ph}})_2]^{2+}$ reacts with Ag(I) ions to form a simple tri-nuclear complex cation, which further self-assembles into a nonanuclear non-coordinatively bonded structure *via* extensive π-stacking and hydrogen-bonding interactions with the bound anions.

3.4 Experimental

Metal salts and all organic reagents were purchased from Alfa or Sigma-Aldrich and used as received. NMR spectra were recorded on Bruker DRX 500 MHz, Bruker AV-III 400 MHz or AV-1 800 MHz instruments. Electrospray mass spectra were recorded on a Micromass LCT instrument. UV/Vis absorption spectra were measured on a Cary 50 spectrophotometer.

Cyclic voltammetric measurements were performed with an Ecochimie Autolab 100 potentiostat using a conventional three-electrode cell with a Pt disc working electrode and Ag/AgCl electrode as reference; the base electrolyte was 0.1 M Bu_4NPF_6 and the solvent was MeCN (purified by distillation over CaH_2). Ferrocene was added at the end of each experiment as an internal standard and all potentials are quoted vs the ferrocene/ferricinium couple (Fc/Fc^+).

3.4.1 Ligand Synthesis

3-(2-pyridyl)pyrazole, $L^{o\text{-}Ph}$, $L^{m\text{-}Ph}$, $L^{p\text{-}Ph}$, $L^{1,5\text{-}nap}$, $L^{3,3\text{-}Bi}$ and $L^{1,4\text{-}nap}$ were prepared following the literature procedures.[28,32,51,67,69-71]

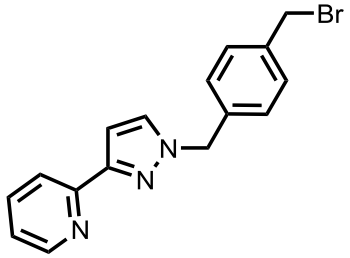

Synthesis of $Int^{p\text{-}Ph}$

A mixture of 1,4-bis(bromomethyl)benzene (1.5 g, 3.68 mmol), 3-(2-pyridyl)pyrazole (0.4 g, 2.75 mmol), tetrahydrofuran (THF, 70 cm^3) and aqueous NaOH (7.5 M, 10 cm^3) was stirred at 40°C for 1 hour. The resultant yellow solution was diluted with H_2O (100 cm^3) and the organic layer separated, dried over $MgSO_4$ and concentrated before purification by column chromatography on alumina (20 % hexane / dichloromethane) to give $Int^{p\text{-}Ph}$ as a white solid (Yield: 0.20 g, 22.2%). ^{1}H-NMR (400 MHz, $CDCl_3$): δ 8.66 (1H, ddd; pyridyl H^6), 7.96 (1H, d; pyridyl H^3), 7.74 (1H, td; pyridyl H^4), 7.45 (1H, d;

pyrazolyl H^5), 7.42–7.37 (2H, m; phenyl), 7.27–7.20 (3H, m; 2 x phenyl, and pyridyl H^5), 6.93 (1H, d; pyrazolyl H^4), 5.42 (2H, s; CH_2- pz), 4.50 (2H, s, CH_2Br). EI MS: *m/z* 327 (M^+). Found: C, 56.3; H, 4.3; N, 11.9%: Required for $C_{16}H_{14}N_3Br$: C, 56.9; H, 4.5; N, 12.5%. Data is in accordance with the literature.[72]

3.4.2 Mononuclear complex synthesis

$Ru(DMSO)_4Cl_2$ was prepared by the literature method;[73] *mix*-, *mer*- and *fac*-$[Ru(PyPzH)_3](PF_6)_2$, and *mer* and *fac*- $[Ru(L^{Me})_3](PF_6)_2$ were made by the method detailed in Chapter 2.[47]

Synthesis of *mix*-$[Ru(L^{p\text{-}Ph})_3](PF_6)_2$

A mixture of $L^{p\text{-}Ph}$ (0.41 g, 1.0 mmol), $RuCl_2(DMSO)_4$ (0.10g, 0.2 mmol), ethanol (48 cm^3) and water (12 cm^3) were heated to reflux with stirring for 4 h. After cooling the red mixture, excess ligand was removed by washing with chloroform. Addition of saturated $KPF_{6\ (aq)}$ afforded a yellow precipitate, which was collected by filtration and washed with diethyl ether and water (1:5 mixture of *fac* and *mer* isomers). Yield: 0.24 g, 77.7%. ESMS *m/z* 1423 (M - PF_6^-)$^+$, 639 (M - $2PF_6^-$)$^{2+}$. Found: C, 54.2; H, 4.2; N, 15.7%. Required for $C_{72}H_{60}N_{18}P_2F_{12}Ru{\bullet}H_2O$: C, 54.5; H, 3.9; N, 15.9%.

Synthesis of *mix*-$[Ru(L^{1,5\ nap})_3](PF_6)_2$

A solution of $L^{1,5\text{-}nap}$ (0.20 g, 0.45 mmol, 5.4 eq) was stirred rapidly in refluxing ethylene glycol (40 cm^3) until dissolved. To this was added a solution of $RuCl_2(dmso)_4$ (0.04 g, 0.08 mmol) in H_2O / ethylene glycol (12 : 1, 65 cm^3) by dropping funnel over 3 hours, and then the orange mixture was stirred at reflux in the dark for 14 h. The solution was cooled to 25 ^oC and excess saturated $KPF_{6\ (aq)}$ was added. The product was extracted with dichloromethane, dried over $MgSO_4$ and evaporated to dryness. The product was purified by column chromatography on silica. Elution with MeCN–water–saturated aqueous KNO_3 (100 : 10 : 1) resulted in a broad yellow band moving down the column which was collected. After removing acetonitrile by rotary evaporation, excess saturated aqueous KPF_6 was added and the product was extracted from the suspension into dichloromethane. The organic layer was separated, dried over $MgSO_4$, and the solvent removed *in vacuo* to yield $[Ru(L^{1,5\text{-}nap})_3](PF_6)_2$ as a yellow

solid (1:3 mixture of *fac* and *mer* isomers which were not separated). Yield: 0.11 g, 77 %. ESMS: *m/z* 1573 $(M - PF_6)^+$, 714 $(M - 2PF_6)^{2+}$. Found: C, 56.7; H, 4.1; N, 13.7. $C_{84}H_{66}F_{12}N_{18}P_2Ru \bullet 4H_2O$ requires C, 56.3; H, 4.2; N, 14.1%. UV/Vis in MeCN [λ_{max}/nm ($10^{-3}\varepsilon$ / M^{-1} cm^{-1})]: 398 (16.6), 282 (103.1), 226 (196.0).

Synthesis of *mix*-$[Ru(L^{m\text{-}Ph})_3](PF_6)_2$

A solution of $L^{m\text{-}Ph}$ (0.30 g, 0.76 mmol, 6.9 eq) in ethanol (100 cm^3) and H_2O (20 cm^3) was stirred under reflux until fully dissolved. To this was added a solution of $RuCl_2(dmso)_4$ (0.05 g, 0.11 mmol) in ethanol / H_2O (7 : 5, 60 cm^3) by dropping funnel over 3 hours, and then the yellow mixture was stirred at reflux in the dark for 14 h. After cooling the red mixture and diluting with H_2O, excess ligand was removed by washing with chloroform. Addition of saturated $KPF_{6\,(aq)}$ afforded a yellow precipitate, which was purified by column chromatography on silica. Elution with MeCN–water–saturated aqueous KNO_3 (100 : 10 : 1) resulted in a broad yellow band moving down the column which was collected. After removing acetonitrile by rotary evaporation, excess saturated aqueous KPF_6 was added and the product was extracted from the suspension into dichloromethane. The organic layer was separated, dried over $MgSO_4$, and the solvent removed *in vacuo* to yield $[Ru(L^{m\text{-}Ph})_3](PF_6)_2$ as a yellow solid (1:7 mixture of *fac* and *mer* isomers). Yield: 0.24 g, 77.7%. ESMS *m/z* 1423 (M^+ - PF_6^-), 639 (M^{2+} - $2PF_6^-$). Found: C, 54.7; H, 4.1; N, 15.8%. Required for $C_{72}H_{60}N_{18}P_2F_{12}Ru$: C, 55.1; H, 3.9; N, 16.1%.

Synthesis of $[Ru(L^{o\text{-}Ph})_2](PF_6)_2$

A mixture of $L^{o\text{-}Ph}$ (0.60 g, 1.52 mmol, 6 eq) in EtOH/H_2O (5 : 1, 60 cm^3) was heated to reflux until the ligand had dissolved. A solution of $RuCl_2(dmso)_4$ (0.12 g, 0.25 mmol) in in EtOH/H_2O (1 : 1, 10 cm^3) was then added dropwise over 2 h, and the clear orange mixture was stirred under reflux in the dark for 16 h. After cooling to room temperature the solvent was removed by rotary evaporation and the resultant crude yellow solid was partitioned between H_2O and $CHCl_3$. The aqueous layer was collected, and excess saturated aqueous KPF_6 was added to precipitate the product, before purification of the yellow solid by column chromatography on silica. Elution with MeCN–water–saturated aqueous KNO_3 (100 : 10 : 2) resulted in a single yellow band moving down the column which was collected. After removing

acetonitrile by rotary evaporation, excess saturated aqueous KPF_6 was added and the product was extracted from the suspension into dichloromethane. The organic layer was separated, dried over $MgSO_4$, and the solvent removed *in vacuo* to yield $[Ru(L^{o\text{-}Ph})_2](PF_6)_2$ as a yellow solid. Slow diffusion of di-ethyl ether vapour into a solution of the complex in acetone/nitromethane afforded the product as yellow shards. Yield: 0.20 g, 68 %. ^{1}H NMR (400 MHz, CD_3CN): δ 8.57 (1H, d, *J* = 4.9 Hz), δ 8.16 – 8.06 (3H, m), δ 8.01 (1H, td, *J* = 7.9, 1.4 Hz), δ 7.95 – 7.69 (8H, m), δ 7.57 (1H, d, *J* = 2.3 Hz; pyrazolyl), δ 7.48 (2H, d, *J* = 6.7 Hz), δ 7.42 – 7.31 (3H, m), δ 7.31 – 7.20 (4H, m), δ 7.19 (1H, d, *J* = 2.9 Hz; pyrazolyl), δ 7.04 (1H, d, *J* = 7.7 Hz), δ 7.01 – 6.94 (2H, m), δ 6.89 (1H, d, *J* = 2.3 Hz; pyrazolyl), δ 6.67 (1H, d, *J* = 7.9 Hz), δ 6.39 (1H, ddd, *J* = 7.9, 5.6, 1.4 Hz), δ 6.08 (1H, d, *J* = 5.6 Hz), δ 6.00 (1H, d, *J* = 7.7 Hz), δ 5.60 (1H, d, *J* = 18.4 Hz; CH_2), δ 5.43 (1H, d, *J* = 17.0 Hz; CH_2), δ 4.95 (1H, d, *J* = 15.7 Hz; CH_2), δ 4.77 (2H, s, 2 x CH_2), δ 4.62 (1H, d, *J* = 18.4 Hz; CH_2), δ 4.55 (1H, d, *J* = 17.0 Hz; CH_2), δ 2.47 (1H, d, *J* = 15.7 Hz; CH_2). ESMS: *m/z* 1032 $(M - PF_6)^+$, 443 $(M - 2PF_6)^{2+}$. Found: C, 48.6; H, 3.8; N, 13.8. $C_{48}H_{40}F_{12}N_{12}P_2Ru{\bullet}H_2O$ requires C, 48.3; H, 3.6; N, 14.1%. UV/Vis in MeCN [λ_{max}/nm (10^{-3} ε/M^{-1} cm^{-1})]: 399 (13.4), 282 (60.9), 243 (52.0).

Synthesis of *fac*-$[Ru(L^{p\text{-}Ph})_3](PF_6)_2$

A mixture of *fac*-$[Ru(PyPzH)_3](PF_6)_2$ (0.05 g, 0.05 mmol) and $Int^{p\text{-}Ph}$ (0.11 g, 0.33 mmol), Cs_2CO_3 (0.15 g, 0.46 mmol), Bu_4NI (0.10 g, 0.27 mmol) and CH_2Cl_2 (20 cm^3) was heated to reflux in the dark with stirring for 48 h. After cooling to room temperature, excess Cs_2CO_3 was filtered off and the solvent removed by rotary evaporation, before purification of the yellow solid by column chromatography on silica by elution with MeCN–water–saturated aqueous KNO_3 (100:10:5 ratio by volume). After removing acetonitrile by rotary evaporation, excess saturated aqueous KPF_6 was added and the product was extracted from the suspension into dichloromethane. The organic layer was separated, dried over $MgSO_4$, and the solvent removed *in vacuo* to yield *fac*–$[Ru(L^{p\text{-}Ph})_3][PF_6]_2$ as a yellow solid in 68% yield. Slow diffusion of di-isopropyl ether vapour into a solution of the complex in acetone afforded the product as yellow needles. ^{1}H NMR (400 MHz, CD_3CN): δ 8.58 (1H, ddd, *J* = 4.7, 1.8, 0.8 Hz; pendant pyridyl H^6), 8.00 (1H, td, *J* = 8.0, 1.0 Hz; pendant pyridyl H^3), 7.83 (1H, d, *J* = 2.2 Hz; pendant pyrazolyl), 7.79 (1H, td, *J* = 7.8, 1.8 Hz; pendant pyridyl H^4), 7.71 (1H, d, *J* = 2.9 Hz; coordinated

pyrazolyl), 7.61 (1H, td, *J* = 7.8, 1.4 Hz; coordinated pyridyl H^4), 7.27 (1H, ddd, *J* = 7.4, 4.9, 1.1 Hz; pendant pyridyl H^5), 7.24 (1H, d, *J* = 8.0 Hz; coordinated pyridyl H^3), 7.03 (1H, ddd, *J* = 7.9, 5.7, 1.4 Hz; coordinated pyridyl H^5), 6.98 (1H, d, *J* = 2.2 Hz; pendant pyrazolyl), 6.94 (1H, d, *J* = 5.7 Hz; coordinated pyridyl H^6), 6.88 (2H, d, *J* = 8.2 Hz; phenyl H^3), 6.54 (1H, d, *J* = 2.9 Hz; coordinated pyrazolyl), 5.91 (2H, d, *J* = 8.2 Hz; phenyl H^2), 5.48 (1H, d, *J* = 17.3 Hz; CH_2 closer to Ru), 5.29 (2H, s; CH_2 further from Ru), 4.78 (1H, d, *J* = 17.3 Hz; CH_2 closer to Ru). ESMS: *m/z* 1424 $(M - PF_6)^+$, 639 $(M - 2PF_6)^{2+}$. Found: C, 54.9; H, 3.9; N, 16.0. $C_{72}H_{60}F_{12}N_{18}P_2Ru$ requires C, 55.1; H, 3.9; N, 16.1%. UV/Vis in MeCN [λ_{max}/nm (10^{-3} ε/M^{-1} cm^{-1})]: 399 (12.6), 282 (64.4), 250 (66.3).

Synthesis of *mer*-[Ru($L^{p\text{-}Ph}$)$_3$](PF$_6$)$_2$

The same method was used as for *fac*–[Ru($L^{p\text{-}Ph}$)$_3$][PF_6]$_2$, except starting with *mer*-[Ru(PyPzH)$_3$](PF_6)$_2$. The product was isolated as a yellow solid in 64 % yield. ^{1}H NMR (400 MHz, acetone-d_6): δ 8.64 – 8.55 (3H, m), 8.38 (1H, d, *J* = 8.0 Hz), 8.22 (1H, d, *J* = 2.8 Hz; pyrazolyl), 8.14 – 8.01 (6H, m), 8.00 – 7.94 (3H, m), 7.92 (1H, d, *J* = 2.8 Hz), 7.85 – 7.69 (6H, m), 7.62 – 7.56 (2H, m), 7.54 (1H, d, *J* = 8.1 Hz), 7.43 (1H, d, *J* = 8.1 Hz), 7.39 (1H, d, *J* = 5.5 Hz), 7.35 (1H, d, *J* = 8.1 Hz), 7.32 – 7.18 (9H, m), 7.05 – 7.00 (3H, m), 6.98 (4H, d, *J* = 7.7 Hz), 6.92 (2H, d, *J* = 8.1 Hz), 6.88 (1H, d, *J* = 2.8 Hz; pyrazolyl), 6.73 (1H, d, *J* = 2.8 Hz; pyrazolyl), 6.62 (1H, d, *J* = 2.8 Hz; pyrazolyl), 6.14 (2H, d, *J* = 8.1 Hz; phenyl), 6.01 (2H, d, *J* = 8.1 Hz; phenyl), 5.96 (2H, d, *J* = 8.1 Hz; phenyl), 5.78 (1H, d, *J* = 17.4 Hz; CH_2 closer to Ru), 5.66 (1H, d, *J* = 17.4 Hz; CH_2 closer to Ru), 5.58 (1H, d, *J* = 17.4 Hz; CH_2 closer to Ru), 5.43 – 5.32 (6H, m, CH_2 further from Ru), 5.15 (1H, d, *J* = 17.0 Hz; CH_2 closer to Ru), 5.11 (1H, d, *J* = 17.0 Hz; CH_2 closer to Ru), 5.02 (1H, d, *J* = 17.4 Hz; CH_2 closer to Ru). ESMS: *m/z* 1424 $(M - PF_6)^+$, 639 $(M - 2PF_6)^{2+}$.

Synthesis of *fac*-[Ru($L^{3\text{-}Py}$)$_3$](PF$_6$)$_2$

A mixture A mixture of *fac*-[Ru(PyPzH)$_3$](PF_6)$_2$ (0.04 g, 0.05 mmol) and 3-(bromomethyl) pyridine hydrobromide (0.15 g, 0.60 mmol, 11.6 eq), Cs_2CO3 (0.61 g, 1.89 mmol), Bu_4NI (0.05 g, 0.12 mmol) and acetonitrile (50 cm^3) was stirred in the dark for 5 days. Excess Cs_2CO_3 was filtered off and the solvent removed by rotary evaporation, before purification of the orange solid by column

chromatography on silica by elution with MeCN–water–saturated aqueous KNO_3 (100:10:10 ratio by volume); the second major yellow band was collected. After removing acetonitrile by rotary evaporation, excess saturated aqueous KPF_6 was added and the product was extracted from the suspension into dichloromethane. The organic layer was separated, dried over $MgSO_4$, and the solvent removed *in vacuo* to yield *fac*–$[Ru(L^{3\text{-}Py})_3][PF_6]_2$ as a yellow solid in 47% yield. Slow diffusion of di-isopropyl ether vapour into a solution of the complex in acetone afforded the product as yellow needles. ^{1}H NMR (250 MHz, acetone-d_6): δ 8.40 (1H, dd, *J* = 4.7, 0.9 Hz; pendant pyridyl H^6), 8.22 (1H, d, *J* = 3.0 Hz; pyrazolyl), 8.06 (1H, td, *J* = 7.8, 1.4 Hz; coordinated pyridyl H^5), 7.97 (1H, ddd, *J* = 7.8, 1.4, 0.7 Hz; coordinated pyridyl H^6), 7.54 (1H, d, *J* = 5.7 Hz; coordinated pyridyl H^3), 7.47 – 7.38 (2H, m; pendant pyridyl H^2 and coordinated pyridyl H^4), 7.19 (1H, d, *J* = 3.0 Hz; pyrazolyl), 7.05 (1H, dd, *J* = 7.9, 4.7 Hz; pendant pyridyl H^5), 6.54 (1H, d, *J* = 7.9 Hz; pendant pyridyl H^4), 5.90 (1H, d, *J* = 17.3 Hz; CH_2), 5.09 (1H, d, *J* = 17.3 Hz; CH_2). ESMS: *m/z* 956 $(M - PF_6)^+$, 405 $(M - 2PF_6)^{2+}$. Found: C, 44.5; H, 3.1; N, 14.6. $C_{42}H_{36}F_{12}N_{12}P_2Ru \bullet 0.5CH_2Cl_2$ requires C, 44.7; H, 3.3; N, 14.7%. UV/Vis in MeCN [λ_{max}/nm (10^{-3} ε/M^{-1} cm^{-1})]: 398 (15.6), 281 (55.1), 241 (42.9).

3.4.3 Cage synthesis

$[Cd_3L^{1\text{-}4\text{-}nap}{}_3](BF_4)_6$ was prepared by the literature method.[29]

Synthesis of $[Ru_4Cd_4(L^{1,5\text{-}nap})_{12}](ClO_4)_{16}$

To a stirred solution of $[Ru(L^{1,5\text{-}nap})_3](PF_6)_2$ (0.038 g, 0.022 mmol) in nitromethane (20 cm^3) was added an excess of $Cd(ClO_4)2.6H_2O$ (0.091 g, 0.217 mmol) causing a colour change from yellow to orange. After an overnight stir, the mixture was passed through a membrane filter and then precipitated with di-isopropyl ether. The light orange solid was collected by filtration and washed thoroughly with diisopropyl ether. X-ray quality crystals were grown by slow diffusion of di-isopropyl ether into a solution of the complex in nitromethane. Yield: 0.032 g, 75 %. ESMS: *m/z* 1839 $(M - 4ClO_4)^{4+}$, 1451

$(M - 5ClO_4)^{5+}$, 1193 $(M - 6ClO_4)^{6+}$, 1009 $(M - 7ClO_4)^{7+}$, 870 $(M - 8ClO_4)^{8+}$, 762 $(M - 9ClO_4)^{9+}$. UV/Vis in MeCN [λ_{max}/nm (10^{-3} ε / M^{-1} cm^{-1})]: 398 (61.5), 286 (366.3), 226 (707.0).

Synthesis of $[Ru_4Co_4(L^{1,5\text{-nap}})_{12}](BF_4)_{16}$

To a stirred solution of $[Ru(L^{1,5\text{-nap}})_3](PF_6)_2$ (0.003 g, 0.002 mmol) in nitromethane (20 cm^3) was added an excess of $Co(BF_4)_2.6H_2O$ (0.004 g, 0.013 mmol). After an overnight stir, the mixture was evaporated to dryness and then washed with dichloromethane and methanol. Slow diffusion of diisopropyl ether into the nitromethane solution gave the product as very small orange blocks. Yield: 0.002 g, 50 %. ESMS: *m/z* 1748 $(M - 4BF4)^{4+}$, 1381 $(M - 5BF_4)^{5+}$, 1136 $(M - 6BF_4)^{6+}$, 962 $(M - 7BF_4)^{7+}$, 831 $(M - 8BF_4)^{8+}$, 729 $(M - 9BF_4)^{9+}$.

Synthesis of $[Ru_4Co_4(L^{m\text{-Ph}})_{12}](BF_4)_8(PF_6)_8$

To a stirred solution of $[Ru(L^{m\text{-Ph}})_3](PF_6)_2$ (0.073 g, 0.047 mmol) in dichloromethane (10 cm^3) was added a solution of $Co(BF4)_2.6H_2O$ (0.016 g, 0.047 mmol) in methanol (10 cm^3). After an overnight stir, the mixture was evaporated to dryness and then washed with dichloromethane and methanol. The mixture was then collected on a membrane filter and then extracted with nitromethane. Slow diffusion of diisopropyl ether into the nitromethane solution gave the product as yellow blocks and orange shards. ESMS (selected peaks): *m/z* 2835, $([Ru_4Co_4(L^{m\text{-Ph}})_{12}](BF_4)(PF_6))^{5+}$; 2348, $([Ru_4Cd_{12}(L^{p\text{-Ph}})_{12}(L^{1,4\text{-nap}})_{12}]\text{-}(BF_4)_{25}(PF_6))^{6+}$; 2000, $([Ru_4Cd_{12}(L^{p\text{-Ph}})_{12}(L^{1,4\text{-nap}})_{12}](BF_4)_{24}(PF_6))^{7+}$.

Elemental analytical data was consistent with the presence of water of crystallisation due to the desolvated material being hygroscopic, Found: C, 46.19; H, 3.55; N, 13.03 %. Required for $C_{288}H_{240}B_9NaCo_4F_{84}N_{72}P_8Ru_4{\cdot}12H_2O$: C, 45.94; H, 3.53; N, 13.39 %.

Synthesis of $[Ru_4Ag_6(L^{p\text{-Ph}})_{12}](PF_6)_{14}$

To a solution of *fac*-$[Ru(L^{p\text{-Ph}})_3](PF_6)_2$ (0.023 g, 0.015 mmol) in CH_3CN (1 cm^3) was added a solution of $AgPF_6$ (0.007 g, 0.028 mmol, 1.8 eq) in CH_3CN (1 cm^3). The solution was mixed vigorously for 16 hr and then evaporated to dryness. The yellow residue was washed with MeOH and dried *in vacuo*.

Slow diffusion of di-isopropyl ether vapour into a solution of the complex in acetonitrile afforded the product as yellow blocks.

ESMS: m/z 2452 $\{(Ru_4Ag_6(L^{p\text{-}Ph})_{12})(PF_6)_{11}\}^{3+}$; 1803 $\{(Ru_4Ag_6(L^{p\text{-}Ph})_{12})(PF_6)_{10}\}^{4+}$; 1678 $\{(RuAg(L^{p\text{-}Ph})_3)(PF_6)\}^{+}$; 1154 $\{(Ru_4Ag_6(L^{p\text{-}Ph})_{12})(PF_6)_8\}^{6+}$; 892 $\{(RuAg_2(L^{p\text{-}Ph})_3)(PF_6)_2\}^{2+}$; 546 $\{(RuAg_2(L^{p\text{-}Ph})_3)(PF_6)\}^{3+}$. The vacuum-dried material gave elemental analyses consistent with absorption of large numbers of H_2O molecules. Anal. Calcd for $[Ru_4Ag_6(L^{p\text{-}Ph})_{12}](PF_6)_{14}\bullet 9H_2O$: C, 43.5; H, 3.3; N, 12.7%. Found: C, 43.8; H, 3.6; N, 12.8%. Yield based on this formulation: ca. 80%.

Synthesis of $[Ru_4Cd_{12}(L^{p\text{-}Ph})_{12}(L^{1,4\text{-}nap})_{12}](PF_6)_{n\text{-}32}(BF_4)_{32\text{-}n}$

A Teflon lined autoclave was charged with $[Cd_3L^{1\text{-}4\text{-}nap}{}_3](BF_4)_6$ (11 mg, 0.005 mmol), $[Ru(L^{p\text{-}Ph})_3](PF_6)_2$ (7 mg, 0.005 mmol) and acetonitrile (10 cm^3). Heating to 180 °C for twelve hours followed by slow cooling to room temperature yielded a yellow solid which was recrystallised by slow diffusion of diisopropyl ether into a solution of the complex in acetonitrile. (Yield: 16 mg, 0.004 mmol, 80 %). ESMS (selected peaks): *m/z* 2835, $([Ru_4Cd_{12}(L^{p\text{-}Ph})_{12}(L^{1,4\text{-}nap})_{12}](BF_4)_{26}(PF_6))^{5+}$; 2348, $([Ru_4Cd_{12}(L^{p\text{-}Ph})_{12}(L^{1,4\text{-}nap})_{12}](BF_4)_{25}(PF_6))^{6+}$; 2000, $([Ru_4Cd_{12}(L^{p\text{-}Ph})_{12}(L^{1,4\text{-}nap})_{12}](BF_4)_{24}(PF_6))^{7+}$.

Synthesis of $[Ag\{Ru(L^{o\text{-}Ph})_2\}_2](PF_6)_5$

A solution of $AgPF_6$ (0.004 g, 0.015 mmol) in MeOH (5 cm^3) was added to a stirring solution of $[Ru(L^{o\text{-}Ph})_2](PF_6)_2$ (0.030 g, 0.026 mmol) in DCM (5 cm^3) and the mixture was stirred in the dark for 16 h. The solvent was removed by rotary evaporation to yield a crude yellow solid. Slow diffusion of toluene vapour into a solution of the complex in acetonitrile afforded the product as yellow blocks. Yield: 0.027 g, 73 %. ESMS: m/z 2460 $\{[Ru_6Ag_3(L^{o\text{-}Ph})_{12}](PF_6)_{12}\}^{3+}$; 1809 $\{[Ru_6Ag_3(L^{o\text{-}Ph})_{12}](PF_6)_{11}\}^{4+}$; 1592 $\{[Ru_4Ag_2(L^{o\text{-}Ph})_8](PF_6)_7\}^{3+}$; 1157 $\{[Ru_2Ag(L^{o\text{-}Ph})_4](PF_6)_3\}^{2+}$; 723 $\{[Ru_2Ag(L^{o\text{-}Ph})_4](PF_6)_2\}^{3+}$.

Synthesis of $[Ag_3Ru_2(L^{3\text{-}Py})_6](PF_6)_7$

A solution of *fac*–$[Ru(L^{3\text{-}Py})_3][PF_6]_2$ (0.018 g, 0.016 mmol) in acetone-d_6 (0.8 cm^3) was treated with $AgPF_6$ (0.006 g, 0.024 mmol, 1.5 eq) and the mixture was left in the dark overnight. The solvent was removed by rotary evaporation to give the product as a yellow solid. Yield: 0.024 g, quantitative. ^1H

NMR (250 MHz, acetone-d_6): δ 8.56 (1H, d, *J* = 4.0 Hz; pendant pyridyl H^6), 8.23 (1H, d, *J* = 2.8 Hz; pyrazolyl), 8.14 – 7.94 (2H, m; coordinated pyridyl H^5 + H^6), 7.69 (1H, s; pendant pyridyl H^2), 7.54 – 7.39 (2H, m; coordinated pyridyl H^3 + H^4), 7.34 (1H, dd, *J* = 8.1, 5.4 Hz; pendant pyridyl H^5) 7.23 (1H, d, *J* = 2.8 Hz; pyrazolyl), 6.75 (1H, d, *J* = 8.0 Hz; pendant pyridyl H^4), 5.99 (1H, d, *J* = 17.8 Hz; CH_2), 5.12 (1H, d, *J* = 17.8 Hz; CH_2). ESMS: *m/z* 1208 $\{[\{Ru(L^{3\text{-}Py})_3\}_2Ag_2](PF_6)_4\}^{2+}$.

3.5 X-ray crystallography

Details of the crystal, data collection and refinement parameters are summarised. Data were corrected for absorption using empirical methods (SADABS)[74] based upon symmetry-equivalent reflections combined with measurements at different azimuthal angles. The structures were solved by direct methods and refined by full-matrix least squares on weighted F^2 values for all reflections using the SHELX suite of programs.[75] Non-hydrogen atoms were refined anisotropically. Hydrogen atoms were placed in calculated positions, refined using idealized geometries (riding model) and were assigned fixed isotropic displacement parameters.

The structures of *fac*–$[Ru(L^{p\text{-}Ph})_3][PF_6]_2$ and $[Ru_4Ag_6(L^{p\text{-}Ph})_{12}](PF_6)_{14}$ were collected at the National Crystallography Service at the University of Southampton.[76] In each other case a suitable crystal was mounted in a stream of cold N_2 on a Bruker APEX-2 or SMART CCD diffractometers (at the University of Sheffield) equipped with graphite-monochromated Mo-Kα radiation from a sealed-tube source. Details of each structure are given in their individual CIFs.

For the polynuclear complexes the crystals scattered weakly – as is usual for compounds of this type – due to a combination of poor crystallinity and extensive disorder of anions/solvent molecules. The weakness of the data required extensive use of restraints and/or constraints, to keep the geometries of anions, aromatic rings or solvent molecules reasonable, and the disorder meant that in some cases not all anions could be located. In all these cases, and for *fac*–$[Ru(L^{p\text{-}Ph})_3][PF_6]_2$, there were extensive areas

of residual electron density which could not sensibly be modelled as solvent or anions, which were removed *via* application of the 'Squeeze' function in PLATON.[77] Full details of these issues and how they were handled is given in the individual CIFs, but it should be noted that the composition/formula of the crystal as given in the crystallographic data table is necessarily an approximation (regarding anions / solvents). We emphasise that the complex cations are well defined in all cases with reasonable displacement parameters and with esd's for atomic coordinates and for bond distances / angles that are unremarkable.

Summary of crystallographic data for the new crystal structures:

Compound	**$[Ru_4Cd_4(C_{28}H_{22}N_6)_{12}](ClO_4)_{16}$ • 11$MeNO_2$ • 0.5$[Cd(OH_2)_6](ClO_4)_2$**	**$[Ru_4Co_4(L^{m\text{-}Ph})_{12}]$ $Na(BF_4)_{12}(PF_6)_5$●8$MeNO_2$**
Formula	$C_{347}H_{309}Cd_{4.5}Cl_{17}N_{83}O_{96}Ru_4$	$C_{296}H_{264}B_{12}Co_4F_{78}N_{80}NaO_{16}P_5Ru_4$
Molecular weight	8441.94	7627.42
T / *K*	100(2)	100(2)
Crystal system	Monoclinic	Tetragonal
Space group	*P*2(1)/c	*P*-42$_1$*m*
a / Å	23.0027(14)	31.3553(12)
b / Å	40.888(2)	31.3553(12)
c / Å	50.529(3)	21.7210(8)
α / °	90	90
β / °	100.989(3)	90
γ / °	90	90
V / Å^3	46653(5)	21355.1(18)
Z	4	2
ρ / g cm^{-3}	1.237	1.186
μ / mm^{-1}	0.5	0.398
Data, restraints, parameters, R_{int}	61008 / 4310 / 3721 / 0.176	14221 / 941 / 809 / 0.0630
Final *R*1, *wR*2[a]	0.1301, 0.3777	0.0766, 0.2199

Compound	***fac*–[Ru(L$^{p\text{-}Ph}$)$_3$][PF$_6$]$_2$ ●acetone**	**[{Ru(L$^{p\text{-}Ph}$)$_3$}$_4$Ag$_6$](PF$_6$)$_{14}$**
Formula	$C_{75}H_{66}F_{12}N_{18}OP_2Ru$	$C_{288}H_{240}Ag_6F_{84}N_{72}P_{14}Ru_4$
Molecular weight	1626.47	7790.59
T / *K*	100(2)	100(2)
Crystal system	Orthorhombic	Monoclinic
Space group	*P*bca	*P*2/n
a / Å	23.2400(17)	24.688(3)
b / Å	13.2721(9)	30.324(4)
c / Å	47.443(3)	25.247(3)
α / °	90	90
β / °	90	102.819(2)
γ / °	90	90
V / Å^3	14633.5(17)	18430(4)
Z	8	2
ρ / g cm^{-3}	1.477	1.404
μ / mm^{-1}	0.348	0.630
Data, restraints, parameters, R_{int}	8193 / 597 / 984 / 0.0991	24082 / 1746 / 1560 / 0.0646
Final *R*1, *wR*2[a]	0.1329, 0.3103	0.1405, 0.4293

Compound	***fac*–[Ru(L$^{3\text{-}Py}$)$_3$]-[PF$_6$]$_2$ ●acetone**	**2{[Ru(L$^{o\text{-}Ph}$)$_2$]-(PF$_6$)$_2$}●0.5MeNO$_2$**	**[AgRu$_2$(L$^{o\text{-}Ph}$)$_4$]-(PF$_6$)$_5$●2toluene**
Formula	$C_{48}H_{48}F_{12}N_{12}O_2P_2Ru$	$C_{96.50}H_{81.50}F_{24}N_{24.50}OP_4Ru_2$	$C_{330}H_{288}Ag_3F_{90}N_{72}P_{15}Ru_6$
Molecular weight	1215.99	2382.38	8366.90
T / *K*	100(2)	100(2)	100(2)
Crystal system	Triclinic	Monoclinic	Rhombohedral
Space group	*P* -1	*P*2(1)/c	*R*32
a / Å	11.4654(2)	19.9334(5)	21.5946(9)
b / Å	12.1681(3)	32.4345(8)	21.5946(9)
c / Å	19.4636(4)	17.3266(4)	70.537(4)
α / °	93.6490(10)	90	90
β / °	94.0130(10)	97.023(2)	90
γ / °	110.0760(10)	90	120
V / Å^3	2533.00(9)	11118.1(5)	28486(2)
Z	2	2	3
ρ / g cm^{-3}	1.594	1.423	1.463
μ / mm^{-1}	0.471	0.426	0.551
Data, restraints, parameters, R_{int}	11403 / 259 / 749 / 0.0195	30492 / 96 / 1358 / 0.0591	10839 / 616 / 540 / 0.0777
Final *R*1, *wR*2[a]	0.0621, 0.1642	0.0749, 0.02490	0.1220, 0.3643

[a] The value of R1 is based on 'observed' data with I>2σ(I); the value of wR2 is based on all data.

3.6 References

1. M. D. Ward and P. R. Raithby, *Chem. Soc. Rev.*, 2013, **42**, 1619.

2. M. M. J. Smulders, I. A. Riddell, C. Browne and J. R. Nitschke, *Chem. Soc. Rev.*, 2013, **42**, 1728.

3. M. Wang, V. Vajpayee, S. Shanmugaraju, Y.-R. Zheng, Z. Zhao, H. Kim, P. S. Mukherjee, K.-W. Chi and P. J. Stang, *Inorg. Chem.*, 2011, **50**, 1506.

4. Y. Sakata, S. Hiraoka and M. Shionoya, *Chem.-Eur. J.*, 2010, **16**, 3318.

5. C. Piguet, G. Bernardinelli and G. Hopfgartner, *Chem. Rev.*, 1997, **97**, 2005.

6. O. Chepelin, J. Ujma, X. Wu, A. M. Z. Slawin, M. B. Pitak, S. J. Coles, J. Michel, A. C. Jones, P. E. Barran and P. J. Lusby, *J. Am. Chem. Soc.*, 2012, **134**, 19334.

7. K. Suzuki, M. Tominaga, M. Kawano and M. Fujita, *Chem. Commun.*, 2009, 1638.

8. K.-i. Yamashita, M. Kawano and M. Fujita, *Chem. Commun.*, 2007, 4102.

9. W. J. Ramsay, T. K. Ronson, J. K. Clegg and J. R. Nitschke, *Angew. Chem. Int. Ed.*, 2013, **52**, 13439.

10. X. K. Sun, D. W. Johnson, D. L. Caulder, K. N. Raymond and E. H. Wong, *J. Am. Chem. Soc.*, 2001, **123**, 2752.

11. S. Hiraoka, Y. Sakata and M. Shionoya, *J. Am. Chem. Soc.*, 2008, **130**, 10058.

12. H. B. Wu and Q. M. Wang, *Angew. Chem. Int. Ed.*, 2009, **48**, 7343.

13. A. J. Metherell and M. D. Ward, *RSC. Adv.*, 2013, **3**, 14281.

14. M. M. J. Smulders, A. Jimenez and J. R. Nitschke, *Angew. Chem. Int. Ed.*, 2012, **51**, 6681.

15. M. L. Saha and M. Schmittel, *J. Am. Chem. Soc.*, 2013, **135**, 17743.

16. F. Reichel, J. K. Clegg, K. Gloe, K. Gloe, J. J. Weigand, J. K. Reynolds, C.-G. Li, J. R. Aldrich-Wright, C. J. Kepert, L. F. Lindoy, H.-C. Yao and F. Li, *Inorg. Chem.*, 2014, **53**, 688.

17. I. S. Tidmarsh, H. Fenton and M. D. Ward, *Dalton Trans.*, 2010, **39**, 3805.

18. P. de Wolf, P. Waywell, M. Hanson, S. L. Heath, A. Meijer, S. J. Teat and J. A. Thomas, *Chem.-Eur. J.*, 2006, **12**, 2188.

19. G. Cooke, G. M. O. Maille, R. Quesada, L. S. Wang, S. Varughese and S. M. Draper, *Dalton Trans.*, 2011, **40**, 8206.

20. N. C. Fletcher, M. Nieuwenhuyzen, R. Prabarahan and A. Wilson, *Chem. Commun.*, 2002, 1188.

21. R. T. Brown, N. C. Fletcher, M. Nieuwenhuyzen and T. E. Keyes, *Inorg. Chim. Acta.*, 2005, **358**, 1079.

22. N. C. Fletcher, R. T. Brown and A. P. Doherty, *Inorg. Chem.*, 2006, **45**, 6132.

23. R. Hage, J. G. Haasnoot, J. Reedijk and J. G. Vos, *Inorg. Chim. Acta.*, 1986, **118**, 73.

24. Y. Luo, P. G. Potvin, Y. H. Tse and A. B. P. Lever, *Inorg. Chem.*, 1996, **35**, 5445.

25. M. Kyakuno, S. Oishi and H. Ishida, *Inorg. Chem.*, 2006, **45**, 3756.

26. S. Torelli, S. Delahaye, A. Hauser, G. Bernardinelli and C. Piguet, *Chem.-Eur. J.*, 2004, **10**, 3503.

27. M. D. Ward, *Chem. Commun.*, 2009, 4487.

28. J. S. Fleming, K. L. V. Mann, C. A. Carraz, E. Psillakis, J. C. Jeffery, J. A. McCleverty and M. D. Ward, *Angew. Chem. Int. Ed.*, 1998, **37**, 1279.

29. R. L. Paul, Z. R. Bell, J. C. Jeffery, J. A. McCleverty and M. D. Ward, *Proc. Nat. Acad. Sci. U.S.A*, 2002, **99**, 4883.

30. M. D. Ward, I. S. Tidmarsh, B. F. Taylor, M. J. Hardie, L. Russo and W. Clegg, *New. J. Chem.*, 2009, **33**, 366.

31. Z. R. Bell, J. C. Jeffery, J. A. McCleverty and M. D. Ward, *Angew. Chem. Int. Ed.*, 2002, **41**, 2515.

32. I. S. Tidmarsh, T. B. Faust, H. Adams, L. P. Harding, L. Russo, W. Clegg and M. D. Ward, *J. Am. Chem. Soc.*, 2008, **130**, 15167.

33. A. M. Najar, I. S. Tidmarsh, H. Adams and M. D. Ward, *Inorg. Chem.*, 2009, **48**, 11871.

34. B. R. Hall, L. E. Manck, I. S. Tidmarsh, A. Stephenson, B. F. Taylor, E. J. Blaikie, D. A. Vander Griend and M. D. Ward, *Dalton Trans.*, 2011, **40**, 12132.

35. A. Stephenson, S. P. Argent, T. Riis-Johannessen, I. S. Tidmarsh and M. D. Ward, *J. Am. Chem. Soc.*, 2011, **133**, 858.

36. Q.-H. Wei, S. P. Argent, H. Adams and M. D. Ward, *New. J. Chem.*, 2008, **32**, 73.

37. M. H. W. Lam, S. T. C. Cheung, K. M. Fung and W. T. Wong, *Inorg. Chem.*, 1997, **36**, 4618.

38. G. Canard and C. Piguet, *Inorg. Chem.*, 2007, **46**, 3511.

39. D. Ghosh, H. Ahmad and J. A. Thomas, *Chem. Commun.*, 2009, 2947.

40. Y.-T. Chan, X. Li, J. Yu, G. A. Carri, C. N. Moorefield, G. R. Newkome and C. Wesdemiotis, *J. Am. Chem. Soc.*, 2011, **133**, 11967.

41. L. Aboshyan-Sorgho, M. Cantuel, S. Petoud, A. Hauser and C. Piguet, *Coord. Chem. Rev.*, 2012, **256**, 1644.

42. S. Turega, M. Whitehead, B. R. Hall, A. J. H. M. Meijer, C. A. Hunter and M. D. Ward, *Inorg. Chem.*, 2013, **52**, 1122.

43. R. L. Paul, Z. R. Bell, J. S. Fleming, J. C. Jeffery, J. A. McCleverty and M. D. Ward, *Heteroatom Chem.*, 2002, **13**, 567.

44. N. C. A. Baker, N. McGaughey, N. C. Fletcher, A. V. Chernikov, P. N. Hortonb and M. B. Hursthouse, *Dalton Trans.*, 2009, 965.

45. N. C. Fletcher, M. Nieuwenhuyzen and S. Rainey, *J. Chem. Soc., Dalton Trans.*, 2001, 2641.

46. E. A. P. Armstrong, R. T. Brown, M. S. Sekwale, N. C. Fletcher, X. Q. Gong and P. Hu, *Inorg. Chem.*, 2004, **43**, 1714.

47. A. J. Metherell, W. Cullen, A. Stephenson, C. A. Hunter and M. D. Ward, *Dalton Trans.*, 2014, **43**, 71.

48. M. Whitehead, S. Turega, A. Stephenson, C. A. Hunter and M. D. Ward, *Chem. Sci.*, 2013, **4**, 2744.

49. S. Turega, W. Cullen, M. Whitehead, C. A. Hunter and M. D. Ward, *J. Am. Chem. Soc.*, 2014, **136**, 8475.

50. Z. R. Bell, L. P. Harding and M. D. Ward, *Chem. Commun.*, 2003, 2432.

51. S. P. Argent, H. Adams, L. P. Harding and M. D. Ward, *Dalton Trans.*, 2006, 542.

52. B. Whittle, S. R. Batten, J. C. Jeffery, L. H. Rees and M. D. Ward, *J. Chem. Soc., Dalton Trans.*, 1996, 4249.

53. M. S. Lah and V. L. Pecoraro, *J. Am. Chem. Soc.*, 1989, **111**, 7258.

54. A. J. Stemmler, J. W. Kampf and V. L. Pecoraro, *Inorg. Chem.*, 1995, **34**, 2271.

55. A. J. Stemmler, A. Barwinski, M. J. Baldwin, V. Young and V. L. Pecoraro, *J. Am. Chem. Soc.*, 1996, **118**, 11962.

56. B. R. Gibney, H. Wang, J. W. Kampf and V. L. Pecoraro, *Inorg. Chem.*, 1996, **35**, 6184.

57. A. Stephenson and M. D. Ward, *Chem. Commun.*, 2012, **48**, 3605.

58. A. Stephenson and M. D. Ward, *RSC. Adv.*, 2012, **2**, 10844.

59. J. M. Lehn and A. V. Eliseev, *Science*, 2001, **291**, 2331.

60. F. A. Cotton, C. A. Murillo and R. M. Yu, *Dalton Trans.*, 2005, 3161.

61. A. Stephenson, D. Sykes and M. D. Ward, *Dalton Trans.*, 2013, **42**, 6756.

62. N. Guex and M. C. Peitsch, *Electrophoresis*, 1997, **18**, 2714.

63. L. Wang, Y. Li, Y. Peng, Z. Liang, J. Yu and R. Xu, *Dalton Trans.*, 2012, **41**, 6242.

64. X. Kuang, X. Wu, R. Yu, J. P. Donahue, J. Huang and C.-Z. Lu, *Nature Chem.*, 2010, **2**, 461.

65. T. Shiga, G. N. Newton, J. S. Mathieson, T. Tetsuka, M. Nihei, L. Cronin and H. Oshio, *Dalton Trans.*, 2010, **39**, 4730.

66. T. Shiga, T. Tetsuka, K. Sakai, Y. Sekine, M. Nihei, G. N. Newton and H. Oshio, *Inorg. Chem.*, 2014, **53**, 5899.

67. R. L. Paul, S. M. Couchman, J. C. Jeffery, J. A. McCleverty, Z. R. Reeves and M. D. Ward, *J. Chem. Soc., Dalton Trans.*, 2000, 845.

68. S. Turega, M. Whitehead, B. R. Hall, M. F. Haddow, C. A. Hunter and M. D. Ward, *Chem. Commun.*, 2012, **48**, 2752.

69. A. J. Amoroso, A. M. C. Thompson, J. C. Jeffery, P. L. Jones, J. A. McCleverty and M. D. Ward, *J. Chem. Soc.-Chem. Commun.*, 1994, 2751.

70. S. P. Argent, H. Adams, T. Riis-Johannessen, J. C. Jeffery, L. P. Harding and M. D. Ward, *J. Am. Chem. Soc.*, 2006, **128**, 72.

71. A. Stephenson and M. D. Ward, *Dalton Trans.*, 2011, **40**, 7824.

72. S. P. Argent, H. Adams, L. P. Harding, T. Riis-Johannessen, J. C. Jeffery and M. D. Ward, *New. J. Chem.*, 2005, **29**, 904.

73. I. P. Evans, A. Spencer and Wilkinso.G, *J. Chem. Soc., Dalton Trans.*, 1973, 204.

74. G. M. Sheldrick, *SADABS: A program for absorption correction with the Siemens SMART system*, University of Göttingen, Germany, 1996.

75. G. M. Sheldrick, *Acta Cryst. Sect. A*, 2008, **64**, 112.

76. S. J. Coles and P. A. Gale, *Chem. Sci.*, 2012, **3**, 683.

77. P. Vandersluis and A. L. Spek, *Acta Cryst. Sect. A*, 1990, **46**, 194.

4. A tetrameric hetero-octanuclear cyclic helicate formed from a bridging ligand with two inequivalent binding sites

4.1 Introduction

As discussed in Chapter 3, the synthesis of heterometallic coordination complexes is currently the subject of intense research with the potential for very interesting and useful functional behaviour.[1-5] Two methods that are used in the synthesis of heterometallic structures are described in Chapter 2; the thermodynamic control approach, and the kinetic control approach. The research conducted using Ru(II) focuses on the latter approach, with a kinetically inert 'complex as ligand'[6] used as the basis of a supramolecular assembly. The Ru(II) complex functions as a pre-organised tris-bidentate metalloligand due to its three pendant binding sites. The stepwise heterometallic complex synthesis requires the initial isolation of the kinetically inert complex as a 'sub-component', before reaction with the labile components under self-assembly conditions.

An alternative approach to the kinetic control approach is the aforementioned thermodynamic control approach, a method which is applicable when all metal ions are sufficiently kinetically labile to allow rearrangement. The differing coordination preferences of different metal ions are exploited using an asymmetric bridging ligand which will have at least two different binding sites that exclusively bind to one metal ion (see Figure 4.1.1). This system has been termed the thermodynamic control approach, as the combination of metal ions and ligand are be able to rearrange, assembling and disassembling in such a way that initial 'mistakes' are corrected, eventually resulting in a structure that represents the thermodynamic minimum.

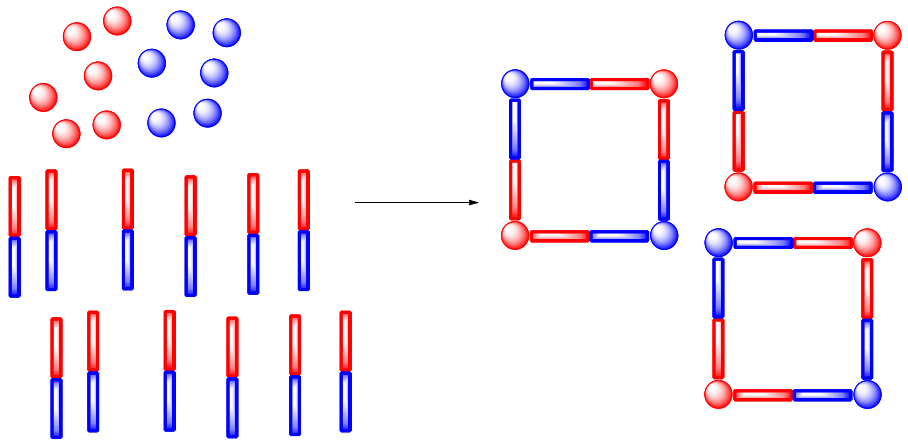

Figure 4.1.1 A schematic representation of heterometallic self-assembly using the thermodynamic control approach. Red and blue spheres depict different kinetically labile metal ions. Red and blue rectangles represent unsymmetrical bridging ligands.

Two different classes of unsymmetrical ligand have been used to achieve the synthesis of heterometallic structures. The first of these consists of ligands which possess binding sites with differing denticities, such that the affinity of each end of the ligand to bind to particular metals is primarily based on the preferred coordination geometry of each metal. For example, Piguet and co-workers have prepared heterometallic triple helicates which contain one transition metal ion and one lanthanide ion by using a ligand which contains one tridentate binding site and one bidentate binding site (see Figure 4.1.2a).[7] This is the only arrangement of ligands and metal ions which allows the Zn(II) ion to have its preferred octahedral geometry, and the Eu(III) to be nine-coordinate. The Nitschke group have used subcomponent self-assembly to form a cubic coordination cage containing six Pt(II) ions and eight Fe(II) ions bridged by a pyridyl-bis-imine ligand (see Figure 4.1.2b); the ligand is formed *in situ* from 2-formyl pyridine and 4-(4-pyridyl)aniline. Again, this structure forms because each metal's coordination preferences are satisfied. The square planar Pt(II) ions are coordinated to four monodentate pyridyl groups, and the octahedral Fe(II) ions are coordinated to three bientate imino-pyridyl groups. The final example is from the Ward group, and consists of another ligand with bidentate and monodentate binding groups (see Figure 4.1.2c). In this instance, the monodentate group is a benzonitrile group which coordinates to pyramidal Ag(I) ions, and the bidentate group is a pyridine-pyrazolyl (PyPz) unit which coordinates to octahedral Ni(II) ions.

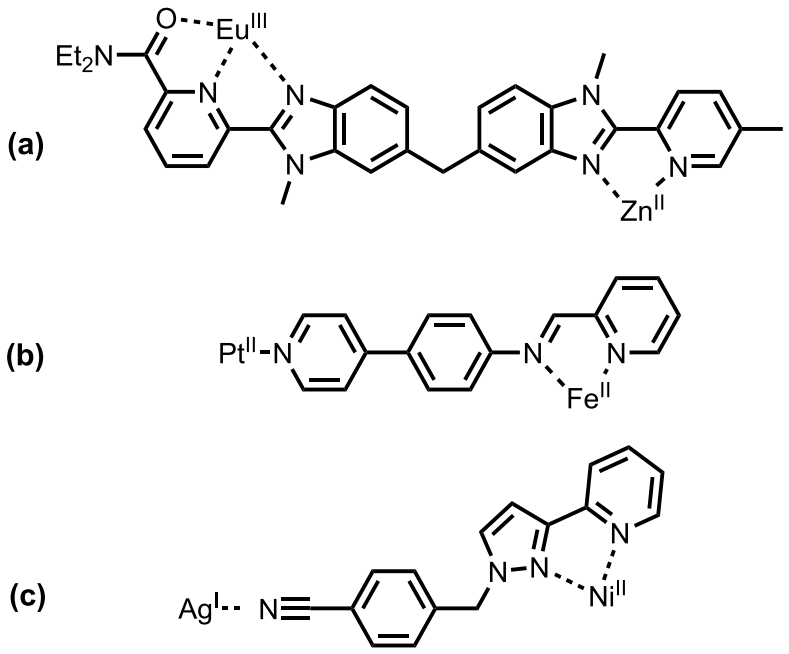

Figure 4.1.2 Three examples of ligands with unsymmetrical denticity: (a) $[EuZnL_3]^{5+}$ triple helicate[7]; (b) $[Fe_8Pt_6L_{24}]^{28+}$ cubic cage[8], and; (c) $[AgNiL_3]^{3+}$ coordination network.[9]

The second class of unsymmetrical ligand used in the design of heterometallic structures is those possessing hard and soft donor atoms at different binding sites. Recent examples in the literature where this type of approach has been used typically rely on the differing coordination preferences of hard donors (such as phenolates or catecholates) and soft donors (such as phosphine or pyridyl groups). Shionoya and co-workers have utilised a ligand with a pyridyl group at one end and a catecholate at the other, which bind to Pd(II) ions and Ti(IV) ions, respectively, to form a cage or ring, depending on the reaction stoichiometry and reaction conditions (see Chapter 1, Figure 1.5.4).[4,10] Further to this, the cage and the ring are interconvertible with each other under appropriate conditions. For example, their $[Pd_3Ti_2L_6Cl_6]^{4-}$ cage shown in Figure 1.5.4 interconverts to a $[Pd_2Ti_2(HL_2)_2(acac)_2Cl_4]$ ring on addition of $TiO(acac)_2$ and trifluoroacetic acid.

A notable feature of Shionoya's synthesis is that the $[TiL_3]^{2-}$ unit can be isolated and used as a metalloligand, a precursor to the heterometallic coordination cage. This method of using a metalloligand to form heterometallic structures has also been used by Wang and co-workers, who used a ligand furnished with a pyridyl and acetylacetonate binding sites to create an aluminium(III) tris-catecholate

metalloligand. This reacts with Pd(II) ions to form a $[Pd_6(AlL_3)_8](NO_3)_{12}$ cube (see Figure 1.5.5).[11] In a collaboration with Stang's group, reaction of the same metalloligand with a 60° diplatinum(II) acceptor yielded a structurally similar trigonal cage, in this case making use of the more inert Pt(II) ion to increase the solution stability of the cage once the desired product had been formed.

Raymond and co-workers have used a phosphino-catechol ligand that forms a tripodal metalloligand with Ti(IV). Mixing this with Pd(II) ions causes two of these metalloligands to assemble into a trigonal pyramidal heterometallic cage (see Figure 4.1.3).[12] Such complexes take advantage of not only the metals' preferred ligand type, but also the symmetry requirements of each metal to form the heterometallic structure. In this case - octahedral $[Ti^{IV}(cat)_3]^{2-}$ and linear $PdCl_2(phosphine)_2$.

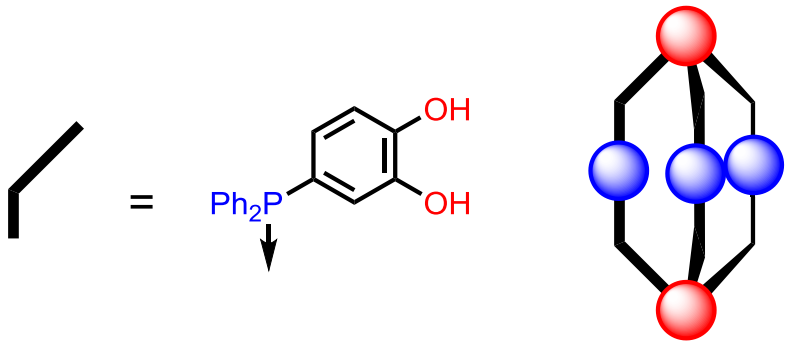

Figure 4.1.3 Raymond's phosphino-catechol ligand and the pentanuclear complex it forms on reaction with Ti(IV) and Pd(II) ions (red and blue spheres represent Ti(IV) and Pd(II), respectively). Reproduced from reference 12).[12]

4.2 Results and discussion

4.2.1 Ligand design and synthesis

The initial problem in the synthesis of heterometallic coordination structures with an asymmetric ligand is the design of such a ligand. As shown above, recent examples of such ligands utilise monodentate pyridyl or phosphine groups as the soft binding site, and catechol or acetylacetonate groups as the hard binding sites. Examples where bis-bidentate asymmetric ligands have been used in heterometallic synthesis are restricted to catechol-thiolates, and these only result in dinuclear helicates.[13] To the best

of the author's knowledge, no examples exist where a bis-bidentate asymmetric ligand has been used to create a heterometallic cage structure with a defined cavity that may be used for host-guest chemistry.

With the idea of a bis-bidentate ligand, two binding sites became immediately obvious as candidates in the prototype ligand; the PyPz binding site frequently used in the Ward group, and a catecholamide unit frequently used by the Raymond group.[14, 15] A prototype ligand might separate these two binding sites with an aromatic spacer, which frequently form aromatic π-stacks with the PyPz units, thus increasing the stability of the resulting supramolecular structures.[16]

Both binding sites can be easily introduced into one ligand, as a simple disconnection of the 1,3-phenylene substituted ligand reveals easily accessible synthetic equivalents (see Figure 4.2.1). The PyPz unit can be introduced by an S_N2 substitution of an alkyl bromide, whereas the catecholamide is introduced by an amide condensation between an acid chloride and an amine.

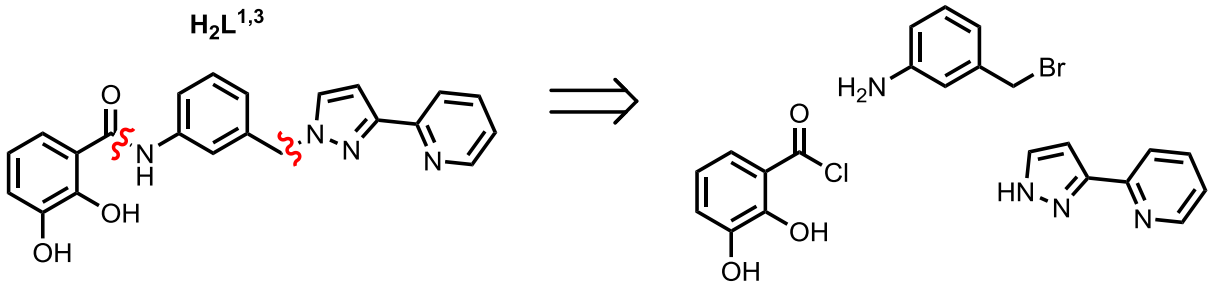

Figure 4.2.1 Prototype asymmetric ligand $H_2L^{1,3}$, with two disconnections that reveal the three synthetic building blocks.

With the simple disconnection strategy established, it is evident that there will be selectivity issues due to the presence of many reactive functional groups in one reaction. The bromomethylaniline could easily react with itself, and the catechol acid chloride would be difficult to prepare from the carboxylic acid without first protecting the catechol oxygens. A synthetic route was devised that protects the aniline group with the acid-labile butoxycarbonyl (Boc) protecting group, and the catechol was protected as the methyl ether (see Figure 4.2.2).

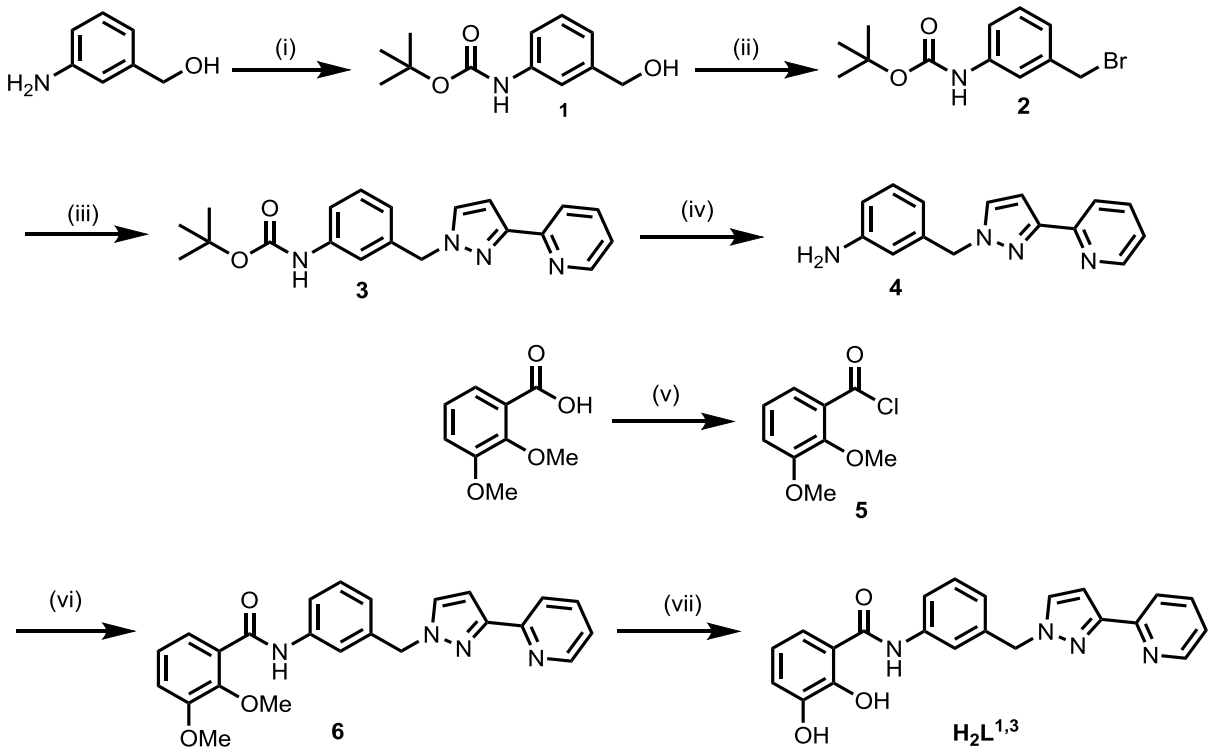

Figure 4.2.2 Reaction scheme for the preparation of $H_2L^{1,3}$. (i) Boc_2O, THF; (ii) CBr_4, PPh_3, DCM; (iii) PyPzH, THF, $NaOH_{(aq)}$; (iv) TFA, DCM; (v) $SOCl_2$, dmf; (vi) **5**, DCM, Et_3N; (vii) BBr_3, DCM, H_2O.

Starting from 3-aminobenzyl alcohol, the amine group was protected by a routine Boc protection with Boc_2O in tetrahyrofuran (THF), giving the carbamate **1** in nearly quantitative yield.[17] The alcohol was then converted to a leaving group by an Appel bromination with 1.5 equivalent of CBr_4 and PPh_3 in dichloromethane (DCM) at 0 ^oC to give alkyl bromide **2**. Once isolated by column chromatography as a white solid, the alkyl bromide was substituted by reaction with PyPzH in THF and aqueous sodium hydroxide at reflux to give **3**. The Boc group was then removed by an overnight stir in dichloromethane (DCM) with trifluoroacetic acid (TFA), and neutralised with potassium carbonate to give the amine **4**. The separate acid chloride **5** was prepared by refluxing the carboxylic acid in thionyl chloride with catalytic dimethylformamide (dmf). This was then reacted with the de-protected amine **4** in dry DCM with triethylamine in an amide condensation reaction that proceeded in excellent yield. The final step was the deprotection of the catechol methyl ether by reaction with BBr_3 in dry DCM at -78 ^oC followed by solvolysis in boiling water, yielding the target ligand $H_2L^{1,3}$ as its HBr salt as a white solid.

Compounds **3**, **4**, **6** and **$H_2L^{1,3}$** are new compounds and so were characterised by ^{1}H NMR spectroscopy, electrospray mass spectrometry (ESMS) and elemental analysis. The aromatic regions of the ^{1}H NMR spectra of **6** and **$H_2L^{1,3}$** are relatively complicated with 13 closely overlapping signals; a 2D COSY spectrum allows full assignment of these compounds (see Figure 4.2.3 for the assignment of compound **6**). The demethylated ligand **$H_2L^{1,3}$** is markedly less soluble than its precursor **6**, and its ^{1}H NMR spectrum is shown below in deuterated dimethylsulfoxide (see Figure 4.2.4).

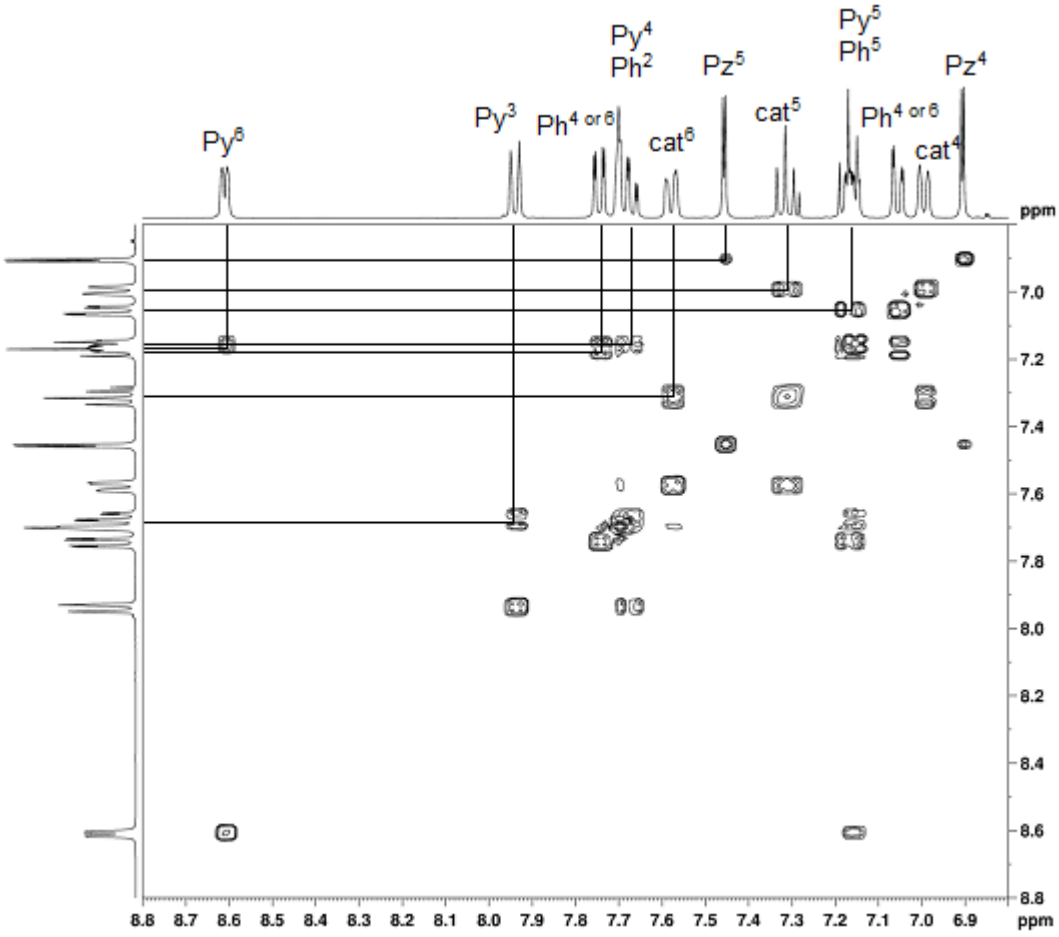

Figure 4.2.3 Part of the ^{1}H COSY NMR (400 MHz, $CDCl_3$) spectrum of **6,** showing the full assignment of the aromatic region. Py = pyridine, Pz = pyrazole, Ph = phenyl, cat = catechol.

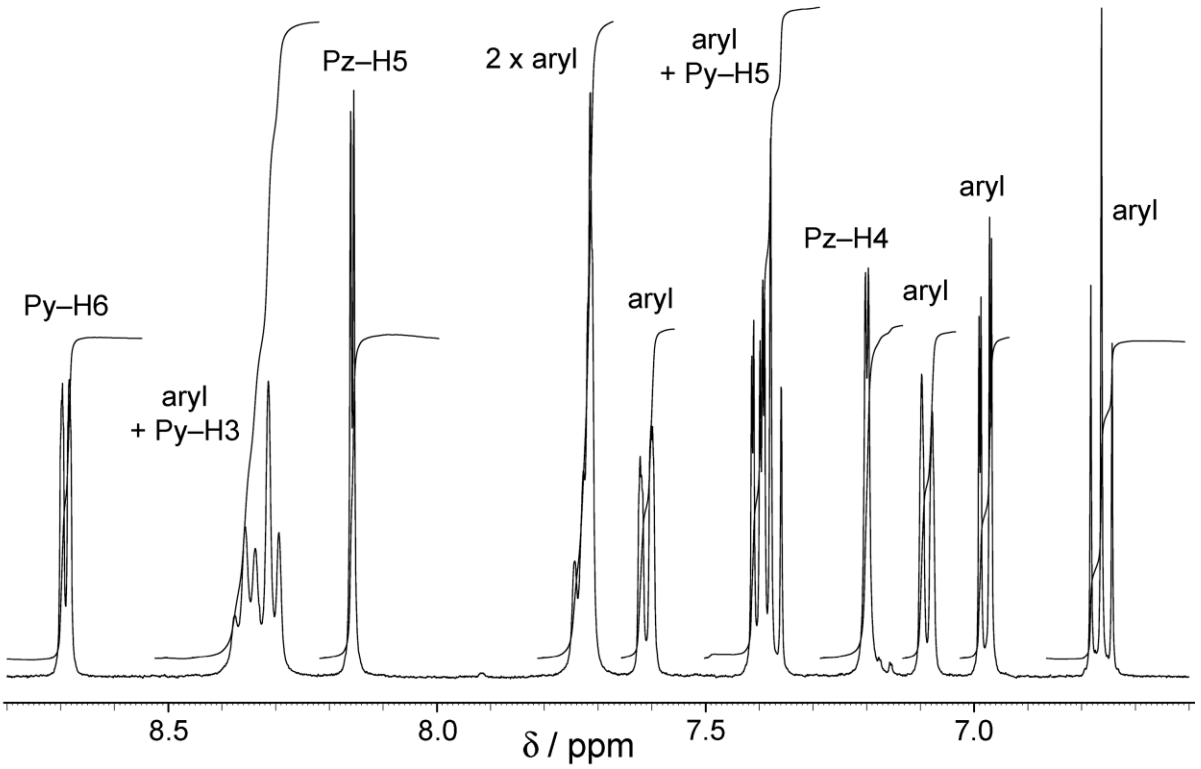

Figure 4.2.4 Part of the ^{1}H NMR (400 MHz, $(CD_3)_2SO$) spectrum of $H_2L^{1,3}$.HBr (Py = pyridyl; Pz = pyrazolyl). Not shown are the NH and OH protons at > 10 ppm and the methylene protons at 5.53 ppm.

The ligand $H_2L^{1,3}$.HBr was recrystallised from methanol/chloroform solution by slow diffusion of diethyl ether vapour. This resulted in the formation of very fine X-ray quality colourless needles, and the crystal structure is shown below (Figure 4.2.5). There is one complete ligand (and one HBr) in the asymmetric unit. The catechol oxygen atoms are arranged *syn* to the amide carbonyl, as this allows the formation of a 6-membered hydrogen-bonded ring with the catechol O-H bonded to the carbonyl oxygen. Raymond and co-workers have reported this effect with their catecholamide ligands.[15] The crystal structure also reveals that the bromide anion forms a variety of close contacts with protonated ligand molecules (numerous H•••Br contacts of ca. 2.9 – 3 Å involving CH and NH bonds), with one interaction being notably shorter than the others: this is an N^{+}–H•••Br^{-} hydrogen bond involving a protonated pyridine ring [N(11)•••Br(1), 3.21 Å; H(11)•••Br(1), 2.41 Å].

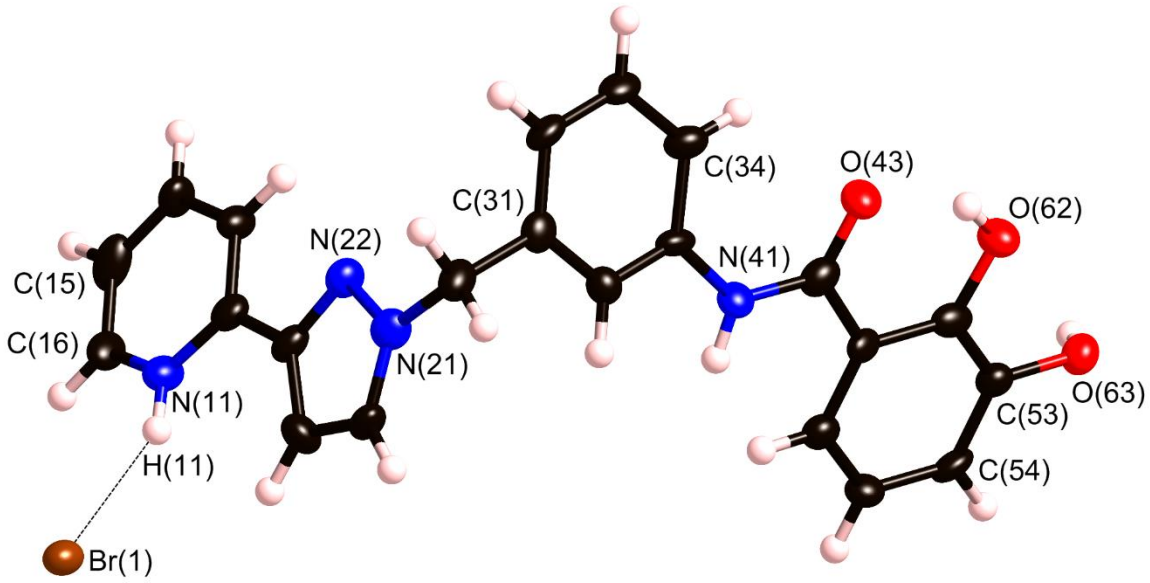

Figure 4.2.5 Molecular structure of $H_2L^{1,3}$·HBr. Non-H atoms are shown with 50% thermal ellipsoids, the hydrogen-bond between the protonated pyridine and the bromide anion is shown with a dotted line.

4.2.2 A tetrameric hetero-octanuclear cyclic helicate

With the synthesis and the characterisation of the ligand complete, the next step was the synthesis of heterometallic complexes. Deprotonated catecholates will provide a relatively hard binding environment, which will bind hard metal ions such as Ti(IV) and Ga(III) with a high affinity. The PyPz unit presents a relatively soft binding environment, and binds strongly to relatively soft metal ions such as transition metal dications. It is hoped that the bis-bidentate ligand will allow both metal ion types to form tris-chelates, such that complexes of the type $[Ti_nM_n(L^{1,3})_{3n}]$ or $[Ga_nM_n(L^{1,3})_{3n}]^{n-}$ will be formed, where M = a soft metal dication. If the hard and soft binding sites exclusively bind to their intended metal partners, then a polynuclear complex can not form with two of the equivalent metal ions connected by the same ligand. Based on these assumptions and the principle of maximum site occupancy,[18] then one might predict a simple dinuclear helicate $[TiML^{1,3}_3]$ or $[GaML^{1,3}_3]^-$, or even an octanuclear cube $[Ti_4M_4L^{1,3}_{12}]$ or $[Ga_4M_4L^{1,3}_{12}]^{4-}$ which might be structurally similar to those seen with PyPz ligands in the Ward group (see Figure 4.2.6).[19] Of course, the actual structure of any complexes

formed will depend not only on the principal metal-ligand interactions described above, but also the more subtle secondary interactions such as π-stacking and hydrogen bonding of ligands.[2] The best way to understand these interactions, one could argue, would be to isolate complexes and then rationalise the structures which are formed, and finally using these rationalisations to successfully design a target complex.

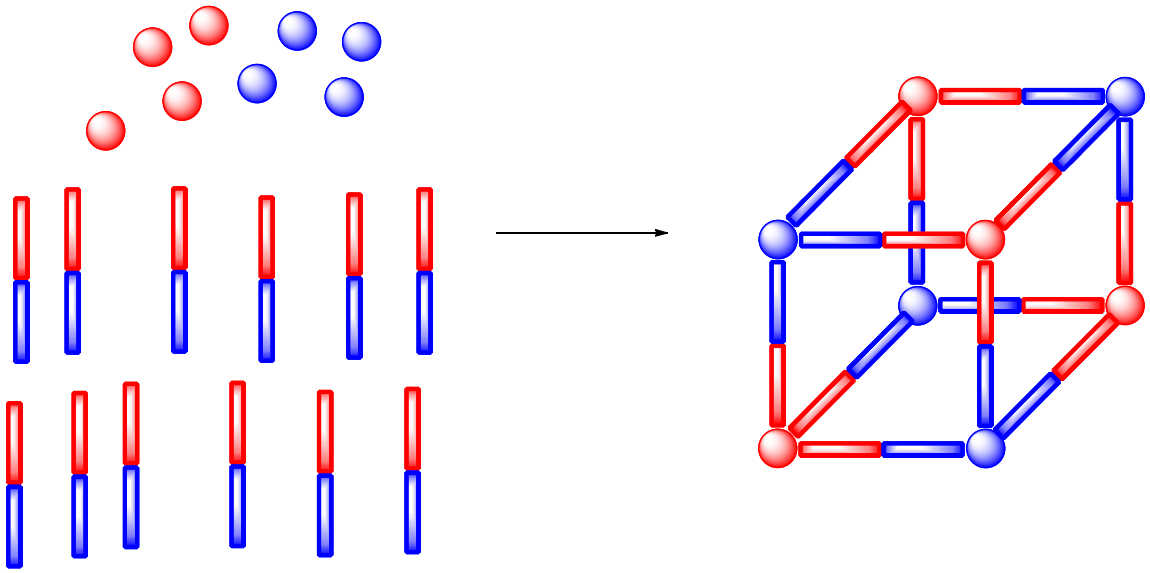

Figure 4.2.6 Predicted self-assembly of the asymmetric ligand $H_2L^{1,3}$ and two different metal ions into an octanuclear cube.

Reactions were set up with $M(BF_4)_2$ salts (where M = Cd, Co, Cu, Ni or Zn), $Ti(OiPr)_4$ and $H_2L^{1,3}$.HBr in a 1 : 1 : 3 mixture stirring in methanol with excess triethylamine at room temperature. In all cases, an orange precipitate formed instantly. These precipitates were collected and washed with methanol and diethyl ether before dissolving in dmf and filtering. Slow diffusion of diethyl ether, THF, diisopropyl ether, acetone or methanol vapour led to, in most instances, a precipitation of a powder. However, with Zn(II) as the soft ion and methanol vapour as the anti-solvent, a crop of x-ray quality orange plate crystals were collected, and the resultant crystal structure is shown below (see Figures 4.2.7 and 4.2.8).

The complex has the formulation $[Ti_4Zn_4(L^{1,3})_8(\mu\text{–}OMe)_8]$•4MeOH•4dmf and has an unusual structure which is a square array of four heterodinuclear $\{TiZnL_2\}^{2+}$ double helicates that are connected head-to-

tail [i.e. Zn(II) terminus to Ti(IV) terminus] by a pair of methoxide bridges. Each double helicate fragment – an edge of the square assembly – has the two bridging ligands oriented in the same direction, such that the Zn(II) ion is coordinated by two pzpy units at one end and the Ti(IV) ion is coordinated by two cat^{2-} units at the other, i.e. the ligands are arranged so as to define 'hard' and 'soft' binding pockets.

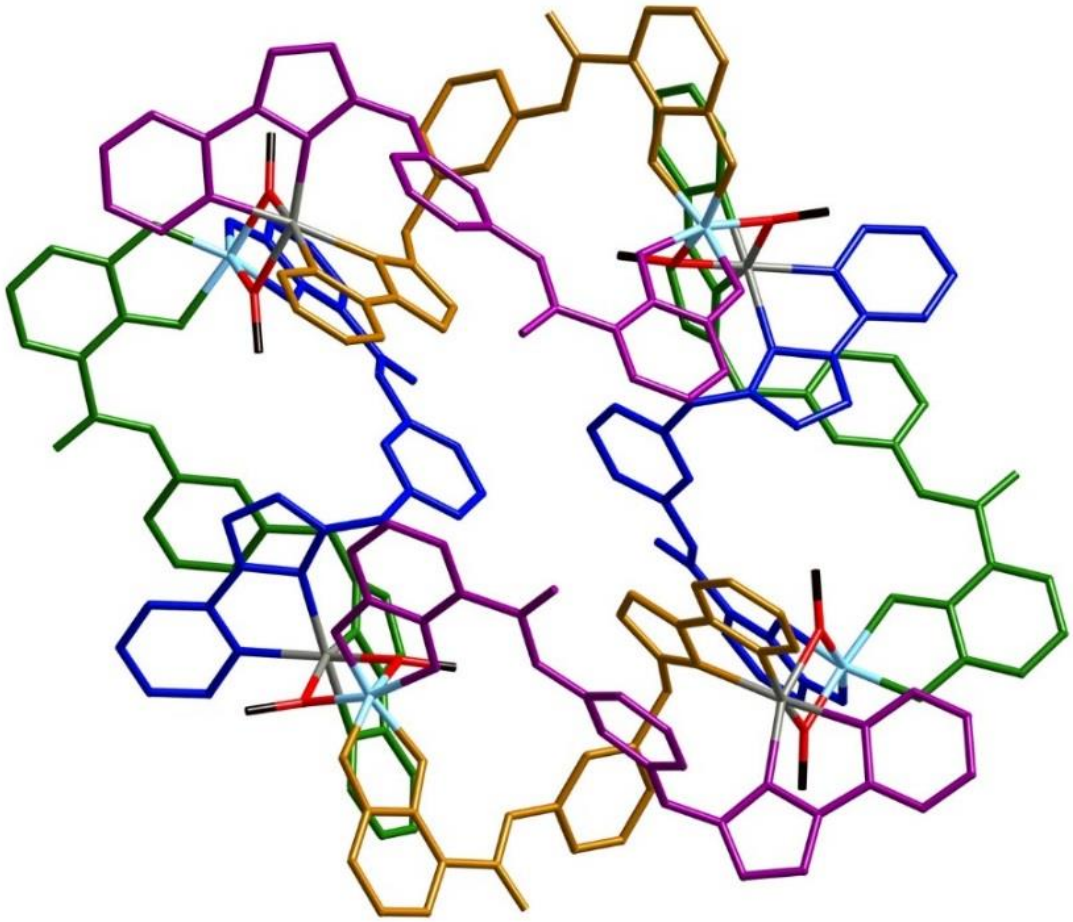

Figure 4.2.7 A view of the complete tetrameric assembly of $[Ti_4Zn_4(L^{1,3})_8(\mu\text{–}OMe)_8]$. The dinuclear double helicate units are shown with the atoms of each ligand coloured green/blue or purple/gold; Zn = grey; Ti = cyan; O = red; C = black.

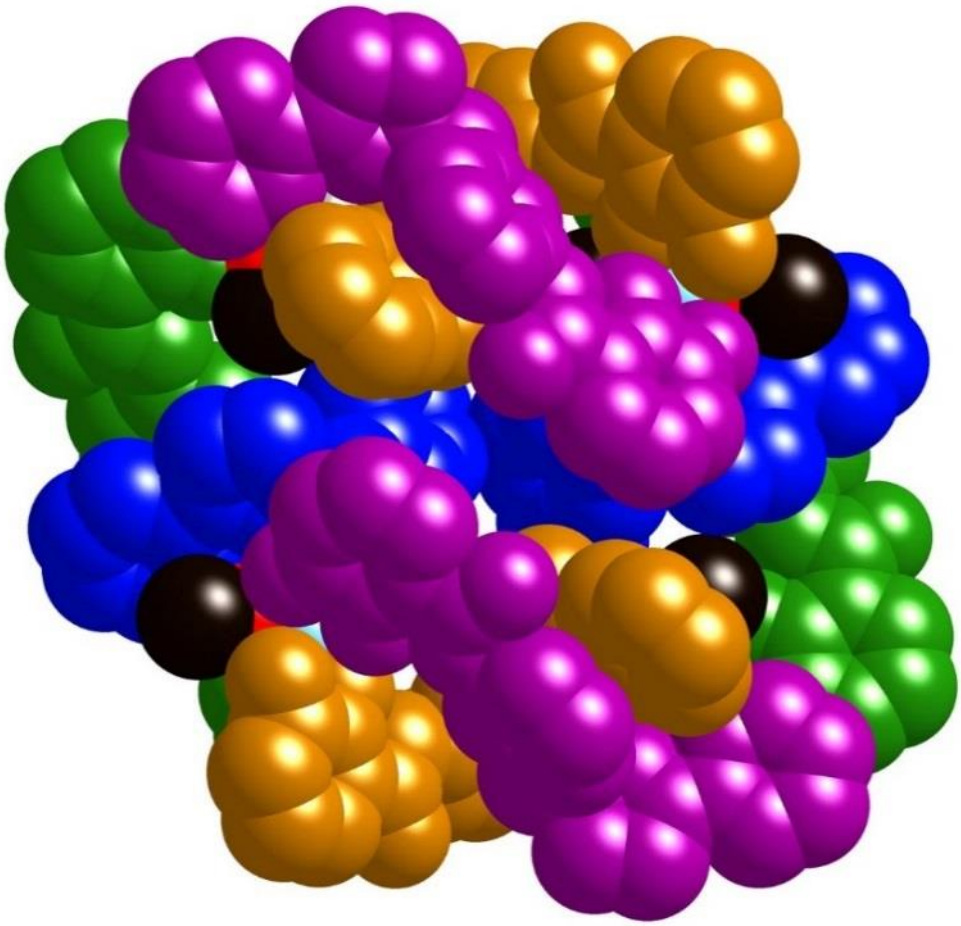

Figure 4.2.8 A space-filling view of the whole complex $[Ti_4Zn_4(L^{1,3})_8(\mu\text{–}OMe)_8]$ with the bridging ligands coloured as in Figure 4.2.7 (the individual dinuclear double helicate components are green/blue or purple/gold).

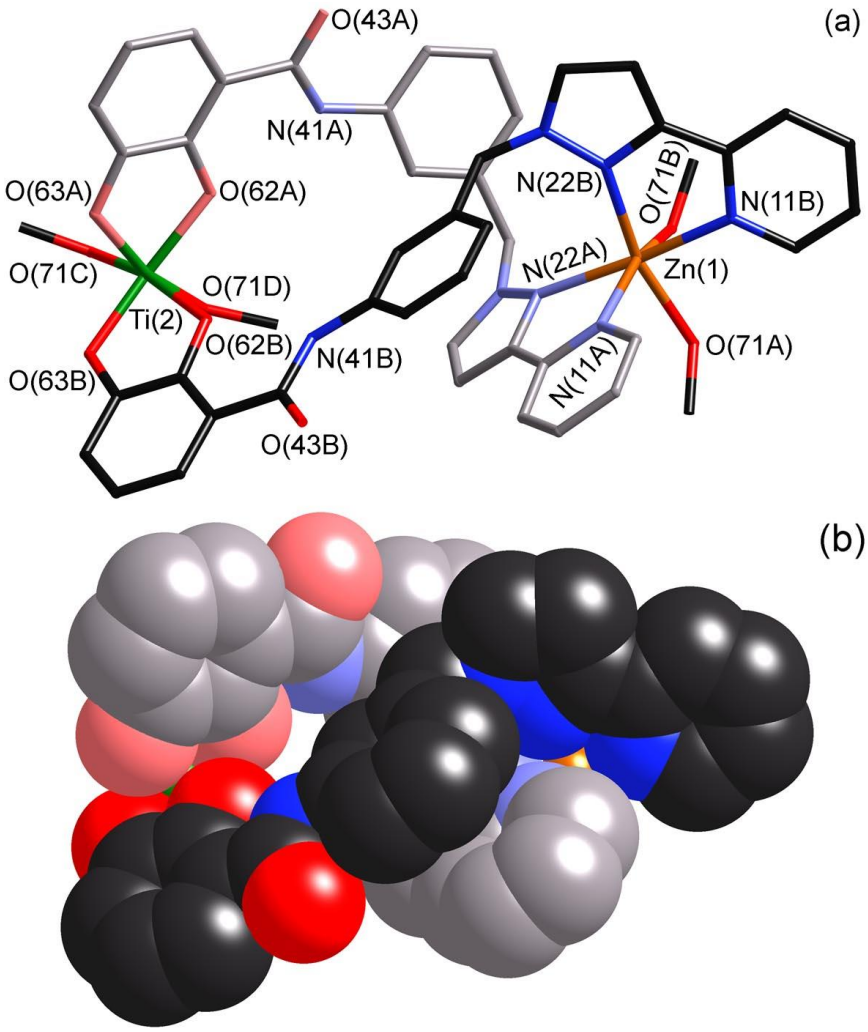

Figure 4.2.9 Two views of one of the four dinuclear double helical subunits that form the edges of tetrameric assembly. (a) A wire-frame view showing the atomic numbering scheme; the methoxide ligands are shown (but not the adjacent atoms to which they bridge). (b) A space-filling view from the same perspective, with one of the ligands shown in paler colours for clarity (methoxide ligands omitted).

There are two crystallographically independent types of double helicate unit, one containing Ti(1)/Zn(2) and the other containing Ti(2)/Zn(1), with Ti•••Zn separations of 9.67 and 9.63 Å respectively; as such the tetrameric $\{TiZn\}_4$ array has crystallographically-imposed twofold symmetry. The Ti(2)/Zn(1) double helicate unit is shown in wire-frame and space-filling modes in Figure 4.2.9, and thermal ellipsoid plots of both double helicates are shown in Figure 4.2.10. Weak interactions between ligands (π-π and CH•••π) within each double helicate subunit are evident; for example Figure 4.2.9a illustrates

a π-stacking interaction between a phenyl spacer of one ligand and a coordinated pyrazolyl-pyridine unit of the other.

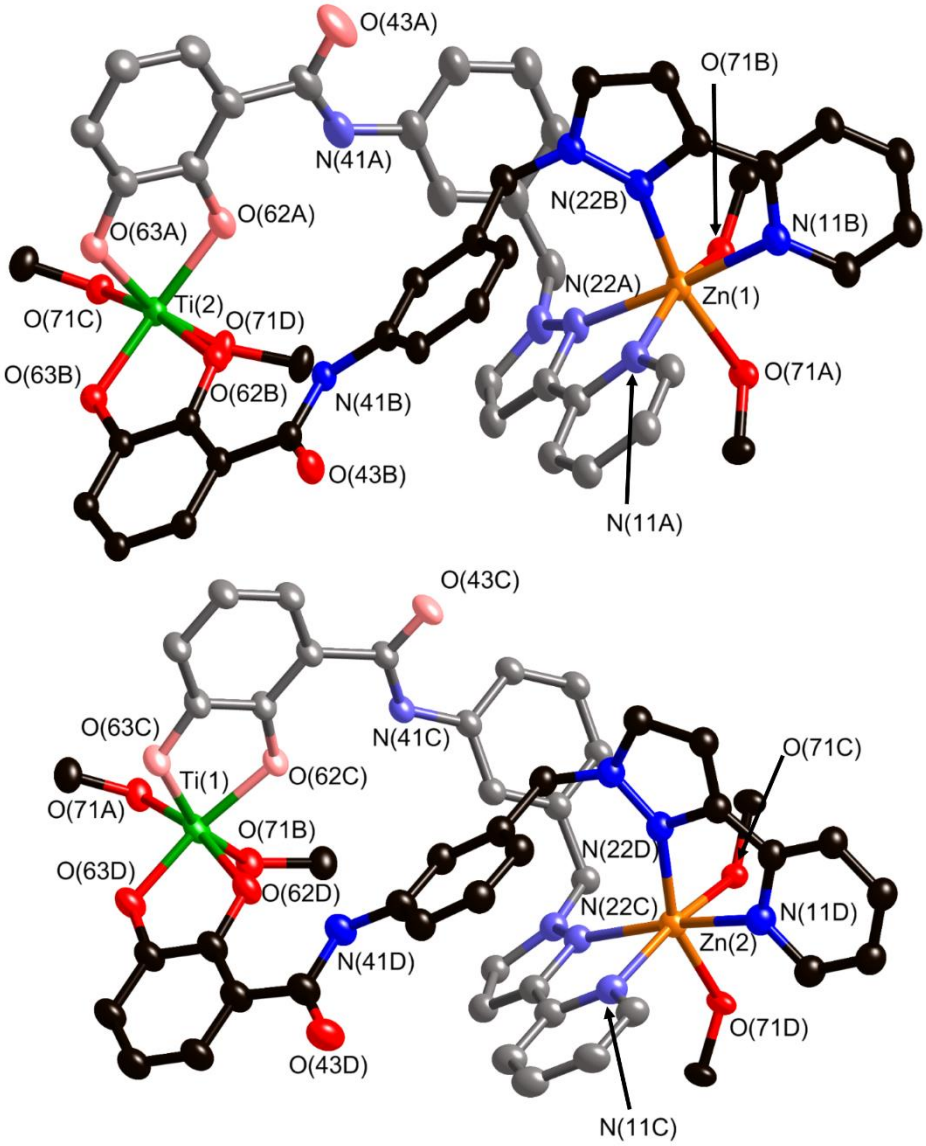

Figure 4.2.10 Thermal ellipsoid plots of the two crystallographically independent dinuclear double helical subunits shown at 30% probability.

All four dinuclear double helicate units have the same sense of twist within the assembly, *i.e.* the whole tetrameric assembly is homochiral. A pair of bridging methoxide ions connecting each helicate to the next in the cyclic tetramer means that each Zn(II) ion has an N_4O_2 donor set and each Ti(IV) ion has an O_6 donor set. The Zn(1)•••Ti(1) and Zn(2)•••Ti(2) separations across the methoxide bridges in the $ZnTi(\mu\text{–}OMe)_2$ units are 3.18 and 3.20 Å respectively. Individual bond lengths and angles around the

approximately octahedral metal ions are unremarkable. Figure 4.2.7 shows the entire complex, with the two Zn(1)/Ti(2) double helicates (approximately vertical in the figure) shown with blue and green bridging ligands, and the two Zn(2)/Ti(1) double helicates (approximately horizontal in the figure) shown with purple and gold ligands. A space filling view showing both 'front' and 'back' faces of the assembly is in Figure 4.2.8, and Figure 4.2.11 shows just the octanuclear metal skeleton and the methoxide bridges that hold the four double helicates together.

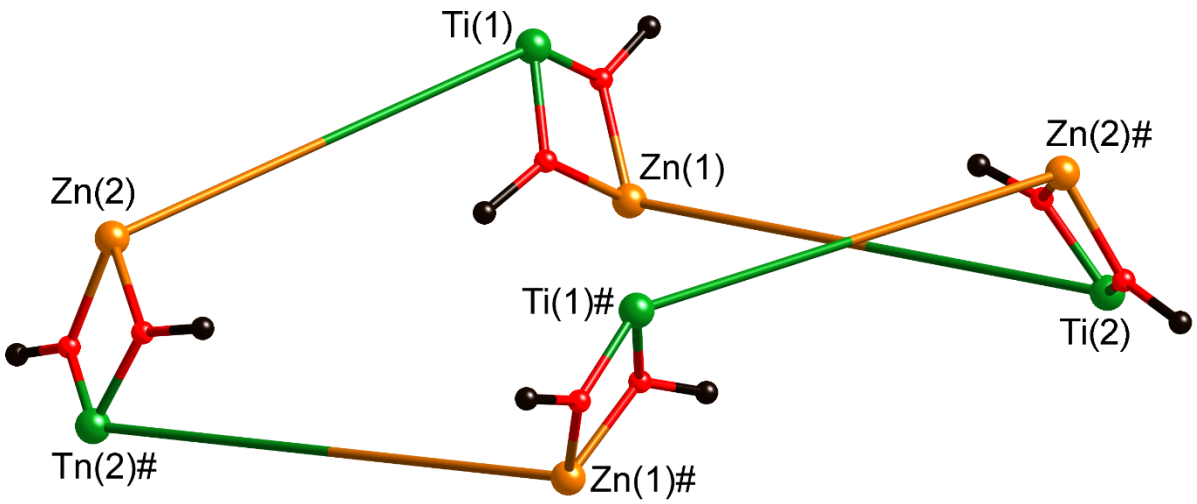

Figure 4.2.11 A view of the complex $[Ti_4Zn_4L^{1,3}{}_8(\mu\text{-}OMe)_8]$ showing only the eight metal ions and the bridging methoxide ligands which connect each Ti/Zn double helicate (a long 'edge' in this view) into a cyclic tetramer (C = black, O = red). Atoms labeled '#' are at equivalent position (–x, y, 0.5–z).

Once formed, the crystals are highly insoluble and can only be redissolved in a strongly competitive solvent like dmso; ES mass spectra on the resultant solutions showed, unsurprisingly, only fragments with no evidence for the intact complex under those conditions. Unfortunately, no further crystals of x-ray quality have been grown from the reactions with other transition metal ions, and the poor solubility of the products formed precludes their solution studies. Only one of the reactions provided any evidence of a heterometallic array persisting in solution to some extent (see Figure 4.2.12). The reaction mixture of $H_2L^{1,3}$, $Ti(O^iPr)_4$ and $Co(BF_4)_2$ displayed a peak for $\{[CoTi(L^{1,3})_3]H\}^+$ at *m/z* 1260 in the ES positive ionisation mode mass spectrum, as confirmed by overlays with the theoretical isotope pattern (see Figure 4.2.13).

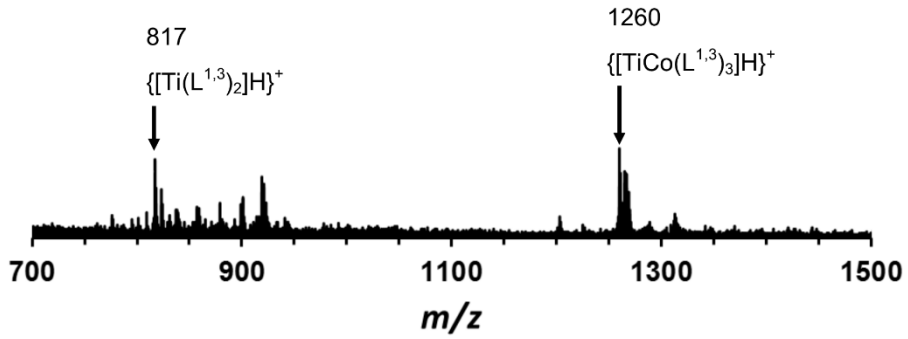

Figure 5.2.12 Electrospray mass spectrum (positive) of $[CoTi(L^{1,3})_3]$.

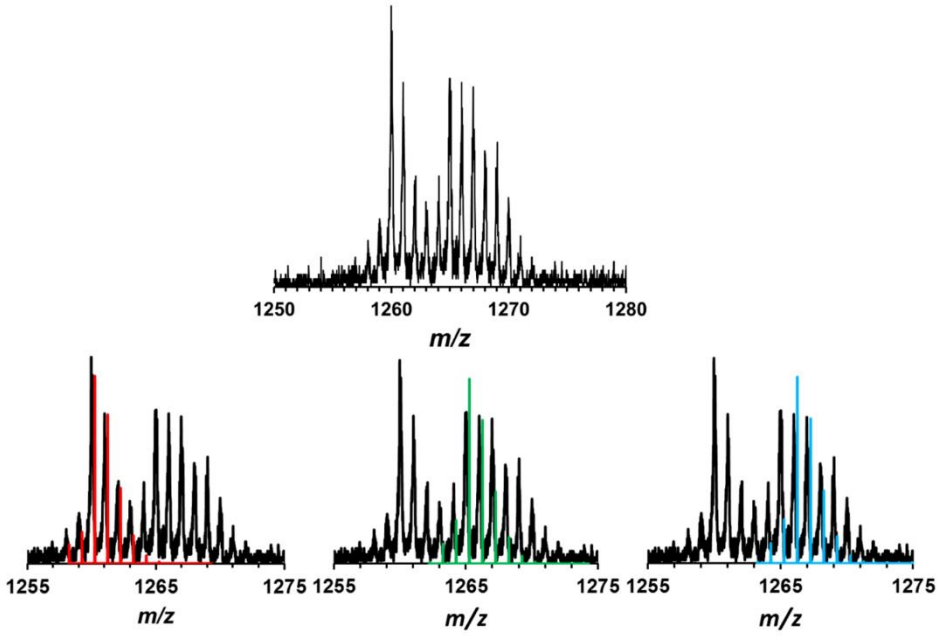

Figure 5.2.13 Top: Electrospray mass spectrum (positive) expansion of $[CoTi(L^{1,3})_3]$. Bottom: Theoretical isotope patterns overlaid; (red) $\{[Co^{II}Ti(L^{1,3})_3]H\}^+$; (green) $\{[Co^{III}Ti(L^{1,3})_3]Li\ -H\}^+$; (blue) $\{[Co^{II}Ti(L^{1,3})_3]Li\}^+$.

Cyclic helicate structures in general are now well known[20-26] but the above example is unprecedented for two reasons. Firstly, a one-pot self-assembly reaction results in formation of a cyclic heteronuclear array in which Zn(II) and Ti(IV) ions alternate around the circumference due to the presence of two quite different binding sites in the non-symmetrical ligand; this contrasts with the usual situation in cyclic helicates in which all metal ions are the same. Whilst the author is not aware of any other heterometallic cyclic helicates, it is noted that Rice *et al.* recently reported a three-component cyclic helicates from a single reaction which contains Cu(II) ions and two types of bridging ligand.[27] In addition, this cyclic structure is unusual in being formed from four distinct dinuclear double helicates

connected by methoxide bridges, rather than the more usual type of structure in which ditopic or tritopic bridging ligands overlap in a continuous sequence around the periphery of the complex.[20-26] Using the same methodology as employed for $H_2L^{1,3}$ we can readily synthesise a wide range of heterotopic catecholate / pyrazolyl-pyridine bridging ligands as a basis for self-assembled heterometallic arrays.

4.2.3 Analogous ligand and complex syntheses

Analogous syntheses were designed for the 1,2- and 1,4-substituted isomers of $H_2L^{1,3}$. The synthesis of the ligand $H_2L^{1,2}$ was attempted first, but this proved more problematic than the original synthesis of $H_2L^{1,3}$ (see Figure 4.2.14). The product of the bromination step **8** was found to degrade rapidly, and the PyPz substitution step introduced an entirely new problem. Instead of cleanly converting the alkyl bromide **8** to the desired product **9**, ^{1}H NMR spectroscopy revealed the presence of two products in a 1 : 1 ratio, with identical molecular weights, as determined by the HPLC trace of the ESMS spectrum. It was assumed that the products were stereoisomers of each other, with the pyrazole ring substituted on different nitrogen atoms (see Figure 4.2.15). The two products had very similar R_f values, but elution with ethyl acetate/ dichloromethane (4 : 1) on silica allowed their separation, and their resultant ^{1}H NMR spectra helped confirm the identity of each component.

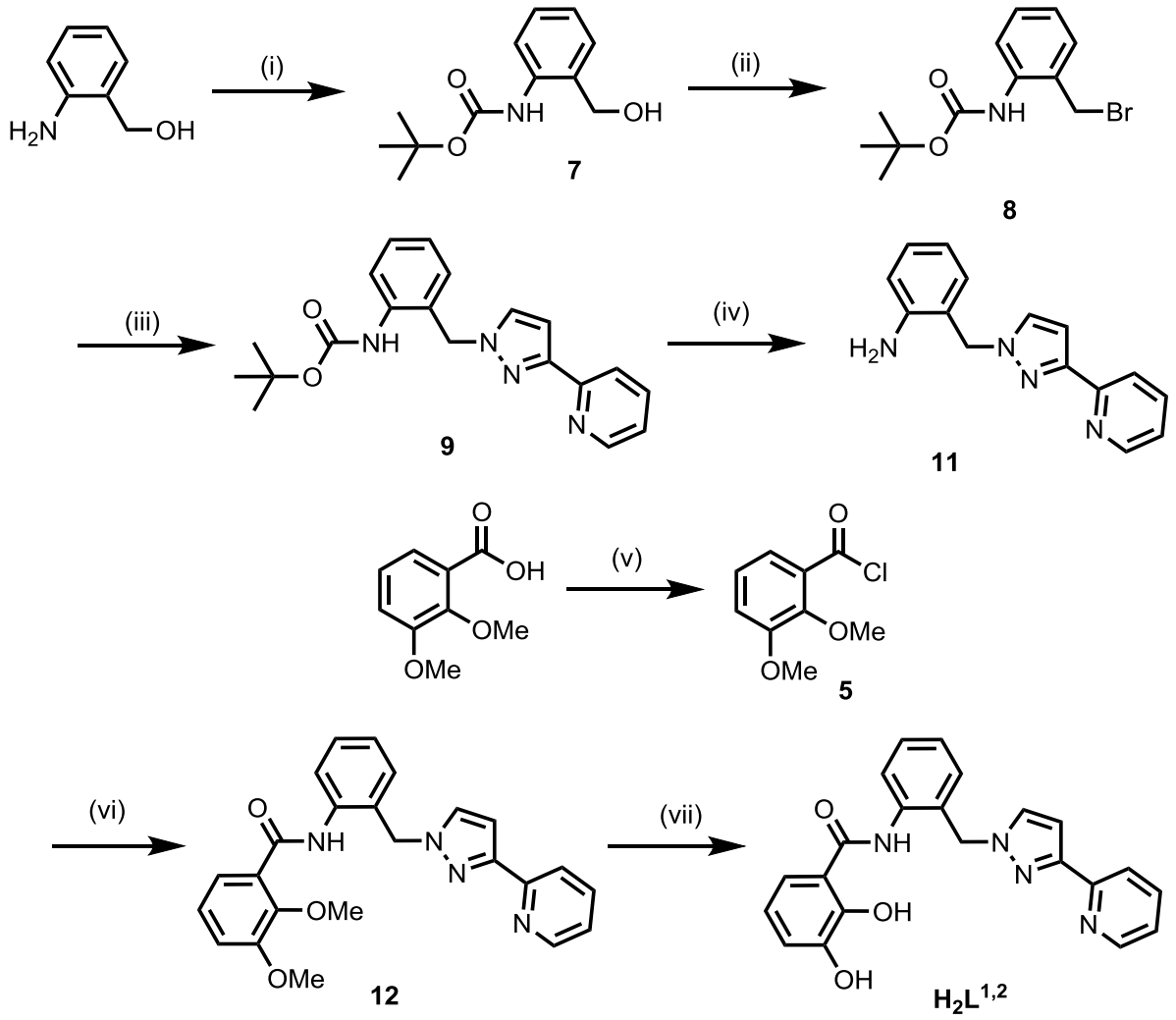

Figure 4.2.14 Reaction scheme for the preparation of $H_2L^{1,2}$. (i) Boc_2O, THF; (ii) CBr_4, PPh_3, DCM; (iii) PyPzH, THF, $NaOH_{(aq)}$; (iv) TFA, DCM; (v) $SOCl_2$, dmf; (vi) **5**, DCM, Et_3N; (vii) BBr_3, DCM, H_2O.

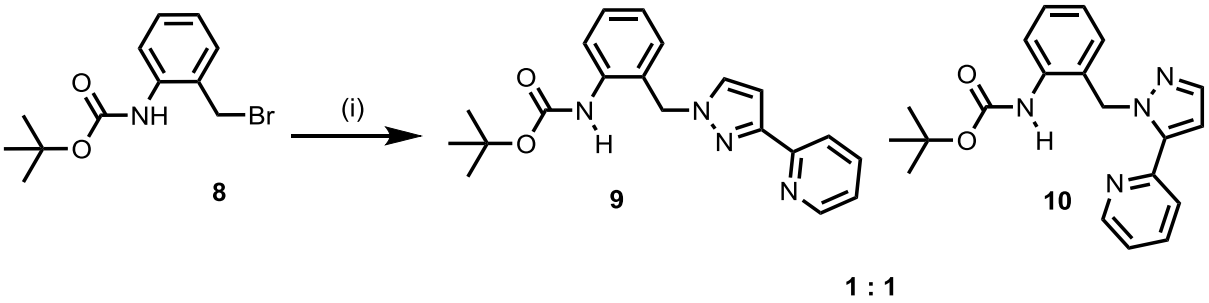

Figure 4.2.15 Nucleophilic substitution of bromide with PyPz leads to two stereoisomers in an approximately 1 : 1 ratio. (i) PyPzH, THF, $NaOH_{(aq)}$.

All ligands containing 1-alkyl substituted 3-(2-pyridyl)pyrazole show two distinctive sharp doublets for the pyrazole protons, and in most cases the two peaks are separated by approximately 0.5 ppm in $CDCl_3$. The first of the two fractions has a separation of approximately 1.0 ppm, and the second fraction approximately 0.5 ppm (see Figure 4.2.16). This led us to assign the first fraction as the side product **10**, and the second fraction as the desired compound **9**. After the subsequent Boc deprotection of the compound **9**, the crystal structure of a colourless block of **11**·$\mathbf{H_2O}$ was collected, irrefutably confirming the structure as the intended product (see Figure 4.2.17). The amine crystallised as a monohydrate, and there are numerous H•••O and H•••N hydrogen-bonding interactions of *ca.* 2.0 – 2.1 Å between the water molecule and the pyridyl and aniline groups of the ligand (see Figure 4.2.18). There is also an intramolecular hydrogen bond between the pyrazolyl N(22) and the aniline H(41A) (H•••N 2.2 Å).

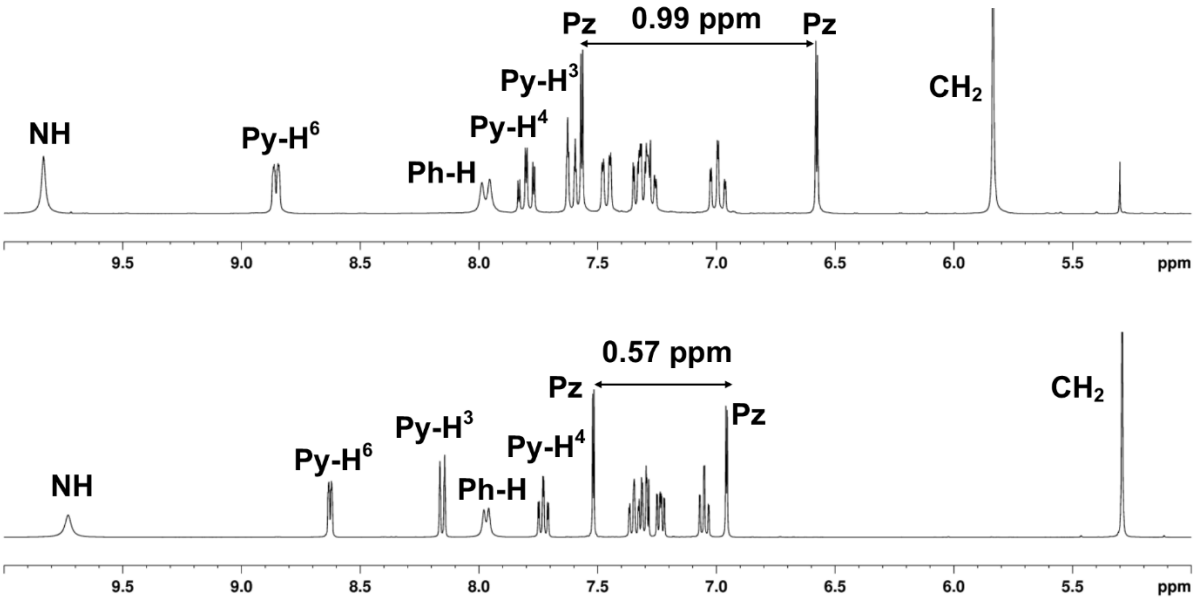

Figure 4.2.16 Partially assigned ^{1}H NMR (400 MHz, $CDCl_3$) spectra of compounds **10** (top) and **9** (bottom), highlighting the characteristic splitting distance between the protons of di-substituted pyrazole rings (Py = pyridine, Pz = pyrazole, Ph = phenyl).

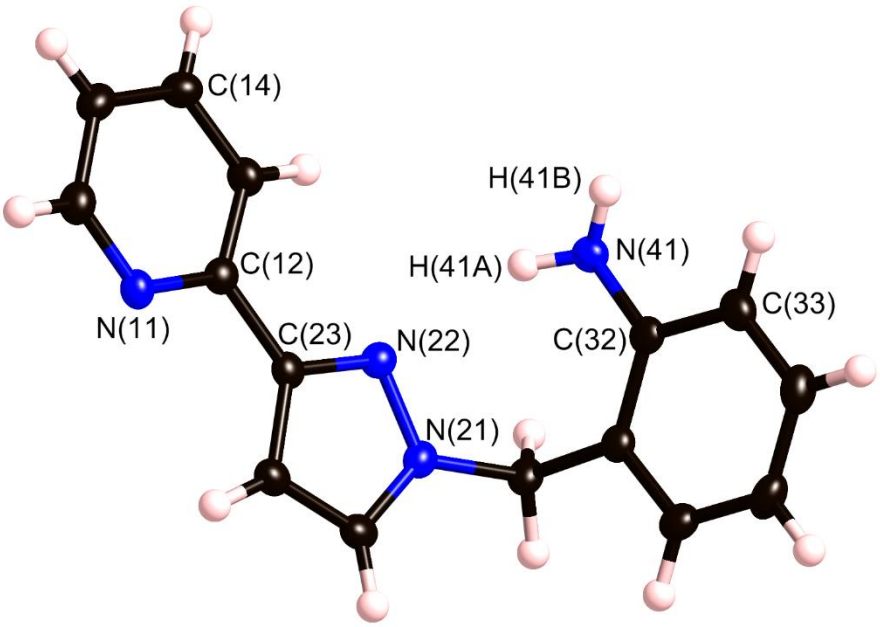

Figure 4.2.17 Thermal ellipsoid of the ligand **11**.H_2O plot with non-hydrogen atoms shown at 50 % probability.

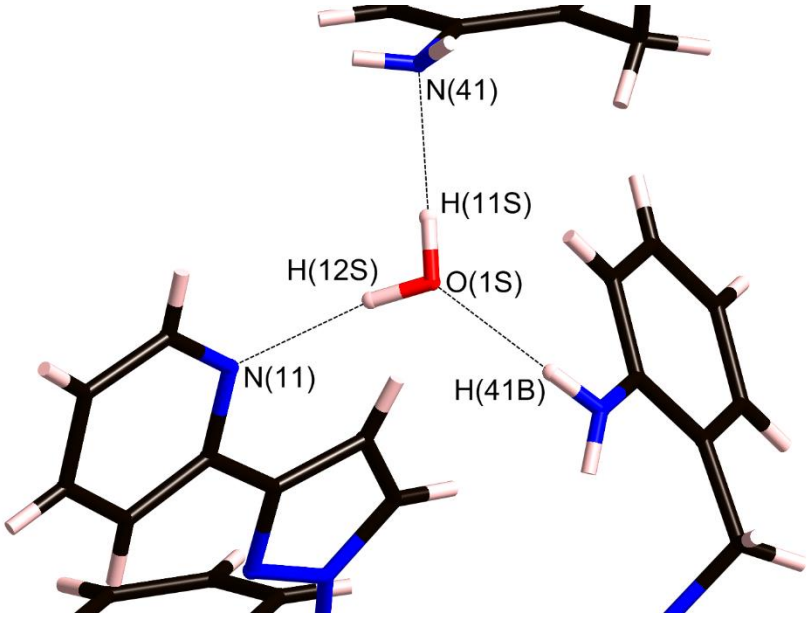

Figure 4.2.18 Hydrogen-bonding interactions in the crystal structure of **11**.H_2O.

Once the correct isomer of the deprotected amine had been isolated, the synthesis of the methoxy-protected ligand **12** was completed by the same amide condensation method as described above, although the ^{1}H NMR spectrum could not be fully assigned due to its convoluted aromatic region (see Figure 4.2.19). The final step in the synthesis of $H_2L^{1,2}$ posed yet another problem. Upon using identical

conditions to those described above, the crude product isolated from the reaction mixture was not the pure demethylated $H_2L^{1,2}$ as expected, but a mixture of the desired ligand and a mono-deprotected $HMeL^{1,2}$ (see Figure 4.2.20) in an approximate ratio of 0.7 : 1.0 (by ^{1}H NMR integration of equivalent protons, see Figure 4.2.21). Separation of these products by column chromatography proved surprisingly difficult, with incomplete separation achieved. It was decided at this point that due to the numerous synthetic difficulties associated with this synthesis that a different ligand should be targeted which may prove to be easier to isolate on an acceptable scale.

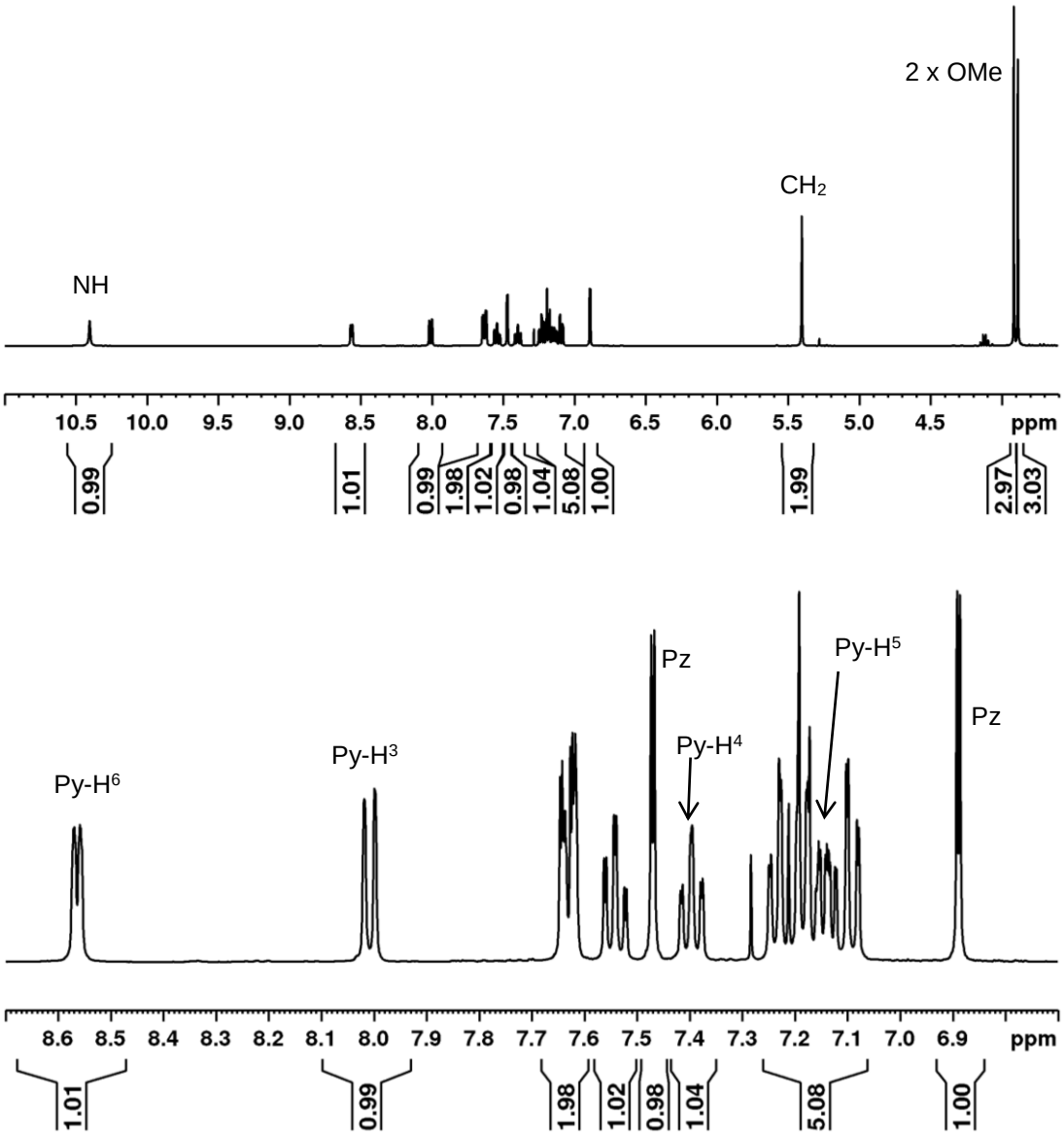

Figure 4.2.19 Top: Full ^{1}H NMR spectrum (400 MHz, $CDCl_3$) of **12**; Bottom: Expansion in the aromatic region with partial assignment.

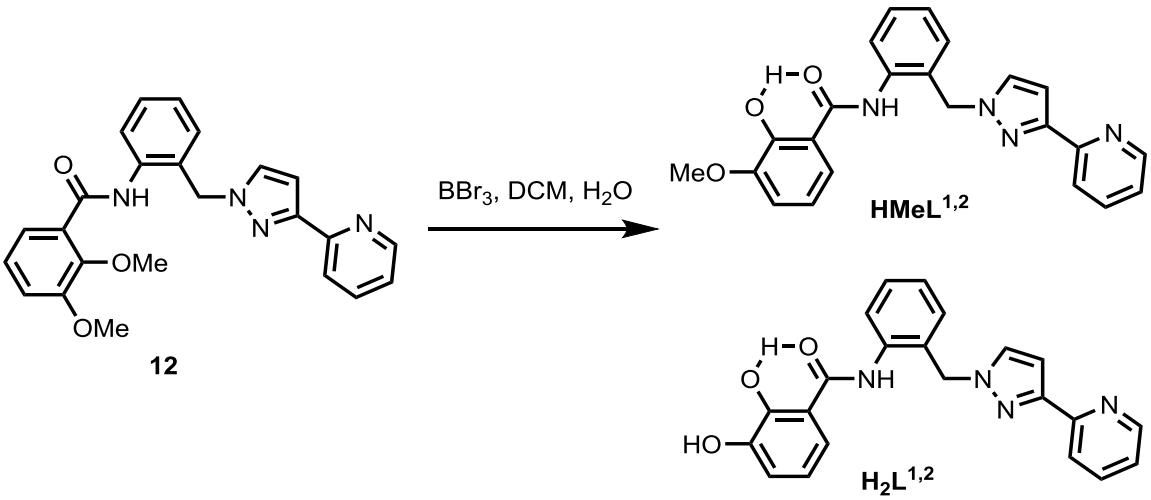

Figure 4.2.20 The two products arising from the incomplete demethylation of compound **12**.

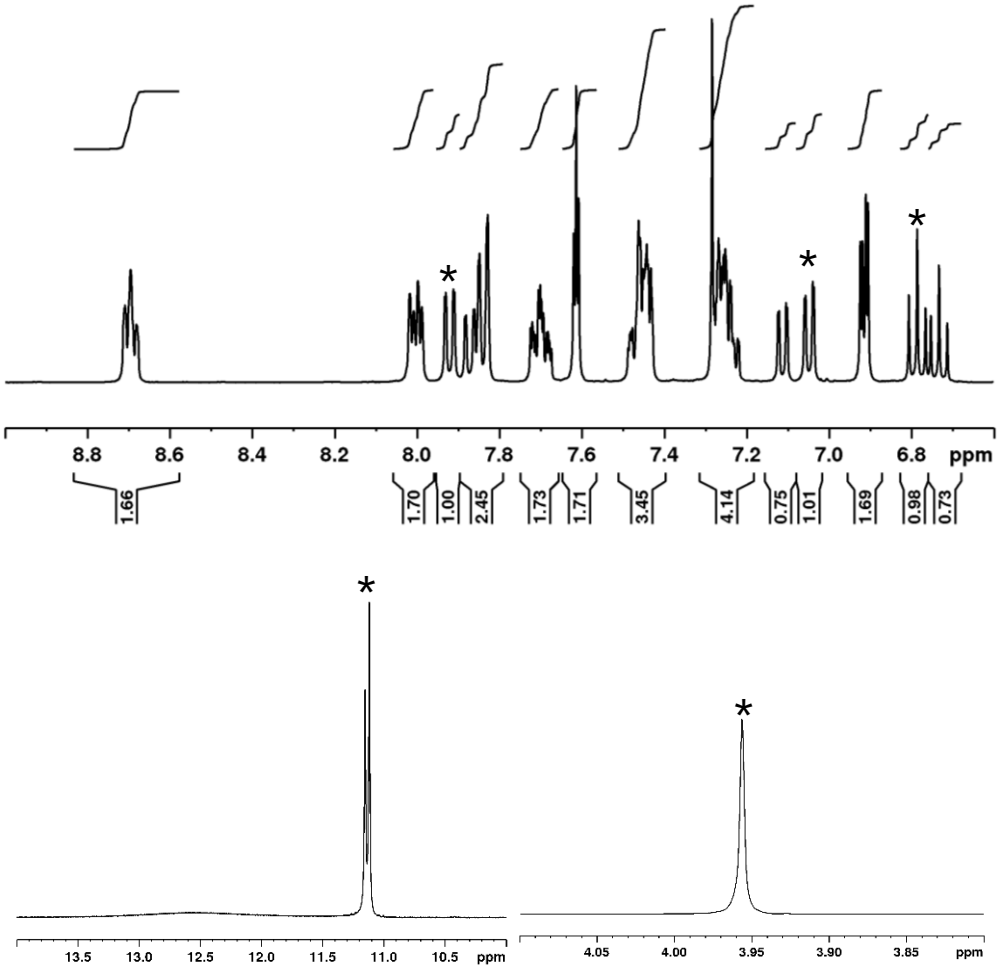

Figure 4.2.21 Top: Partial ^{1}H NMR spectrum (400 MHz, $CDCl_3$) of $HMeL^{1,2}$ and $H_2L^{1,2}$ (peaks that can be assigned as $HMeL^{1,2}$ are marked with *). Bottom: (Left) Expansion in the downfield region (note the broad singlet at 12.5 ppm for O-H•••O); (Right) Single methoxide peak attributable to $HMeL^{1,2}$.

The analogous synthesis of $H_2L^{1,4}$ was therefore undertaken (see Figure 4.2.22), and it was hoped that the distance between the two arms of the ligand would prevent problems in the alkylation step which may have been caused by amide NH group directing the undesired reaction. Protection of the aniline with Boc is routine,[28] but it was again found that the bromination step in this synthesis is problematic, with the alkyl bromide **14** appearing to degrade rapidly, making the next step difficult. However, the PyPz substitution, Boc deprotection and amide condensation reactions were all performed successfully affording the methoxy protected ligand **17** as a yellow oil. This was recrystallised from DCM and diethyl ether, providing colourless needle crystals of x-ray quality. Despite the temperature failing during collection, the crystal structure could be solved by integrating all the runs performed at room temperature, revealing the structure of the ligand (see Figure 4.2.23). As expected, the catechol methoxy groups are arranged in an *anti* fashion to the amide carbonyl, in contrast to the *syn* fashion displayed by the deprotected ligand $H_2L^{1,3}$.[15]

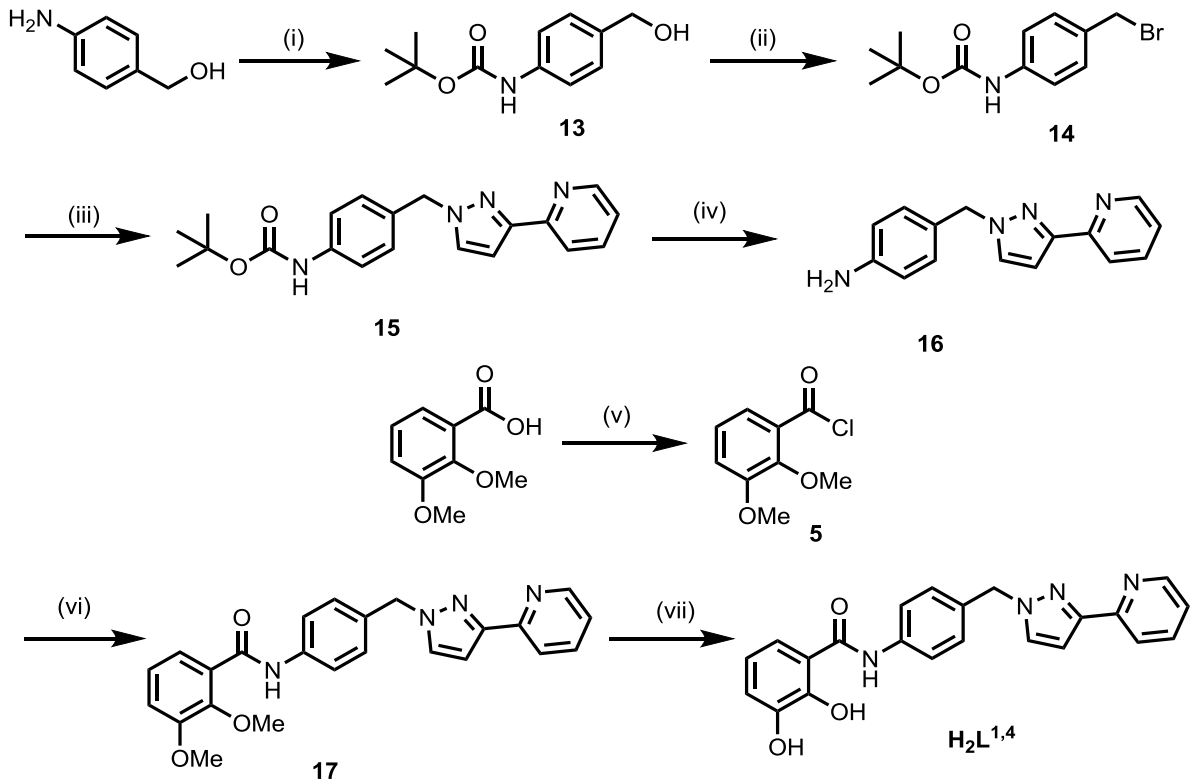

Figure 4.2.22 Reaction scheme for the preparation of $H_2L^{1,4}$. (i) Boc_2O, THF; (ii) CBr_4, PPh_3, DCM; (iii) PyPzH, THF, $NaOH_{(aq)}$; (iv) TFA, DCM; (v) $SOCl_2$, DMF; (vi) **5**, DCM, Et_3N; (vii) BBr_3, DCM, H_2O.

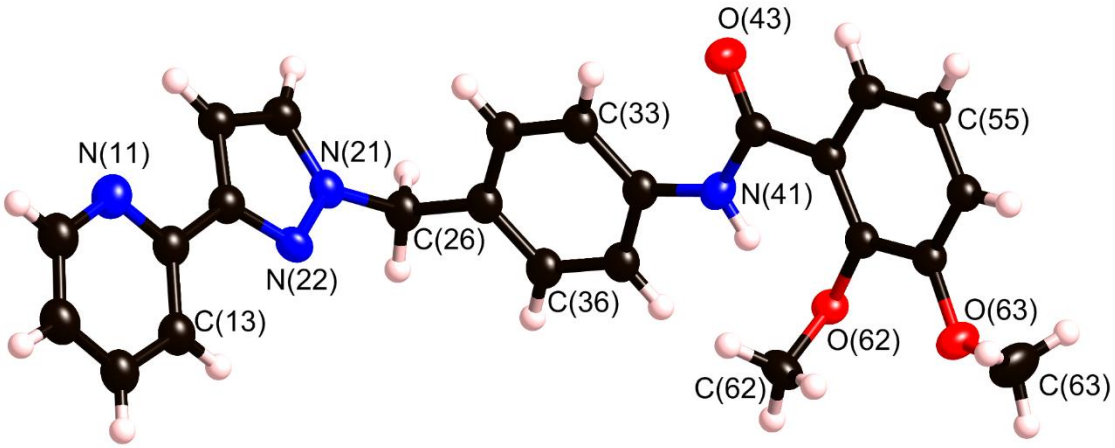

Figure 4.2.23 Thermal ellipsoid plot of the ligand **17** with non-hydrogen atoms shown at 30 % probability.

The methoxy-protected ligand **17** was deprotected successfully with BBr_3 in this instance to yield an off white solid after solvolysis in water. The ligand was found to be soluble in methanol with gentle heating, and consequently the ^{1}H NMR spectrum in deuterated methanol was obtained, with all acidic proton environments absent due to fast exchange with the solvent (see Figure 4.2.24).

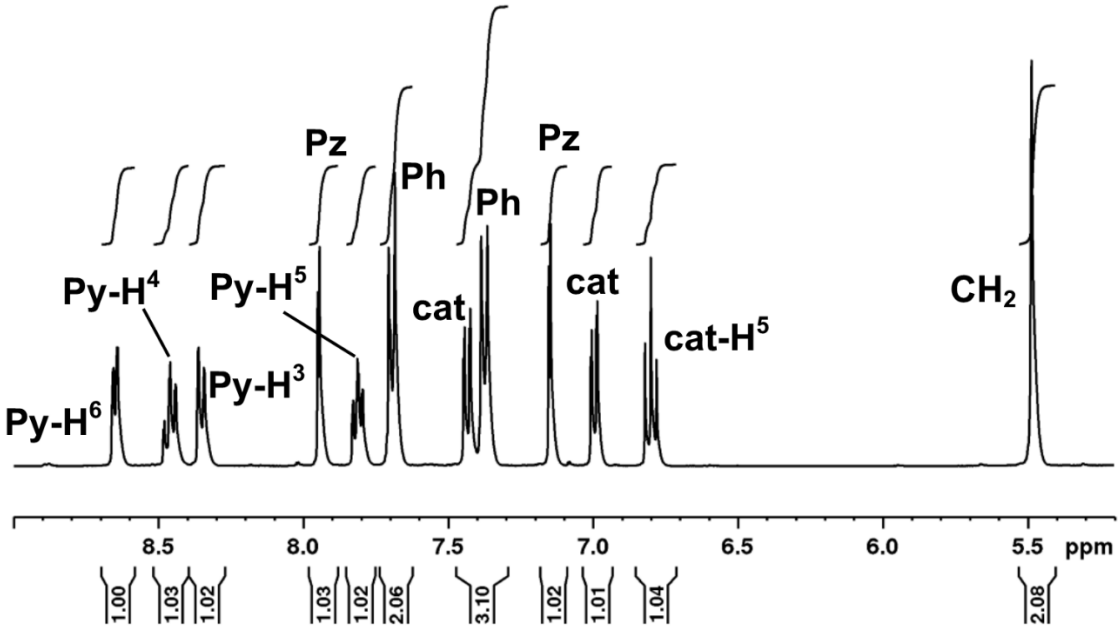

Figure 4.2.24 Fully assigned ^{1}H NMR (400 MHz, MeOD) spectrum of $H_2L^{1,4}$.HBr (Py = pyridine, Pz = pyrazole, Ph = phenyl, cat = catechol).

Complexation reactions were performed in the same way as described above, with a mixture of the ligand $H_2L^{1,4}$, $M(BF_4)_2$ (where M = Cd, Ni and Zn) and $Ti(OiPr)_4$ (3 : 1 : 1) stirred in methanol with excess triethylamine at room temperature. Peaks were observed in the electrospray negative ionisation mode mass spectra in all cases which correspond to $[Ti(L^{1,4})_3]^{2-}$ (*m/z* 600) and $[TiH(L^{1,4}{}_3]^-$ (*m/z* 1201) (see Figure 4.2.25 for an example when M = Zn), but no peaks are observed which can be unequivocally assigned to a heteronuclear complex. Interestingly, there are a series of intense peaks for titanium(IV) complexes with abstracted fluoride, as confirmed by theoretical isotopic distribution overlays with the mass spectra expansions (see Figure 4.2.26). This is presumably due to the decomposition of the tetrafluoroborate counterions used, and is a known phenomenom when these metal salts are used.[16, 19] No complex peaks were observed in the electrospray positive ionisation mode mass spectra.

Unfortunately, despite numerous attempts, no crystals could be obtained of any structures incorporating this ligand, and any products which were obtained were extremely insoluble in all solvents apart from dmf, as was the case with complexes of the ligand $H_2L^{1,3}$.

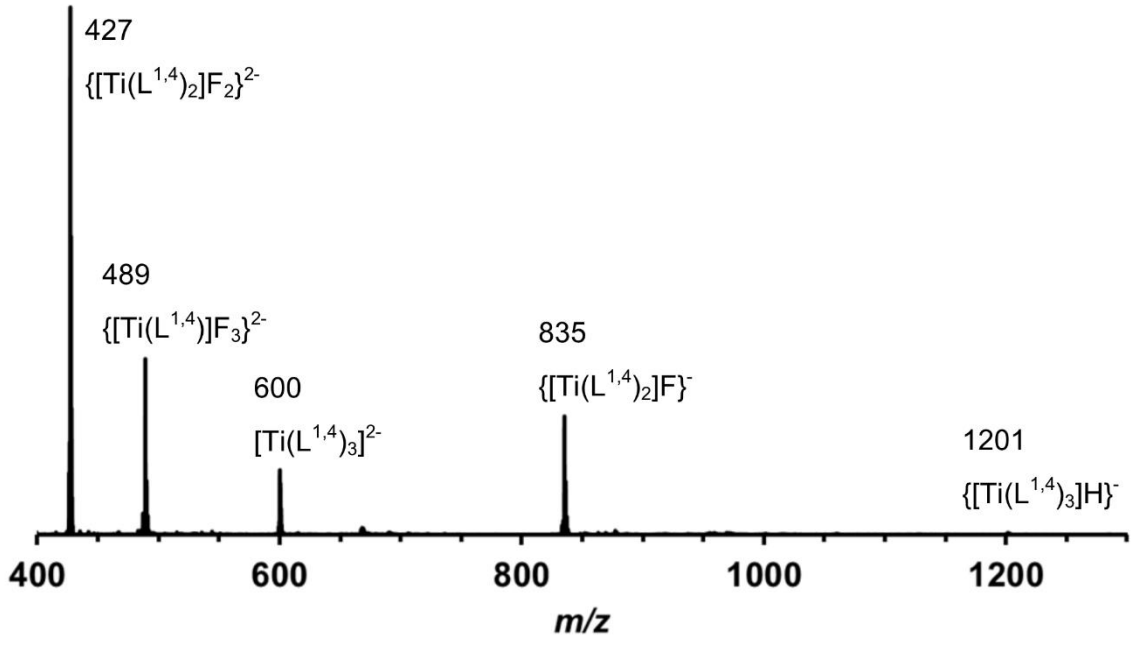

Figure 4.2.25 Electrospray mass spectrum (negative) of the reaction mixture of Ti(IV), Zn(II) and $H_2L^{1,4}$.

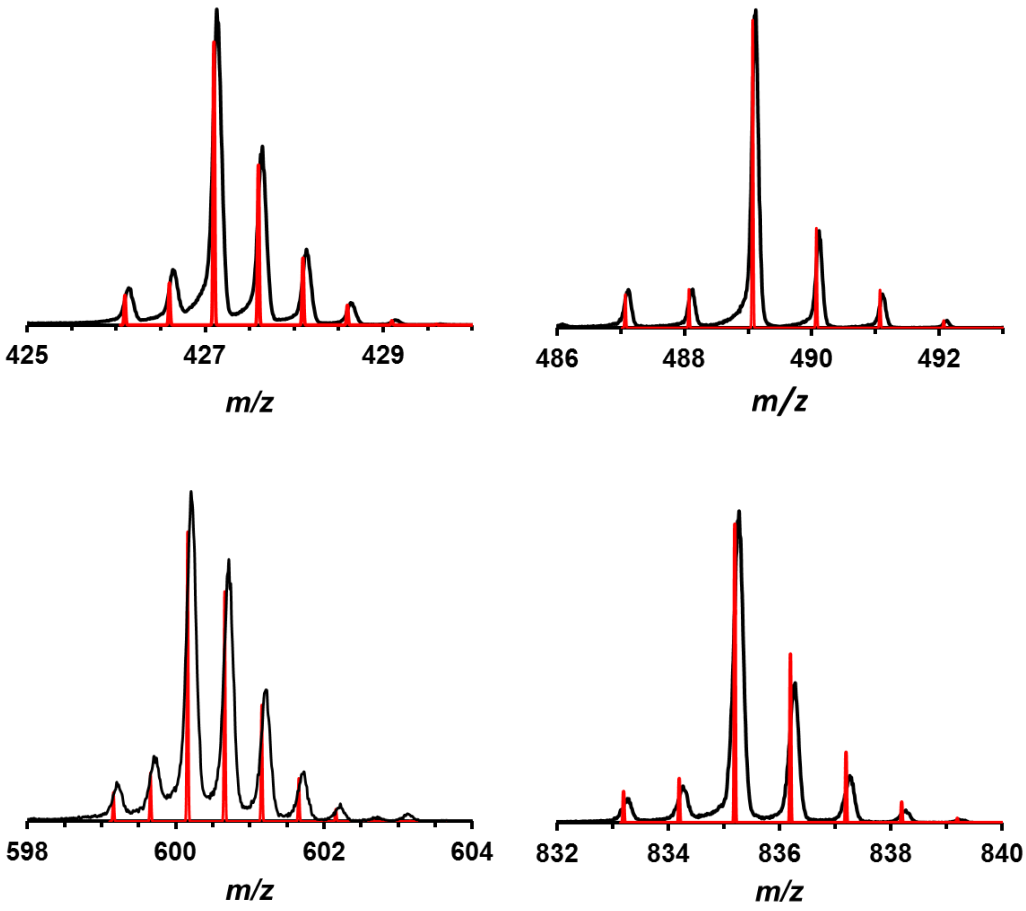

Figure 4.2.26 Theoretical isotopic distribution (red) and experimental mass spectra (black) for $\{[Ti(L^{1,4})_2]F_2\}^{2-}$ (top left), $\{[Ti(L^{1,4})_2]F_3\}^{2-}$ (top right), $\{[Ti(L^{1,4})_3]\}^{2-}$ (bottom left) and $\{[Ti(L^{1,4})_2]F\}^{2-}$ (bottom right).

4.3 Conclusion

A potentially general synthetic route for a family of asymmetric ligands based on bromomethyl-substitued aniline starting materials has been developed; two examples have been demonstrated based on a *meta*- and *para*- substituted phenyl ring, and a third example based on the *ortho*- ring was partially successful. A heterometallic square of double helicates has been synthesised with the *meta*- substituted ligand $H_2L^{1,3}$ based on the orthogonality of the catecholamide and pyrazolyl-pyridine binding sites, acting as proof-of-principle for this work. The poor solubility of the complexes formed precluded detailed NMR and mass spectral studies; future designs of these complexes would need to improve their solubility to enable any useful function.

4.4 Experimental

4.4.1 Ligand synthesis

3-(2-pyridyl)pyrazole was used as prepared.[29] Dry dichloromethane was obtained by distillation over calcium hydride.

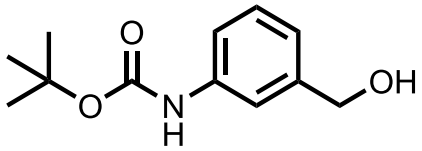

Synthesis of 1

A mixture of 3-(hydroxymethy1)aniline (7.50 g, 60.90 mmol) and di-*tert*-butyl dicarbonate (13.50 g, 61.86 mmol) was stirred in THF (150 cm^3) at 25 ^oC for 48 h. The resultant brown solution was reduced to dryness before purification of the crude brown oil by purified by column chromatography on silica. Elution with ethyl acetate/ 40:60 petroleum ether (1:2, R_f = 0.36) followed by sonication for 10 minutes in hexane yielded **1** as a white solid (Yield: 13.01 g, 58.27 mmol, 96 %). ^{1}H-NMR (400 MHz, $CDCl_3$): δ 7.48 (1H, s; ArH), 7.32 – 7.23 (2H, m; ArH), 7.08 – 7.06 (1H, m; ArH), 6.52 (1H, bs; NH), 4.69 (2H, s; CH_2), 1.75 (1H, s; OH), 1.54 (9H, s; ^{t}Bu). ESMS: *m/z* 262 $[M + K]^+$, 246 $[M + Na]^+$, 150 $[M - {}^-O^tBu]^+$; Found: C, 64.60; H, 7.67; N, 6.17 %. Required for $C_{12}H_{17}NO_3$: C, 64.55; H, 7.67; N, 6.27 %. Data is in accordance with the literature.[17]

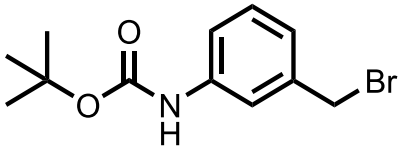

Synthesis of 2

A solution of **1** (3.22 g, 14.42 mmol) in DCM (70 cm^3) was maintained at 0 ^oC with stirring. To this was added PPh_3 (6.10 g, 23.26 mmol) and CBr_4 (7.94 g, 23.94 mmol) sequentially, and the resultant yellow solution was stirred at 0 ^oC for 1.5 h. The reaction mixture was then diluted with EtOAc and

stirred for a further 0.5 h, before washing with brine. The organic layer was extracted with EtOAc, dried over $MgSO_4$ and concentrated before purification by column chromatography on silica. Elution with ethyl acetate/ 40:60 petroleum ether (1:12, R_f = 0.55) yielded **2** as a white solid (Yield: 2.95 g, 10.31 mmol, 67 %). ^{1}H-NMR (400 MHz, $CDCl_3$): δ 7.54 (1H, s; ArH), 7.31 – 7.21 (2H, m; ArH), 7.10 – 7.07 (1H, m; ArH), 6.52 (1H, bs; NH), 4.48 (2H, s; CH_2), 1.55 (9H, s; ^{t}Bu). ESMS *m/z* 286 $[M + H]^+$, 288 $[M + H]^+$. Found: C, 50.53; H, 5.42; N, 4.77 %. Required for $C_{12}H_{16}BrNO_2$, 50.37; H, 5.64; N, 4.89 %. Data is in accordance with the literature.[17]

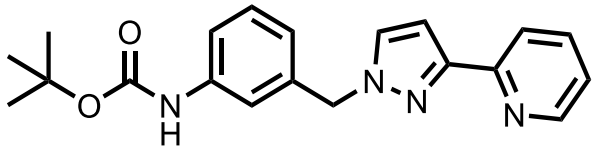

Synthesis of 3

A mixture of **2** (2.95 g, 10.29 mmol), 3-(2- pyridyl)pyrazole (1.50 g, 10.33 mmol), THF (120 cm^3) and aqueous NaOH (13 M, 7.5 cm^3) was stirred at 75 ^{o}C for 24 h. The organic layer was separated, dried over $MgSO_4$ and concentrated before purification by column chromatography on silica. Elution with EtOAc/ DCM (4:1, R_f = 0.70) yielded **3** as a white solid (Yield: 2.55 g, 71 %). ^{1}H-NMR (400 MHz, $CDCl_3$): δ 8.65 (1H, ddd, *J* = 5.0, 1.8, 1.0 Hz; pyridyl H^6), 7.97 (1H, dt, *J* = 8.0, 1.0 Hz; pyridyl H^3), 7.73 (1H, td, *J* = 8.0, 1.8 Hz; pyridyl H^4), 7.43 (1H, d, *J* = 2.4 Hz; pyrazolyl H^5), 7.34 – 7.25 (3H, m; ArH), 7.21 (1H, ddd, *J* = 7.5, 5.0, 1.0 Hz; pyridyl H^5), 6.94 – 6.92 (2H, m; Ar-H and pyrazolyl H^4), 6.55 (1H, bs; NH), 5.38 (2H, s; CH_2), 1.52 (9H, s; ^{t}Bu). ESMS: *m/z* 373 $[M + Na]^+$, 351 $[M + H]^+$. Found: C, 68.46; H, 6.35; N, 15.78 %. Required for $C_{20}H_{22}N_4O_2$: C, 68.55; H, 6.33; N, 15.99 %.

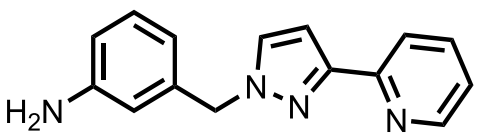

Synthesis of 4

To a solution of **3** (1.51 g, 4.31 mmol) in DCM (20 cm^3) was added TFA (20 cm^3) and the resultant yellow mixture was stirred at 25 ^oC for 14 h. The solvent was removed *in vacuo* and the clear brown oil was repeatedly washed with DCM/ MeOH (1:1) and evaporated to dryness in order to remove traces of TFA. The cream-coloured solid was washed with an aqueous solution of K_2CO_3 (2M) and the organic layer extracted with DCM, dried over $MgSO_4$ and evaporated to dryness, yielding **4** as a white solid (Yield: 0.81 g, 75 %). ^{1}H-NMR (400 MHz, $CDCl_3$): δ 8.65 (1H, ddd, *J* = 4.9, 2.0, 0.8 Hz; pyridyl H^6), 7.97 (1H, d, *J* = 8.0 Hz; pyridyl H^3), 7.72 (1H, td, *J* = 7.8, 1.7 Hz; pyridyl H^4), 7.42 (1H, d, *J* = 2.4 Hz; pyrazolyl H^5), 7.20 (1H, ddd, *J* = 7.4, 4.9, 1.2 Hz; pyridyl H^5), 7.14 (1H, t, *J* = 7.8 Hz; Ar-H), 6.92 (1H, d, *J* = 2.4 Hz; pyrazolyl H^4), 6.68 – 6.61 (2H, m; Ar-H), 6.53 (1H, t, *J* = 1.7 Hz; Ar-H), 5.31 (2H, s; CH_2), 3.56 (2H, bs; NH_2). ESMS: *m/z* 251 $[M + H]^+$. Found: C, 70.70; H, 5.46; N, 21.64 %. Required for $C_{15}H_{14}N_4$: C, 71.98; H, 5.64; N, 22.38 %.

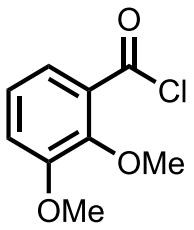

Synthesis of 5

2,3-dimethoxybenzoic acid (4.70 g, 25.8 mmol), $SOCl_2$ (7 cm^3, 96.5 mmol) and a drop of DMF were heated to reflux with stirring for 6 h. The condenser was fitted with a $CaCl_2$ drying tube to absorb liberated SO_2 and HCl. The resultant clear yellow solution was diluted with $CHCl_3$ and evaporated to dryness under reduced pressure three times. Drying under high vacuum yielded **5** as an off white solid, which was used without any further purification, assuming quantitative yield (Yield: 5.10 g, 99 %). ^{1}H-NMR (250 MHz, $CDCl_3$): δ 7.55 (1H, dd; Ar-H), 7.20-7.15 (2H, m; Ar-H), 3.94 (3H, s; OMe), 3.92 (3H, s; OMe). EIMS *m/z* 224 $[M + Na]^+$, 165 $[M - Cl^-]^+$. Data is in accordance with the literature.[30]

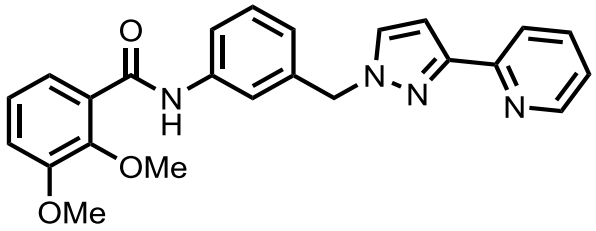

Synthesis of 6

A mixture of **4** (0.51 g, 2.0 mmol) and **5** (0.44 g, 2.2 mmol) were stirred in dry DCM (25 cm^3) under nitrogen flow. To the cloudy solution was added Et_3N (0.55 cm^3, 4.0 mmol), and the resultant clear solution was stirred at room temperature for 1 h. The mixture was then sequentially washed with 1M HCl (50 cm^3) and 1M NaOH (50 cm^3). The organic layer was extracted with DCM, dried over $MgSO_4$ and concentrated before purification by column chromatography on silica. Elution with EtOAc/DCM (1:1, R_f = 0.29) yielded **6** as a clear yellow oil (Yield: 0.80 g, 97%). ^{1}H-NMR (400 MHz, $CDCl_3$): δ 10.05 (1H, s; NH), 8.62 (1H, d, *J* = 4.5 Hz; pyridyl H^6), 7.95 (1H, d, *J* = 7.9 Hz; pyridyl H^3), 7.75 (1H, dd, *J* = 8.0, 1.4 Hz; Ph-H), 7.72 – 7.66 (2H, m; Ph-H and pyridyl H^4), 7.58 (1H, d, *J* = 8.0 Hz; cat-H), 7.46 (1H, d, *J* = 2.3 Hz; pyrazolyl H^5), 7.33 (1H, t, *J* = 8.0 Hz; cat-H), 7.22 – 7.13 (2H, m; Ph-H and pyridyl H^5), 7.07 (1H, dd, *J* = 8.2, 1.4 Hz; Ph-H), 7.00 (1H, d, *J* = 7.9 Hz; cat-H), 6.92 (1H, d, *J* = 2.3 Hz; pyrazolyl H^4), 5.40 (2H, s; CH_2), 3.95 (3H, s; OMe); 3.89 (3H, s; OMe). ESMS: *m/z* 415 $[M + H]^+$. Found: C, 60.67; H, 4.51; N, 11.52 %. Required for $C_{24}H_{22}N_4O_3 \cdot$ DCM: C, 60.13; H, 4.84; N, 11.22 %.

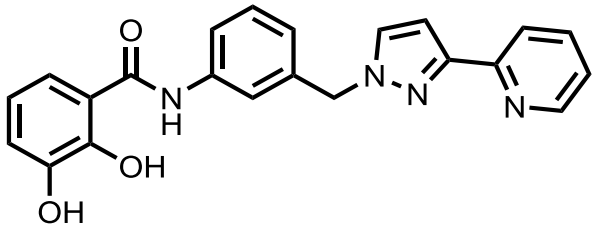

Synthesis of $H_2L^{1,3}$

BBr_3 (1M solution in DCM, 17 cm^3, 17 mmol) was added dropwise to a solution of **6** (0.80 g, 1.9 mmol) in dry DCM (50 cm^3) maintained at -78 °C and then stirred at room temperature overnight. The reaction

mixture was quenched with MeOH and the volatiles were removed under reduced pressure. The resultant black residue was suspended in H_2O at 100 ^oC for 2 h and the brown solution was cooled and filtered. The pink precipitate was washed with water and DCM, and the resultant white solid was recrystallized from MeOH, yielding a white solid (Yield: 0.61 g, 83%). ^{1}H-NMR (400 MHz, $(CD_3)_2SO$): δ 11.51 (1H, bs; Ar-OH), 10.39 (1H, s; NH), 8.69 (1H, d, *J* = 5.6 Hz; pyridyl H^6), 8.41 – 8.25 (2H, m; Ar-H and pyridyl H^3), 8.16 (1H, d, *J* = 2.4 Hz; pyrazolyl H^5), 7.78 – 7.68 (2H, m; Ar-H), 7.61 (1H, d, *J* = 8.0 Hz; Ar-H), 7.44 – 7.33 (2H, m; Ar-H and pyridyl H^5), 7.20 (1H, d, *J* = 2.4 Hz; pyrazolyl H^4), 7.09 (1H, d, *J* = 7.8 Hz; Ar-H), 6.98 (1H, dd, *J* = 7.8, 1.5 Hz; Ar-H), 6.76 (1H, t, *J* = 8.0 Hz; Ar-H), 5.53 (2H, s; CH_2). ESMS: *m/z* 387 $[M + H]^+$. Found: C, 56.50; H, 4.04; N, 11.81 %. Required for $C_{22}H_{18}N_4O_3$.HBr: C, 56.54; H, 4.10; N, 11.99 %.

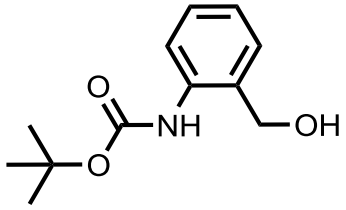

Synthesis of 7

A mixture of 2-(hydroxymethy1)aniline (8.8 g, 71.5 mmol) and di-*tert*-butyl dicarbonate (15.8 g, 72.4 mmol) was stirred in THF (150 cm^3) at 25 ^oC for 5 days. The solution was concentrated to a brown oil before purification by column chromatography on silica. Elution with ethyl acetate/ hexane (1:3, R_f = 0.40) yielded **7** as a clear yellow oil (Yield: 14.8 g, 66.3 mmol, 93 %). ^{1}H-NMR (400 MHz, $CDCl_3$): δ 7.90 (1H, d, *J* = 8.0 Hz; ArH), 7.69 (1H, bs; NH), 7.31 (1H, td, *J* = 7.9, 1.5 Hz; ArH), 7.17 (1H, dd, *J* = 7.6, 1.5 Hz; ArH), 7.02 (1H, td, *J* = 7.6, 1.2 Hz; ArH), 4.67 (2H, s; CH_2), 2.50 (1H, t, *J* = 5.7 Hz; OH), 1.54 (9H, s; ^{t}Bu). ESMS *m/z* 246 $[M + Na]^+$, 224 $[M + H]^+$, 150 $[M - {}^-O^tBu]^+$; Found: C, 64.28; H, 7.69; N, 6.19 %. Required for $C_{12}H_{17}NO_3$: C, 64.55; H, 7.67; N, 6.27 %. Data is in accordance with the literature.[31]

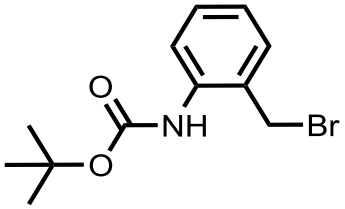

Synthesis of 8

A solution of **7** (2.07 g, 9.27 mmol) in DCM (20 cm^3) was maintained at 0 ^oC with stirring under nitrogen flow. To this was added CBr_4 (3.73 g, 11.25 mmol) and PPh_3 (2.93 g, 11.17 mmol) sequentially, and the resultant orange solution was stirred at 0 ^oC for 2.5 h. The reaction mixture was concentrated by rotary evaporation before purification by column chromatography on silica. Elution with ethyl acetate/ hexane (1:7, R_f = 0.41) yielded **8** as an off-white solid (Yield: 1.80 g, 6.29 mmol, 68 %). ^{1}H-NMR (400 MHz, $CDCl_3$): δ 7.86 (1H, d, *J* = 8.0 Hz; ArH), 7.36 (1H, td, *J* = 7.8, 1.5 Hz; ArH), 7.31 (1H, dd, *J* = 7.8, 1.5 Hz; ArH), 7.08 (1H, td, *J* = 7.5, 1.0 Hz; ArH), 6.71 (1H, bs; NH), 4.53 (2H, d; CH_2), 1.57 (9H, s; ^{t}Bu). ESMS *m/z* 286 $[M + H]^+$, 288 $[M + H]^+$. Found: C, 50.41; H, 5.91; N, 4.94; Br 27.63 %. Required for $C_{12}H_{16}BrNO_2$, 50.37; H, 5.64; N, 4.89; 27.92 %. Data is in accordance with the literature.[31]

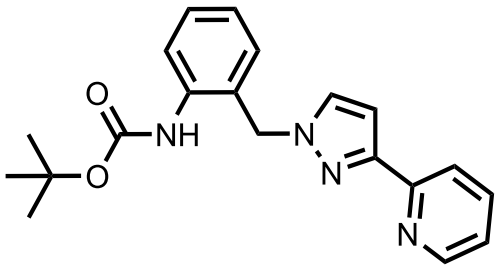

Synthesis of 9

A mixture of **8** (2.05 g, 7.16 mmol), 3-(2-pyridyl)pyrazole (1.43 g, 9.86 mmol), THF (120 cm^3) and aqueous NaOH (9.5 M, 10 cm^3) was stirred at 75 ^oC for 48 h. The organic layer was extracted with DCM, separated, dried over $MgSO_4$ and concentrated before purification by column chromatography on silica. Elution with EtOAc/ DCM (4:1, R_f = 0.73) yielded **9** as a yellow solid (Yield: 0.98 g, 39 %).

^{1}H-NMR (400 MHz, $CDCl_3$): δ 9.73 (1H, bs; NH), 8.63 (1H, ddd, *J* = 5.0, 1.9, 1.0 Hz; pyridyl H^6), 8.15 (1H, d, *J* = 8.0 Hz; pyridyl H^3), 7.97 (1H, d, *J* = 8.1 Hz; ArH), 7.73 (1H, td, *J* = 7.7, 1.7 Hz; pyridyl H^4), 7.52 (1H, d, *J* = 2.3 Hz; pyrazolyl H^5), 7.35 (1H, td, *J* = 7.8, 1.5 Hz; ArH), 7.30 (1H, dd, *J* = 8.0, 1.5 Hz; ArH), 7.23 (1H, ddd, *J* = 7.5, 5.0, 1.1 Hz; pyridyl H^5), 7.05 (1H, td, *J* = 7.5, 1.1 Hz; ArH), 6.96 (1H, d, *J* = 2.3 Hz; pyrazolyl H^4), 5.29 (2H, s; CH_2), 1.63 (9H, s; ^{t}Bu). ESMS: *m/z* 373 $[M + Na]^+$, 351 $[M + H]^+$, 295 $[M - {}^tBu^+, +2H]^+$. Found: C, 68.45; H, 6.89; N, 15.43 %. Required for $C_{20}H_{22}N_4O_2$: C, 68.55; H, 6.33; N, 15.99 %.

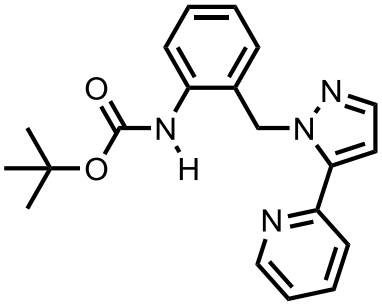

Synthesis of 10

Same method as **9**. Elution with EtOAc/ DCM (4:1, R_f = 0.88) yielded **10** as a clear yellow oil (Yield: 0.95 g, 38 %). ^{1}H-NMR (400 MHz, $CDCl_3$): δ 9.84 (1H, bs; NH), 8.85 (1H, ddd, *J* = 4.9, 2.0, 0.9 Hz; pyridyl H^6), 7.97 (1H, d, *J* = 8.1 Hz; ArH), 7.80 (1H, td, *J* = 7.8, 1.9 Hz; pyridyl H^4), 7.61 (1H, dt, *J* = 7.8, 1.0 Hz; pyridyl H^3), 7.57 (1H, d, *J* = 1.9 Hz; pyrazolyl H), 7.46 (1H, dd, *J* = 7.6, 1.6 Hz; ArH), 7.36 – 7.24 (2H, m; ArH), 6.99 (1H, td, *J* = 7.5, 1.2 Hz; pyridyl H^5), 6.58 (1H, d, *J* = 1.9 Hz; pyrazolyl H), 5.84 (2H, s; CH_2), 1.52 (9H, s; ^{t}Bu). ESMS: *m/z* 373 $[M + Na]^+$, 351 $[M + H]^+$, 295 $[M - {}^tBu^+, +2H]^+$.

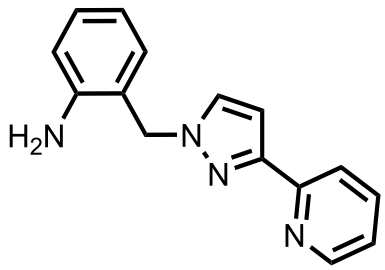

Synthesis of 11

To a solution of **9** (0.98 g, 2.80 mmol) in DCM (5 cm^3) was added TFA (5 cm^3) and the resultant yellow mixture was stirred at 25 ^oC for 14 h. The solvent was removed *in vacuo* and the clear brown oil was repeatedly washed with DCM/ MeOH (1:1) and evaporated to dryness in order to remove excess TFA. The cream-coloured solid was washed with an aqueous solution of K_2CO_3 (2M) and the organic layer extracted with DCM, dried over $MgSO_4$ and evaporated to dryness, yielding **11** as a brown solid (Yield: 0.65 g, 92 %). ^{1}H-NMR (400 MHz, $CDCl_3$): δ 8.63 (1H, d, *J* = 4.4 Hz; pyridyl H^6), 7.95 (1H, d, *J* = 7.9 Hz; pyridyl H^3), 7.73 (1H, td, *J* = 7.7, 1.5 Hz; pyridyl H^4), 7.43 (1H, d, *J* = 2.2 Hz; pyrazolyl H^5), 7.24 – 7.13 (3H, m; pyridyl H^5 and ArH), 6.90 (1H, d, *J* = 2.2 Hz; pyrazolyl H^4), 6.77 (1H, t, *J* = 2.3 Hz; Ar-H), 6.70 (1H, d, *J* = 7.9 Hz; ArH), 5.31 (2H, s; CH_2), 4.40 (2H, bs; NH_2). ESMS: *m/z* 251 $[M + H]^+$. Found: C, 60.56; H, 4.79; N, 17.88 %. Required for $C_{15}H_{14}N_4 \cdot 0.5H_2O \cdot 0.5$TFA: C, 60.75; H, 4.94; N, 17.71 %.

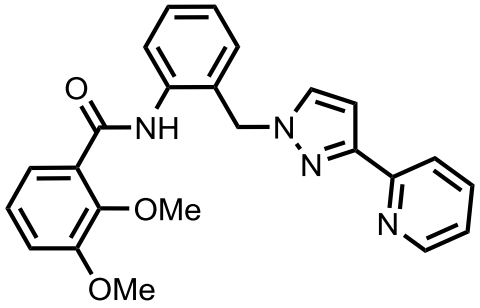

Synthesis of 12

A mixture of **11** (0.52 g, 2.1 mmol) and **5** (0.42 g, 2.1 mmol) were stirred in dry DCM (40 cm^3) under nitrogen flow. To the cloudy solution was added Et_3N (0.7 cm^3, 5.1 mmol), and the resultant clear solution was stirred at room temperature for 20 h. The mixture was washed with H_2O and the product

extracted with DCM, dried over $MgSO_4$ and concentrated before purification by column chromatography on silica. Elution with EtOAc/DCM (1:1, R_f = 0.45) yielded **6** as a clear yellow oil (Yield: 0.60 g, 69 %). ^{1}H-NMR (400 MHz, $CDCl_3$): δ 10.41 (1H, s; NH), 8.57 (1H, ddd, *J* = 5.0, 2.0, 0.9 Hz; pyridyl H^6), 8.01 (1H, d, *J* = 7.8 Hz; pyridyl H^3), 7.66 – 7.60 (2H, m; Ar-H and pyridyl H^4), 7.54 (1H, td, *J* = 7.7, 1.7 Hz; Ar-H), 7.47 (1H, d, *J* = 2.2 Hz; pyrazolyl H^5), 7.40 (1H, td, *J* = 7.7, 1.7 Hz; Ar-H), 7.24 (1H, dd, *J* = 7.8, 1.5 Hz; Ar-H), 7.22 – 7.11 (3H, m; Ar-H and pyridyl H^5), 7.09 (1H, dd, *J* = 8.2, 1.5 Hz; Ar-H), 6.89 (1H, d, *J* = 2.2 Hz; pyrazolyl H^4), 5.40 (2H, s; CH_2), 3.91 (3H, s; OMe); 3.88 (3H, s; OMe). ESMS: *m/z* 415 $[M + H]^+$.

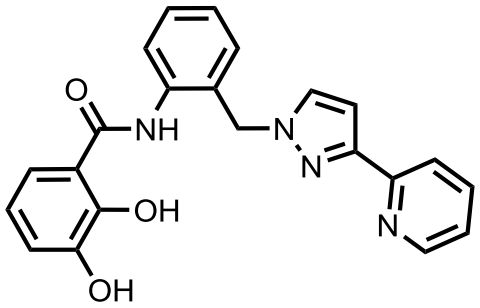

Synthesis of $H_2L^{1,2}$

BBr_3 (1.0 cm^3, 10.4 mmol, 7.2 eq) was added dropwise to a solution of **12** (0.60 g, 1.5 mmol) in dry DCM (50 cm^3) maintained at -78 ^oC and then stirred at room temperature overnight. The reaction mixture was quenched with MeOH and the volatiles were removed under reduced pressure. The resultant residue was suspended in H_2O at 100 ^oC for 4 h and the pink solution was cooled and extracted with EtOAc. Removal of the solvent under reduced pressure followed by washing with Et_2O yielded the product as a pink solid (Yield: 0.55 g). ^{1}H-NMR – see text. ESMS: *m/z* 387 $[M + H]^+$, 401 $[M + Me + H]^+$.

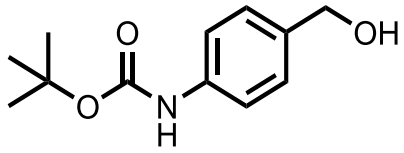

Synthesis of 13

A mixture of 4-(hydroxymethy1)aniline (5.00 g, 40.60 mmol) and di-*tert*-butyl dicarbonate (8.92 g, 40.87 mmol) was stirred in THF (100 cm^3) at 25 ^oC for 3 days. The resultant brown solution was concentrated and purified by column chromatography on silica. Elution with ethyl acetate/ hexane (1:2, R_f = 0.37) yielded **13** as a white solid (Yield: 8.43 g, 37.76 mmol, 93 %). ^{1}H-NMR (400 MHz, $CDCl_3$): δ 7.40 – 7.24 (4H, m; ArH), 6.60 (1H, bs; NH), 4.64 (2H, s; CH_2), 1.86 (1H, bs; OH), 1.54 (9H, s; ^{t}Bu). ESMS *m/z* 246 $[M + Na]^+$, 150 $[M - {}^-O^tBu]^+$; Found: C, 64.28; H, 7.69; N, 6.19 %. Required for $C_{12}H_{17}NO_3$: C, 64.55; H, 7.67; N, 6.27 %. Data is in accordance with the literature.[28]

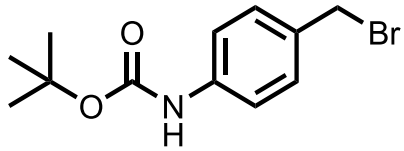

Synthesis of 14

A solution of **13** (2.42 g, 10.8 mmol) in DCM (60 cm^3) was maintained at 0 ^oC with stirring. To this was added PPh_3 (4.40 g, 16.8 mmol) and CBr_4 (5.40 g, 16.3 mmol) sequentially, and the resultant yellow solution was stirred at 0 ^oC for 1.5 h. The reaction mixture was then diluted with EtOAc and stirred for a further 0.5 h, before washing with brine. The organic layer was extracted with EtOAc, dried over $MgSO_4$ and concentrated before purification by passage through a short silica plug. Elution with ethyl acetate/ hexane (1:4, R_f = 0.50) yielded **14** as a yellow solid (Yield: 1.21 g, 10.3 mmol, 67 %). ^{1}H-NMR (400 MHz, $CDCl_3$): δ 7.39 – 7.31 (4H, m; ArH), 6.53 (1H, bs; NH), 4.50 (2H, s; CH_2), 1.54 (9H, s; ^{t}Bu). Data is in accordance with the literature.[32]

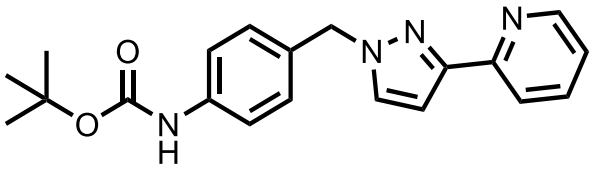

Synthesis of 15

A mixture of **14** (0.88 g, 3.1 mmol), 3-(2-pyridyl)pyrazole (0.45 g, 3.1 mmol), THF (50 cm^3) and aqueous NaOH (12.5 M, 3 cm^3) was stirred at 75 ^oC for 24 h. The organic layer was separated, dried over $MgSO_4$ and concentrated before purification by column chromatography on silica. Elution with EtOAc/ DCM (4:1, R_f = 0.55) yielded **15** as a white solid (Yield: 0.84 g, 77 %). ^{1}H-NMR (400 MHz, $CDCl_3$): δ 8.58 (1H, ddd, *J* = 4.9, 1.9, 0.8 Hz; pyridyl H^6), 7.93 (1H, dt, *J* = 8.0, 1.0 Hz; pyridyl H^3), 7.67 (1H, td, *J* = 7.8, 1.8 Hz; pyridyl H^4), 7.36 – 7.30 (3H, m; Ar-H pyrazolyl H^5), 7.18 – 7.12 (4H, m; ArH, NH and pyridyl H^5), 6.88 (1H, d, *J* = 2.4 Hz; pyrazolyl H^4), 5.27 (2H, s; CH_2), 1.46 (9H, s; ^{t}Bu). ESMS: *m/z* 373 $[M + Na]^+$, 351 $[M + H]^+$.

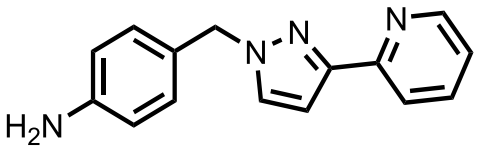

Synthesis of 16

To a solution of **15** (0.84 g, 2.39 mmol) in DCM (10 cm^3) was added TFA (10 cm^3) and the resultant yellow mixture was stirred at 25 ^oC for 14 h. The solvent was removed *in vacuo* and the clear brown oil was repeatedly washed with DCM/ MeOH (1:1) and evaporated to dryness in order to remove excess TFA. The cream-coloured solid was washed with an aqueous solution of K_2CO_3 (2M) and the organic layer extracted with DCM, dried over $MgSO_4$ and evaporated to dryness, yielding **16** as a light brown solid (Yield: 0.47 g, 79 %). ^{1}H-NMR (400 MHz, $CDCl_3$): δ 8.64 (1H, ddd, *J* = 5.0, 1.9, 0.9 Hz; pyridyl H^6), 7.96 (1H, dt, *J* = 8.0, 0.9 Hz; pyridyl H^3), 7.72 (1H, td, *J* = 7.8, 1.8 Hz; pyridyl H^4), 7.35 (1H, d, *J* = 2.4 Hz; pyrazolyl H^5), 7.20 (1H, ddd, *J* = 7.5, 5.0, 1.0 Hz; pyridyl H^5), 7.12 (2H, m; Ar-H), 6.88 (1H, d, *J* = 2.4 Hz; pyrazolyl H^4), 6.67 (2H, m; Ar-H), 5.28 (2H, s; CH_2), 3.81 (2H, bs; NH_2). ESMS: *m/z*

273 $[M + Na]^+$, 251 $[M + H]^+$. Found: C, 68.97; H, 5.31; N, 20.82 %. Required for $C_{15}H_{14}N_4 \cdot 0.15$ TFA: C, 68.72; H, 5.33; N, 20.95 %.

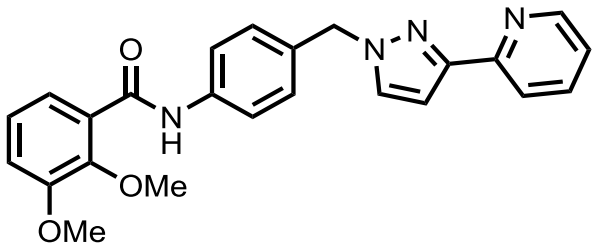

Synthesis of 17

A mixture of **16** (0.25 g, 1.0 mmol) and **5** (0.22 g, 1.1 mmol) were stirred in dry DCM (25 cm^3) under nitrogen flow. To the cloudy solution was added Et_3N (0.30 cm^3, 2.2 mmol), and the resultant clear solution was stirred at room temperature for 1 h. The mixture was then sequentially washed with 1M HCl (50 cm^3) and 1M NaOH (50 cm^3). The organic layer was extracted with DCM, dried over $MgSO_4$ and evaporated to dryness, yielding **17** as a light brown solid, which was used without any further purification (Yield: 0.26 g, 63 %). ^{1}H-NMR (400 MHz, $CDCl_3$): δ 10.05 (1H, s; NH), 8.61 (1H, ddd, *J* = 5.0, 1.9, 0.9 Hz; pyridyl H^6), 7.94 (1H, dt, *J* = 7.9, 1.0 Hz; pyridyl H^3), 7.78 – 7.62 (4H, m; Ar-H and pyridyl H^4), 7.40 (1H, d, *J* = 2.4 Hz; pyrazolyl H^5), 7.31 – 7.23 (2H, m; Ar-H), 7.22 – 7.13 (2H, m; Ar-H), 7.07 (1H, dd, *J* = 8.1, 1.6 Hz; pyridyl H^5), 6.92 (1H, d, *J* = 2.4 Hz; pyrazolyl H^4), 5.35 (2H, s; CH_2), 3.95 (3H, s; OMe); 3.89 (3H, s; OMe). ESMS: *m/z* 415 $[M + H]^+$. Found: C, 67.86; H, 4.83; N, 13.19 %. Required for $C_{24}H_{22}N_4O_3 \cdot 0.15$DCM: C, 67.90; H, 5.26; N, 13.12 %.

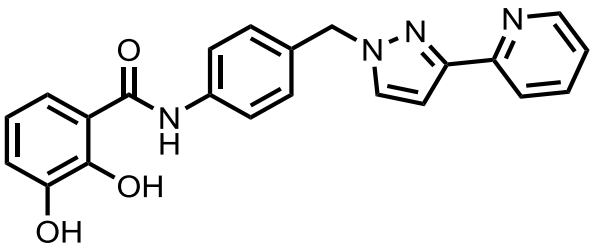

Synthesis of $H_2L^{1,4}$

BBr_3 (1M solution in DCM, 6 cm^3, 6 mmol) was added dropwise to a solution of **17** (0.20 g, 0.48 mmol) in dry DCM (50 cm^3) maintained at -78 ^oC and then stirred at room temperature overnight. The reaction mixture was quenched with MeOH and the volatiles were removed under reduced pressure. The resultant orange residue was suspended in H_2O at 100 ^oC for 2 h and the brown solution was cooled and filtered. The pink precipitate was washed with water and DCM, yielding **$H_2L^{1,4}$** as an off-white solid (Yield: 0.15 g, 81 %). ^{1}H-NMR (400 MHz, MeOD): δ 8.65 (1H, d, *J* = 5.4 Hz; pyridyl H^6), 8.46 (1H, td, *J* = 7.9, 1.5 Hz; pyridyl H^4), 8.35 (1H, d, *J* = 8.1 Hz; pyridyl H^3), 7.95 (1H, d, *J* = 2.5 Hz; pyrazolyl H^5), 7.81 (1H, m; pyridyl H^5), 7.69 (2H, d, *J* = 8.5 Hz; Ph-H), 7.43 (1H, dd, *J* = 7.8, 1.5 Hz; cat-H), 7.37 (2H, d, *J* = 8.5 Hz; Ph-H), 7.15 (1H, d, *J* = 2.5 Hz; pyrazolyl H^4), 6.99 (1H, dd, *J* = 7.8, 1.5 Hz; cat-H) 6.80 (1H, t, *J* = 7.8 Hz; cat-H^5), 5.49 (2H, s; CH_2). ESMS: *m/z* 387 $[M + H]^+$.

4.4.2 Complex synthesis

The complexation reactions were all carried out using the same general method; the example given below is typical.

Synthesis of $Ti_4Zn_4L^{1,3}{}_8OMe_8{\cdot}4dmf{\cdot}4MeOH$

A solution of $Ti(O^iPr)_4$ (8.5 mg, 0.03 mmol) in MeOH (5 cm^3) was added to a stirring solution of **L^1** (39 mg, 0.1 mmol) in MeOH (3 cm^3) causing the solution to turn yellow, to which $Zn(BF_4)_2.6H_2O$ (10.2 mg, 0.03 mmol) in MeOH (2 cm^3) was added. An excess of Et_3N was added (1 cm^3) and the mixture was stirred in the dark at room temperature for 24 h. A fine orange precipitate was collected and washed

with MeOH. X-Ray quality crystals were grown by slow diffusion of MeOH into a solution of the complex in dimethylformamide. (Yield: 13 mg).

4.5 X-ray crystallography

Details of the crystal, data collection and refinement parameters are summarised. Data were corrected for absorption using empirical methods (SADABS)[33] based upon symmetry-equivalent reflections combined with measurements at different azimuthal angles. The structures were solved by direct methods and refined by full-matrix least squares on weighted F^2 values for all reflections using the SHELX suite of programs.[34] Non-hydrogen atoms were refined anisotropically. Hydrogen atoms were placed in calculated positions, refined using idealized geometries (riding model) and were assigned fixed isotropic displacement parameters.

The structures of $[Ti_4Zn_4(L^{1,3})_8(OMe)_8]$ and $H_2L^{1,3}$**.**HBr were collected at the National Crystallography Service at the University of Southampton. The 'Squeeze' function in PLATON was used to eliminate regions of diffuse electron density in solvent-accessible voids for $[Ti_4Zn_4(L^{1,3})_8(OMe)_8]$, information is given in the CIF.

In each other case a suitable crystal was mounted in a stream of cold N_2 on a Bruker APEX-2 or SMART CCD diffractometers (at the University of Sheffield) equipped with graphite-monochromated Mo-Kα radiation from a sealed-tube source. Details of each structure are given in their individual CIFs.

Summary of crystallographic data for the new crystal structures:

Compound	**$[Ti_4Zn_4(L^{1,3})_8(OMe)_8]$. 4MeOH . 4DMF**	**$H_2L^{1,3}$ · HBr**
Formula	$C_{200}H_{196}N_{36}O_{40}Ti_4Zn_4$	$C_{22}H_{19}BrN_4O_3$
Molecular weight	4197.01	467.32
T / *K*	100(2)	100(2)
Crystal system	Monoclinic	Monoclinic
Space group	*C 2/c*	*P2(1)/c*
a / Å	45.96(3)	4.807(3)
b / Å	14.997(8)	18.377(13)
c / Å	34.57(2)	22.149(15)
α / °	90	90
β / °	119.729(8)	91.68(3)
γ / °	90	90
V / Å^3	20692(21)	1956(2)
Z	4	4
ρ / g cm^{-3}	1.347	1.587
μ / mm^{-1}	0.683	2.135
Data, restraints, parameters, R_{int}	14644 / 1120 / 1041 / 0.0682	2780 / 0 / 271 / 0.1065
Final *R*1, *wR*2[a]	0.1090, 0.3000	0.0752, 0.2140

Compound	**11 · H_2O**	**17**
Formula	$C_{15}H_{16}N_4O$	$C_{24}H_{22}N_4O_3$
Molecular weight	268.32	414.46
T / *K*	100(2)	298(2)
Crystal system	Orthorhombic	Monoclinic
Space group	*Pca2(1)*	*P2(1)/c*
a / Å	8.4025(8)	17.311(7)
b / Å	10.1318(10)	13.104(5)
c / Å	16.0412(16)	9.212(4)
α / °	90	90
β / °	90	101.380(6)
γ / °	90	90
V / Å^3	1365.6(2)	2048.6(15)
Z	4	4
ρ / g cm^{-3}	1.305	1.344
μ / mm^{-1}	0.086	0.091
Data, restraints, parameters, R_{int}	3103 / 4 / 198 / 0.0248	2932 / 169 / 283 / 0.0815
Final *R*1, *wR*2[a]	0.0278, 0.0713	0.0612, 0.1731

[a] The value of R1 is based on 'observed' data with I>2σ(I); the value of wR2 is based on all data.

4.6 References

1. M. D. Ward and P. R. Raithby, *Chem. Soc. Rev.*, 2013, **42**, 1619.

2. M. M. J. Smulders, I. A. Riddell, C. Browne and J. R. Nitschke, *Chem. Soc. Rev.*, 2013, **42**, 1728.

3. M. Wang, V. Vajpayee, S. Shanmugaraju, Y.-R. Zheng, Z. Zhao, H. Kim, P. S. Mukherjee, K.-W. Chi and P. J. Stang, *Inorg. Chem.*, 2011, **50**, 1506.

4. Y. Sakata, S. Hiraoka and M. Shionoya, *Chem.-Eur. J.*, 2010, **16**, 3318.

5. C. Piguet, G. Bernardinelli and G. Hopfgartner, *Chem. Rev.*, 1997, **97**, 2005.

6. P. de Wolf, P. Waywell, M. Hanson, S. L. Heath, A. Meijer, S. J. Teat and J. A. Thomas, *Chem.-Eur. J.*, 2006, **12**, 2188.

7. C. Piguet, J. C. G. Bunzli, G. Bernardinelli, G. Hopfgartner, S. Petoud and O. Schaad, *J. Am. Chem. Soc.*, 1996, **118**, 6681.

8. M. M. J. Smulders, A. Jimenez and J. R. Nitschke, *Angew. Chem. Int. Ed.*, 2012, **51**, 6681.

9. I. S. Tidmarsh, H. Fenton and M. D. Ward, *Dalton Trans.*, 2010, **39**, 3805.

10. S. Hiraoka, Y. Sakata and M. Shionoya, *J. Am. Chem. Soc.*, 2008, **130**, 10058.

11. H. B. Wu and Q. M. Wang, *Angew. Chem. Int. Ed.*, 2009, **48**, 7343.

12. X. K. Sun, D. W. Johnson, D. L. Caulder, K. N. Raymond and E. H. Wong, *J. Am. Chem. Soc.*, 2001, **123**, 2752.

13. F. E. Hahn, M. Offermann, C. S. Isfort, T. Pape and R. Frohlich, *Angew. Chem. Int. Ed.*, 2008, **47**, 6794.

14. M. D. Ward, *Chem. Commun.*, 2009, 4487.

15. D. L. Caulder, C. Bruckner, R. E. Powers, S. Konig, T. N. Parac, J. A. Leary and K. N. Raymond, *J. Am. Chem. Soc.*, 2001, **123**, 8923.

16. A. Stephenson, D. Sykes and M. D. Ward, *Dalton Trans.*, 2013, **42**, 6756.

17. F. J. Brown, P. R. Bernstein, L. A. Cronk, D. L. Dosset, K. C. Hebbel, T. P. Maduskuie, H. S. Shapiro, E. P. Vacek, Y. K. Yee, A. K. Willard, R. D. Krell and D. W. Snyder, *J. Med. Chem.*, 1989, **32**, 807.

18. J. M. Lehn, *Science*, 2002, **295**, 2400.

19. I. S. Tidmarsh, T. B. Faust, H. Adams, L. P. Harding, L. Russo, W. Clegg and M. D. Ward, *J. Am. Chem. Soc.*, 2008, **130**, 15167.

20. J. F. Ayme, J. E. Beves, D. A. Leigh, R. T. McBurney, K. Rissanen and D. Schultz, *J. Am. Chem. Soc.*, 2012, **134**, 9488.

21. O. R. Clegg, R. V. Fennessy, L. P. Harding, C. R. Rice, T. Riis-Johannessen and N. C. Fletcher, *Dalton Trans.*, 2011, **40**, 12381.

22. S. P. Argent, H. Adams, T. Riis-Johannessen, J. C. Jeffery, L. P. Harding, O. Mamula and M. D. Ward, *Inorg. Chem.*, 2006, **45**, 3905.

23. J. Hamblin, F. Tuna, S. Bunce, L. J. Childs, A. Jackson, W. Errington, N. W. Alcock, H. Nierengarten, A. Van Dorsselaer, E. Leize-Wagner and M. J. Hannon, *Chem.-Eur. J.*, 2007, **13**, 9286.

24. O. Mamula, A. von Zelewsky, P. Brodard, C. W. Schlapfer, G. Bernardinelli and H. Stoeckli-Evans, *Chem.-Eur. J.*, 2005, **11**, 3049.

25. B. Hasenknopf, J. M. Lehn, N. Boumediene, A. DupontGervais, A. VanDorsselaer, B. Kneisel and D. Fenske, *J. Am. Chem. Soc.*, 1997, **119**, 10956.

26. C. S. Campos-Fernandez, B. L. Schottel, H. T. Chifotides, J. K. Bera, J. Bacsa, J. M. Koomen, D. H. Russell and K. R. Dunbar, *J. Am. Chem. Soc.*, 2005, **127**, 12909.

27. K. E. Allen, R. A. Faulkner, L. P. Harding, C. R. Rice, T. Riis-Johannessen, M. L. Voss and M. Whitehead, *Angew. Chem. Int. Ed.*, 2010, **49**, 6655.

28. T. Schadendorf, C. Hoppmann and K. Rueck-Braun, *Tet. Lett.*, 2007, **48**, 9044.

29. A. J. Amoroso, A. M. C. Thompson, J. C. Jeffery, P. L. Jones, J. A. McCleverty and M. D. Ward, *J. Chem. Soc., Chem. Commun.*, 1994, 2751.

30. M. Meyer, B. Kersting, R. E. Powers and K. N. Raymond, *Inorg. Chem.*, 1997, **36**, 5179.

31. C. Mukai, M. Kobayashi, S. Kubota, Y. Takahashi and S. Kitagaki, *J. Org. Chem.*, 2004, **69**, 2128.

32. D. W. Ma, S. H. Yu, B. Li, L. Chen, R. H. Chen, K. Q. Yu, L. Q. Zhang, Z. W. Chen, D. F. Zhong, Z. Gong, R. X. Wang, H. L. Jiang and G. Pei, *Chemmedchem*, 2007, **2**, 187.

33. G. M. Sheldrick, *SADABS: A program for absorption correction with the Siemens SMART system*, University of Göttingen, Germany, 1996.

34. G. M. Sheldrick, *Acta Cryst. Sect. A*, 2008, **64**, 112.

5. Coordination chemistry of a 3,5-substituted aniline ligand: Towards exohedral functionalisation of M_8L_{12} coordination cages

5.1 Introduction

In the well-established field of self-assembled coordination cages, the focus of many research groups has shifted from serendipitous discovery of new cage structures to the design and application of functional cage molecules.[1-3] In the majority of coordination cages described in the literature hitherto, the organic spacer which links the coordinating termini of the ligand is unfunctionalised; typically an unsubsituted aryl or alkynyl moeity.[4-6] Guest-binding and reactivity modulation occur as a result of the micro-environment within the cavity, which is quite different from that outside the container, along with the complementary size and shape of the guest. Functional cage behaviour associated with substituted ligand backbones is a relatively unexplored area in comparison, with few literature examples.

The Fujita group have prepared a series of ligands based on a 1,3-bis(4-pyridyl)benzene backbone (see Figure 5.1.1). The unsubstituted ligand, when mixed with half an equivalent of $Pd(NO_3)_2$ under self-assembly conditions, forms an approximately spherical $M_{12}L_{24}$ cage complex. Substitution at the 5-position of the phenylene spacer allows the formation of a series of $M_{12}L_{24}$ cages which have 24 pendant substituents decorating the exterior of the cage; this is known as exohedral functionalisation.[7] Examples of substituents used include metallo-porphyrins, saccharides, DNA strands and hexapeptide aptamers. These substituents contribute to strong and selective interaction of the spherical complexes with a wide variety of substrates, which do not occur when the unfunctionalised ligand is used; for example, the saccharide coated molecular sphere forms aggregates with the protein concanavalin A.[8]

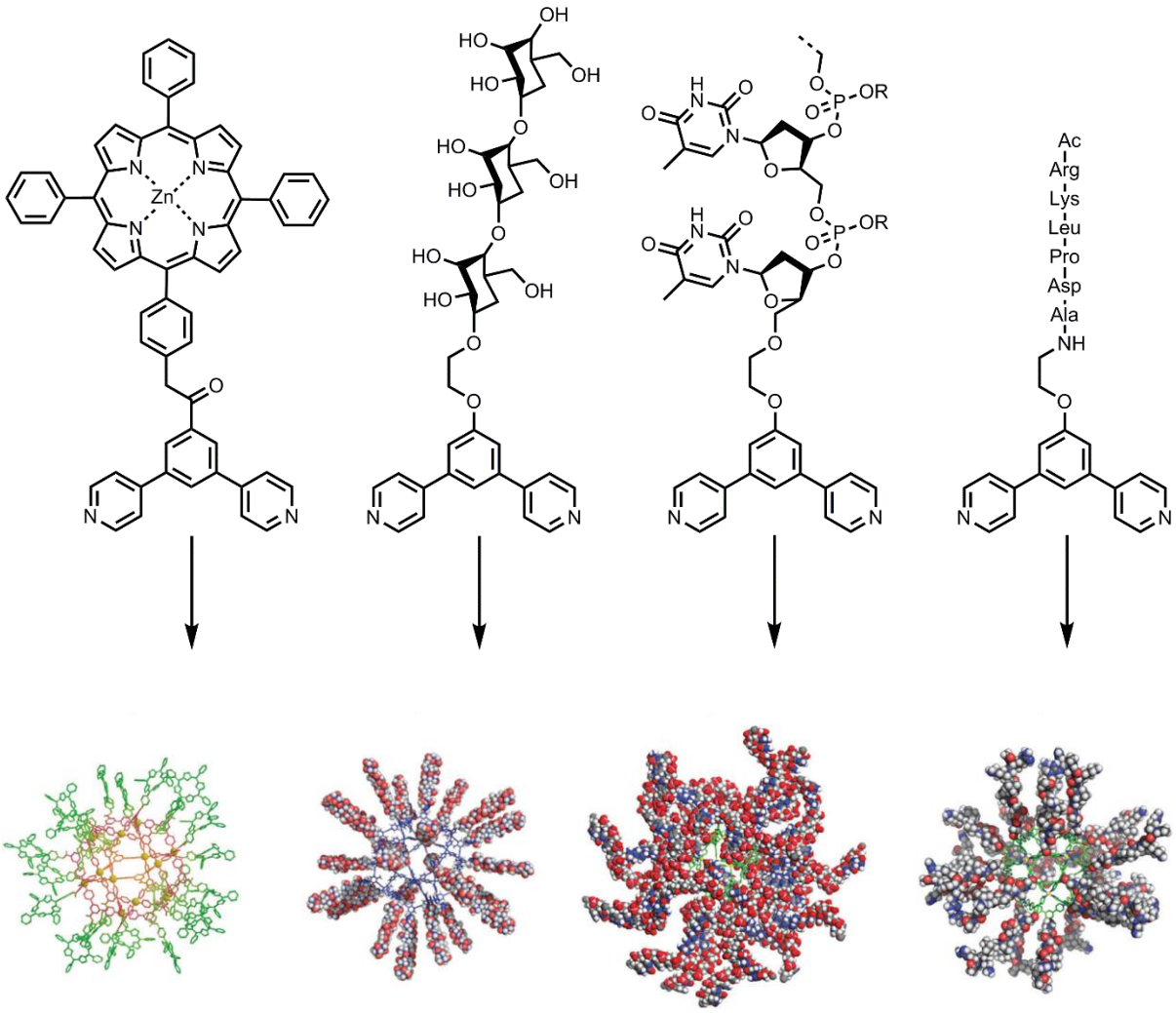

Figure 5.1.1 Examples of exohedrally functionalised $M_{12}L_{24}$ spherical complexes from the Fujita group. Reproduced from Ref. 7 with permission from The Royal Society of Chemistry.

Fujita's group have also used a series of ligands which are substituted at the 2-position of the phenyl spacer (i.e. the concave position) of an elongated ligand.[7] Formation of $M_{12}L_{24}$ molecular spheres with these ligands results in structures with 24 inwardly directed substituents, an example of endohedral functionalisation. By lining the interior surface of the cage with sugar, alkyl, tetra(ethylene glycol), perfluoroalkyl or peptide chains, the host-guest chemistry of the cage is drastically altered. For example, with 24 inwardly directed sugar groups, precisely monodisperse silica nanoparticles can be formed within the cage cavity.[9]

Nitschke's group have prepared a ligand which contains 4,4-difluoro-4-bora-3*a*,4*a*-diaza-*s*-indacene (BODIPY) and pyrene fluorophores (se Figure 5.1.2).[10] Reaction with $Fe(OTf)_2$ yields a Fe_4L_6

tetrahedron which can act as an anion sensor at nanomolar concentrations, and as a white-light-emitting ensemble when a host-guest complex with the aromatic guest perylene is formed. As with the above examples, the useful behaviour of the cage complex is a result of the functionality incorporated within the ligand backbone.

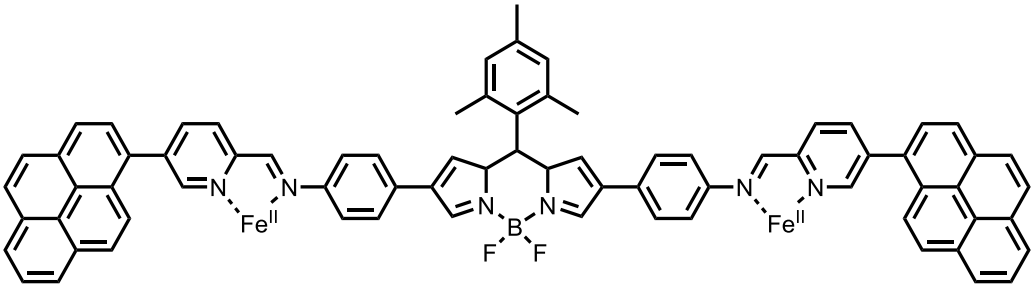

Figure 5.1.2 The fluorphore incorporating ligand used by the Nitschke group.[10]

The Ward group has synthesised a range of ligands with heteroaromatic spacer groups connecting two pyrazolyl-pyridine termini *via* flexible methylene hinges (see Figure 5.1.3).[11-13] Reaction of the furan, thiophene or pyridyl containing ligand with labile transition metal dications [e.g. Zn(II) or Co(II)] results in a series of structures with the usual 2M : 3L ratio observed with this family of ligands; the heteroatom of the aromatic spacer does not participate in coordinative bonding with the metal centres. For example, combination of the 2,6-pyridyl ligand with $Zn(ClO_4)_2$ or $Co(BF_4)_2$ led to the formation of a M_8L_{12} cube. It was hoped that the 12 "free" pyridyl nitrogens would be endohedrally directed, providing a three-dimensional H-bond accepting array, but unfortunately this is not what was observed; the nitrogen atoms are oriented in a variety of directions, some inwards and some outwards.

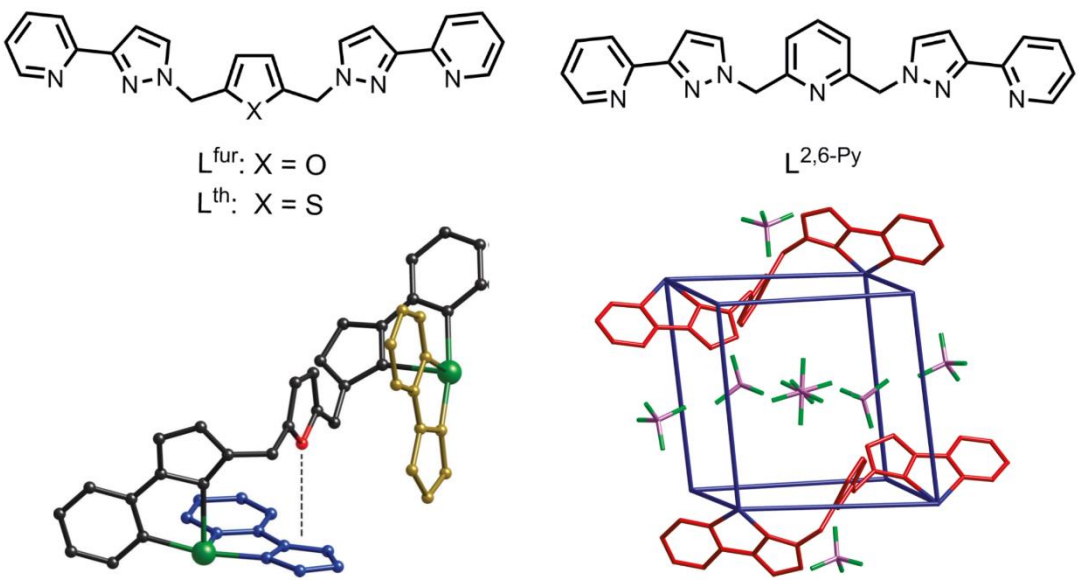

Figure 5.1.3 Ligands prepared by the Ward group with heteroaromatic spacer groups (Bottom left; Reproduced from Ref. 11 with permission from The Royal Society of Chemistry; bottom right: Reproduced with permission from Ref. 12. Copyright 2009 American Chemical Society).

A recent focus in the Ward group has been the appendage of a hydroxymethyl substituent to the coordinated pyridyl ring of the 1,5-naphthalene substituted ligand. While not directly altering the function of the interior of the cage, the 24 externally-directed pendant alcohol groups render the cage water soluble, something which has not previously been achieved with ligands in this family.[14,15] A tantalising prospect would be to introduce a substituent in the ligand backbone which would allow the solubility *and* functionality of the resultant cage to be easily altered. One such way that this could be achieved is by the introduction of an aniline group as the central spacer, something that has not previously been explored within the Ward group; this will allow easy functionalization *via* amide condensation reactions with a range of acid chlorides.

5.2 Results and discussion

5.2.1 Ligand synthesis

When one considers a potential bis(pyridyl-pyrazolyl)-substituted aniline ligand, two candidates become immediately obvious due to their symmetrical nature; the 3,5- and 2,6- disubstituted isomers (see Figure 5.2.1). On closer inspection of the availability of the starting materials and the relative ease of synthesis, the 3,5-disubstituted isomer was identified as the principal target **L^{an}**. It is noted that the 3,5-substituted phenylene spacer, with no amine group, is known to give M_8L_{12} cubes.[12]

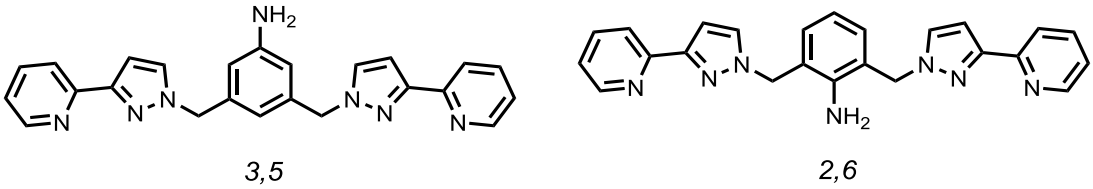

Figure 5.2.1 Potential bis(pyridyl-pyrazolyl)-substituted aniline ligands.

Synthesis of the ligand **L^{an}** was achieved in 5 steps starting from the readily available starting material dimethyl 5-aminoisophthalate (see Figure 5.2.2), and followed the same general synthetic route as seen for the ligands in Chapter 4.[16] The di-ester was reduced to the di-alchohol **18** by treatment with excess $LiAlH_4$ in tetrahyrofuran (THF),[17] and subsequently N-protected as the carbamate **19** by reaction with Boc_2O in THF.[18] Conversion to the di-alkyl bromide **20** by an Appel bromination was achieved in good yield following a literature procedure,[18] which was then substituted by reaction with PyPzH in THF and aqueous sodium hydroxide at reflux to give **21**. The Boc group was then removed by an overnight stir in dichloromethane (DCM) with trifluoroacetic acid (TFA), and neutralised with potassium carbonate to give the desired ligand **L^{an}**.

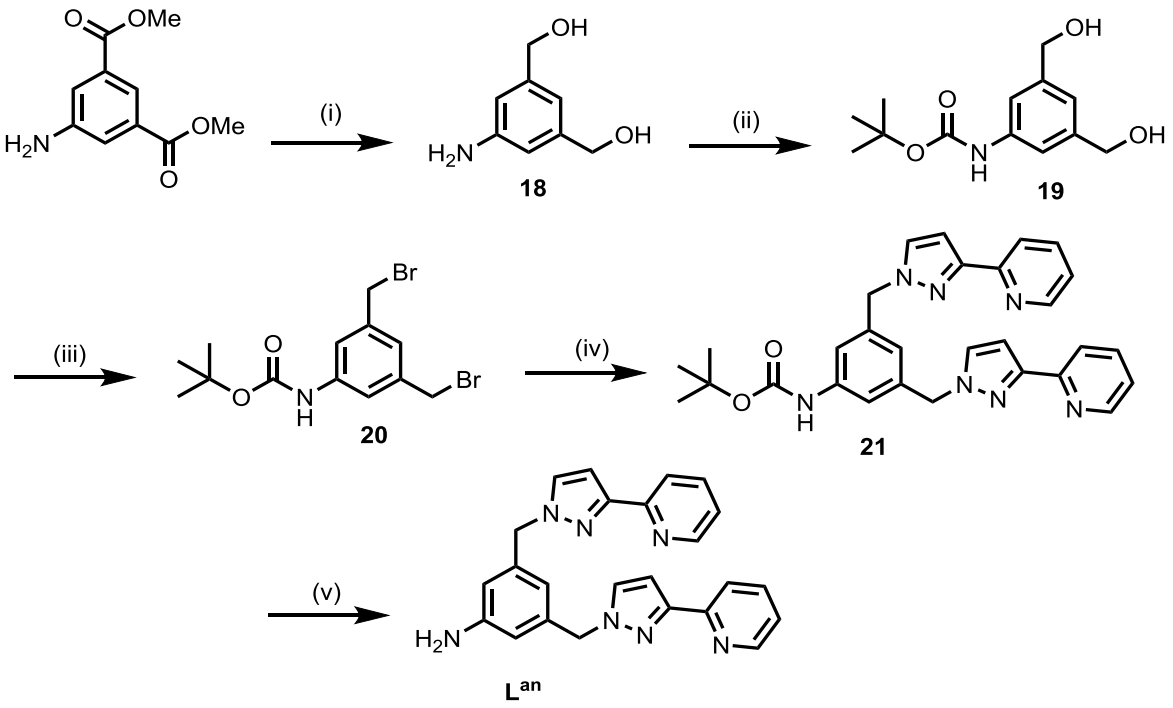

Figure 5.2.2 Reaction scheme for the preparation of L^{an}. (i) a. $LiAlH_4$, THF, b. H_2O, KOH, EtOAc (ii) Boc_2O, THF; (iii) CBr_4, PPh_3, DCM; (iv) PyPzH, THF, NaOH(aq); (v) TFA, DCM.

The compounds **21** and $\mathbf{L^{an}}$ were new and so were fully characterised by ^{1}H NMR spectroscopy, electrospray mass spectrometry (ESMS) and elemental analysis; the full ^{1}H NMR spectrum of the ligand $\mathbf{L^{an}}$ is shown below, which is simplified due to the C_2 symmetry of the ligand (see Figure 5.2.3). Slow evaporation of a solution of $\mathbf{L^{an}}$ in ethyl acetate and hexane resulted in the formation of crystals of x-ray quality; the crystal structure is shown below (see Figure 5.2.4). The structure is typical for ligands of this type, with a transoid arrangement of the two near-planar rings in each pyrazolyl-pyridine fragment. There are hydrogen bonding interactions between the lattice water molecules and one of the pyrazolyl nitrogens [N(22) to O(1S) separation 2.88 Å], and also two hydrogen-bonds between the aniline group and pyridyl nitrogens of two adjacent molecules [N(57) to N(11) separation 3.09 Å, N(57) to N(31) separation 3.24 Å].

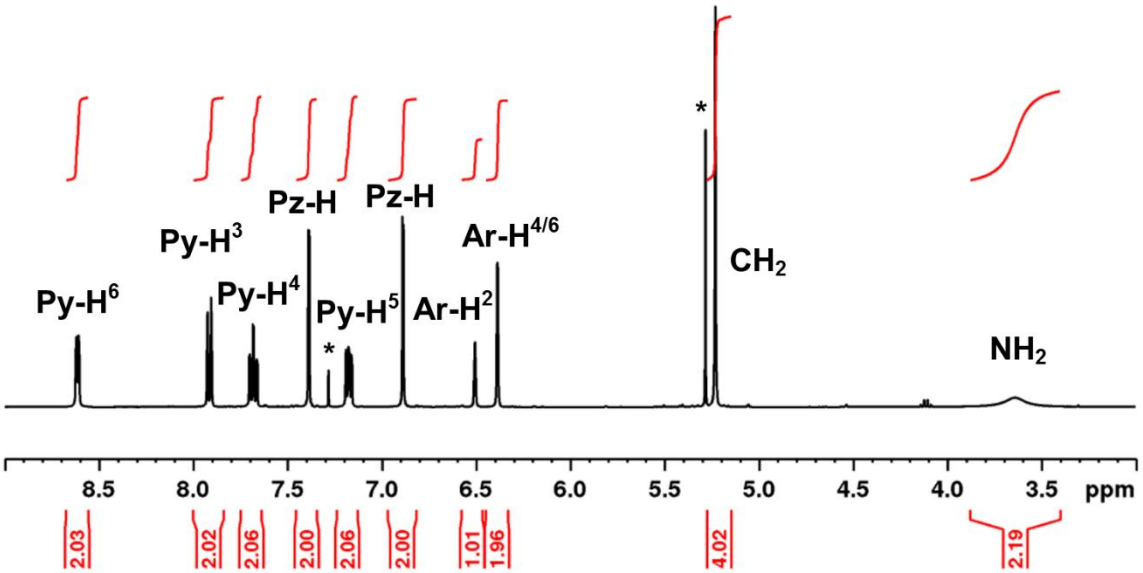

Figure 5.2.3 ^{1}H NMR (400 MHz, $CDCl_3$) spectrum of **L^{an}** (* = traces of protonated solvent).

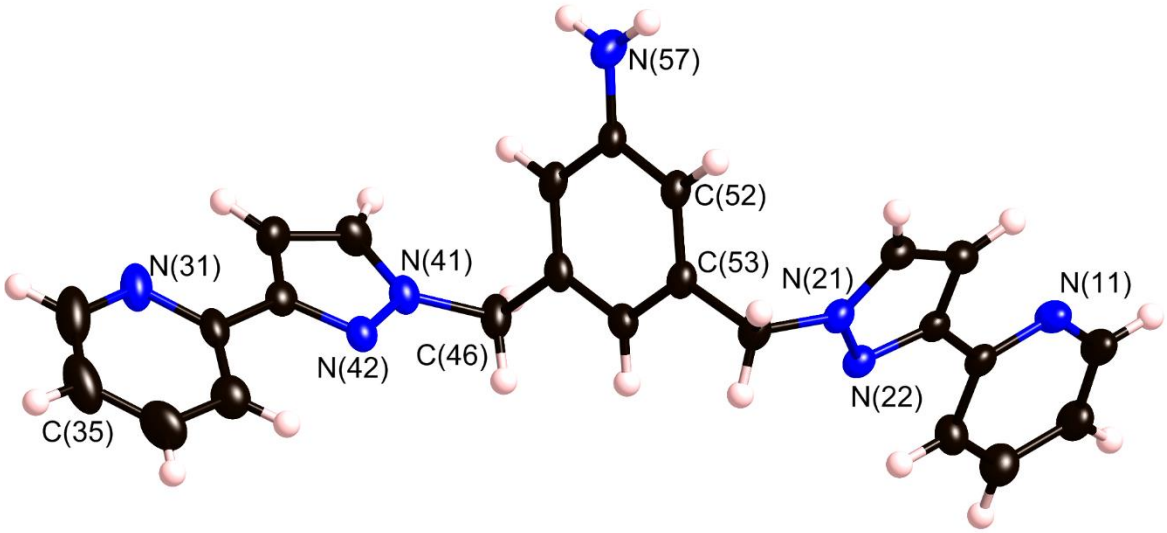

Figure 5.2.4 Molecular structure of L^{an}·2.25(H_2O). Non-H atoms are shown with 30% thermal ellipsoids.

5.2.2 Coordination chemistry of L^{an}

With the synthesis and the characterisation of the ligand complete, the coordination chemistry of the ligand with labile transition metal mono- and dications was studied. Previously in the Ward group, the structurally related ligands L$^{m\text{-}Ph}$ and L$^{2,6\text{-}Py}$ have been studied (see Figure 5.2.5, top).[12,13,19] These ligands from a range of structures when mixed with perchlorate or tetrafluorborate M(II) salts (where M = Co,

Ni or Zn), including M_4L_6 squares and M_6L_9 open-books, but both ligands form a M_8L_{12} cube when mixed with $Co(BF_4)_2$ (see Figure 5.2.5, bottom). It might be expected that similar complexes form when the structurally similar ligand $\mathbf{L^{an}}$ is mixed with the same metal salts.

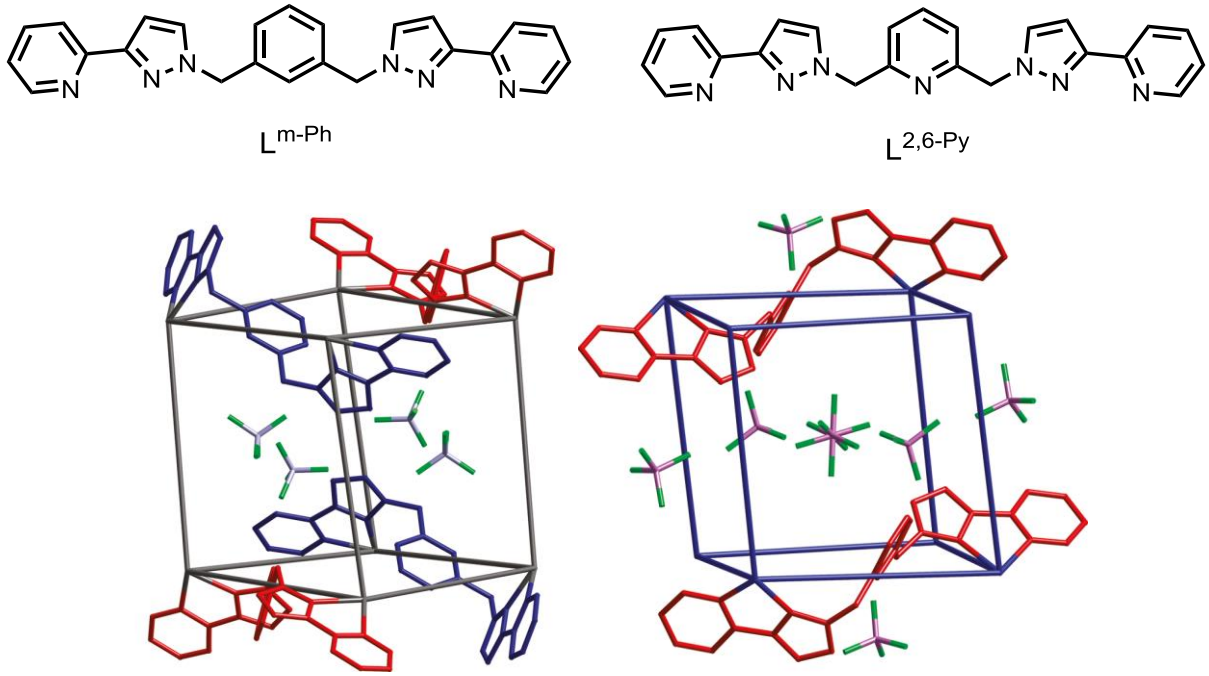

Figure 5.2.5 Ligands used previously by the Ward group with a meta-subsituted aromatic spacer, and the $[Co_8L_{12}](BF_4)_{16}$ cubic coordination cages that result from their reaction with $Co(BF_4)_2$. Reproduced with permission from Ref. 12. Copyright 2009 American Chemical Society.

Thus, reactions were set up with $M(BF_4)_2$ or $M(ClO_4)_2$ salts (where M = Cd, Co, Cu and Zn) and $\mathbf{L^{an}}$ in a 2 : 3 ratio in methanol and dichloromethane solution stirring at room temperature, and also with $Ag(PF_6)$ and $\mathbf{L^{an}}$ in a 1 : 1 ratio. After removing the solvent and washing the powders with methanol and dichloromethane, the reaction products were analysed by ^1H NMR and electrospray positive ionisation mode mass spectrometry (ESMS). Unfortunately, in most cases (M = Ag, Cd, Cu and Zn) the dominant product in solution as determined by ESMS was a mononuclear M_1L_1 complex and with $Co(BF_4)_2$ no product peaks were observed in the mass spectrum.

It has been reported previously that with the potentially pentadentate ligand L^{fur} (see Figure 5.1.3), Ag(I)[20] and Cd(II)[11] salts form mononuclear complexes in which the pyridyl-pyrazolyl termini form a tetradentate chelate around the metal ion, and the furan oxygen atom is inwardly directed towards the

metal ion providing a weak attractive interaction. For the Cd(II) complex, a fluorine atom from a tetrafluoroborate anion fills the vacant coordination site. It is possible that the ligand $\mathbf{L^{an}}$ is a good pentadentate ligand for large metal ions with less strict coordination environment preferences (e.g. Cd(II) and Ag(I)), with the aniline nitrogen also participating in weak attractive bonding to the metal ion. Of course, a crystal structure would help to confirm this hypothesis, but unfortunately no crystals of x-ray quality could be grown. In the case of Ag(I), the ^{1}H NMR spectrum in CD_3CN has a full set of resonances corresponding to a whole ligand environment (see Figure 5.2.6). Interestingly, there are two doublets (4.31 and 5.14 ppm) corresponding to one of the diastereotopic CH_2 groups, whereas the other CH_2 peak is obscured by one of the doublets (5.14 ppm). This observation, coupled with the full ligand environment observed in the ^{1}H NMR spectrum (*c.f.* half ligand environment for $[AgL^{fur}]^+$) suggests a different coordination mode than the expected tetradentate chelate (see Figure 5.2.7a). It may be possible that the ligand acts as a tridentate chelate *via* one of the PyPz termini and the aniline nitrogen, with a pendant uncooridnated PyPz arm (see Figure 5.2.7b). This binding mode would explain the inequivalence of the protons of one of the methylene groups and not the other, and this theory is further supported by the ESMS mass spectrum, which has a peak at *m/z* 684.9 corresponding to $[Ag_2(\mathbf{L^{an}})(NO_3)]^+$, in which a Ag(I) has coordinated to the pendant PyPz arm (see Figure 5.2.8).

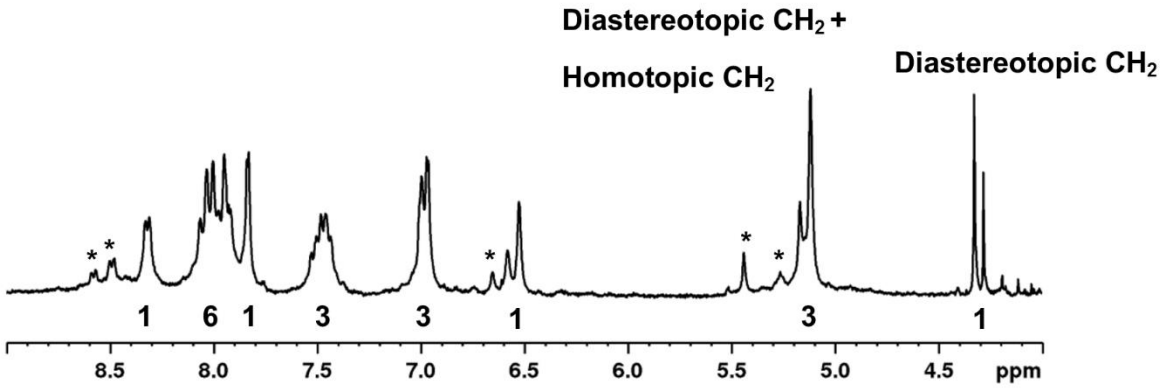

Figure 5.2.6 ^{1}H NMR (250 MHz, CD_3CN) spectrum of $[Ag\mathbf{L^{an}}](PF_6)$ (* = minor component associated with some rearrangement or dissociation in solution).

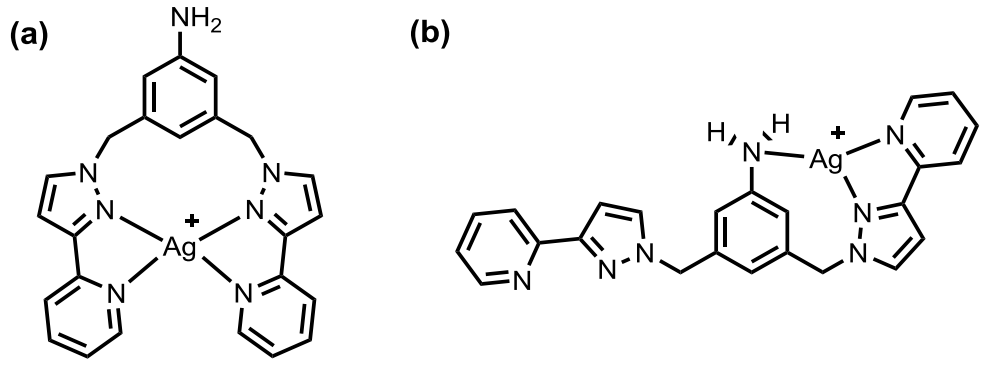

Figure 5.2.7 Two possible coordination modes of the ligand Lan with Ag(I): (a) expected tetradentate chelate, and; (b) tridentate chelate.

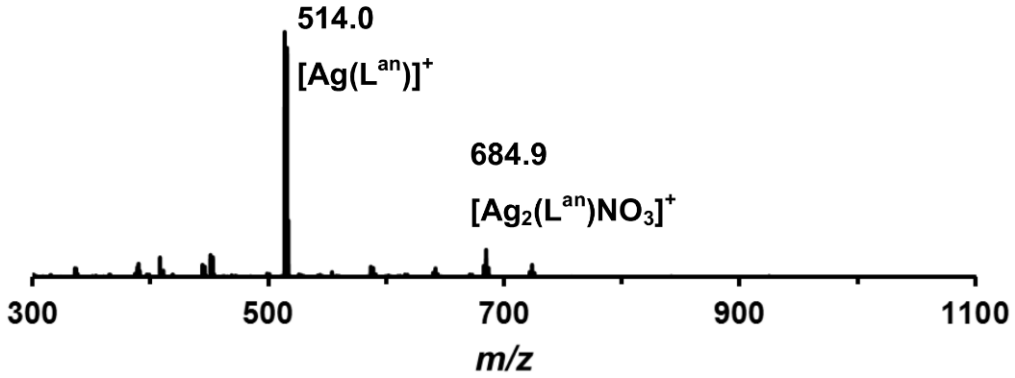

Figure 5.2.8 Electrospray mass spectrum of [Ag**L**^{an}](PF_6).

The combination of $Zn(ClO_4)_2$ and **L**^{an} gave a very complicated mixture of products. This was evidenced by the ESMS spectrum (see Figure 5.2.10), in which peaks are observed for the following species: M_1L_1, M_1L_2, M_2L_2, M_2L_3 and M_3L_3. The ^{1}H NMR spectrum recorded in CD_3CN was consistent with a mixture of different species, with a large number of poorly resolved peaks between 9.0 – 3.5 ppm (see Figure 5.2.11). Heating the sample to 60 ^{o}C and re-recording the spectrum after 1 or 2 days did not significantly change any of the peaks, and after 1 week of heating the product degraded and precipitated out of solution. It was clear, therefore, that a different strategy was necessary to form any type of coordination cage structure with the ligand **L**^{an}.

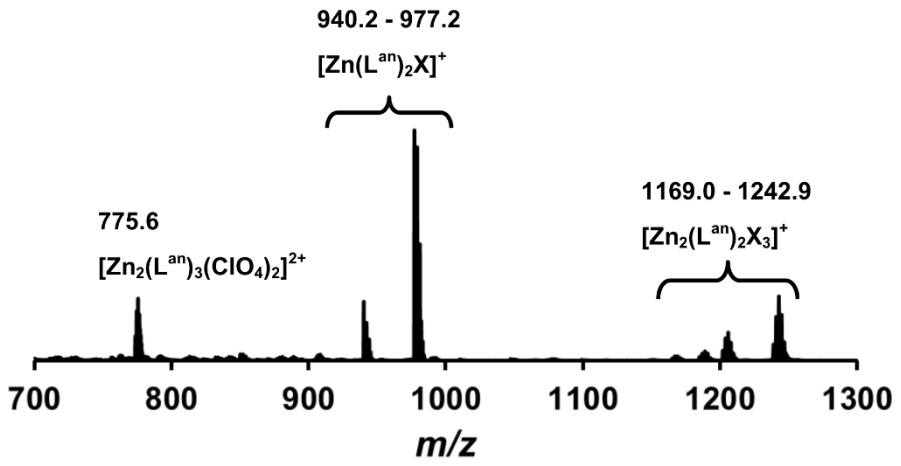

Figure 5.2.10 Partial electrospray mass spectrum of the product mixture arising from $Zn(ClO_4)_2$ and $\mathbf{L^{an}}$.

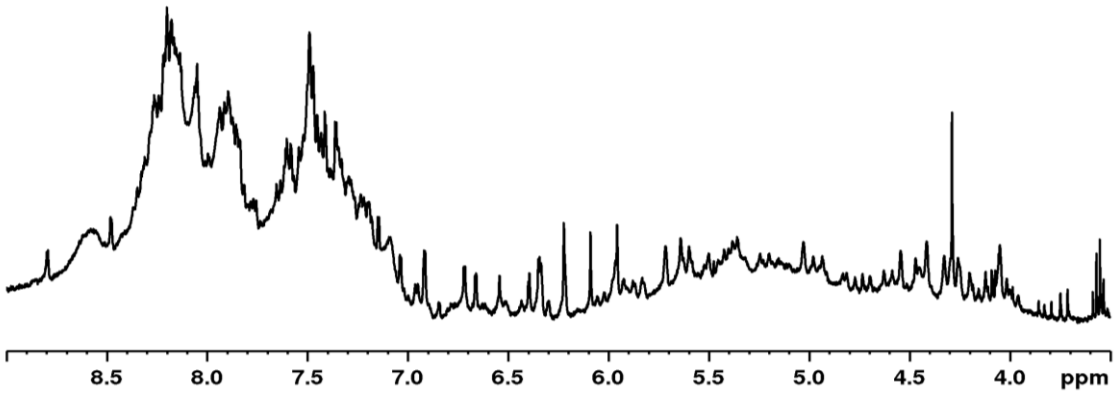

Figure 5.2.11 ^{1}H NMR (400 MHz, CD_3CN) spectrum of the product mixture arising from $Zn(ClO_4)_2$ and $\mathbf{L^{an}}$.

The complexation reactions were repeated, but this time using a solvothermal method in which a mixture of the ligand $\mathbf{L^{an}}$ and the appropriate transition metal salt were mixed in a 3 : 2 ratio in methanol and then transferred to a Teflon lined autoclave. The autoclave was then heated to 100 ^oC for 12 hours and then slowly cooled to room temperature. This method can sometimes allow the recrystallization of the product, with the possibility of X-ray quality crystals being formed. Unfortunately, again in most cases only mononuclear complexes were formed, with the product precipitating out of solution as a powder. However, with the reaction of $Co(BF_4)_2$ and $\mathbf{L^{an}}$, a positive result was observed. Small pink crystals had been formed during the slow cooling, which analysed as $[Co_8\mathbf{L^{an}}_{12}][BF_4]_{16}$ by ESMS (see Figure 5.2.12). The mass spectrum displayed a pleasing series of peaks for sequential loss of tetrafluoroborate anions from the complete complex, a commonly seen characteristic of cages of this

type.[5] High-resolution mass spectrometry analysis performed on an Orbitrap mass spectrometer confirmed the charge spacings of these peaks; the 5+ peak is shown below (see Figure 5.2.13).

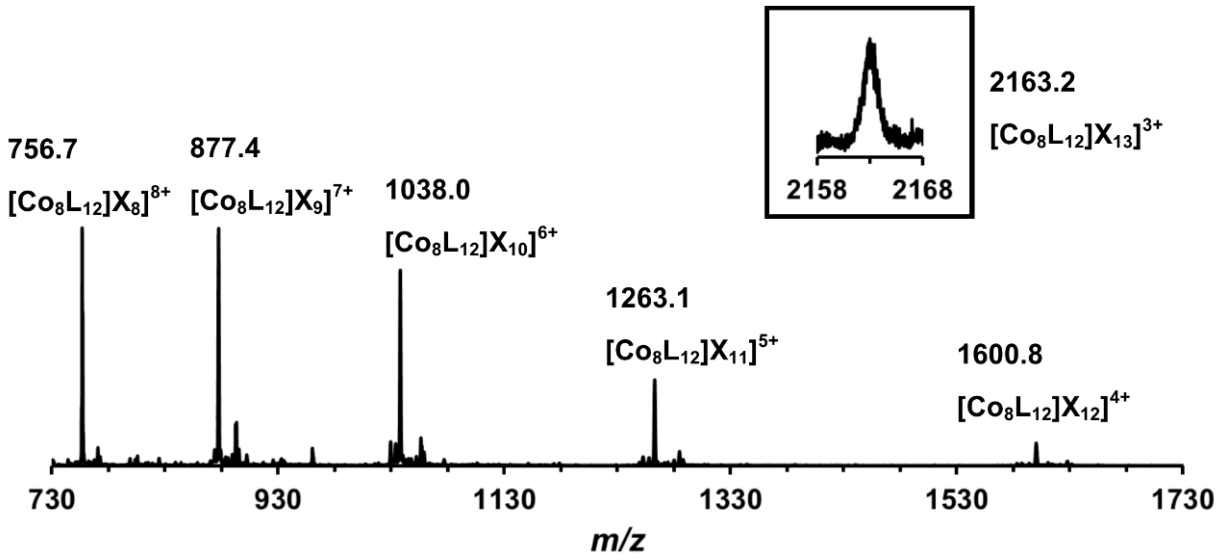

Figure 5.2.12 Electrospray mass spectrum of $[Co_8\mathbf{L}^{an}_{12}][BF_4]_{16}$ showing a sequence of peaks corresponding to $[Co_8\mathbf{L}^{an}_{12}(BF_4)_{16-z}]^{z+}$, i.e. loss of 3–8 tetrafluoroborate anions from the complete complex.

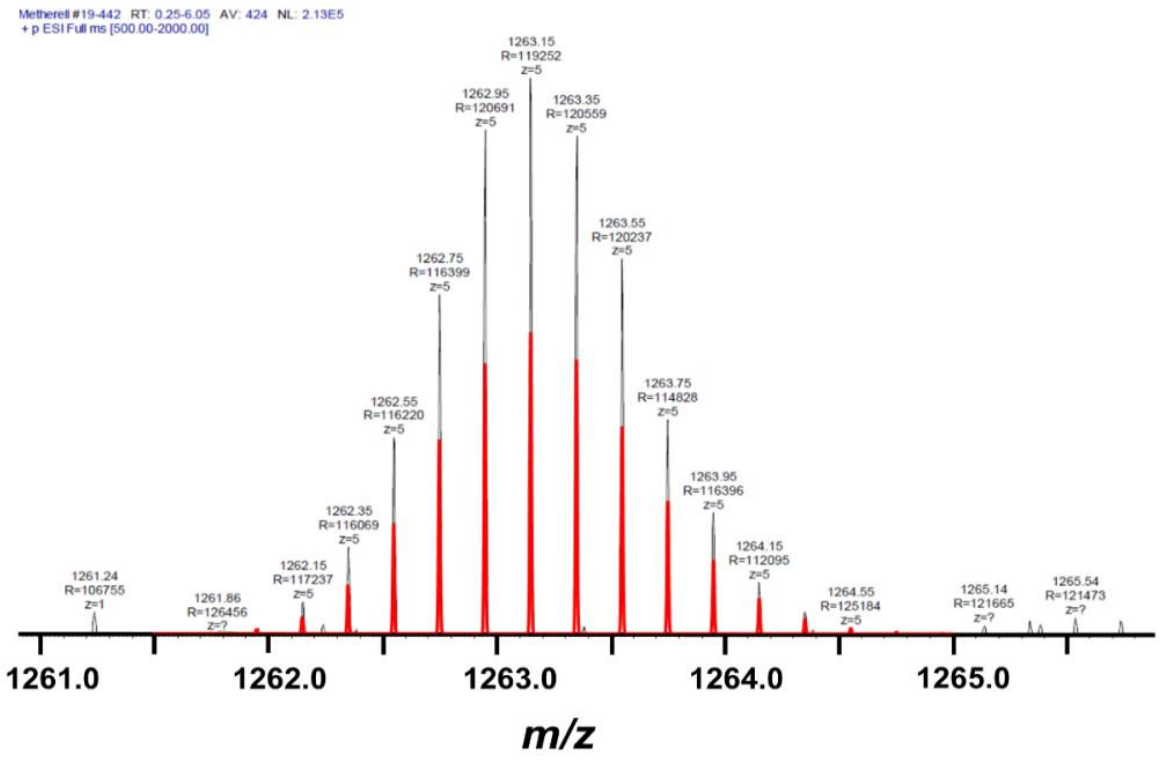

Figure 5.2.13 Expansions of high-resolution ESMS+ mass spectra of redissolved crystals of $[Co_8\mathbf{L}^{an}_{12}][BF_4]_{16}$, showing theoretical (red) and experimental (grey) isotope patterns and accurate masses for the 5+ peak cluster.

The paramagnetic ^{1}H NMR spectrum of the pink crystals, however, is not perfectly clean (see Figure 5.2.14). There is a clear main series of peaks in which 41 different peaks can be identified (as indicated by peaks marked with an asterisk, *), one peak short of the 42 required for two inequivalent ligand environments; the other peak is presumably hidden under the solvent peak or is too broad to identify. The smaller peaks are due to a minor component associated with some rearrangement or dissociation in solution. Two observed ligand environments is consistent with the formation of a $Co_8(\mathbf{L}^{an})_{12}$ cube, provided the metal geometries within the cage are identical to those seen in the $Co_8(L^{m\text{-}Ph})_{12}$ and $Co_8(L^{2,6\text{-}Py})_{12}$ cubes (see Figure 5.2.15).[12,13,19] Two of the metal centres at opposite vertices have *fac* tris chelate geometry [Co(3)/Co(3A) in Figure 5.2.15], whereas the other six metals have *mer* tris chelate geometry. The four metal centres labelled with an 'A' have opposite optical configuration to those without the label; consequently, there is an inversion centre in the centre of the cage, which results in overall S_6 geometry, and therefore two inequivalent ligand environments. A crystal structure would prove this rationalisation of the ^{1}H NMR spectrum, and also provide information as to whether the amine groups are directed exohedrally or endohedrally. However, no X-ray quality crystals could be grown despite repeated attempts.

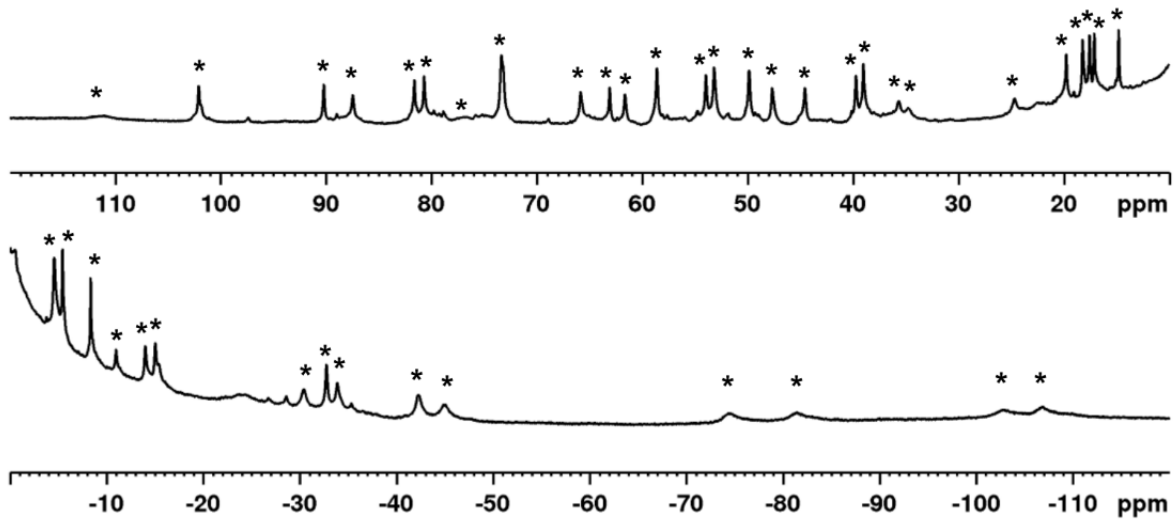

Figure 5.2.14 Paramagnetic ^{1}H NMR (400 MHz, CD_3NO_2) spectrum of $[Co_8\mathbf{L}^{an}_{12}][BF_4]_{16}$. Signals that can be clearly identified are denoted by an asterisk, *; 41 of the expected 42 signals can be located.

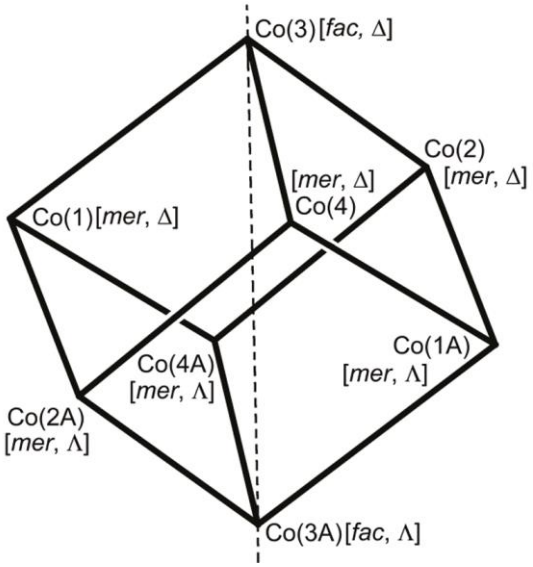

Figure 5.2.15 A sketch showing the expected symmetry of the $[Co_8\mathbf{L}^{an}{}_{12}][BF_4]_{16}$ cage cation with the C_3/S_6 axis shown as a dotted line. Reproduced with permission from Ref. 12. Copyright 2009 American Chemical Society.

5.2.3 Functionalisation of the aniline group with a catecholamide

With good evidence for the formation of an amine decorated $[Co_8\mathbf{L}^{an}{}_{12}][BF_4]_{16}$ cube, efforts were directed to forming exo-functionalised cubic cages. Based on the similarity of the synthesis of the ligand $\mathbf{L}^{an}$ with the unsymmetrical ligands seen in Chapter 4,[16] the first effort at forming cages with external functionality was by the introduction of catecholamide groups at the aniline position.

The synthesis of the three-armed ligand $\mathbf{H_2L}^{TRI}$ was essentially analogous to the last two steps in the syntheses of the ligands in Chapter 4 (see Figure 5.2.16). Starting from the amine $\mathbf{L}^{an}$, the protected catecholamide **22** was formed *via* a routine amide condensation reaction with the acid chloride **5**. Deprotection of the methyl ether groups was achieved by reaction BBr_3 in DCM, followed by solvolysis in boiling water. The ligand $\mathbf{H_2L}^{TRI}$ was ultimately isolated as an off-white solid, with an elemental analysis result consistent with 2.75 HBr molecules per ligand. The ^{1}H NMR spectrum (400 MHz, MeOD) of the ligand could be fully assigned on the basis of a 2D COSY spectrum (see Figure 5.2.17 and 5.2.18). It is worth noting that the assignment is facilitated by the presence of a set of peaks with double the intensity of the others, as these correspond to the two equivalent PyPz arms.

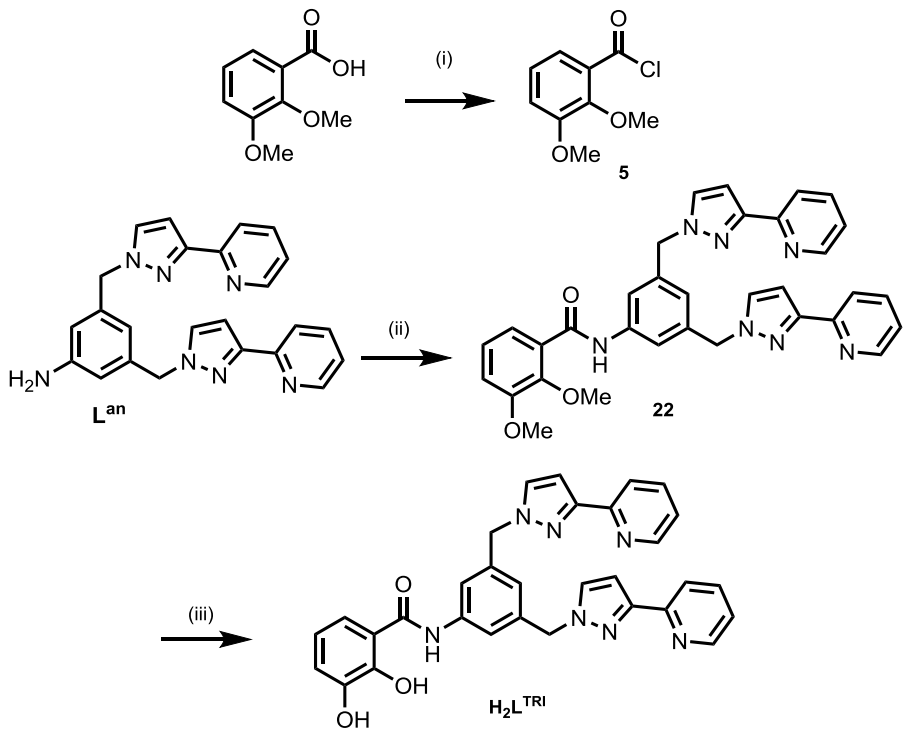

Figure 5.2.16 Reaction scheme for the preparation of $\mathbf{H_2L^{TRI}}$. (i) a. $SOCl_2$, dmf; (ii) **5**, DCM, Et_3N; (iii) BBr_3, DCM, H_2O.

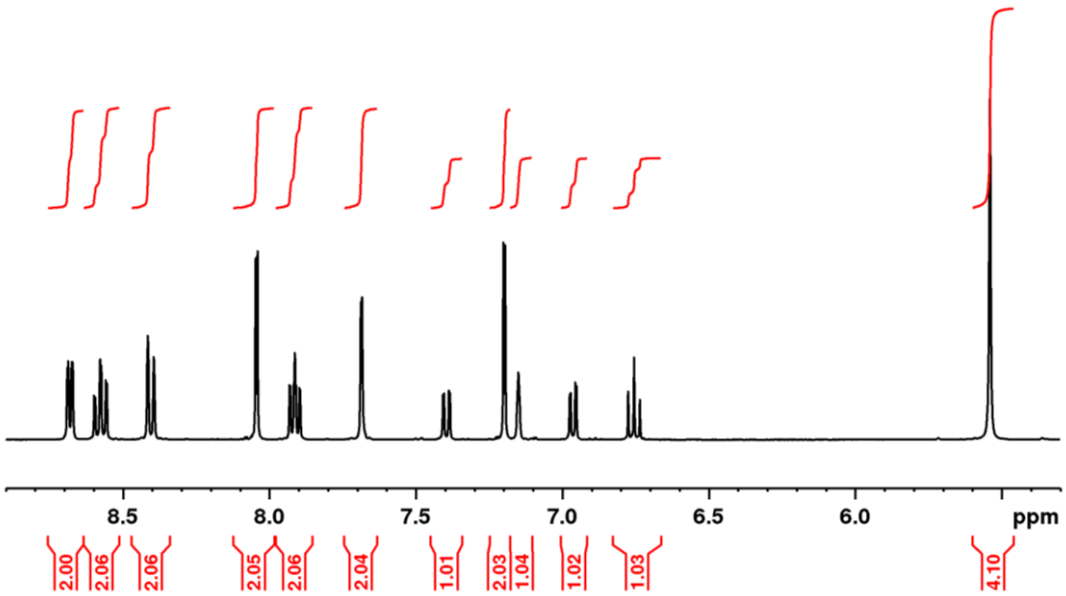

Figure 5.2.17 Full ^1H NMR (400 MHz, CD_3OD) spectrum of H_2L^{TRI}.

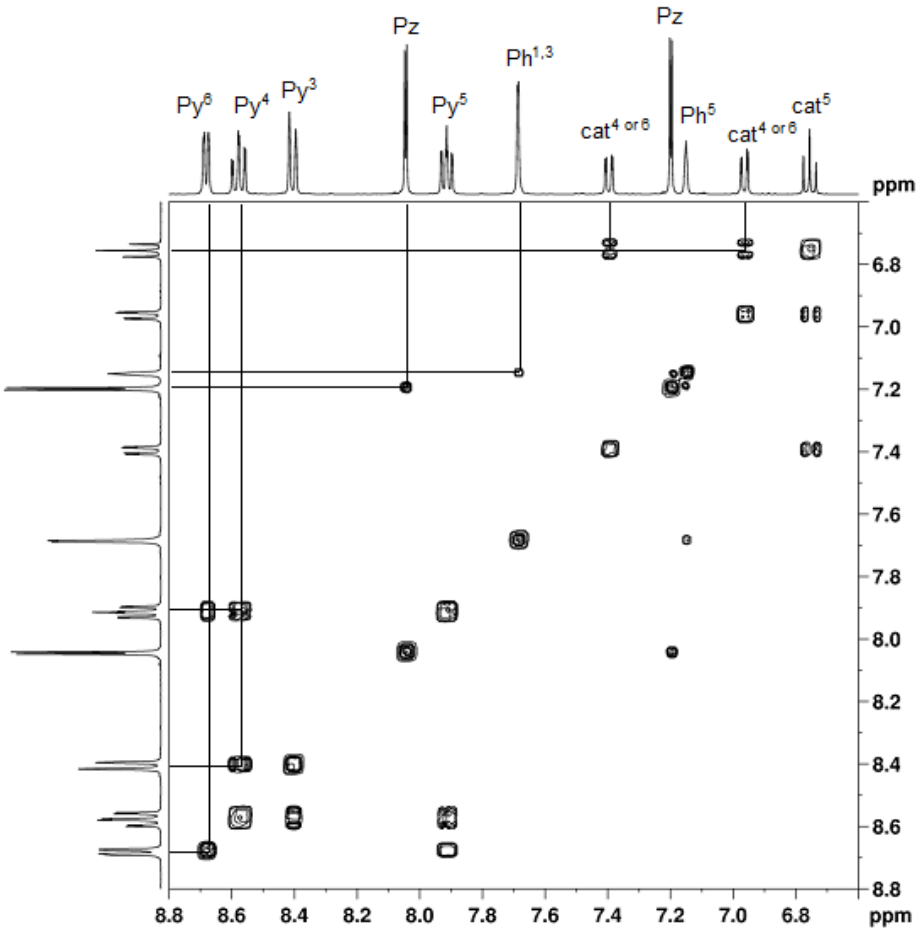

Figure 5.2.18 Part of the ^{1}H COSY NMR (400 MHz, MeOD) spectrum of H_2L^{TRI}.2.75HBr **,** showing the full assignment of the aromatic region. Py = pyridine, Pz = pyrazole, Ph = phenyl, cat = catechol.

Like the ligands in Chapter 4, $\mathbf{H_2L^{TRI}}$ possesses both hard and soft binding sites. Unlike the previously seen bis-bidentate ligands, the new tritopic ligand has the potential to form coordination cages in two distinct ways when mixed with octahedral hard and soft metal ions. The first is with all the hard and soft metal ions defining the vertices of a heterometallic cage. As the ligand has 4 nitrogen donor atoms and 2 oxygen donor atoms, this would necessarily lead to a cage formulation of $[M^{H}_{n}M^{S}_{2n}\mathbf{L^{TRI}}_{3n}]^{n+}$ (where M^{H} is a hard metal and M^{S} a soft metal), providing the hard metal ion is octahedrally coordinated to 6 oxygen atoms, and the soft metal ion is octahedrally coordinated to 6 nitrogen atoms (see Figure 5.2.19). It should be noted that a cage of this type could also form with mixed N/O donor vertices if there is no distinct coordination preference for either metal. The second way a coordination cage could be formed with the ligand $\mathbf{H_2L^{TRI}}$ is by only the soft metals (i.e. those bound to the PyPz termini) defining the cage vertices of a homonuclear cage, such as the M_8L_{12} cubes seen above. The catechol

termini would be pendant groups of this cage, and will thus provide binding sites for hard metal ions external to the cage.

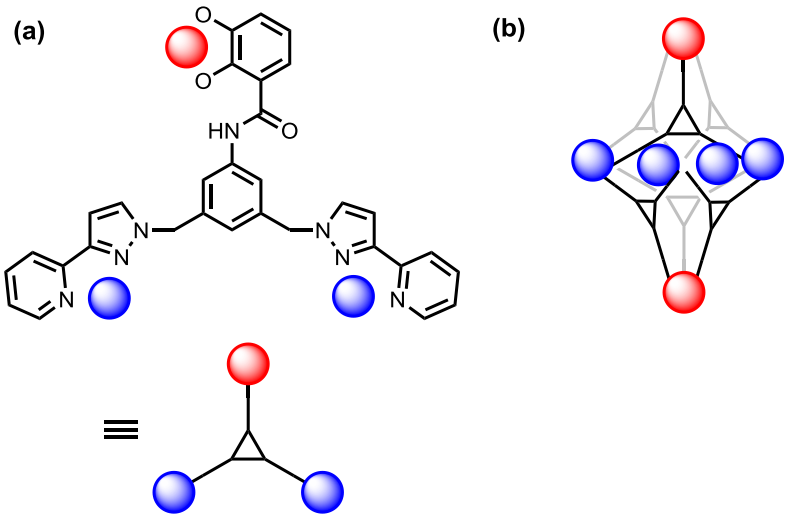

Figure 5.2.19 (a) Schematic representation of the ligand $(\mathbf{L}^{\mathbf{TRI}})^{2-}$ coordinating to a hard metal ion M^H and two soft metal ions M^S (denoted by red and blue spheres, respectively), and; (b) Sketch showing one possible cage topology based on this coordination mode with the formulation $[M^H_2M^S_4(\mathbf{L}^{\mathbf{TRI}})_6]^{2+}$.

Based on its use in the formation of catecholamide cages by Raymond and co-workers, $Ga(acac)_3$ was used as the source of hard metals in a complexation reaction.[21] Reaction of $\mathbf{H_2L^{TRI}}$ with $Ga(acac)_3$ and $Co(BF_4)_2$ in a 3 : 1 : 2 ratio in methanol with 6 equivalents of potassium hydroxide could theoretically lead to a structure of the type $[Ga_nCo_{2n}L_{3n}]^{n+}$, in which all Ga(III) ions are octahedrally coordinated to three catecholates, and the Co(II) ions are coordinated to three PyPz units. The beige precipitate collected from the reaction was analysed by ESMS and appears to suggest the formation of a similar but different complex type (see Figure 5.2.20). The two most intense peaks above *m/z* 500 can be assigned to different charge states of the complex cation $[GaCo_3(L^{TRI})_4]^{4+}$, in which all cobalt atoms would exist as Co(III) ions in an N_4O_2 donor environment, a coordination environment it is known to adopt.[22] The Ga(III) ions would also have to exist in an N_4O_2 donor environment, but there are examples when it has adopted a N_3O_3 donor environment.[23]

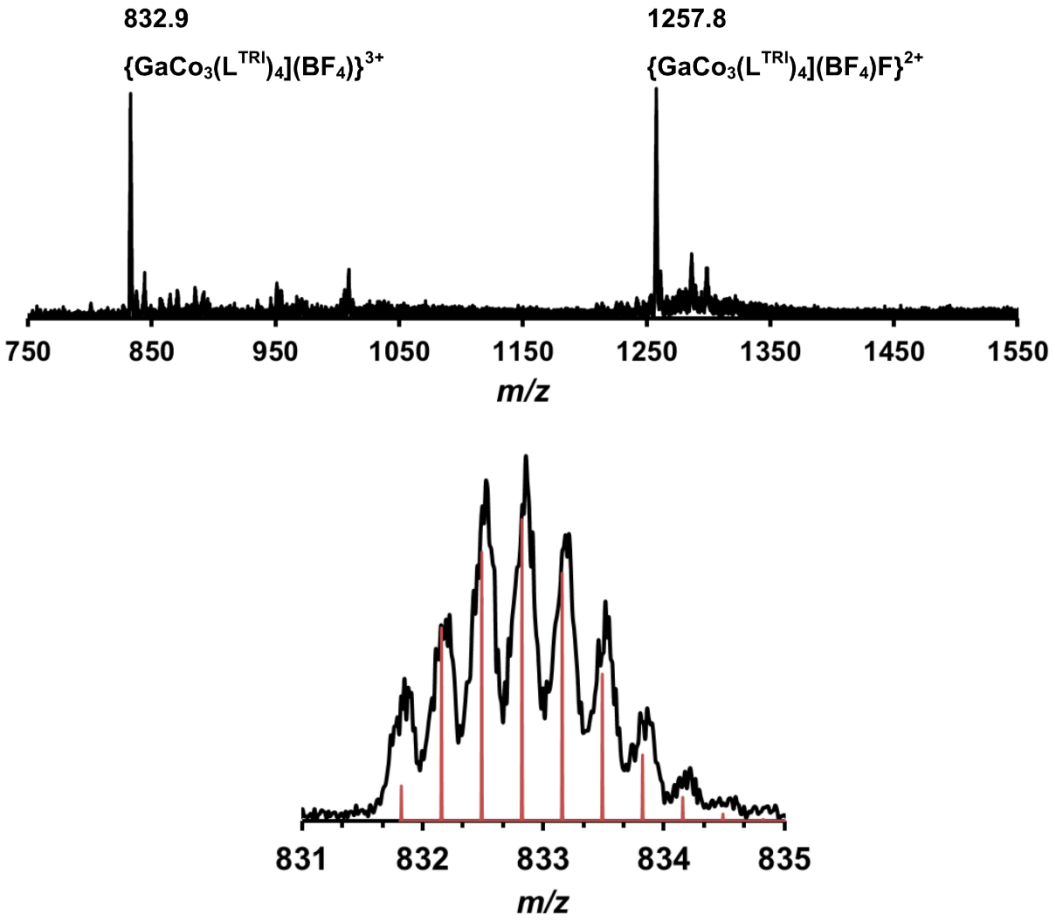

Figure 5.2.20 Top: Part of the electrospray mass spectrum of $([GaCo_3(L^{TRI})_4](BF_4))^{3+}$. Bottom: An expansion of the ESMS peak attributable to $([GaCo_3(L^{TRI})_4](BF_4))^{3+}$ (black), and the theoretical peak shape (red).

The peak at *m/z* 833 can be attributed to $([GaCo_3(L^{TRI})_4](BF_4))^{3+}$, in which the tetrafluoroborate anion may reside in the cavity of the presumably tetrahedral complex cation. This assignment correlates well with the predicted peak shape (see Figure 5.2.20, bottom). This peak is accompanied by a less intense peak at *m/z* 838 in which the tetrafluoroborate anion is substituted for an acetylacetonate anion. A peak at *m/z* 1258 could be attributable to $([GaCo_3(L^{TRI})_4](BF_4)F)^{2+}$, as there are many examples of the abstraction of fluoride ions from the tetrafluoroborate anion.[24-26] No crystals could be grown in order to confirm the structure of the complex, and NMR analysis was inconclusive.

A synthesis was attempted with 3 equivalents of $Ti(O^iPr)_4$ and 1 equivalent of ligand $\mathbf{H_2L^{TRI}}$ with excess Cs_2CO_3 in order to preform the $[Ti(\mathbf{L^{TRI}})_3]^{2-}$ component, in a method similar to those used by Shionoya and Raymond.[27,28] A yellow powder was isolated which gave a very clean ESMS mass

spectrum consistent with the formation of $Cs_2[Ti(\mathbf{L}^{TRI})_3]$ (see Figure 5.2.21), with the only major peak corresponding to $[Ti(\mathbf{L}^{TRI})_3]^{2-}$ (*m/z* 837.3). The ^{1}H NMR spectrum revealed that the ligand still possessed C_2 symmetry; the PyPz arms are still equivalent even when the catecholate is coordinated to a metal centre. Unfortunately the spectrum revealed impurities which could not be removed by washing with methanol, precluding detailed analysis. Even more disappointingly, reaction of the preformed $Cs_2[Ti(\mathbf{L}^{TRI})_3]$ component with $Cd(ClO_4)_2$ did not result in the formation of any cages which could be detected by ESMS.

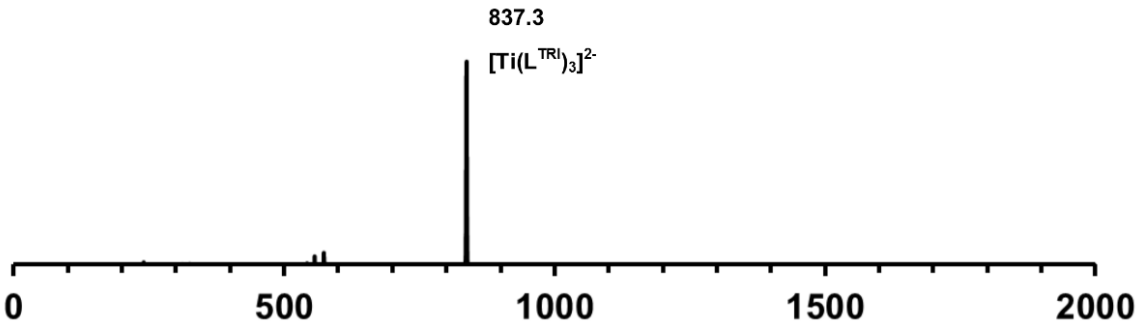

Figure 5.2.21 Electrospray mass spectrum of $Cs_2[Ti(\mathbf{L}^{TRI})_3]$.

5.2.4 Functionalisation of the aniline group with ferrocene

As the attempted introduction of catechol groups to the exterior of coordination cages had been unsuccessful, a simpler method to introduce functionality to the exterior of a M_8L_{12} cube was sought. Ferrocene was identified as a candidate for this purpose, as it can be easily introduced *via* its carboxylic acid derivative and also provides the potential for redox active cage behaviour. The synthesis of the ligand $\mathbf{L}^{Fc}$ was achieved simply by reacting $\mathbf{L}^{an}$ in dichloromethane in triethylamine with the acid chloride **23**, which was easily prepared from ferrocenecarboxylic acid and oxalyl chloride in dichloromethane (see Figure 5.2.22). After purification by column chromatography on alumina, the new ligand was determined to be pure by ESMS and ^{1}H NMR spectroscopy (see Figure 5.2.23).

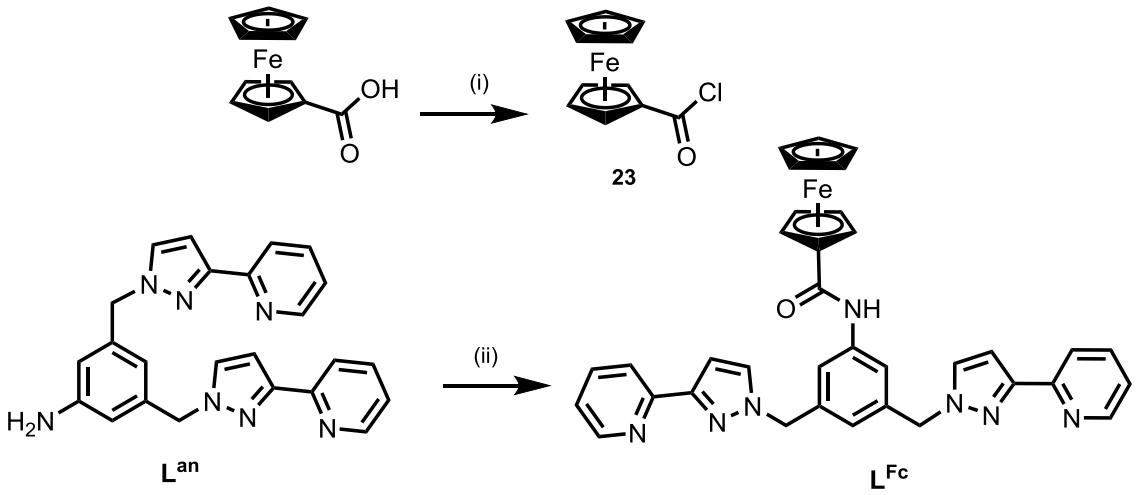

Figure 5.2.22 Reaction scheme for the preparation of $\mathbf{L^{Fc}}$. (i) $(COCl)_2$, DCM; (ii) **23**, DCM, Et_3N.

Reaction of 3 equivalents of $\mathbf{L^{Fc}}$ with 2 equivalents of $Co(BF_4)_2$ in methanol and dichloromethane resulted in the formation of an orange powder. After washing with methanol, the powder was analysed by ESMS and ^{1}H NMR spectroscopy to give some results that might seem quite surprising. Whereas with the parent ligand $\mathbf{L^{an}}$ a M_8L_{12} cubic coordination cage was determined to be the major product, it was apparent that this was not the major product in this instance; instead, a M_6L_9 assembly dominates the electrospray mass spectrum (see Figure 5.2.24). Peaks at m/z 2237.1, 1655.4, 1307.6 and 1057.5 correspond to the loss of 3-6 anions, respectively, from the complete complex $[Co_6\mathbf{L^{Fc}}_9][BF_4]_{12}$. A peak at *m/z* 1575.5 corresponds to $[Co_2\mathbf{L^{Fc}}_2(BF_4)_2(CHO_2)]^+$, as confirmed by the isotope pattern, and is presumably a fragmentation product arising from the addition of formic acid during the mass spectrum preparation. The paramagnetic ^{1}H NMR spectrum is quite poorly resolved (see Figure 5.2.25), but it is clear that it is more complicated than the spectrum of the $M_8\mathbf{L^{an}}_{12}$ cube (see Figure 5.2.14). These two observations can be rationalised based on previous results in the Ward group.[12]

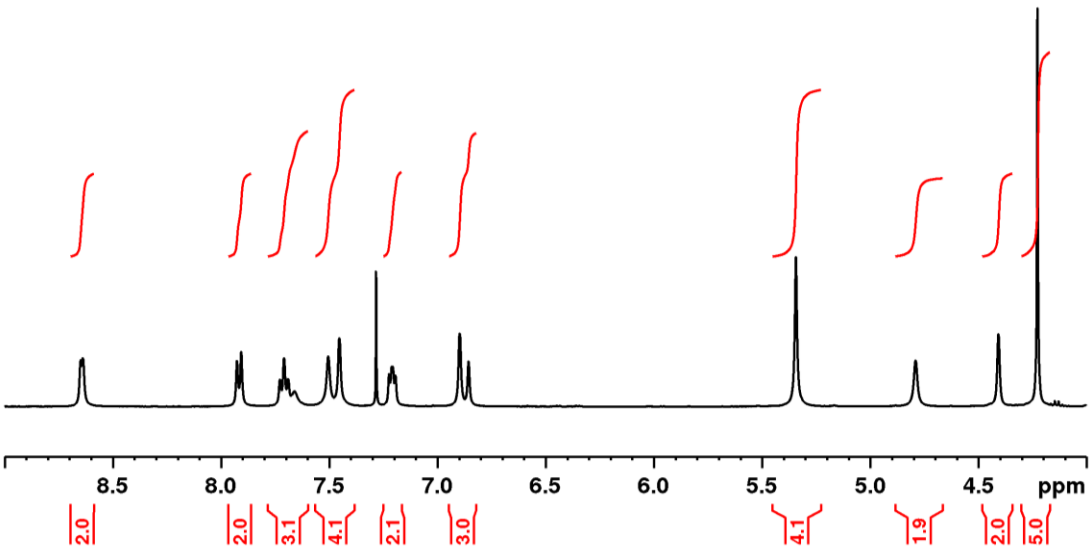

Figure 5.2.23 ^{1}H NMR (400 MHz, $CDCl_3$) spectrum of $\mathbf{L^{Fc}}$.

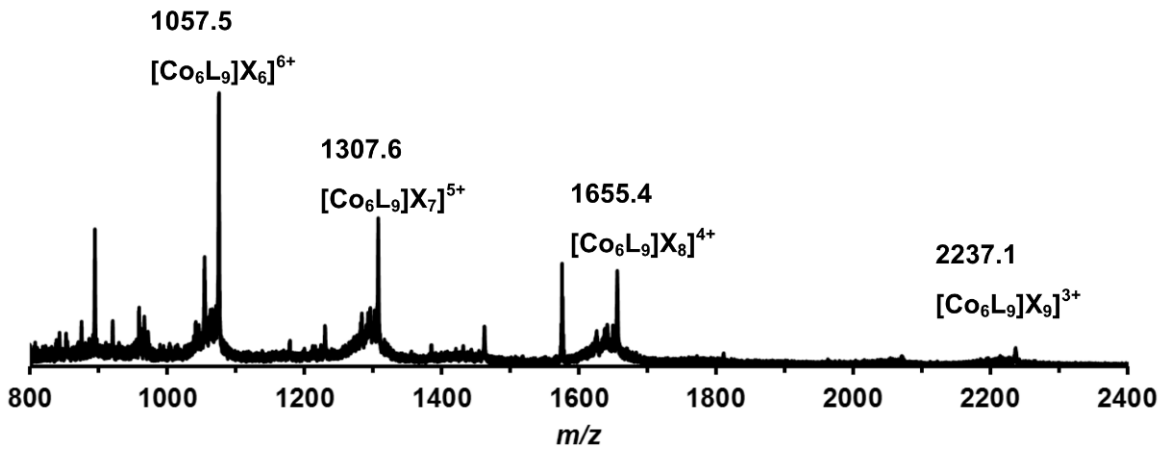

Figure 5.2.24 Electrospray mass spectrum of $[Co_6\mathbf{L^{Fc}}_9][BF_4]_{12}$ showing a sequence of peaks corresponding to $[Co_6\mathbf{L^{Fc}}_9(BF_4)_{12-z}]^{z+}$, i.e. loss of 3–6 tetrafluoroborate anions from the complete complex.

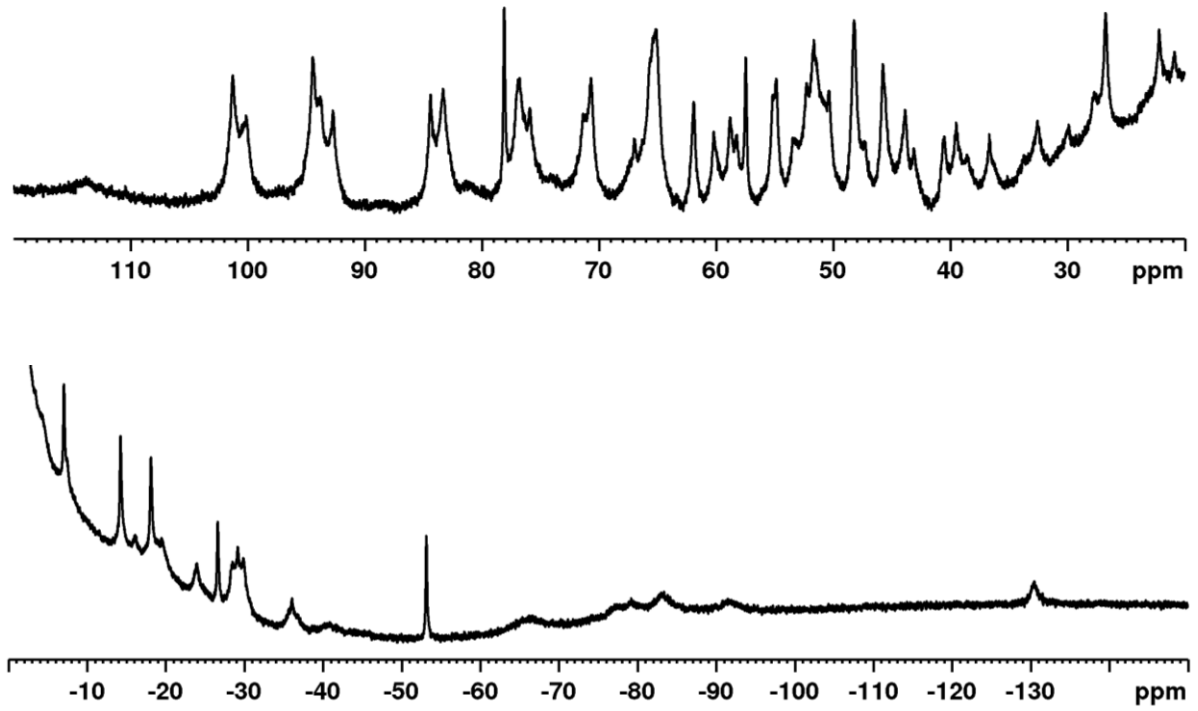

Figure 5.2.25 Paramagnetic ^{1}H NMR (400 MHz, CD_3NO_2) spectrum of $[Co_6\mathbf{L}^{\mathbf{Fc}}{}_9][BF_4]_{12}$.

It was found in earlier work[12] that the M_8L_{12} cubic and M_6L_9 open-book structures can interconvert readily, even through use of different anions of the same charge and shape with the same metal cation; the two assemblies are clearly of very similar energy. Therefore, it might be not surprising that adding a bulky ferrocenyl group to the ligand causes a different structure to be formed, due to the change in sterics of the ligand packing in the cage structures. It is likely that the $Co_6\mathbf{L}^{\mathbf{Fc}}{}_9$ assembly is indeed the open-book assembly as seen with $L^{m\text{-}Ph}$ and $L^{2,6\text{-}Py}$, and not the trigonal prism also reported within the Ward group.[12, 29] This is on the basis of the paramagnetic ^{1}H NMR spectrum; the open-book structure requires 4.5 inequivalent ligand environments, whereas the trigonal prism requires 1.5 ligand environments. Although the ^{1}H NMR spectrum is quite poorly resolved, it is apparent that there are far more than the 30 paramagnetically shifted peaks required for the trigonal prism.

5.3 Conclusion

A general synthetic route for a family of amide-substituted ligands based on a meta-phenylene spacer has been designed, *via* the parent aniline ligand $\mathbf{L^{an}}$. The ligand $\mathbf{L^{an}}$ can be prepared in 5 steps in an overall 17 % yield from readily available starting materials. A range of functionality can be introduced to the ligand by simple amide condensation reactions with an appropriate acid chloride. This will enable the exterior functionalisation of coordination cages, thus improving their practical use. The ligand $\mathbf{L^{an}}$ reacts with $Co(BF_4)_2$ to give a M_8L_{12} (presumably) cubic coordination cage, whereas the ferrocenyl substituted ligand $\mathbf{L^{Fc}}$ reacts with $Co(BF_4)_2$ to give a M_6L_9 (presumably) open-book assembly. Based on previous work in the group, the two types of framework are likely to be of very similar energy to each other, and can even interconvert in solution. This work suggests that a better starting point for exo-functionalised coordination cages would be from ligands that tend to give only one type of cage structure.

5.4 Experimental

5.4.1 Ligand synthesis

3-(2-Pyridyl)pyrazole was used as prepared.[30] Dry dichloromethane was obtained by distillation over calcium hydride.

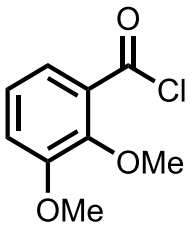

Synthesis of 5

2,3-Dimethoxybenzoic acid (4.70 g, 25.8 mmol), $SOCl_2$ (7 cm^3, 96.5 mmol) and a drop of DMF were heated to reflux with stirring for 6 h. The condenser was fitted with a $CaCl_2$ drying tube to absorb liberated SO_2 and HCl. The resultant clear yellow solution was diluted with $CHCl_3$ and reduced to

dryness three times. Drying under high vacuum yielded **5** as an off white solid, which was used without any further purification, assuming quantitative yield (Yield: 5.10 g, 99 %). ^{1}H-NMR (250 MHz, $CDCl_3$): δ 7.55 (1H, dd; Ar-H), 7.20-7.15 (2H, m; Ar-H), 3.94 (3H, s; OMe), 3.92 (3H, s; OMe). EIMS *m/z* 224 $[M + Na]^+$, 165 $[M - Cl^-]^+$. Data is in accordance with the literature.[31]

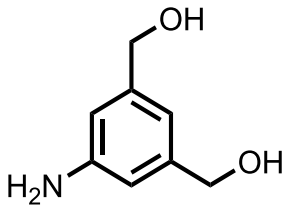

Synthesis of 18

A solution of dimethyl 5-aminoisophthalate (5.0 g, 23.9 mmol) in dry THF (90 cm^3) was maintained at 0 °C in an N_2 atmosphere. To this was added $LiAlH_4$ (2.4 M in THF, 60 cm^3, 144 mmol, 6 eq) by disposable plastic syringe. A colour change from yellow to green and finally to purple was observed. After stirring for 1 h at 0 °C, the mixture was heated to reflux overnight. The following day, the resultant white solution was cooled to 0 °C and quenched by the slow addition of aqueous KOH (20%, 25 cm^3) and then diluted with EtOAc (200 cm^3). The cream solution was filtered through celite and rinsed with EtOAc. The resultant yellow solution was evaporated to dryness under reduced pressure before purification by column chromatography on silica. Elution with EtOAc → 10 % MeOH/EtOAc and collection of the 2nd fraction (R_f = 0.21 in EtOAc) yielded **18** as a pale yellow solid (Yield: 1.30 g, 8.5 mmol, 36 %). ^{1}H-NMR (400 MHz, MeOD): δ 6.71 (1H, s; ArH), 6.66 (2H, s; ArH), 4.51 (4H, s; CH_2). ESMS: *m/z* 154 $[M + H]^+$; Data is in accordance with the literature.[17]

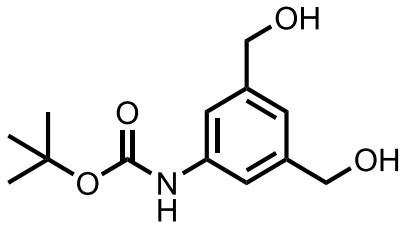

Synthesis of 19

A mixture of **18** (1.30 g, 8.5 mmol) and di-*tert*-butyl dicarbonate (1.88 g, 8.6 mmol) was stirred in THF (50 cm^3) at 25 ^oC for 2 days. The solvent was removed under reduced pressure before purification of the crude brown oil by column chromatography on silica. Elution with ethyl acetate (R_f = 0.60) yielded **19** as a white solid (Yield: 1.60 g, 6.3 mmol, 74 %). ^{1}H-NMR (250 MHz, MeOD): δ 7.33 (2H, s; ArH), 7.03 (1H, s; ArH), 4.58 (4H, s; CH_2), 1.53 (9H, s; ^{t}Bu). ESMS: *m/z* 262 $[M - H]^-$; Found: C, 61.77; H, 7.55; N, 5.46 %. Required for $C_{13}H_{19}NO_4$: C, 61.64; H, 7.56; N, 5.53 %. Data is in accordance with the literature.[18]

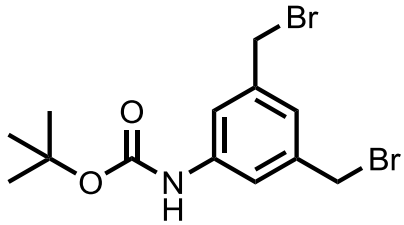

Synthesis of 20

To a solution of **19** (1.37 g, 5.4 mmol) in dry THF (20 cm^3) under an atmosphere of N_2 was added PPh_3 (3.51 g, 13.4 mmol) and CBr_4 (4.56 g, 13.8 mmol) sequentially. A white precipitate quickly formed from the initially clear solution, and the mixture was stired at room temperature for 2 h. The solvent was removed under reduced pressure before purification of the crude residue by column chromatography on silica. Elution with DCM/ hexane (40:60, R_f = 0.16) yielded **20** as a white solid (Yield: 1.89 g, 5.0 mmol, 92 %). ^{1}H-NMR (400 MHz, $CDCl_3$): δ 7.39 (2H, s; ArH), 7.11 (1H, s; ArH), 6.54 (1H, bs; NH), 4.45 (4H, s; CH_2), 1.54 (9H, s; ^{t}Bu). ESMS: *m/z* 378 $[M - H]^-$; Data is in accordance with the literature.[18]

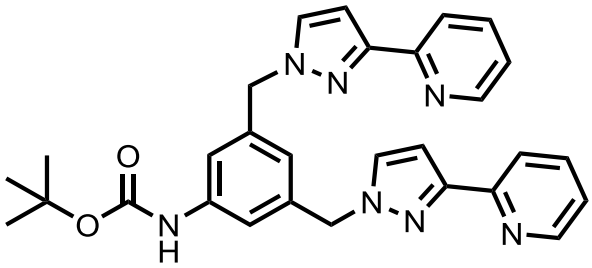

Synthesis of 21

A mixture of **20** (1.88 g, 5.0 mmol), 3-(2-pyridyl)pyrazole (1.54 g, 10.6 mmol), THF (50 cm^3) and aqueous NaOH (17.5 M, 6 cm^3) was stirred at 75 ^oC for 3 days. The organic layer was separated, dried over $MgSO_4$ and concentrated before purification by column chromatography on silica. Elution with EtOAc/ DCM (4:1) → 100% EtOAc yielded two fractions. The first fraction collected yielded **21** as an off-white solid (R_f = 0.51 in EtOAc, yield: 1.78 g, 3.5 mmol, 70 %), and the second fraction yielded the Boc-deprotected **22** as an off-white solid (R_f = 0.14 in EtOAc, yield: 0.41 g, 1.0 mmol, 20 %; total yield 90 %). ^{1}H-NMR (400 MHz, $CDCl_3$): δ 8.57 (2H, ddd, *J* = 5.0, 1.9, 1.0 Hz; pyridyl H^6), 7.87 (2H, dt, *J* = 7.8, 1.0 Hz; pyridyl H^3), 7.63 (2H, td, *J* = 7.8, 1.8 Hz; pyridyl H^4), 7.37 (1H, s; ArH), 7.35 (2H, d, *J* = 2.3 Hz; pyrazolyl H^5), 7.20 (2H, s; ArH), 7.14 (2H, ddd, *J* = 7.4, 4.9, 1.1 Hz; pyridyl H^5), 6.84 (2H, d, *J* = 2.3 Hz; pyrazolyl H^4), 6.71 (1H, bs; NH), 5.22 (4H, s; CH_2), 1.41 (9H, s; ^{t}Bu). ESMS: *m/z* 530 $[M + Na]^+$, 508 $[M + H]^+$, 452 $[M - {}^tBu^+, + 2H]^+$, 255 $[M + 2H]^{2+}$, 227 $[M - {}^tBu^+, + 3H]^{2+}$.

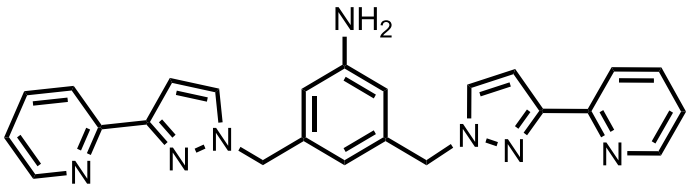

Synthesis of L^{an}

To a solution of **21** (1.78 g, 3.5 mmol) in DCM (10 cm^3) was added TFA (10 cm^3) and the resultant clear yellow solution was stirred at 25 ^oC for 14 h. The solvent was removed *in vacuo* and the clear brown oil was repeatedly washed with DCM/ MeOH (1:1) and evaporated to dryness in order to remove

all traces of TFA. The brown solid was washed with an aqueous solution of K_2CO_3 (2M) and the organic layer extracted with DCM, dried over $MgSO_4$ and evaporated to dryness, yielding **L^{an}** as a white solid (Yield: 1.13 g, 79 %). ^{1}H-NMR (400 MHz, $CDCl_3$): δ 8.62 (2H, ddd, *J* = 5.0, 1.9, 1.0 Hz; pyridyl H^6), 7.92 (2H, dt, *J* = 8.0, 1.0 Hz; pyridyl H^3), 7.68 (2H, td, *J* = 7.8, 1.8 Hz; pyridyl H^4), 7.39 (2H, d, *J* = 2.3 Hz; pyrazolyl H^5), 7.18 (2H, ddd, *J* = 7.8, 4.9, 1.1 Hz; pyridyl H^5), 6.89 (2H, d, *J* = 2.3 Hz; pyrazolyl H^4), 6.51 (1H, s; ArH), 6.39 (2H, s; ArH), 5.23 (4H, s; CH_2), 3.64 (2H, bs; NH_2). ESMS: *m/z* 430 [M + Na]$^+$, 408 [M + H]$^+$, 205 [M + 2H]$^{2+}$. Found: C, 64.40; H, 5.53; N, 21.92 %. Required for $C_{24}H_{21}N_7 \cdot 2.25H_2O$: C, 64.34; H, 5.74; N, 21.89 %

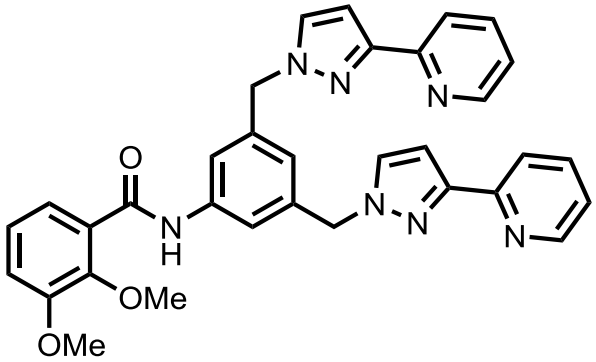

Synthesis of 22

A mixture of **L^{an}** (1.57 g, 3.9 mmol) and **5** (0.85 g, 4.2 mmol) were stirred in dry DCM (50 cm^3) under nitrogen flow. To the cloudy solution was added Et_3N (2 cm^3, 14.4 mmol), and the resultant clear solution was stirred at room temperature for 14 h. The mixture was then sequentially washed with 1M HCl (50 cm^3) and 1M NaOH (50 cm^3). The organic layer was extracted with DCM, dried over $MgSO_4$ and concentrated before purification by column chromatography on silica. Elution with EtOAc (R_f = 0.17) yielded **22** as a white solid (Yield: 1.81 g, 82 %). ^{1}H-NMR (400 MHz, $CDCl_3$): δ 10.04 (1H, s; NH), 8.62 (2H, ddd, *J* = 5.0, 1.9, 1.0 Hz; pyridyl H^6), 7.92 (2H, dt, *J* = 8.0, 1.0 Hz; pyridyl H^3), 7.74 (1H, dd, *J* = 8.1, 1.5 Hz; ArH), 7.69 (2H, td, *J* = 7.8, 1.8 Hz; pyridyl H^4), 7.57 (2H, d, *J* = 1.1 Hz; ArH), 7.45 (2H, d, *J* = 2.3 Hz; pyrazolyl H^5), 7.22 – 7.15 (3H, m; ArH and pyridyl H^5), 7.08 (1H, dd, *J* = 8.1, 1.5 Hz; ArH), 6.90 (2H, d, *J* = 2.3 Hz; pyrazolyl H^4), 6.89 (1H, s; ArH), 5.37 (4H, s; CH_2), 3.91 (3H, s; OMe); 3.89 (3H, s; OMe). ESMS: *m/z* 572 [M + H]$^+$, 287 [M + 2H]$^{2+}$.

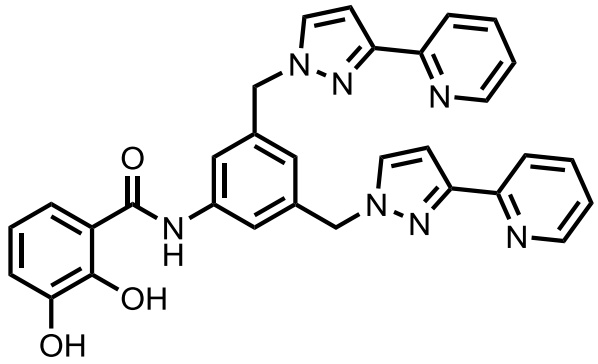

Synthesis of H_2L^{TRI}

To a solution of **22** (1.80 g, 3.2 mmol) in dry DCM (100 cm^3) under nitrogen flow at -78 ^oC was added BBr_3 (3.5 cm^3, 36.3 mmol) dropwise by disposable plastic syringe. The reaction was maintained at -78 ^oC for 1 h and then stirred at room temperature overnight. The volatiles were removed under reduced pressure and the resultant orange residue was suspended in H_2O at 100 ^oC for 4 h. Upon cooling to room temperature a white precipitate formed which was collected by filtration and washed with water, EtOH, Et_2O and DCM, yielding H_2L^{TRI}.HBr as a white solid (Yield: 1.60 g, 95 %). ^{1}H-NMR (400 MHz, (MeOD) 8.68 (2H, d, *J* = 5.9 Hz; pyridyl H^6), 8.58 (2H, td, *J* = 7.9, 1.4 Hz; pyridyl H^4), 8.40 (2H, d, *J* = 7.9 Hz; pyridyl H^3), 8.05 (2H, d, *J* = 2.5 Hz; pyrazolyl H^5), 7.91 (2H, ddd, *J* = 7.9, 5.9, 1.2 Hz; pyridyl H^5), 7.69 (2H, d, *J* = 1.3 Hz; Ph-H), 7.40 (1H, dd, *J* = 8.1, 1.4 Hz; cat-H), 7.20 (2H, d, *J* = 2.5 Hz; pyrazolyl H^4), 7.15 (1H, s; Ph-H), 6.96 (1H, dd, *J* = 8.0, 1.5 Hz; cat-H), 6.76 (1H, t, *J* = 8.0 Hz; cat-H), 5.54 (4H, s; CH_2). ESMS: *m/z* 566 $[M + Na]^+$, 544 $[M + H]^+$, 273 $[M + 2H]^{2+}$. Found: C, 49.00; H, 3.86; N, 12.75 %. Required for $C_{31}H_{25}N_7O_3 \cdot 2.75HBr$: C, 48.60; H, 3.65; N, 12.80 %.

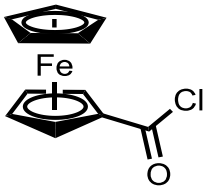

Synthesis of 23

A modified literature procedure was used.[32] A mixture of ferrocenecarboxylic acid (0.26 g, 1.0 mmol) and oxalyl chloride (0.38 g, 3.0 mmol) were stirred in DCM (15 cm^3) at room temperature for 2 h. After removing the volatiles *in vacuo*, the mixture was washed with hexane and then evaporated to dryness once more. The resultant brown oil was used without further purification.

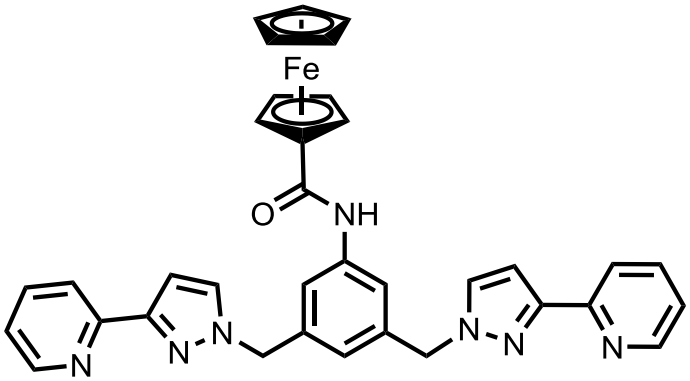

Synthesis of L^{Fc}

A mixture of $\mathbf{L^{an}}$ (0.33 g, 0.8 mmol) and **23** (0.23 g, 1.0 mmol) were stirred in DCM (30 cm^3) under nitrogen flow. To the cloudy solution was added Et_3N (0.60 cm^3, 4.3 mmol), and the resultant clear solution was stirred at room temperature for 14 h after which time the mixture was quenched with water (30 cm^3). The organic layer was extracted with DCM, washed with brine, dried over $MgSO_4$ and concentrated before purification by column chromatography on alumina. Elution with 1: 3 EtOAc/DCM and collection of the second major fraction yielded $\mathbf{L^{Fc}}$ as an orange solid (Yield: 0.34 g, 69 %). ^{1}H-NMR (400 MHz, $CDCl_3$): δ 8.65 (2H, d, *J* = 4.0 Hz; pyridyl H^6), 7.92 (2H, d, *J* = 7.8 Hz; pyridyl H^3), 7.71 (2H, t, *J* = 7.5 Hz; pyridyl H^4), 7.67 (1H, br s; NH), 7.51 (2H, s; Ar-H), 7.45 (2H, s; pyrazolyl), 7.21 (2H, dd, *J* = 7.5, 4.8 Hz; pyridyl H^5), 6.90 (2H, s; pyrazolyl), 6.86 (1H, s; Ar-H), 5.34 (4H, s;

CH_2), 4.79 (2H, s; Cp), 4.41 (2H, s; Cp), 4.23 (5H, s; Cp). ESMS: *m/z* 620 $[M + H]^+$, 311 $[M + 2H]^{2+}$. Found: C, 67.92; H, 4.78; N, 15.66 %. Required for $C_{35}H_{29}FeN_7O$: C, 67.86; H, 4.72; N, 15.83 %.

5.4.2 Complex synthesis

Synthesis of $[Co_8(L^{an})_{12}](BF_4)_{16}$

A Teflon lined autoclave was charged with **L^{an}** (0.050 g, 0.12 mmol), $Co(BF_4)_2.6H_2O$ (0.036 g, 0.10 mmol) and methanol (5 cm^3). Heating to 100 ^oC for 12 hr followed by slow cooling to room temperature yielded a crop of small pink crystals, which were washed with methanol and dried to give $[Co_8(\mathbf{L}^{an})_{12}](BF_4)_{16}$ as a pink solid in 76 % yield.

ESMS: *m/z*; 2163.2, $\{[Co_8(\mathbf{L}^{an})_{12}](BF_4)_{13}\}^{3+}$; 1600.8, $\{[Co_8(\mathbf{L}^{an})_{12}](BF_4)_{12}\}^{4+}$; 1263.1, $\{[Co_8(\mathbf{L}^{an})_{12}](BF_4)_{11}\}^{5+}$, 1038.0 $\{[Co_8(\mathbf{L}^{an})_{12}](BF_4)_{10}\}^{6+}$; 877.4, $\{[Co_8(\mathbf{L}^{an})_{12}](BF_4)_9\}^{7+}$; 756.7, $\{[Co_8(\mathbf{L}^{an})_{12}](BF_4)_8\}^{8+}$.

Elemental analytical data was consistent with the presence of water of crystallisation due to the desolvated material being hygroscopic, Found: C, 47.52; H, 4.17; N, 15.76 %. Required for $C_{288}H_{252}B_{16}Co_8F_{64}N_{84}{\cdot}32H_2O$: C, 47.21; H, 4.35; N, 16.06 %.

Synthesis of $[Cd(L^{an})](ClO_4)_2$

A Teflon lined autoclave was charged with **L^{an}** (0.050 g, 0.12 mmol), $Cd(ClO_4)_2.6H_2O$ (0.035 g, 0.08 mmol) and methanol (5 cm^3). Heating to 100 ^oC for 12 hr followed by slow cooling to room temperature yielded a white powder, which was washed with methanol and dried to give $[Cd(\mathbf{L}^{an})]$-$(ClO_4)_2$ in 62 % yield.

ESMS: *m/z*; 620, $\{[Cd(\mathbf{L}^{an})](ClO_4)\}^+$; 583, $\{[Cd(\mathbf{L}^{an})](NO_3)\}^+$. Found: C, 40.44; H, 3.65; N, 13.27 %. Required for $C_{24}H_{21}CdCl_2N_7O_8{\cdot}MeOH$: C, 39.99; H, 3.36; N, 13.06 %.

Synthesis of [Ag(L^{an})](PF_6)

A mixture of $\mathbf{L^{an}}$ (0.050 g, 0.12 mmol) and $Ag(PF_6)$ (0.040 g, 0.16 mmol), methanol (5 cm^3) and DCM (5 cm^3) was stirred at room temperature overnight. The resultant precipitate was filtered off and washed with methanol and DCM, and then dried in vacuo to give [Ag($\mathbf{L^{an}}$)](PF_6) as a grey powder in 65 % yield.

ESMS: *m/z*; 685, {[Ag_2($\mathbf{L^{an}}$)](NO_3)}$^+$; 514, {Ag($\mathbf{L^{an}}$)}$^+$.

Synthesis of [Co_6(L^{Fc})$_9$](BF_4)$_{12}$

A mixture of $\mathbf{L^{Fc}}$ (0.051 g, 0.08 mmol) and $Co(BF_4)_2.6H_2O$ (0.022 g, 0.06 mmol), methanol (5 cm^3) and DCM (5 cm^3) was stirred at room temperature overnight. The resultant precipitate was filtered off and washed with methanol and then dried *in vacuo* to give [Co_6($\mathbf{L^{Fc}}$)$_9$](BF_4)$_{12}$ as an orange powder in 70 % yield.

ESMS: *m/z*; 2237.1, {[Co_6($\mathbf{L^{Fc}}$)$_9$](BF_4)$_9$}$^{3+}$; 1655.4, {[Co_6($\mathbf{L^{Fc}}$)$_9$](BF_4)$_8$}$^{4+}$; 1575.5 {[Co_2($\mathbf{L^{Fc}}$)$_2$](BF_4)$_2CHO_2$}$^+$; 1462.3 {[Co_8($\mathbf{L^{Fc}}$)$_{12}$](BF_4)$_{10}$}$^{6+}$; 1307.6 {[Co_6($\mathbf{L^{Fc}}$)$_9$](BF_4)$_7$}$^{5+}$; 1057.5 {[Co_6($\mathbf{L^{Fc}}$)$_9$](BF_4)$_6$}$^{6+}$.

Synthesis of [$GaCo_3$(L^{TRI})$_4$](BF_4)$_4$

To a solution of $\mathbf{L^{TRI}}$**.2.75HBr** (0.162 g, 0.21 mmol) in methanol (10 cm^3) was added KOH (0.036 g, 0.65 mmol) in methanol (1 cm^3). Upon the cloudy mixture becoming clear, $Ga(acac)_3$ (0.037 g, 0.10 mmol) and then $Co(BF_4)_2.6H_2O$ (0.068 g, 0.20 mmol) were added, and the mixture was stirred at room temperature overnight. The resultant precipitate was filtered off and washed with methanol, water and acetone, and then dried *in vacuo* to give [$GaCo_3$($\mathbf{L^{TRI}}$)$_4$](BF_4)$_4$ as a beige powder in 59 % yield.

ESMS: *m/z*; 1257.8, {[$GaCo_3$($\mathbf{L^{TRI}}$)$_4$](BF_4)F}$^{2+}$; 837.9, {[$GaCo_3$($\mathbf{L^{TRI}}$)$_4$](acac)}$^{3+}$; 832.9 {[$GaCo_3$($\mathbf{L^{TRI}}$)$_4$](BF_4)}$^{3+}$.

Elemental analytical data was consistent with the presence of water of crystallisation due to the desolvated material being hygroscopic, Found: C, 49.00; H, 4.03; N, 12.41 %. Required for $C_{124}H_{92}B_4Co_3F_{16}GaN_{28}O_{12}{\cdot}16H_2O$: C, 48.86; H, 4.10; N, 12.87 %.

Synthesis of $Cs_2[Ti(L^{TRI})_3]$

To a solution of **L^{TRI}·2.75HBr** (0.199 g, 0.26 mmol) and Cs_2CO_3 (0.388 g, 1.19 mmol) in methanol (20 cm^3) was added $Ti(^iOPr)_4$ (0.025 g, 0.09 mmol) in methanol (1 cm^3) *via* plastic disposable syringe. The mixture was stirred at room temperature overnight. An insoluble solid was filtered off and washed with methanol, and removal of the solvent by rotary evaporation gave $Cs_2[Ti(\mathbf{L^{TRI}})_3]$ as a yellow solid in 51 % yield.

ESMS(-): *m/z*; 857.3, $[Ti(\mathbf{L^{TRI}})_3]^{2-}$.

5.5 X-ray crystallography

Details of the crystal, data collection and refinement parameters are summarised. Data were corrected for absorption using empirical methods (SADABS)[33] based upon symmetry-equivalent reflections combined with measurements at different azimuthal angles. The structures were solved by direct methods and refined by full-matrix least squares on weighted F^2 values for all reflections using the SHELX suite of programs.[34] Non-hydrogen atoms were refined anisotropically. Hydrogen atoms were placed in calculated positions, refined using idealized geometries (riding model) and were assigned fixed isotropic displacement parameters.

A suitable crystal was mounted in a stream of cold N_2 on a Bruker APEX-2 CCD diffractometer (at the University of Sheffield) equipped with graphite-monochromated Mo-Kα radiation from a sealed-tube source. Detail of the structure is given in the CIF.

Summary of crystallographic data for the new crystal structure:

Compound	**$L^{an.}$ 2.25H_2O**
Formula	$C_{24}H_{25.5}N_7O_{2.25}$
Molecular weight	448.01
T / *K*	100(2)
Crystal system	Monoclinic
Space group	P 21/n
a / Å	11.4574(3)
b / Å	10.1888(3)
c / Å	19.1554(5)
α / °	90
β / °	95.3053(12)
γ / °	90
V / Å^3	2226.57(11)
Z	4
ρ / g cm^{-3}	1.336
μ / mm^{-1}	0.090
Data, restraints, parameters, *R*int	5183 / 0 / 315 / 0.0249
Final *R*1, *wR*2[a]	0.0485, 0.1368

[a] The value of R1 is based on 'observed' data with I>2σ(I); the value of wR2 is based on all data.

5.6 References

1. M. D. Ward and P. R. Raithby, *Chem. Soc. Rev.*, 2013, **42**, 1619.

2. B. Breiner, J. K. Clegg and J. R. Nitschke, *Chem. Sci.*, 2011, **2**, 51.

3. M. Yoshizawa, J. K. Klosterman and M. Fujita, *Angew. Chem., Int. Ed.*, 2009, **48**, 3418.

4. M. Fujita, *Chem. Soc. Rev.*, 1998, **27**, 417.

5. M. D. Ward, *Chem. Commun.*, 2009, 4487.

6. R. Chakrabarty, P. S. Mukherjee and P. J. Stang, *Chem. Rev.*, 2011, **111**, 6810.

7. K. Harris, D. Fujita and M. Fujita, *Chem. Commun.*, 2013, **49**, 6703.

8. N. Kamiya, M. Tominaga, S. Sato and M. Fujita, *J. Am. Chem. Soc.*, 2007, **129**, 3816.

9. K. Suzuki, S. Sato and M. Fujita, *Nature Chem.*, 2010, **2**, 25.

10. P. P. Neelakandan, A. Jimenez and J. R. Nitschke, *Chem. Sci.*, 2014, **5**, 908.

11. A. Stephenson and M. D. Ward, *Dalton Trans.*, 2011, **40**, 10360.

12. A. M. Najar, I. S. Tidmarsh, H. Adams and M. D. Ward, *Inorg. Chem.*, 2009, **48**, 11871.

13. Z. R. Bell, L. P. Harding and M. D. Ward, *Chem. Commun.*, 2003, 2432.

14. S. Turega, W. Cullen, M. Whitehead, C. A. Hunter and M. D. Ward, *J. Am. Chem. Soc.*, 2014, **136**, 8475.

15. M. Whitehead, S. Turega, A. Stephenson, C. A. Hunter and M. D. Ward, *Chem. Sci.*, 2013, **4**, 2744.

16. A. J. Metherell and M. D. Ward, *RSC Adv.*, 2013, **3**, 14281.

17. R. Neelarapu, D. L. Holzle, S. Velaparthi, H. Bai, M. Brunsteiner, S. Y. Blond and P. A. Petukhov, *J. Med. Chem.*, 2011, **54**, 4350.

18. H. Onagi and J. Rebek, *Chem. Commun.*, 2005, 4604.

19. S. P. Argent, H. Adams, L. P. Harding and M. D. Ward, *Dalton Trans.*, 2006, 542.

20. A. Stephenson and M. D. Ward, *RSC Adv.*, 2012, **2**, 10844.

21. D. L. Caulder, R. E. Powers, T. N. Parac and K. N. Raymond, *Angew. Chem. Int. Ed.*, 1998, **37**, 1840.

22. A. Panja, *RSC Adv.*, 2013, **3**, 4954.

23. M. Albrecht and R. Frohlich, *J. Am. Chem. Soc.*, 1997, **119**, 1656.

24. R. L. Paul, Z. R. Bell, J. C. Jeffery, J. A. McCleverty and M. D. Ward, *Proc. Nat. Acad. Sci. U.S.A*, 2002, **99**, 4883.

25. I. S. Tidmarsh, T. B. Faust, H. Adams, L. P. Harding, L. Russo, W. Clegg and M. D. Ward, *J. Am. Chem. Soc.*, 2008, **130**, 15167.

26. A. Stephenson, D. Sykes and M. D. Ward, *Dalton Trans.*, 2013, **42**, 6756.

27. S. Hiraoka, Y. Sakata and M. Shionoya, *J. Am. Chem. Soc.*, 2008, **130**, 10058.

28. X. K. Sun, D. W. Johnson, D. L. Caulder, K. N. Raymond and E. H. Wong, *J. Am. Chem. Soc.*, 2001, **123**, 2752.

29. A. Stephenson, S. P. Argent, T. Riis-Johannessen, I. S. Tidmarsh and M. D. Ward, *J. Am. Chem. Soc.*, 2011, **133**, 858.

30. A. J. Amoroso, A. M. C. Thompson, J. C. Jeffery, P. L. Jones, J. A. McCleverty and M. D. Ward, *J. Chem. Soc., Chem. Commun.*, 1994, 2751.

31. M. Meyer, B. Kersting, R. E. Powers and K. N. Raymond, *Inorg. Chem.*, 1997, **36**, 5179.

32. A. Aguilar-Aguilar, A. D. Allen, E. P. Cabrera, A. Fedorov, N. Y. Fu, H. Henry-Riyad, J. Leuninger, U. Schmid, T. T. Tidwell and R. Verma, *J. Org. Chem.*, 2005, **70**, 9556.

33. G. M. Sheldrick, *SADABS: A program for absorption correction with the Siemens SMART system*, University of Göttingen, Germany, 1996.

34. G. M. Sheldrick, *Acta Cryst. Sect. A*, 2008, **64**, 112.